

From polarity establishment to fast hyphal growth in the filamentous fungus *Ashbya gossypii*

Inauguraldissertation zur Erlangung der Würde eines Doktors der Philosophie

vorgelegt der

Philosophisch-Naturwissenschaftlichen Fakultät der Universität Basel von

Michael Köhli
aus Kallnach, Bern.

Basel, 2007

Genehmigt von der Philosophisch-Naturwissenschaftlichen Fakultät auf Antrag von
Prof. Dr. Peter Philippsen und Prof. Dr. Yves Barral

Basel, den 26. Juni 2007

Prof. Dr. Hans-Peter Hauri
Dekan

Table of contents

Table of contents

Table of contents	1
Summary	7
<i>Ashbya gossypii</i>	13

Part I

The localization of polarity factors changes with increasing hyphal elongation rate.

Abstract	19
Introduction	19
Results	23
Discussion	35
Materials and methods	40

Part II

AgGic1/2 is important for cell polarity establishment but not for maintenance of fast hyphal growth in *Ashbya gossypii*.

Abstract	53
Introduction	53
Results	55
Discussion	60
Materials and methods	64

Part III

The function of two closely related Rho proteins is determined by regulator specificity, not by effector interaction.

Abstract	73
Introduction	73
Results	75
Discussion	81
Material and methods	84
Appendix	97
References	109
Supplmental movies	117
Acknowledgements	121
Curriculum Vitae	125
Erklärung	129

Summary

Summary

Fungi are an evolutionary successful group of organisms with great ecological importance. The impact of filamentous fungi on human welfare is enormous. They cause the majority of economically significant diseases of crop plants and are becoming increasingly important as human pathogens.

The formation of hyphae (elongated, tubular cells) is a key characteristic of filamentous fungi. Hyphal growth allows them to spread rapidly through various substrates in search of nutrients or mating partners, or to penetrate host organisms. Elucidation of mechanisms that control hyphal growth and fungal morphogenesis may lead to the identification of new fungicide targets, and further may increase the understanding of other hyperpolarized cell types such as neurons in animals, pollen tubes in plants or rhizoids in algae.

Part I

Ashbya gossypii and the budding yeast *Saccharomyces cerevisiae* carry a very similar set of genes. Yet *A. gossypii* is a filamentous fungus displaying constantly polarized growth at hyphal tips resulting in surface expansion rates that are up to 30 times higher than in yeast cells. Polar growth in budding yeast is tightly controlled in a cell cycle-dependent manner. Cell polarity establishment, polar growth and isotropic expansion all take place during formation of a bud, therefore these processes are difficult to separate experimentally. In contrast, growing hyphal tips are ideal systems to study sustained polar growth though the knowledge about the organization of this highly dynamic site is presently limited.

I found that factors that are involved in plasma membrane vesicle fusion, control of the polarized actin cytoskeleton and regulation of cell polarity in *A. gossypii* occupy distinct subcellular regions in the hyphal tip. Core cell polarity factors such as *AgCdc42*, *AgCdc24* and *AgBoi1/2* were restricted to different parts of the tip cortex, whereas the formin *AgBni1*, the polarisome components *AgSpa2* and *AgPea1* and the exocyst were also found in the apical body, which is a vesicle-based structure commonly observed in the apex of growing fungal hyphae. Importantly, localization of these proteins to different zones changes with increasing elongation speed. Slow hyphae with surface expansion rates close to bud growth in *S. cerevisiae* display most polarity factors at the tip cortex independent of the factor's identity, and at slow growth speeds apical bodies are absent. These

findings suggest that fast growing hyphal tips are subdivided into functional zones where different sets of polarity factors exert their function. A model of fast hyphal growth can be postulated based on this hypothesis.

Part II

Establishment of a fungal mycelium depends on constant hyphal elongation and formation of new hyphae, which arise by branching. Emergence of a lateral branch requires establishment of a novel axis of cell polarity at the hyphal cortex, an event which might *a priori* not involve an identical set of polarity factors needed for sustained polar growth. Therefore, I looked for *A. gossypii* candidate genes the deletion of which could generate mycelia with severely reduced or even absent lateral branching while tip expansion was unchanged. I found that loss of *AgGic1/2* resulted in such a phenotype. *AgGic1/2* also plays a role in the first polarity establishment during germination since spores lacking *AgGic1/2* display delayed germ tube emergence. The data reported in this PhD-thesis clearly indicate that *AgGic1/2* is important for cell polarity establishment but dispensable for polarity maintenance in *A. gossypii*. In *S. cerevisiae* the homologous proteins *ScGic1* and *ScGic2* act as effectors of the key polarity factor *ScCdc42*. This molecular function is probably conserved in *A. gossypii* since *AgGic1/2* interacts with *AgCdc42* in a two-hybrid assay. Degradation of *AgGic1/2* is likely to be mediated by its carboxy-terminal PEST domains, which are not predicted in the homologous yeast proteins *ScGic1* and *ScGic2*. *AgGic1/2* may have a regulatory function in branch initiation based on the finding that an *AgGIC1/2* allele lacking the part that encodes the PEST domains induces an increase in branching if expressed from a strong promoter. It is possible that controlled degradation of *AgGic1/2* constitutes a simple mechanism that is involved in regulating emergence of new lateral branches.

Part III

It is generally believed that the vast number of small GTP-binding proteins present in cells of higher organisms today has evolved by gene duplications of a common ancestor. Furthermore it is taken for granted that after duplication mutations alter the protein's effector interactions, thereby changing its function. In contrast to these assumptions we show here for the two duplicated *RHO1* genes

from the filamentous fungus *Ashbya gossypii* that the different functions of the encoded proteins are not due to different effector interactions. Instead we found that both proteins are regulated by different GAP-proteins and that GAP specificity is determined by either a tyrosine or a histidine at a single position in the switch I region of the two Rho1 proteins. An analogous histidine residue is found in some atypical GTP-binding proteins of higher eukaryotes, suggesting that the evolutionary mechanism we describe here might be a common way for diversification of GTP-binding protein function.

Ashbya gossypii

Ashbya gossypii

Stigmatomycosis is a general term for a fungal disease that occurs on different crops. It is used to describe an affection in which fruits are internally infected as a result of punctures made by plant-feeding bugs of the suborder *Heteroptera*. Among other fungi, *Ashbya gossypii*, also known as *Nematospora gossypii* or *Eremothecium gossypii* (Kurtzman, 1995), was identified as a causative agent of stigmatomycosis on cotton bolls (internal boll disease), and was isolated from samples collected in southern Africa and on different Caribbean islands (Ashby and Nowell, 1926). Internal boll disease made it virtually impossible to grow cotton in certain parts of the tropics during the first half of the twentieth century (Batra, 1973). However, insects are essential for the spread of the causative fungi. Thus, control of the insect population by insecticides has proven efficient against stigmatomycosis (Dammer and Grillo-Ravelo, 1996). Nevertheless, *A. gossypii* is still present in nature and was recently isolated from true bugs in Florida (Fred Dietrich, unpublished results).

A. gossypii is a natural overproducer of riboflavin (vitamin B₂), which is responsible for the yellow color of colonies on agar plates (figure 1f; Demain, 1972). Riboflavin is essential only in tiny amounts as a precursor for oxidoreductase coenzymes. The large quantities present in *A. gossypii* probably serve to protect spores against ultraviolet light (Stahmann et al., 2001). Biotechnical riboflavin production by genetically engineered *A. gossypii* strains and other microorganisms are nowadays replacing chemical synthesis of this vitamin, which is widely used as a food colorant (E-101) or as animal feed additive (reviewed by Stahmann et al., 2000).

A. gossypii is closely related to the budding yeast *Saccharomyces cerevisiae*. About 95 % of the 4700 protein-coding *A. gossypii* genes are orthologues of *S. cerevisiae* genes, and 90% map within blocks of synteny (blocks of conserved gene order). These findings suggest that the *A. gossypii* and the *S. cerevisiae* lineage split about 100 million years ago. During this time, about 100 genomic rearrangements, few gene deletions and duplications happened that were maintained in the *A. gossypii* genome. The *S. cerevisiae* genome emerged from a more eventful evolutionary history including the duplication of the entire genome, followed by extensive gene loss. Almost 500 pairs of “twin genes”, which are genes that originally had an identical sequence after the genome duplication, remained in *S. cerevisiae*. Obviously, one syntenic homologue for each pair of twin genes is found in *A. gossypii* (Dietrich et al., 2004). *A. gossypii* is an excellent model organism. Contrary to other filamentous fungi, it integrates linear DNA with high efficiency at the homologous genomic locus and is therefore amenable to targeted genetic manipulation (Wendland et

al., 2000). Furthermore, plasmids carrying an autonomously replicating sequence from budding yeast are maintained in *A. gossypii* (Wright and Philippsen, 1991). In *A. gossypii*, several haploid nuclei occupy a common cytoplasm (Ashby and Nowell, 1926; Gladfelter et al., 2006), which makes it possible to study and maintain recessive mutations that are deleterious or even lethal. A heterokaryotic mycelium contains both mutated and wild-type nuclei and thus displays no defects. The uninucleated spores that are isolated from heterokaryotic mycelium give rise to homokaryotic strains that show the phenotype associated with the mutation.

Like most fungi, *A. gossypii* has the capability to form long, tubular cells called hyphae. Septa, which are chitinous partition walls, subdivide hyphae into compartments that are occupied by several nuclei. (Ashby and Nowell, 1926).

A. gossypii produces needle-shaped conidia (asexual spores, figure 1a). When environmental conditions are good, spores expand in the middle of the spore body and form a spherical germ bubble (figure 1b). Germ tubes emerge perpendicularly to the hyphal axis (figure 1c). At this stage, hyphal elongation rate is about 0.1 $\mu\text{m}/\text{min}$ on rich medium (Knechtle et al., 2003). A second germ tube is established opposite the first one (figure 1d). Hyphal growth and lateral branching (figure 1e) results in formation of a dense network of intertwined hyphae, a so-called mycelium (figure 1f). Hyphal elongation rates can reach 3.5 $\mu\text{m}/\text{min}$ at the border of older mycelia. At this stage, new hyphal tips are generated by tip splitting (figure 1g), which is also called tip branching or dichotomous branching. Tip splitting results in a Y-shaped bifurcation of *A. gossypii* hyphae (figure 1f, arrowheads; Knechtle et al., 2003; Schmitz et al., 2006). Conidia are formed in the center of the fungal mycelium in a poorly described process. Sporangia, the spore-containing structures (figure 1h), are formed by enlargement of successive hyphal segments between septa, so that hyphae are converted into chains of sporangia (Ashby and Nowell, 1926). Little is known about the relationship between *A. gossypii*, its host plants and its insect vectors. For this reason, the life cycle presented here refers to *A. gossypii* grown under laboratory conditions and might be incomplete.

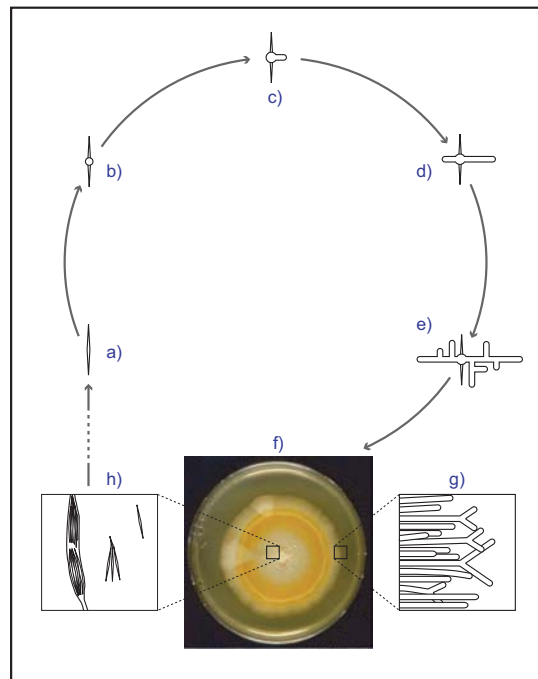


Fig. 1: Life cycle of *A. gossypii*. The figure summarizes the life cycle of *A. gossypii* from germination to sporulation (Ashby and Nowell, 1926; Knechtle et al., 2003; Schmitz et al., 2006, reviewed by Philippsen et al., 2005 and Wendland and Walther, 2005).

Part I

The localization of polarity factors changes with increasing hyphal elongation rate.

Ashbya gossypii and the budding yeast *Saccharomyces cerevisiae* carry a very similar set of genes. Yet *A. gossypii* is a filamentous fungus displaying constantly polarized growth at hyphal tips resulting in surface expansion rates that are up to 30 times higher than in yeast cells. Polar growth in budding yeast is tightly controlled in a cell cycle-dependent manner. Cell polarity establishment, polar growth and isotropic expansion all take place during formation of a bud, therefore these processes are difficult to separate experimentally. In contrast, growing hyphal tips are ideal systems to study sustained polar growth though the knowledge about the organization of this highly dynamic site is presently limited.

I found that factors that are involved in plasma membrane vesicle fusion, control of the polarized actin cytoskeleton and regulation of cell polarity in *A. gossypii* occupy distinct subcellular regions in the hyphal tip. Core cell polarity factors such as *AgCdc42*, *AgCdc24* and *AgBoi1/2* were restricted to different parts of the tip cortex, whereas the formin *AgBni1*, the polarisome components *AgSpa2* and *AgPea1* and the exocyst were also found in the apical body, which is a vesicle-based structure commonly observed in the apex of growing fungal hyphae. Importantly, localization of these proteins to different zones changes with increasing elongation speed. Slow hyphae with surface expansion rates close to bud growth in *S. cerevisiae* display most polarity factors at the tip cortex independent of the factor's identity, and at slow growth speeds apical bodies are absent. These findings suggest that fast growing hyphal tips are subdivided into functional zones where different sets of polarity factors exert their function. A model of fast hyphal growth can be postulated based on this hypothesis.

Introduction

The controlled asymmetric distribution of cellular proteins creates polarity, e.g. polar secretion or maintained polar growth. Polarity is found in almost all cells from neurons and epithelial cells in mammals to single cell organisms like budding yeast and even bacteria. Analysis of different eukaryotic cell types revealed that internal and/or external cues adapt conserved core pathways for cytoskeleton assembly and protein transport to generate cell polarity. One of the best-studied example is the formation of a daughter cell in the budding yeast *Saccharomyces cerevisiae*: landmark proteins that are only found in yeast and closely related species provide a cortical cue to polarize the cytoskeleton and intracellular transport through conserved pathways (reviewed by Nelson, 2003) resulting in outgrowth of a bud.

In this thesis, a novel system, *Ashbya gossypii*, is analyzed, which allows to study an extreme case of polar growth. *A. gossypii* is a filamentous ascomycete with a genome that is unexpectedly closely related to the genome of budding yeast. More than 90% of *A. gossypii* genes show both homology and synteny with *S. cerevisiae* genes (Dietrich et al., 2004). Yet, the sustained filamentous growth-style of *A. gossypii* implies two profound differences to the unicellular *S. cerevisiae*.

Budding yeast cells alternate between polar and isotropic growth phases during cell cycles and couple mitosis and morphogenesis to maintain one nucleus per cell. Initial polarity establishment at the mother cell cortex is followed by a temporally restricted phase of polar growth, subsequent non-polar bud expansion, and finally, reorientation of the polarity axis towards the mother-bud neck to deliver the material for cytokinesis and cell separation (figure 1A.) In contrast, *A. gossypii* forms long, tubular, multinucleated cells called hyphae. At the hyphal tip, cell polarity is maintained and thus polar growth continues as long as conditions are favorable. Neither septation, the process of cytoplasm separation by construction of chitinous partition walls, nor the cell cycle state of the nuclei that are close to the growing tip influence the axis of polarity (Ayad-Durieux et al., 2000; Knechtle, 2002; Philippsen et al., 2005; Wendland and Walther, 2005; Gladfelter et al., 2006). Sites of polar growth, the hyphal tips, separate by ever increasing distances from the original sites of polarity establishment (figure 1A). Thus, hyphal tips harbor autonomous growth control centers. Consequently, *A. gossypii* is a very good system to study sustained polar growth. In *S. cerevisiae* the phase of polar growth is transient and lasts only a few minutes. A second important difference between *A. gossypii* and *S. cerevisiae* is the efficiency of surface growth (Schmitz et al.,

2006). Mature *A. gossypii* tips have a diameter of about 4 μm and can extend with up to 3.3 $\mu\text{m}/\text{min}$ (Knechtle et al., 2003). Thus, 40 μm^2 new cell surface can be synthesized per minute. *S. cerevisiae* synthesizes about 1.5 μm^2 new surface per minute during the bud growth phase. It is obvious that the material transported to one maximally growing *A. gossypii* tip by far exceeds the material needed to build one *S. cerevisiae* bud. Since *A. gossypii* has to focus intracellular transport to the tightly restricted surface area of the hyphal tips, long-range transport must be very efficient in this fungus.

Virtually all genes involved in polar growth of yeast are conserved in *A. gossypii*. Presumably, the basic molecular function of most if not all proteins encoded by these about 200 polarity genes did not change through evolution (table 1) though they might be controlled differently in *A. gossypii* and in yeast (Dietrich et al., 2004, reviewed by Philippsen et al., 2005).

In budding yeast, a small GTP-binding protein, *ScCdc42*, is the key player in cell polarity, and conditional *Scdc42* mutants grow isotropically

resulting in large, round cells under restrictive conditions (Adams et al., 1990). When budding is initiated, *ScCdc42* localizes to cortical landmarks. Its polarized localization and activation involves, among others, *ScBem1* and *ScCdc24*. *ScCdc24* is the sole guanosine nucleotide exchange factor (GEF) of *ScCdc42* and stimulates the exchange of GDP against GTP. Activated *ScCdc42* then recruits the adaptor protein *ScBem1*, which in turn can activate *ScCdc24* resulting in a positive feedback loop (figure 1B, Bose et al., 2001; Butty et al., 2002; Irazoqui et al., 2003; Wedlich-Soldner et al., 2004). The PAK (p21 activated kinase) family kinase *ScCla4* interacts via its CRIB (Cdc42/Rac interactive binding) domain with GTP-bound *ScCdc42* and with its PH-domain with phosphatidylinositol 4-phosphate (PI4P). Both interactions are necessary for *ScCla4* function (Benton et al., 1997; Wild et al., 2004). A peak of *ScCla4* activity after bud emergence is thought to negatively regulate yeast cell polarity by inducing phosphorylation of *ScCdc24*. This phosphorylation triggers dissociation of *ScCdc24* from *ScBem1* and consequently interrupts *ScCdc42* GTP/GDP

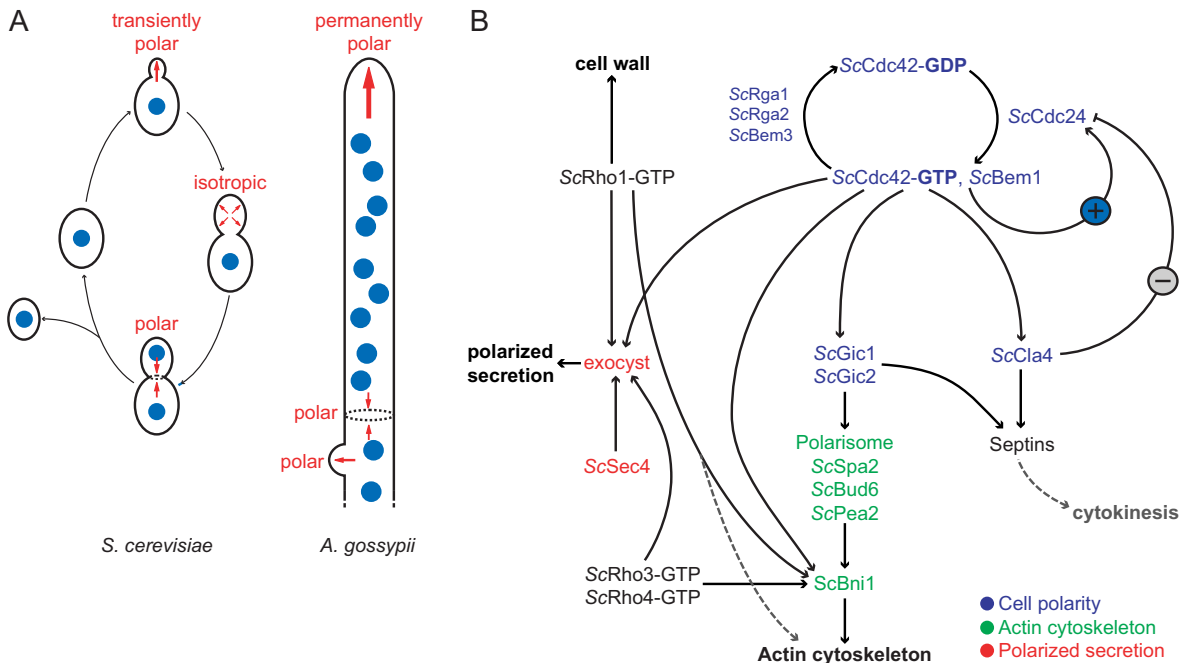


Fig. 1: Cell polarity in *S. cerevisiae* and *A. gossypii*. (A) Morphogenesis and cell polarity of *S. cerevisiae* and *A. gossypii*. Morphogenesis is coupled to the cell cycle in *S. cerevisiae*. Initial polar growth is transient and followed by non-polar expansion of the bud. Cytokinesis only takes place after mitosis and requires reorientation of the axis of polarity towards the mother-bud neck. *A. gossypii* maintains an axis of polarity, new sites of polarity can be established along the cortex. Septation takes place at the same time as hyphal growth. Adapted from Philippsen et al. 2005. (B) Model of cell polarity establishment and actin cytoskeleton polarization in *S. cerevisiae*. Adapted from Pruyne et al. 2004. Protein or protein complexes that are linked with black arrows interact together. The arrows between *ScCdc42-GFP* and *ScCdc42-GDP* indicate cycling between the two nucleotide-bound states. The plus sign indicates a positive feedback loop, the minus sign a shut-off loop. Note that not all known interactions are shown.

exchange thus promoting the switch from polar to isotropic growth. (Benton et al., 1997; Gulli et al., 2000; Bose et al., 2001). Furthermore, *ScCla4* directly phosphorylates septins and is important for organization of the septin ring at the emerging bud (Cvrckova et al., 1995; Versele and Thorner, 2004). Active *ScCdc42* initiates polarization of the actin cytoskeleton towards the incipient bud site by localizing the formin *ScBni1* (Evangelista et al., 1997; Fujiwara et al., 1998). *ScBni1* nucleates actin filaments and protects their growing barbed ends from capping proteins that would terminate

growth. (Evangelista et al., 2002; Sagot et al., 2002; Zigmond et al., 2003; Moseley et al., 2004). It interacts with *ScSpa2*, *ScBud6*, and *ScPea2*, three proteins that were copurified in a protein complex termed the polarisome (Sheu et al., 1998). *ScSpa2* is important for localization of *ScBni1* while *ScBud6* was reported to stimulate *in vitro* actin assembly (Evangelista et al., 1997; Moseley et al., 2004). Interestingly, *ScBni1* recruitment to the incipient bud site turned out not to directly depend on *ScCdc42* binding despite the *in vitro* capacity of *ScCdc42* to interact with the

Table 1: Polarity factors in *A. gossypii* and *S. cerevisiae*

<i>A. g.</i> polarity factor	Homolog(s) in <i>S. cerevisiae</i> *		<i>A. g.</i> ORF size * (aa)	Size(es) of homolog(s) in <i>S. cerevisiae</i> *		Identity to <i>S. c.</i> homolog(s)		<i>A. g.</i> deleti on**	Deletion of <i>S. c.</i> homologs**	
	1°	2°		1°	2°	1°	2°		1°	2°
<i>AgBEM1</i> (<i>AEL241W</i>)	<i>ScBEM1</i> (<i>YBR200W</i>)		549	551		57 %		lethal	viable	
<i>AgBNI1</i> (<i>AFR669W</i>)	<i>ScBNI1</i> (<i>YNL271C</i>)		1918	1953		50 %		lethal	viable	
<i>AgBOI1/2</i> (<i>AGL293C</i>)	<i>ScBOI2</i> (<i>YER114C</i>)	<i>ScBOI1</i> (<i>YBL085W</i>)	984	1040	980	45 %	44 %	viable	viable	viable
									doubleΔ: viable	
<i>AgBUD6</i> (<i>AFR495C</i>)	<i>ScBUD6</i> (<i>YLR319C</i>)		702	788		51 %		viable	viable	
<i>AgCDC24</i> (<i>ADR388C</i>)	<i>ScCDC24</i> (<i>YAL041W</i>)		761	854		60 %		lethal	lethal	
<i>AgCDC42</i> (<i>AGL093W</i>)	<i>ScCDC42</i> (<i>YLR229C</i>)		191	191		94 %		lethal	lethal	
<i>AgCLA4</i> (<i>AEL205W</i>)	<i>ScCLA4</i> (<i>YNL298W</i>)	<i>ScSKM1</i> (<i>YOL113W</i>)	793	842	655	63 %	54 %	viable	viable	viable
									doubleΔ: viable	
<i>AgEXO70</i> (<i>AFR100W</i>)	<i>ScEXO70</i> (<i>YJL085W</i>)		614	623		51 %		lethal	lethal	
<i>AgGIC1/2</i> (<i>AAL047C</i>)	<i>ScGIC2</i> (<i>YDR309C</i>)	<i>ScGIC1</i> (<i>YHR061G</i>)	381	383	314	40 %	38 %	viable	viable	viable
									doubleΔ: viable	
<i>AgPEA2</i> (<i>AGR135C</i>)	<i>ScPEA2</i> (<i>YER149C</i>)		389	420		38 %		viable	viable	
<i>AgRHO1b</i> (<i>ABR183W</i>)	<i>ScRHO1</i> (<i>YPR165W</i>)		207	209		76 %		lethal	lethal	
<i>AgSEC3</i> (<i>ADR012C</i>)	<i>ScSEC3</i> (<i>YER008C</i>)		1319	1336		35 %		lethal	lethal	
<i>AgSEC4</i> (<i>AGL021W</i>)	<i>ScSEC4</i> (<i>YFL005W</i>)		212	215		85 %		lethal	lethal	
<i>AgSPA2</i> (<i>ADL022C</i>)	<i>ScSPA2</i> (<i>YLL021W</i>)	<i>ScSPH1</i> (<i>YLR313C</i>)	3392	1466	661	27 %	25 %	viable	viable	viable
									doubleΔ: viable	

* Data from AGD3 (<http://agd.vital-it.ch/index.html>).

**Data for yeast deletions are taken from SGD (<http://www.yeastgenome.org/>). Data for *A. gossypii* deletion phenotypes from Ayad-Durieux et al. 2000, Brachat S. unpublished, Cavicchioli D. unpublished, Galati V., unpublished, Knechtle et al, 2003, 2006 and unpublished, Schmitz et al. 2006, Wendland et al, 2001, and my own, unpublished results.

Rho-binding domain of *ScBni1* (Evangelista et al., 1997; Ozaki-Kuroda et al., 2001). Therefore, recruitment of *ScBni1* must happen through *ScCdc42* effectors. Two possible candidates are *ScGic1* and *ScGic2*. They both contain a CRIB domain and interact with *ScCdc42*, *ScGic2* was shown to recruit polarisome components and both *ScGic1* and *ScGic2* are involved in initial septin recruitment to the site of bud formation (Brown et al., 1997; Chen et al., 1997; Jaquenoud and Peter, 2000; Iwase et al., 2006). However, *ScGic2* is degraded after initiation of polar growth and strains that lack both *GIC* homologs are still able to bud, thus a parallel pathways must exist to localize *ScBni1* (Jaquenoud et al., 1998). Direct activation of *ScBni1* is mediated by the two Rho GTPases *ScRho3* and *ScRho4*, probably by disruption of an auto-inhibitory intramolecular interaction of *ScBni1* (Alberts, 2001; Dong et al., 2003). From the site of cell polarity establishment, actin cables emanate into the cell serving as tracks

for myosin-V dependent transport of vesicles and mRNA. Once the vesicles arrived at their destination, they fuse with the target membrane, a process that is mediated by the conserved, octameric exocyst protein complex. Deletion of any of the exocyst genes leads to accumulation of secretory vesicles and subsequent cell death (TerBush et al., 1996; Hazuka et al., 1997). Interestingly, the exocyst seems to be at the interface between cell polarity and secretion. *ScSec4*, a Rab GTPase that is active on post-Golgi vesicles, recruits the exocyst component *ScSec15* and triggers interactions between *ScSec15* and other exocyst components thereby assembling the exocyst complex (Salminen and Novick, 1987; Walch-Solimena et al., 1997; Guo et al., 1999). Various exocyst subunits contact components of the polarity machinery: *ScExo70* interacts with *ScRho3*, *ScSec3* with *ScCdc42* and *ScRho1* (see below). The interactions between small Rho GTPases and the exocyst are believed to allosterically regulate exocytosis (Finger et al., 1998; Adamo et al., 1999; Guo et al., 2001; Zhang et al., 2001; Roumanie et al., 2005). Furthermore, *ScSec15* interaction with *ScBem1* is important for *ScSec15* localization especially during early stages of bud growth (France et al., 2006). The small GTPase *ScRho1* plays a dual role in actin cytoskeleton control and cell wall synthesis. Like

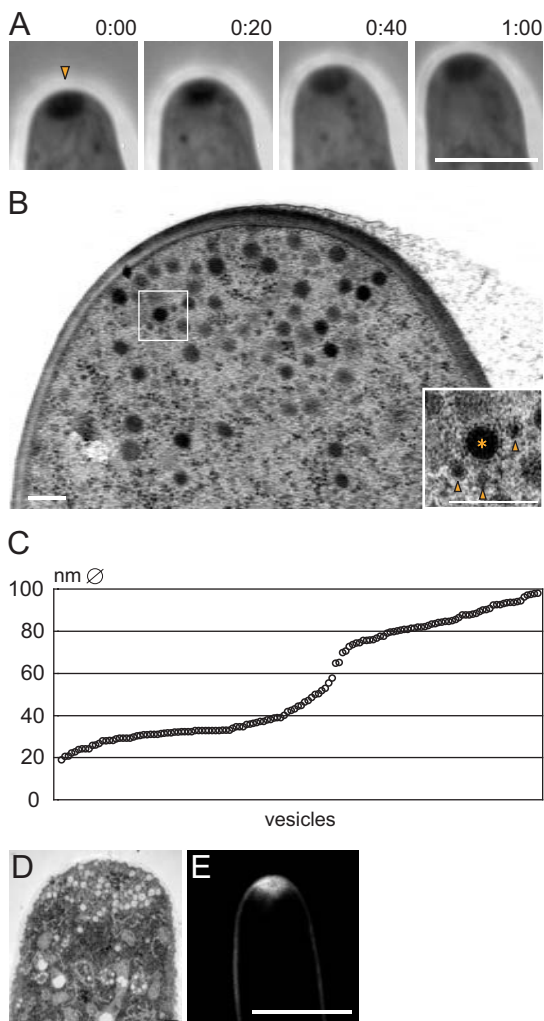


Fig. 2: Vesicles accumulate in the hyphal tip of *A. gossypii* hyphae. (A) Frames from a time-lapse movie of an *A. gossypii* hyphal tip. The time interval between the presented images is 20 s. A phase-dark apical structure is observed in the very apex of the tip (arrowhead). Mycelium from the border of a 2-3 days old colony was inoculated over night on glass slides that were coated with a thin layer of AFM containing 19 % gelatine. The hyphae were covered with a cover slide and allowed to recover for 1-2 hours prior to imaging. Scale bar = 5 μ m. (B) Transmission electron microscopy (TEM) micrograph of a thin section through the hyphal tip of a cryo-fixed *A. gossypii* mycelium. Vesicles are accumulated in the apex of the hyphal tip. The inset shows a higher magnification of the region enclosed by the rectangle in panel. The white arrowheads depict vesicles of different sizes. (C) The diameter of 140 tip-based vesicles was measured and plotted on the y-axis. The vesicle with the lowest diameter marks the left end of the x-axis, the vesicle with the biggest diameter the right end of the x-axis. Clearly, most vesicles had a diameter between 20 and 40 nm or between 70 and 100 nm as indicated by the small slope of the curve in these regions. (D) TEM of a chemically fixed hyphal tip displaying an apical vesicle cluster. Scalebars in B and D = 400 nm. (E) A hyphal tip stained with the live dye FM 4-64 displays a fluorescent, spherical-shaped area in the hyphal tip resembles the phase-dark mass observed by phase contrast microscopy. Mycelium from the border of a 2-4 days old colony was inoculated on a thin layer of AFM microscopy agar and incubated over night at room temperature. 2-4 μ l of 11 μ M FM 4-64 were pipetted to the sample, the mycelium was covered with a cover slide and allowed to recover for 10-15 minutes prior to microscopy. Scale bar = 5 μ m.

ScCdc42, it can interact and activate ScBni1 directly *in vitro*. However, ScRho1 was found to mainly regulate the actin cytoskeleton via its effector ScPkc1 (Kohno et al., 1996; Imamura et al., 1997; Dong et al., 2003). In contrast, cell wall synthesis is controlled by ScRho1 directly via interaction with the $\beta(1,3)$ -glucan synthase ScFks1 and also indirectly through an ScPkc1-dependent pathway (Drgonova et al., 1996; Qadota et al., 1996; Nonaka et al., 1995; Kamada et al., 1996). I analyzed the localization of *A. gossypii* proteins, which are orthologs of *S. cerevisiae* factors involved in secretion, control of the actin cytoskeleton and regulation of cell polarity. These *A. gossypii* proteins have previously been shown or are documented the first time in this PhD thesis to act similarly to their *S. cerevisiae* orthologs. I could locate these polarity factors to distinct regions in the tip where they may execute their function. Furthermore, I found that the locations in the hyphal tip strongly depend on growth speed and distinct zones are most pronounced in fast elongating hyphae. In slow hyphae, the localization of most polarity factors overlap at the tip cortex. We suggest that distinct zones in the hyphal tip fulfill different cellular functions for sustained polar growth and that these zones have speed-dependent, flexible locations.

Results

Vesicles accumulate in the hyphal tip of *A. gossypii*.

A prominent, phase-dense body was observed in the hyphal tip of *A. gossypii* if hyphae were grown in a medium that allows resolution of intracellular details by phase-contrast microscopy (figure 2A, movie S1). The body was roughly spherical ($1.2 \pm 0.1 \mu\text{m}$ in the direction of the hyphal axis and 1.9 ± 0.1 perpendicular to this axis, mean \pm S.E., $n = 25$) but slightly changed its morphology with time emphasising its dynamic nature. Furthermore, this body stayed in close association with the growing hyphal tip. Similar, tip based, phase-dense dynamic bodies were identified in several filamentous fungi where they were named “Spitzenkörper” or “apical body” (Girbardt, 1957, Lopez-Franco, 1996). The organization of the hyphal tip of *A. gossypii* was further characterized by transmission electron microscopy. Samples from the border of 2-3 days old *A. gossypii* mycelia were inoculated on thin dialysis membranes on AFM-agar plates, incubated over night, cryo-fixed and flat-embedded in resin. Virtually all of the hyphae processed for electron microscopy contained an accumulation of vesicles in the tip (figure 2B). Interestingly, 46 % of the vesicles had a diameter between 20 and 40 nm, 41 % a diameter between 70 and 100 nm, and only 13 % displayed an intermediate diameter between 40 and 70 nm indicating the presence of two main types of vesicles that differ in size ($n = 140$,

Table 2: Exocyst components in *A. gossypii*

<i>A. gossypii</i> exocyst	Homolog in <i>S. cerevisiae</i> *	<i>A. gossypii</i> ORF size (aa)	Size of homolog in <i>S. cerevisiae</i> (aa)	Identity to <i>S.c.</i> homolog	<i>A. gossypii</i> deletion**
<i>AgEXO70</i> (<i>AFR100W</i>)	<i>ScEXO70</i> (<i>YJL085W</i>)	615	623	51 %	lethal
<i>AgEXO84</i> (<i>ADL321W</i>)	<i>ScEXO84</i> (<i>YBR102C</i>)	698	753	56 %	lethal
<i>AgSEC10</i> (<i>AGL130C</i>)	<i>ScSEC10</i> (<i>YLR166C</i>)	832	871	48 %	no data
<i>AgSEC15</i> (<i>AFR252C</i>)	<i>ScSEC15</i> (<i>YGL233W</i>)	869	910	53 %	lethal
<i>AgSEC3</i> (<i>ADR012C</i>)	<i>ScSEC3</i> (<i>YER008C</i>)	1320	1336	35 %	lethal
<i>AgSEC5</i> (<i>AGL158C</i>)	<i>ScSEC5</i> (<i>YDR166C</i>)	860	971	51 %	lethal
<i>AgSEC6</i> (<i>ACL047W</i>)	<i>ScSEC6</i> (<i>YIL068C</i>)	793	805	54 %	lethal
<i>AgSEC8</i> (<i>ADL317C</i>)	<i>ScSEC8</i> (<i>YPR055W</i>)	977	1065	40 %	lethal

* Only one syntenic homolog of every *A. gossypii* exocyst component is present in *S. cerevisiae*

** Galati V., unpublished results

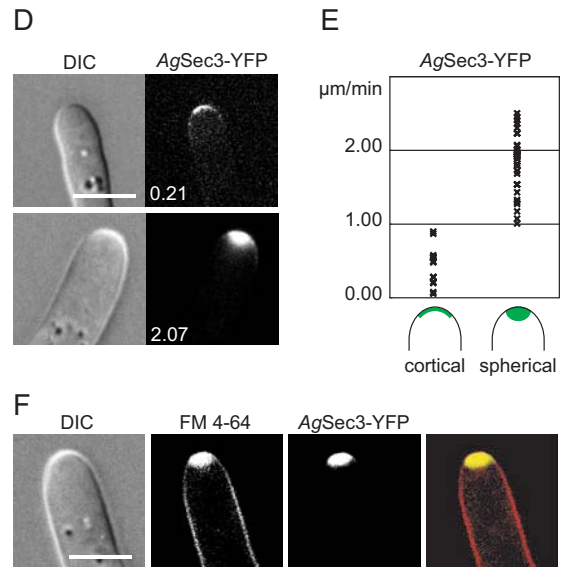
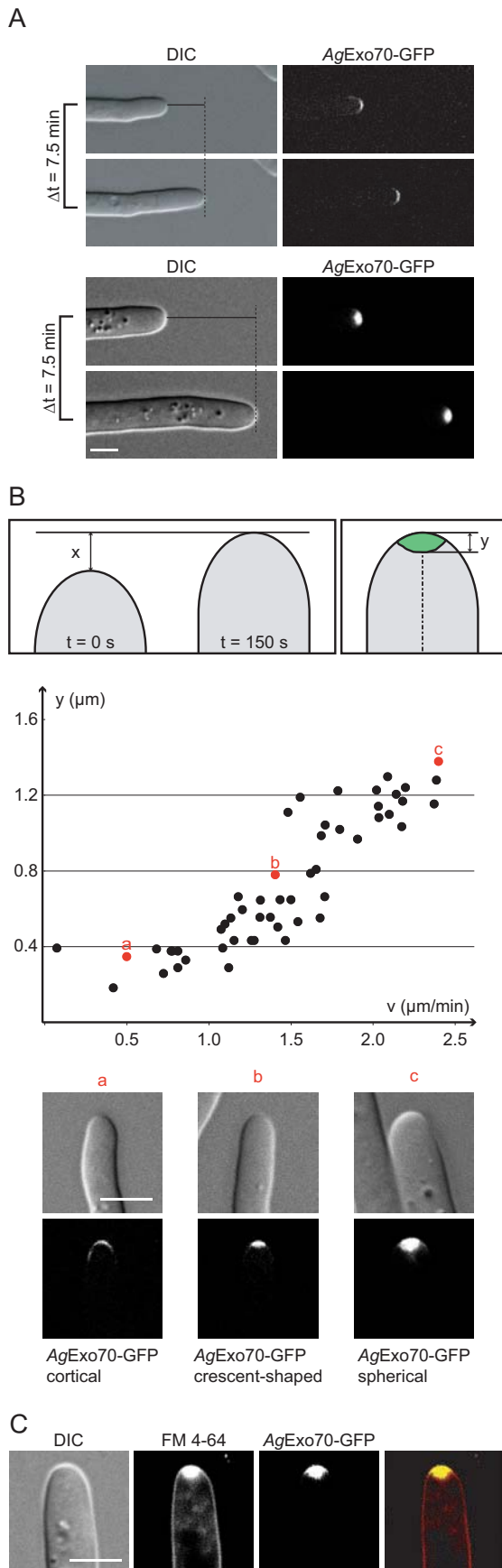


Fig. 3: The localization of Exo70-GFP is growth-speed dependent. (A) Frames of time-lapse movies of *AgEXO70-GFP*. Mycelium from the border of a two to three days old colony was inoculated on a time lapse slide on AFM agar and incubated over night at room temperature prior to microscopy. The two panels are taken from two independent movies; two picture series are shown per panel with a delay of 7.5 minutes between the two series. (B) Assessment of growth speed and *AgExo70-GFP* localization. The first sketch illustrates the hyphal elongation rate measurement: Two DIC-pictures of a hyphae were taken with a delay of $\Delta t = 2.5$ minutes. Growth speed v was estimated by measuring the distance x and dividing it by Δt . Immediately after acquisition of the second DIC image, a GFP image stack was acquired and the extension of the *AgExo70-GFP* signal along the hyphal axis (y) was measured as shown in the second sketch. The *AgExo70-GFP* extension (y) was plotted against growth speed. Images are shown for the data-points labelled in red below the localization/speed plot. (C) FM 4-64 staining of an *AgEXO70-GFP* expressing hypha. *AgExo70-GFP* (green in the overlay) displays a localization pattern that overlaps with the FM 4-64 stained apical body (red in the overlay). (D) Example of a slow and a fast *AgSEC3-YFP* expressing hypha, the white number on the YFP micrograph indicates the growth speed of the hypha shown on the picture in $\mu\text{m}/\text{min}$. (E) Simplified speed/localization plot, the growth speed is given in $\mu\text{m}/\text{min}$ on the y axis, the two different localization patterns are shown on the x-axis. Growth speed of hyphae that displayed *AgSec3-YFP* at the cortex are shown on the left half of the plot, growth speeds of hyphae that showed a spherical *AgSec3-YFP* localization pattern are shown on the right half of the plot. Hyphae that displayed a crescent-like *AgSec3-YFP* localisation were not considered for this measurement. (F) *AgSec3-YFP* (green in the overlay) displays a localization pattern that overlaps with the FM 4-64 stained apical body (red in the overlay). Scale bars = 5 μm .

figure 2C). A correlation between the location of the apical body seen by light microscopy and the area covered with vesicles observed by electron microscopy was not possible since the resin-embedded hypha appeared uniformly black when imaged by phase-contrast microscopy. The findings from cryo-fixed hyphae were confirmed with chemically fixed samples. Cryo-fixation leads to very good conservation of structural details but requires moving of the samples and might induce stress-related artifacts as for example dispersal of the apical body. Chemical fixation on the other hand leads to poor structural preservation but the mycelia are undisturbed until they come in contact with the fixative. Apical body-like structures could be identified by phase-contrast in embedded, chemically fixed samples. As already seen for the cryo-fixed samples, those hyphae displayed tightly clustered vesicles in the tip (figure 2D).

Previous reports show that the apical body can be stained with the lipophilic styryl dye FM 4-64 that fluoresces if inserted in lipid bilayers (Fischer-Parton et al., 2000; Dijksterhuis, 2003). Strong FM 4-64 fluorescence was observed at the plasma membrane and in a spherical zone in the hyphal tip if *A. gossypii* was incubated for 10 to 15 minutes with 11 μM FM 4-64 (Fig 2E). We will refer to the FM 4-64 stained spherical volume as the apical body during this work because the dimensions of the FM 4-64 stained fluorescent area were with $1.2 \pm 0.1 \mu\text{m}$ along the hyphal axis and 1.9 ± 0.1 perpendicular to the hyphal axis (mean \pm S.E., $n = 27$) indistinguishable to the dimensions observed for the apical body visualized by phase-contrast microscopy (see above).

The localization pattern of the exocyst component *AgExo70*-GFP depends on growth speed.

It is generally believed that a substantial part of the vesicles that are clustered in the apical body are exocytic vesicles that transport membrane lipids, cell wall proteins, cell wall synthesizing enzymes and other cargo to the hyphal tip (Bartnicki-Garcia and Lippman, 1969; Gooday, 1971). In *S. cerevisiae* it was shown that a conserved protein complex, the exocyst, mediates tethering of vesicles to sites of growth (TerBush et al., 1996; Guo et al., 1999; Roumanie et al., 2005). Homologs to all eight exocyst-encoding *S. cerevisiae* genes could be identified in the *A. gossypii* genome. Deletions of the seven exocyst genes analyzed so far were lethal (table 2, Galati V. unpublished results). To investigate the site of vesicle incorporation, GFP

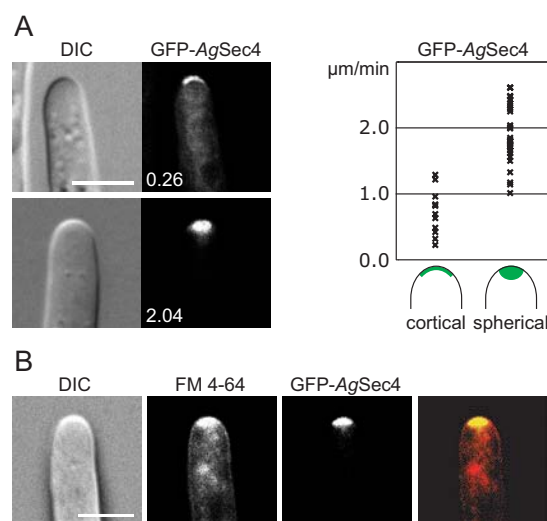


Fig. 4: Growth-speed dependent localization of GFP-*AgSec4*. (A) Growth speed and GFP-*AgSec4* localization. The first panel shows examples of hyphae that display GFP-*AgSec4* at the cortex or in a spherical localization pattern. The white numbers indicate growth speed in $\mu\text{m}/\text{min}$. The right panel shows a speed/localization plot. The speed is given in $\mu\text{m}/\text{min}$ on the y-axis, the localization pattern on the x-axis. (B) GFP-*AgSec4* (green in the overlay) displays a localization pattern that overlaps with the FM 4-64 stained apical body (red in the overlay). Scale bars = 5 μm .

or YFP was fused to two exocyst components, *AgExo70* and *AgSec3* respectively. As expected, *AgExo70*-GFP and *AgSec3*-YFP localized to hyphal tips (figure 3A and 3D). Interestingly, we observed that *AgExo70*-GFP and *AgSec3*-YFP localized cortically in some hyphae while they displayed a spherical localization pattern in others. Time-lapse movies indicated that the extension rate was lower for hyphae with *AgExo70*-GFP at the cortex than for hyphae with *AgExo70*-GFP in a spherical conformation (figure 3A, movie S2). This observation suggested that *AgExo70*-GFP localization is dependent on growth speed. We tested this hypothesis by quantifying growth speed and *AgExo70*-GFP localization as shown in the first panel of figure 3B. Hyphal elongation rate was determined by taking two DIC pictures at a time interval of 2.5 minutes. *AgExo70*-GFP dimensions were measured in direction parallel to the hyphal axis and compared to the hyphal growth speed. Indeed, a correlation between growth speed and *AgExo70*-GFP localization was observed in such that the dimension of *AgExo70*-GFP along the hyphal axis increased gradually with increasing hyphal elongation rate (figure 3B). At growth speeds less than 1.0 $\mu\text{m}/\text{min}$, the layer of *AgExo70*-GFP was not thicker than 0.4 μm , which corresponds to the cortical *AgExo70*-GFP

localization (figure 3Ba). In contrary, hyphae elongating with more than 1.5 $\mu\text{m}/\text{min}$ displayed *AgExo70-GFP* in spherical localization patterns with *AgExo70-GFP* extending about 1.2 μm along the hyphal axis (figure 3Bc). The shape of the *AgExo70-GFP* localization in fast growing hyphae resembled the shape of an apical body. Staining of *AgExo70-GFP* expressing hyphae with FM 4-64 indeed revealed overlapping *AgExo70-GFP* and FM 4-64 fluorescence (figure 3C). No apical body was observed if *AgExo70-GFP* was cortical suggesting that formation of the apical body and the *AgExo70-GFP* stained sphere depends on growth speed. Hyphae that displayed an apical body had an average growth speed of $1.6 \pm 0.4 \mu\text{m}/\text{min}$ (mean \pm S.D., $n = 28$) while no apical body was observed in 97 % of elongating with less than 1.0 $\mu\text{m}/\text{min}$ ($n = 33$) confirming this hypothesis. These results agree with prior findings that the presence of an apical body strongly depends on hyphal growth (Girbardt, 1957; Lopez-Franco, 1996).

The growth-speed dependent localization change of *AgExo70-GFP* is likely to represent the behaviour of the entire exocyst since the YFP-fusion to the second investigated exocyst component, *AgSec3*, displayed the same, speed-dependent localization: slow hyphae displayed *AgSec3-YFP* at the cortex, fast hyphae had *AgSec3* in a spherical configuration, which conferred to the apical body (figure 3D, E and F).

In budding yeast, the small Rab-family GTPase *ScSec4* was shown to be active on post-Golgi vesicles where it recruits the exocyst. A GFP-fusion to *A. gossypii* *Sec4* was used as a marker for exocytic vesicles in a earlier study (Schmitz et

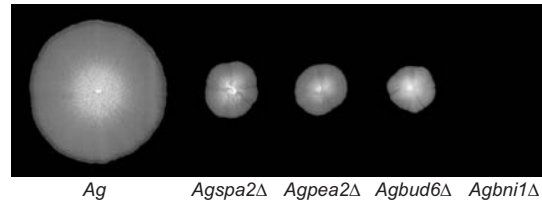


Fig. 6: Radial growth of *Agspa2Δ*, *Agpea2Δ*, *Agbud6Δ* and *Agbni1Δ*. Mycelium of the reference strain (*Ag*), *Agspa2Δ*, *Agpea2Δ* and *Agbud6Δ* was inoculated in the middle of an AFM agar plate, spores of a heterokaryonic *Agbni1Δ* strain were spotted in the middle of a selective AFM agar plate and incubated for 6 days at 30 °C.

al., 2006). Here I show that GFP-*AgSec4* localized to the apical body in a growth speed-dependent manner. In a pattern that was very similar to the exocyst, slow growing hyphae displayed GFP-*AgSec4* at cortex while fast extending tips displayed it in a spherical localization pattern (figure 4).

The polarisome components *AgSpa2* and *AgPea2* and the formin *AgBni1* localize in a spherical localization pattern dependent on growth-speed while *AgBud6* is restricted to the cortex.

Vesicles are transported to the elongating hyphal tip of *A. gossypii* on actin cables, which are nucleated by the tip-located formin *AgBni1* (Schmitz et al., 2006). However, the C-terminal GFP-fusion to *AgBni1* published by Schmitz et al. (2006) showed a very weak GFP signal and this strain displayed a reduced radial growth speed. Apical bodies were not observed in this strain, either due to a direct effect of the GFP-tag on apical body assembly or as consequence of the decreased hyphal growth

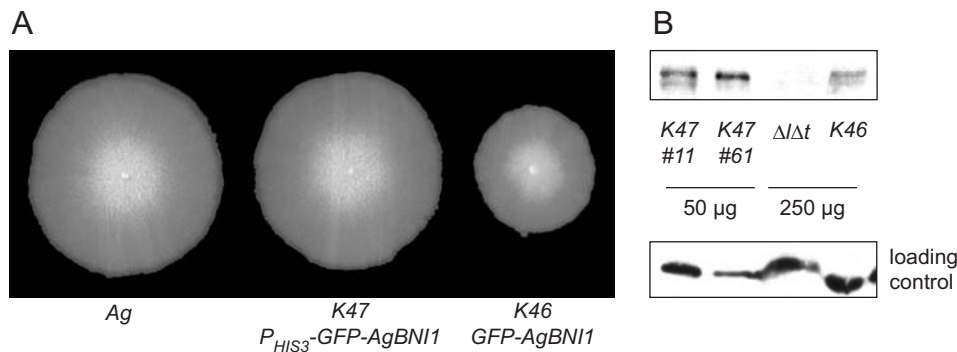


Fig. 5: Amino-terminal GFP-fusions to *AgBni1*. (A) Radial growth assay. The reference strain (*Ag*), *K47* (P_{ScHIS3} -*GFP-AgBNI1*) and *K46* (*GFP-AgBNI1*) were inoculated in the middle of an AFM agar plate and incubated for 6 days at 30 °C. Note that the diameter of the reference strain and *K47* are identical. (B) Estimations of GFP-*AgBni1*-levels. The two *K47* isolates express *GFP-AgBNI1* under the control of the *ScHIS3* promoter, *K46* carries exactly the same construct but under the control of the native *AgBNI1* promoter. 50 μg *K47* protein and 250 μg of reference strain and *K46* protein were separated by SDS-PAGE and probed with antiGFP on a nitrocellulose membrane. GFP-*AgBni1* ran at about 250 kDa (predicted molecular weight: 240 kDa). A crossreacting band of an approximate size of 105 kDa was used as a loading control.

speed. Strains that expressed an amino-terminal GFP-fusion to *AgBni1* displayed apical bodies. The signal intensity of GFP-*AgBni1* could be enhanced by expression of the GFP-fusion under the control of the *ScHIS3* promoter. Overexpression led to a five- to tenfold increase in protein levels compared to expression of the same construct from the endogenous promoter and to reconstitution of wild-type radial growth speed (figure 5). In budding yeast, *ScBni1* was reported to interact with three proteins, *ScSpa2*, *ScPea2*, and *ScBud6*, which were co-purified as a 12S protein complex termed the polarisome (Sheu et al., 1998). Deletions of the genes encoding the putative polarisome components *AgSpa2*, *AgPea2*, and *AgBud6* all

showed a decrease in radial growth speed while deletion of *AgBni1* was lethal (figure 6, Knechtle et al., 2003; Schmitz et al., 2006). In slow growing hyphae, GFP- and YFP fusions to the polarisome components and to *AgBni1* localized to the tip cortex. In fast hyphae, GFP-*AgBni1*, *AgSpa2*-GFP and *AgPea2*-YFP were observed in a spherical localization similar to the pattern observed for *AgExo70*-GFP. Strikingly, GFP-*AgBud6* was restricted to the cortex independent of growth speed (figure 7A and 7B). FM 4-64 staining revealed that the spherical localization patterns of *AgSpa2*-GFP, *AgPea2*-YFP and GFP-*AgBni1* overlapped with the apical body while GFP-*AgBud6* was at the cortex also if an apical body was present (figure 7C).

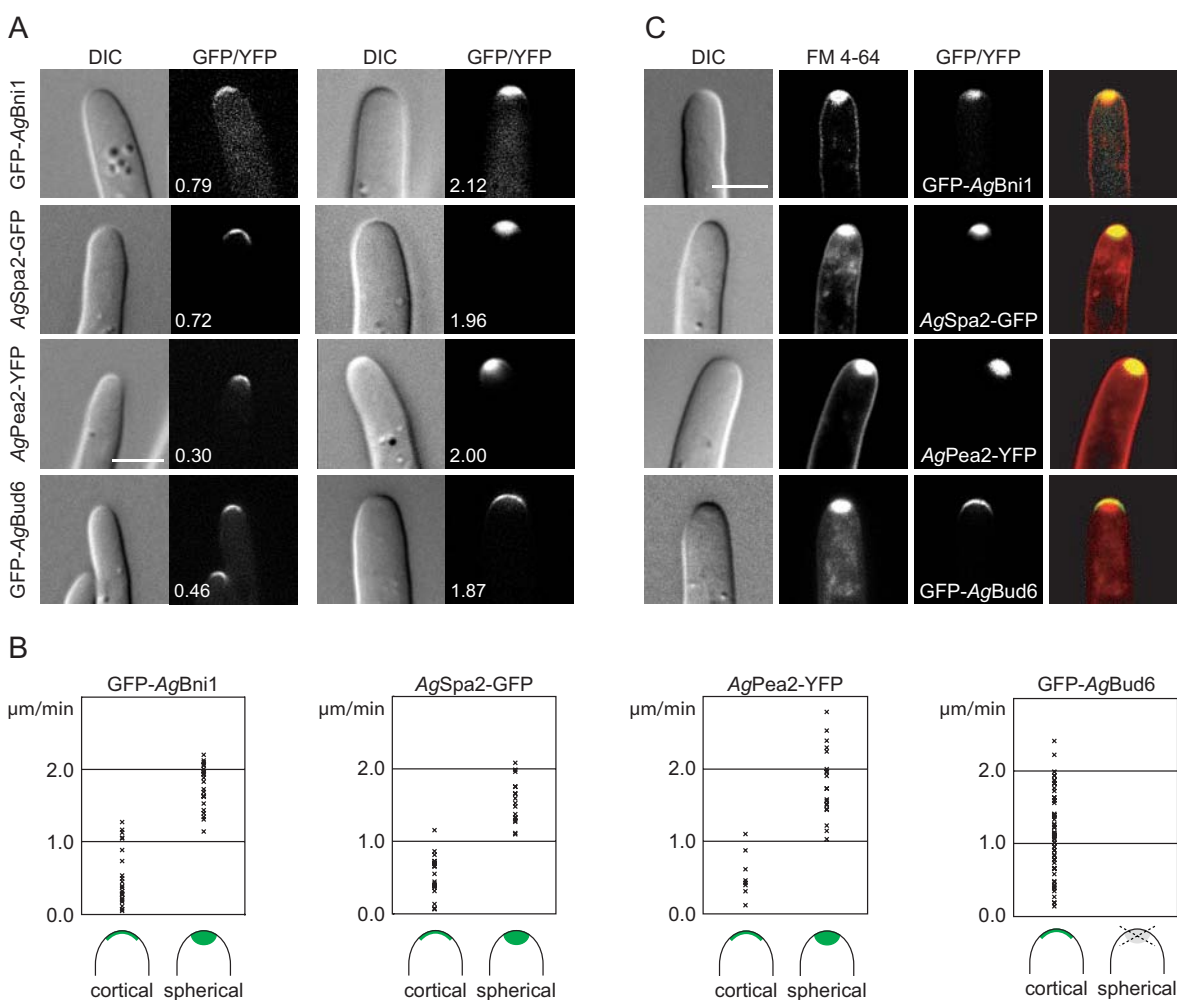


Figure 7: The putative polarisome components *AgSpa2* and *AgPea2* and to the formin *AgBni1* localize in an apical body-like localization pattern dependent on growth speed while another putative polarisome-component, *AgBud6*, is restricted to the cortex. (A) Examples of GFP-*AgBni1*, *AgSpa2*-GFP and *AgPea2*-YFP localizing cortically or spherically. The white numbers indicate the growth speeds of the given hyphae in $\mu\text{m}/\text{min}$. (B) Correlation between localization and growth speed of the formin *AgBni1* and the putative polarisome components. Growth speed is plotted on the y-axis in $\mu\text{m}/\text{min}$, the localization of the GFP- or YFP tagged protein is marked on the x-axis. Note that a spherical GFP-*AgBud6* localization pattern was not observed. (C) GFP-*AgBni1*, *AgSpa2*-GFP, *AgPea2*-YFP and GFP-*AgBud6* are shown in green in the overlay, the FM 4-64 staining in red. Scale bars = 5 μm .

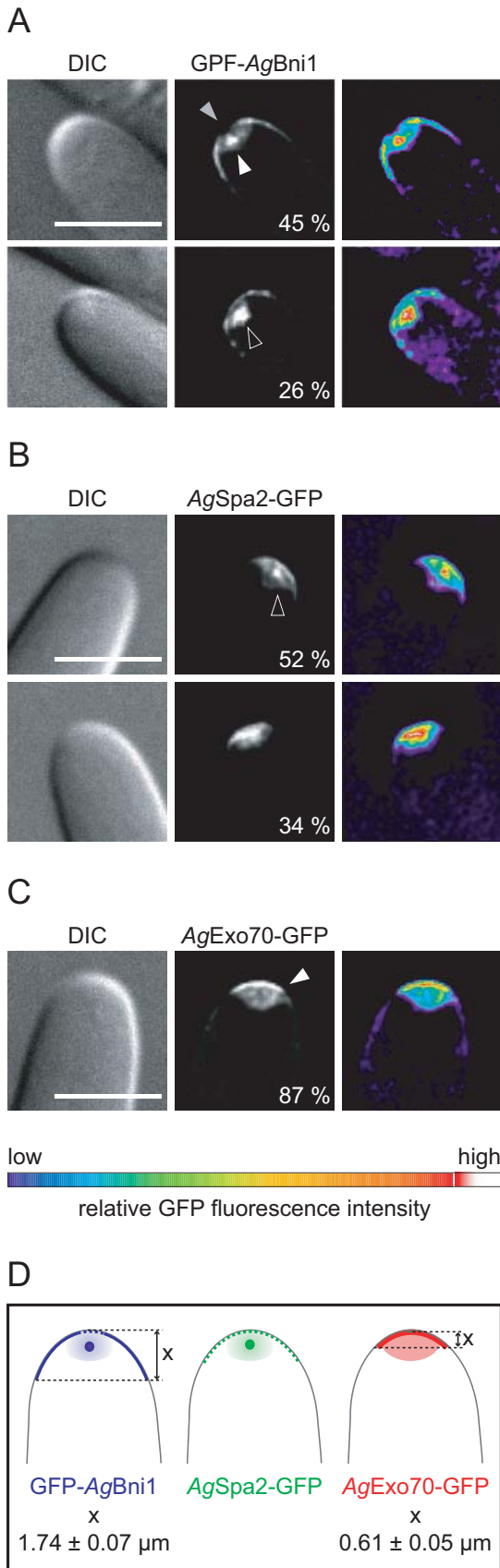


Fig. 8: GFP-AgBni1 and AgSpa2-GFP are enriched in a core-like structure in the apical body while AgExo70-GFP is enriched at the cortex. (A) Stacks of GFP-AgBni1 expressing hypha that grew faster than 1.50 $\mu\text{m}/\text{min}$ were submitted to blind deconvolution, maximum projections of central planes are shown. White or red color in the false color image indicates high GFP-fluorescence, blue and purple low GFP fluorescence. 45 % of all hyphae displayed a localization pattern similar to the one shown in the first image row displaying a discrete GFP-AgBni1 core (white arrowhead). 26 % of the fast hypha displayed a less condensed core region (second image row, black arrowhead, $n = 31$). A reduced GFP-AgBni1 fluorescence at the most apical part of the hyphal cortex was observed in 58 % of all cases (grey arrowhead). (B) 52 % of fast ($v > 1.50 \mu\text{m}/\text{min}$) AgSpa2-GFP hyphae displayed an enrichment of AgSpa2-GFP in a core region in the apical body (first image row, black arrowhead). 34 % of the hyphae displayed an amorphous apical body localization of AgSpa2-GFP without a distinct enrichment (second image row, $n = 29$). (C) AgExo70-GFP was diffusely localized in the region of the apical body but enriched at the cortex in 87 % of fast growing hyphae ($n = 31$). For all three strains, mycelium from the border of a 2-3 days old colony was inoculated on time-lapse slides (glass slides with an AFM agar-filled cavity) and incubated over night at room temperature. Only prior to microscopy the samples were covered with a cover slide, growth speed of the hyphae was assessed before an image stack of the GFP fluorescence was acquired. (D) Model of the localization pattern of GFP-AgBni1, AgSpa2-GFP and AgExo70-GFP. GFP-AgBni1 covered the apical $1.74 \pm 0.07 \mu\text{m}$ of the cortex, AgExo70-GFP the $0.61 \pm 0.05 \mu\text{m}$. Scale bars = 5 μm .

GFP-AgBud6 did not localize to the apical body upon fast growth. However, one could not exclude a subtle localization difference between slow and fast growing GFP-AgBUD6 hyphae. In order to systematically define growth speeds that are characteristic for slow and fast hyphae, the data sets obtained by the speed/localization measurements of AgExo70-GFP, AgSec3-YFP, GFP-AgSec4, AgSpa2-GFP, AgPea2-YFP and GFP-AgBni1 were compared. Two growth speeds were defined based on the localization pattern of the tagged polarity factor. If hyphal elongation rates were slower than $0.83 \mu\text{m}/\text{min}$, 85 % of all hyphae displayed the given, tagged polarity factor at the cortex ($n = 85$). If growth speed exceeded $1.50 \mu\text{m}/\text{min}$, 88 % of all hyphae showed a spherical localization of the given polarity factor ($n = 120$). Based on these findings, hyphae were defined as slow if they extended with less than $0.83 \mu\text{m}/\text{min}$ and as fast if they grew quicker than $1.50 \mu\text{m}/\text{min}$. However, no GFP-AgBud6 localization difference could be seen if fast and slow hyphae were compared.

In conclusion, GFP- or YFP fusions to the two polarisome components *AgSpa2* and *AgPea2* and the formin *AgBni1* localize in a spherical manner depending on hyphal extension rate while GFP-*AgBud6* stayed at the cortex of the hyphal tip regardless of growth speed.

***AgBni1* and *AgSpa2* form a core-like structure in the apical body while *AgExo70* is enriched at the cortex.**

In figure 7C, GFP-*AgBni1* does not seem to occupy the entire FM 4-64 stained apical body like *AgExo70*-GFP or *AgSpa2*-GFP does. This observation suggested that the formin *AgBni1*, the exocyst and the polarisome component *AgSpa2* might display different localizations in the apical body. To test this speculation, we analyzed 30 hyphae by taking image stacks of 32 planes that were submitted to blind deconvolution. Only measurements of hyphae that elongated faster than $1.50 \mu\text{m}/\text{min}$ were taken into account in view of the fact that slower growth speeds had a profound effect on the localization pattern of different polarity factors. We found that the localization patterns of GFP-*AgBni1*, *AgSpa2*-GFP and *AgExo70*-GFP differed from each other slightly. In 45 % of all cases, GFP-*AgBni1* was enriched in an amorphous core structure in the apical dome. In 26 % of the hyphae, a less defined, central region of GFP-*AgBni1* could be distinguished that was separated from a cortical pool of GFP-*AgBni1* (figure 8 A). The remaining 29 % of hyphae either displayed a homogenous GFP-*AgBni1* distribution in the apical body or a large, fuzzy core region of

GFP-*AgBni1* that appeared connected to the cortex (not shown, $n = 31$). Cortex-associated GFP-*AgBni1* reached 1.74 ± 0.07 (mean \pm S.E., $n = 31$) towards distal parts of the hypha measured parallel to the hyphal axis. Furthermore, the cortical GFP-*AgBni1* pool did not cover the cortex evenly: a zone of reduced fluorescence at the very tip proximal to the core-region was observed in 58 % of all cases. Interestingly, *AgSpa2*-GFP was enriched in a core-like region similar to GFP-*AgBni1* in 52 % of all tips though the fluorescence intensity difference between the core-structure and the surrounding *AgSpa2*-GFP cloud was less pronounced than for GFP-*AgBni1*. In 34 % of the hyphae, *AgSpa2* displayed an amorphous, apical body-like localization without a discernible core region ($n = 29$) (figure 8B). Strikingly, *AgExo70*-GFP was not observed in a core-like structure but was distributed almost evenly in the apical body with an enrichment of *AgExo70*-GFP at the cortex (87 %, $n = 31$, figure 8C). The cortical region where *AgExo70*-GFP was strongly enriched was limited to the very apical part of the hyphae and reached only $0.61 \pm 0.05 \mu\text{m}$ measured parallel to the hyphal axis, which is barely larger than the region where the *AgExo70*-GFP marked apical body touches the cortex (mean \pm S.E., $n = 31$). To summarize, we show that GFP-*AgBni1* and *AgSpa2*-GFP are enriched towards the center of the apical body while *AgExo70*-GFP is not (figure 8D).

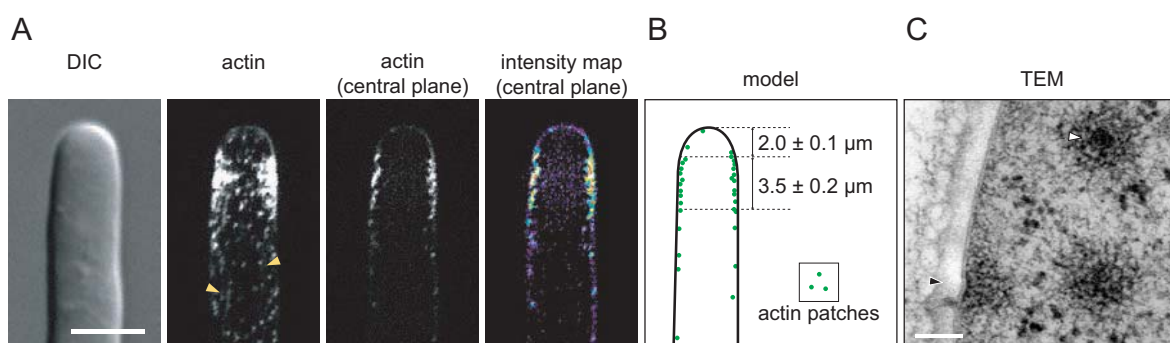


Fig. 9: Actin patches are enriched at the hyphal cortex directly adjacent to the tip. (A) Alexa488-phalloidin staining of fast-growing hyphal tips. The second image displays a maximal projection of an image stack that spans through the entire hyphal tip. Actin cables are depicted by arrowheads. The more prominent, dot-like actin structures are actin patches. The third panel displays a single plane of the entire image stack and the fourth panel a false color representation thereof. Blue and purple colors indicate low, white and red color high relative fluorescence intensity. The reference strain was grown from spores on AFM agar plates for 20 hours at 30°C , fixed and processed for staining as described in material and methods. Scale bar = $5 \mu\text{m}$. (B) Distribution of cortical actin patches. A hyphal outline is indicated in black, the orange dots represent actin patches. Patches were sparse in the first $2 \mu\text{m}$ of the hyphal tip and enriched at the cortex behind this region. (C) Transmission electron micrograph from a cortical region. The cell wall is situated on the left side of the image. The picture shows three electron-dense, filamentous structures. A vesicle is visible in the center of one of these structures (white arrowhead). Filamentous matter is associated with an invagination of the plasma membrane (black arrowhead). Scale bar = $0.1 \mu\text{m}$.

The actin cytoskeleton in fast growing hyphal tips.

Since *AgBni1* is a nucleator of actin cables, it is reasonable to assume that the pool of *AgBni1* in the core region nucleates actin filaments that emanate into the cytoplasm. Contrary to most filamentous fungi, the actin cytoskeleton of *A. gossypii* can be conveniently stained with phalloidin-coupled fluorescent dyes. As described in detail by Knechtle et al., 2003, the *A. gossypii* actin cytoskeleton consists of three main components: long actin cables, cortical actin patches and contractile actin rings at sites of septation. However, actin staining in this and other publications was done with young mycelia that had not reached high growth speeds. Thus, actin-organizations specific to fast growing hyphae are not well described up to now. Spores were spread on AFM agar plates and incubated at 30 °C for 20 hours to obtain fast growing hyphae. The mycelia were fixed by directly pouring the fixative onto the agar plates and processed for actin staining. Unfortunately, no actin cables were visible in the apex, eventually because the background fluorescence is too high in this region (figure 9A). Interestingly, the actin patches were not clustered at the hyphal tip like it was described for young hyphae (Ayad-Durieux et al., 2000; Knechtle et al., 2003). Instead, they were accumulated cortically adjacent to the hyphal tip. The apical zone where

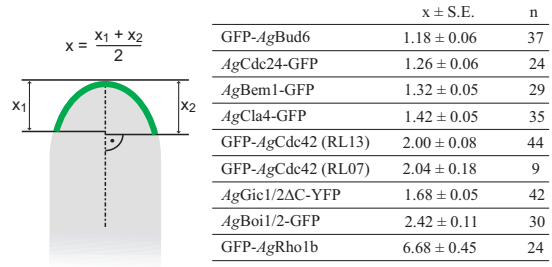


Table 3: Localization of cortex-associated polarity factors. The dimensions of the cortex region occupied by GFP-fusion proteins were estimated by measuring the distances x_1 and x_2 as indicated on the sketch. A schematic hyphal tip is shown, the dotted line represents the hyphal axis and the part of the cortex labelled in green symbolizes the localization of a GFP-fusion protein. For every cortical factor, the parameters x_1 and x_2 were determined for 25 to 50 hyphae that displayed an apical body. One value x was determined per hypha with x being $(x_1 + x_2)/2$ the average of x over all measurements is given in the table.

patches were sparse measured $2.0 \pm 0.1 \mu\text{m}$, the zone where cortical patches were strongly enriched $3.5 \pm 0.2 \mu\text{m}$ (mean ± S.E., $n = 16$, figure 9B). Actin patches are generally regarded as sites of endocytosis (Huckaba et al., 2004; Jonsdottir and Li, 2004). Indeed, by electron microscopy we were able to detect small vesicles or plasma membrane invaginations that were surrounded by a filamentous, electron-dense matter (figure 9C). It is likely that these structures confer to actin patches that are observed by staining with phalloidin-

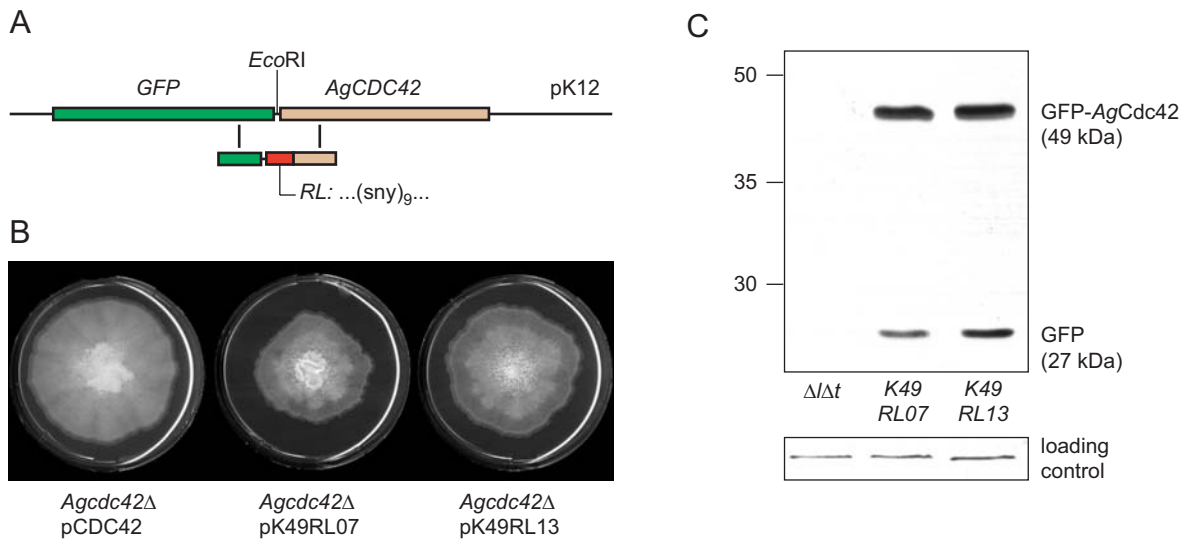


Figure 10: Construction of GFP-*AgCdc42*. (A) Scheme of random-linker insertion between *GFP* and *AgCDC42*. The random linker contains nine (SNY) repeats where S stands for the nucleotides C or G, N for any nucleotide and Y for T or C (IUB Code). (B) Growth of a homokaryonic *Agcdc42Δ* strain that was complemented with either pCDC42 containing *AgCDC42*, pK49RL07 or pK49RL13, which contain GFP-*AgCDC42* fusions with the random linkers RL07 and RL13. Mycelium was inoculated on AFM agar plates and incubated for 8 days at 30 °C. (C) GFP-RL07 and GFP-RL13 on a western blot. 100 μg protein were separated by SDS-PAGE and probed with antiGFP on a nitrocellulose membrane. A GFP-*AgCDC42* band and a band whose size corresponds to GFP are observed. Single GFP-bands were never observed for other GFP- or YFP fusion proteins analyzed by western blotting. A crossreacting 105 kDa band that was always present on western blots probed with antiGFP from Roche was used as a loading control.

coupled dyes in *A. gossypii* since similar “coated vesicles” in budding yeast were shown to contain actin (Mulholland et al., 1994).

***AgCdc42* and its effectors are enriched at the hyphal cortex and show a speed-dependent localization.**

It is known that both the exocyst and the formin *ScBni1* can be activated by the small GTPase *ScCdc42* (Zhang et al., 2001, Evangelista et al., 1997). GTP-bound *ScCdc42*, its GEF *ScCdc24* and the adaptor-protein *ScBem1* supposedly work together in a positive feedback loop to establish a site of polarity. The PAK kinase *ScCla4* is recruited by activated *AgCdc42* and is thought

to be responsible for disruption of the positive feedback loop after bud emergence by inducing an inhibitory phosphorylation of *ScCdc24*. *Cdc42* was identified as a key regulator of cell polarity in *A. gossypii* as well. Deletion of *AgCDC42* leads to uniformly round cells (Wendland and Philippsen, 2001). Furthermore, *AgCdc42* binds to and most probably activates *AgBni1* when it is in its GTP bound, active state (Wendland and Philippsen, 2001; Schmitz et al., 2006). Localization of *AgCdc42* proved to be difficult. In order to create a functional *GFP-AgCDC42* construct, random linker sequences were inserted between *GFP* and *AgCDC42* (figure 10A). The resulting constructs were transformed into yeast strain *DLY3067* that

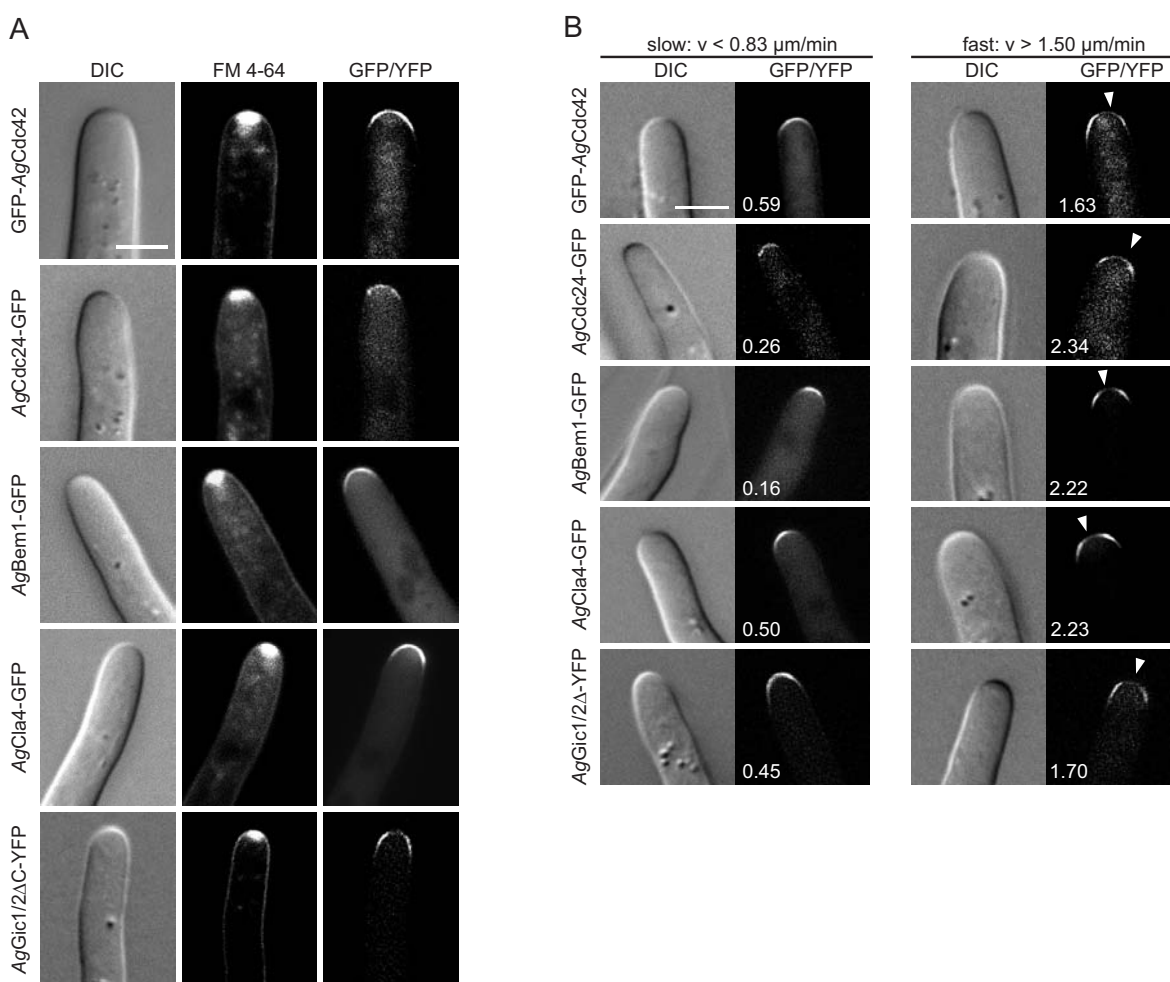


Fig. 11: Putative *AgCdc42* effectors and the *AgCdc42* GEF *AgCdc24* localize to the cortex and show growth speed-dependent reduction of fluorescence at the most apical part of the hyphal tip. (A) GFP-*AgCdc42*, *AgCdc24*-GFP, *AgBem1*-GFP, *AgCla4*-GFP and *AgGic1/2ΔC*-YFP in FM 4-64 stained hyphae. The GFP-labelled polarity factors localize to the cortex also in the presence of a FM 4-64 stained apical body. (B) Growth speed dependent localization of the strains shown under A. Slow (left column, $v < 0.83 \mu\text{m}/\text{min}$) and fast hyphae (right column, $v > 1.5 \mu\text{m}/\text{min}$) were compared. The white number indicates the growth speed of the example hyphae. Slow growing hyphae of *AgCdc24*-GFP, *AgBem1*-GFP and *AgCla4*-GFP and GFP-*AgCdc42* never showed a zone of reduced fluorescence at the very apical part of the hyphal tip while such a zone was observed in 20 – 60 % of fast growing hyphae (arrowheads). Scale bars = 5 μm .

expresses *ScCDC42* under control of the *ScGAL1* promoter. The transformants were selected for the ability to grow on glucose, a condition that represses expression of the endogenous *ScCDC42*. Plasmids that were isolated from these strains were able to complement a homokaryotic *A. gossypii* *cdc42Δ* strain (figure 10B). However, proteolytic cleavage of the linker sequence between GFP and *AgCdc42* was detected in a western blot (figure 10C). It is thus possible that actually only the cleaved *AgCdc42* molecules are active while GFP-*AgCdc42* might not be entirely functional and its localization pattern might not reflect the distribution of untagged *AgCdc42*.

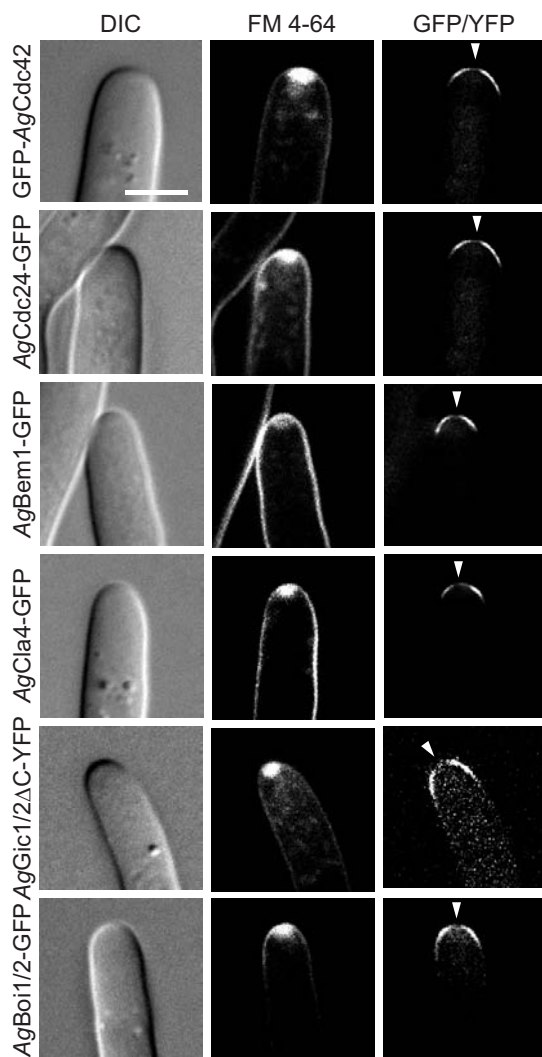


Fig. 12: Reduction of fluorescence intensity at the most apical part of the hyphal tip in FM 4-64 stained hyphae. GFP-*AgCdc42*, *AgCdc24*-GFP, *AgBem1*-GFP, *AgCla4*-GFP, *AgGic1/2ΔC*-YFP and *AgBoi1/2*-GFP in FM 4-64 stained hyphae. The labelled polarity factors display a zone of reduced fluorescence at the hyphal tip (arrowhead). Scale bar = 5 μ m.

GFP-*AgCdc42* localized to the cortex of hyphal tips in all hyphae, also if an apical body was present (figure 11A). *AgCdc24*, the presumably only *AgCdc42* GEF, and the adaptor protein *AgBem1* were investigated because their localization pattern supposedly reflect the zones where the GDP/GTP exchange of *AgCdc42* takes place in analogy to results from yeast. Both *AgCdc24*-GFP and *AgBem1*-GFP were found to localize at the most apical part of the cortex. An apical body-like, spherical localization was not observed (figure 11A). The zones of *AgCdc24* and *AgBem1* localization were quantified by measuring the dimensions of the cortical GFP-signals parallel to the hyphal axis (table 3). Since we showed for the exocyst and the polarisome that protein localization depends on growth speed, we only assessed hyphae that displayed an apical body and thus grew efficiently. The extensions were almost identical for *AgCdc24*-GFP ($1.26 \pm 0.06 \mu\text{m}$) and *AgBem1*-GFP ($1.32 \pm 0.05 \mu\text{m}$, mean \pm S.E., $n = 24$ and $n = 29$ respectively). Also the PAK protein kinase *AgCla4* localized to the cortex of the hyphal tip. The *AgCla4*-GFP signal reached $1.42 \pm 0.05 \mu\text{m}$ along the cortex (mean \pm S.E., $n = 35$) thus occupying the same part of the cortex as *AgCdc24*-GFP and *AgBem1*-GFP. Interestingly, the GFP-*AgCdc42* signal reached with $2.04 \pm 0.08 \mu\text{m}$ (mean \pm S.E., $n = 44$) further along the hyphal cortex than both *AgCdc24*-GFP and *AgBem1*-GFP. Thus, a zone that is enriched in GFP-*AgCdc42* but that lacks the GEF *AgCdc24*, the scaffold protein *AgBem1* and *AgCla4* is observed. CRIB domains, like the one present in *AgCla4*, bind to GTP-bound *Cdc42* or *Rac* (Burbelo et al., 1995), thus it might be possible that GTP-bound *AgCdc42* is restricted to the site where *AgCla4* is observed. To test this hypothesis, we made a construct analogous to

Table 4: Zone of reduced fluorescence in the hyphal tip of fast-growing hyphae.

Strain	% reduced apical GFP fluorescence*	n
GFP- <i>AgCdc42</i>	31%	16
<i>AgCdc24</i> -GFP	47%	19
<i>AgBem1</i> -GFP	40%	25
<i>AgCla4</i> -GFP	25%	20
<i>AgGic1ΔC</i> -YFP	63%	19
<i>AgBoi1</i> -GFP	23%	22
GFP- <i>AgBud6</i>	0%	17

* % fast growing hyphae ($v > 1.50 \mu\text{m}/\text{min}$) that display a reduced GFP-intensity at the very apical part of the hyphal tip (See figures 11B and 13B)

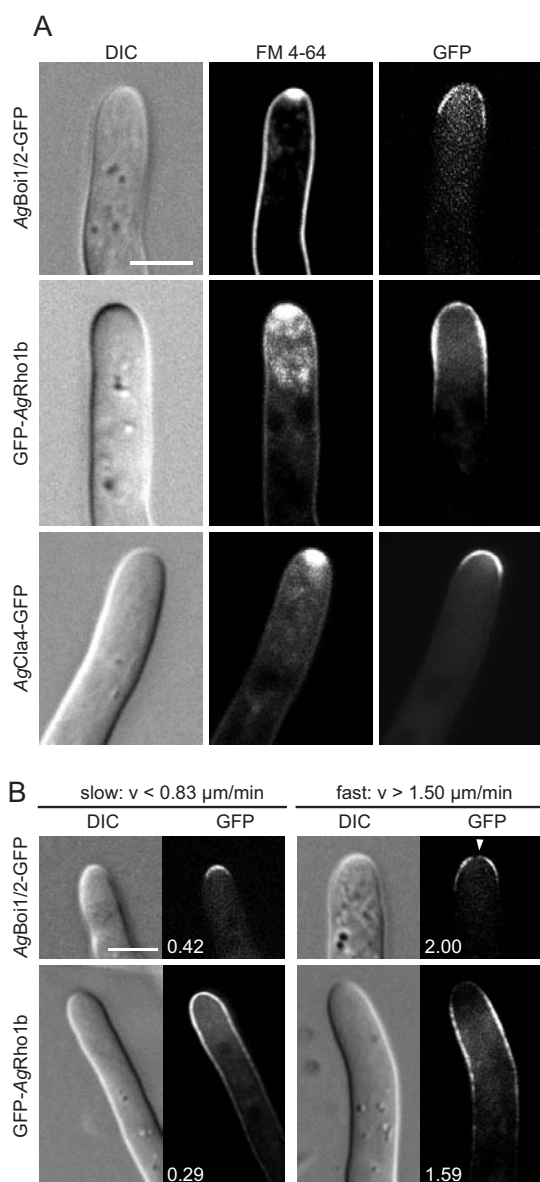


Figure 13: GFP-fusions to *AgBoi1/2* and *AgRho1b* localize to different parts of the hyphal cortex dependent on growth speed. (A) *AgBoi1*-GFP and GFP-*AgRho1b* in hyphae that display a FM 4-64 stained apical body. *AgBoi1*-GFP and GFP-*AgRho1b* cover a larger portion of the apical cortex than *AgCla4* that is shown as a reference. (B) Growth speed dependent localization of *AgBoi1/2*-GFP and GFP-*AgRho1b*. Differences in localization were observed between slow (left column, $v < 0.83 \mu\text{m}/\text{min}$) and fast hyphae (right column, $v > 1.5 \mu\text{m}/\text{min}$). *AgBoi1/2*-GFP localized to the entire apical cortex in 15 % of slow growing hyphae ($n = 13$) and in 82 % of fast growing hyphae ($n = 22$). A reduction of *AgBoi1/2*-GFP fluorescence was observed at the very apical part of fast growing tips (arrowhead) in 23 % of all cases ($n = 22$). *AgGFP-Rho1b* covered the tip of slow growing hyphae evenly (93 %, $n = 15$). Fast GFP-*AgRHO1b* expressing hyphae displayed reduced GFP-*AgRho1b* at the very tip (100 %, $n = 24$). Scale bars = 5 μm .

the one described by Ozbudak et al. (2005), who used a carboxy-terminally truncated version of the CRIB domain protein *ScGic2* fused to GFP to detect activated *ScCdc42* in budding yeast. *AgGic1/2* Δ C-YFP, the C-terminally truncated, YFP-tagged version of *AgGic1/2* we used as a probe, was fully functional as shown in part III of this thesis. Interestingly, *AgGic1/2*-YFP covered a region that was larger than the one occupied by *AgCla4*-GFP. The *AgGic1/2* Δ C-YFP signal reached $1.68 \pm 0.06 \mu\text{m}$ (mean \pm S.E., $n = 42$) towards distal parts of the hyphae along the cortex. In summary, *AgCdc24*-GFP, *AgBem1*-GFP and *AgCla4*-GFP localize to the same part of hyphae, which we termed central apical cortex. Both *AgGic1/2*-YFP and GFP-*AgCdc42* covered a slightly larger region than the other factors (table 3).

We further tested whether the localization of these basic cell polarity factors is influenced by growth speed. All the factors described in this paragraph displayed a very similar growth speed dependence of their localization pattern: the GFP-signal covered the hyphal tip cortex evenly in 100 % of the slow growing hyphae while a reduction of GFP-intensity was observed at the very apical part 20 – 60 % of fast growing hyphae (figure 11B, table 4). A reduction in fluorescence intensity at the very apex was observed also in the hyphae that contained an FM 4-64 stained apical body, which indicates fast growth (figure 12). Importantly, not all factors that localized to the cortex of hyphal tips displayed such a speed-dependent apical reduction of GFP-fluorescence. GFP-*AgBud6* covered the tip cortex evenly in 100 % of fast hyphae and also in 100 % of hyphae that possessed an apical body ($n = 17$ and $n = 37$ respectively).

***AgBoi1/2* and *AgRho1b* define the entire and the extended apical cortex in fast growing hyphal tips.**

A recent report identified *AgBoi1/2* as an important cell polarity factor in *A. gossypii*. Hyphal tips in an *Agboi1/2* Δ strain frequently expand in a non-polar way but can switch back to normal, hyphal growth (Knechtle et al., 2006). *AgBoi1/2*-GFP localized cortically in hyphae that contained an apical body (figure 13A). The *AgBoi1/2*-GFP signal was not restricted to the central apical cortex and extended $2.42 \pm 0.14 \mu\text{m}$ (mean \pm S. D., $n = 30$) towards distal regions of the hypha defining the entire apical cortex (table 3). In slow growing hyphae, *AgBoi1/2*-GFP localized to the entire apical cortex in only 15 % of all cases

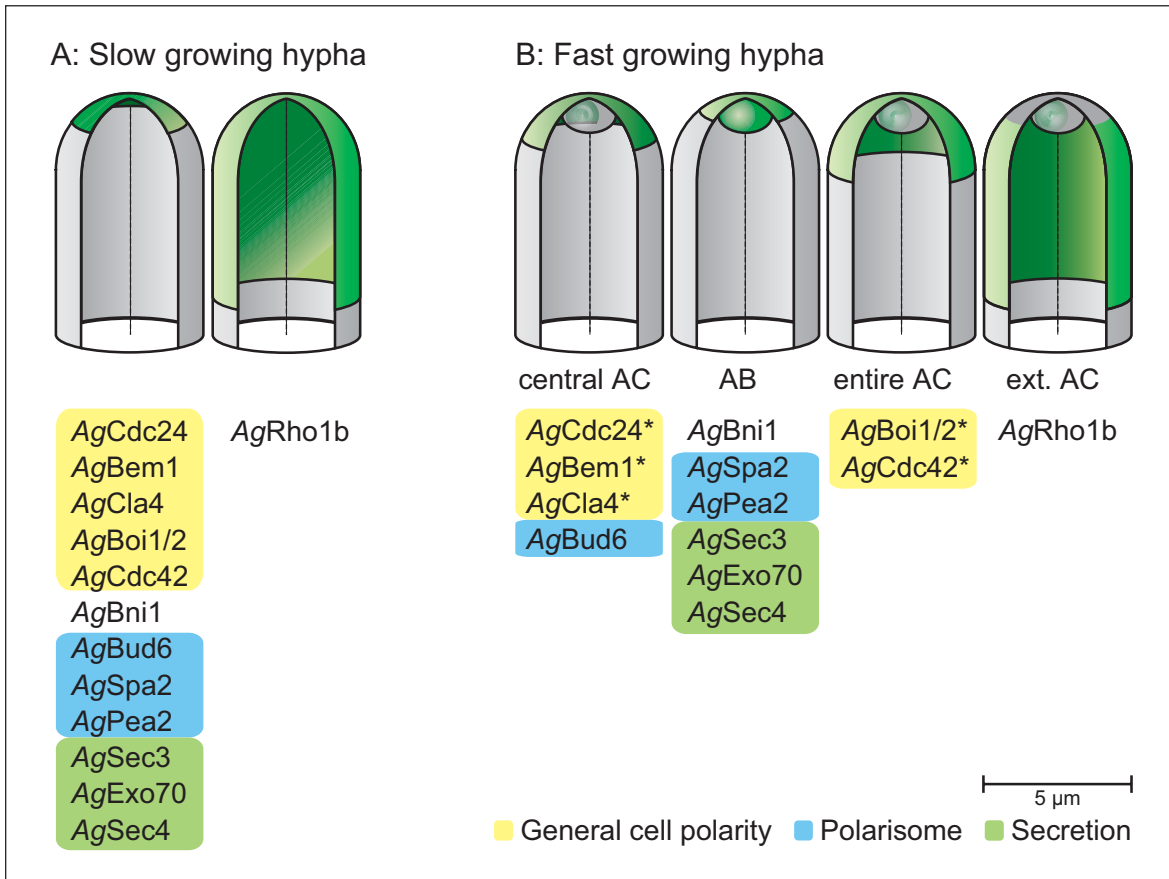


Fig. 14: Localization of factors involved in polar growth in fast and slow growing hyphae. (A) Localization patterns of polar growth factors in slow growing hyphae. The two basic localization modes observed in slow hyphae are represented by two hyphal models. The dotted line denotes the hyphal axis; the regions shaded in green represent the localizations of the factors listed below the models. The polarity factors were assigned to three functional groups (adapted from Irazoqui and Lew, 2004) and shaded in the respective color (yellow for the general cell polarity group, blue for the polarisome, green for the secretion group). (B) Localization patterns of the same factor as shown under (A) in fast growing hyphae. The apical body, which is not seen in slow hyphae, is symbolized by an ellipsoid in the hyphal tip. The central apical cortex (cAC) is defined by the guanosine exchange factor *AgCdc24*, *AgBem1*, the PAK (p21-activated kinase) family member *AgCla4*, the putative polarisome component *AgBud6* also localizes to this region. The other two putative polarisome components of *A. gossypii*, *AgSpa2* and *AgPea2*, were found in the apical body along with the formin *AgBni1*. Proteins involved in polarized secretion like the exocyst components *AgExo70* and *AgSec3* and the small Rab-GTPase *AgSec4* were also enriched in the apical body. *AgBoi1* defines the entire apical cortex (entire AC), *AgCdc42* also localizes to this region. The small Rho-GTPase *AgRho1b* defines the extended apical cortex (ext. AC), maximal enrichment of *AgRho1b* is seen at the hyphal cortex behind the tip in a “corset”-like distribution. GFP-fusions to the polarity factors denoted with a star displayed reduced fluorescence intensity in 20 to 50 % of fast growing hyphae.

(n = 13) while in fast hyphae it was found at the entire apical cortex in 82 % (n = 22). Additionally, a zone of reduced fluorescence at the very apex of the tip could be observed in 23 % of fast hyphae similar to what was found for *AgCdc42* interacting proteins (figure 13B). *AgRho1b* is a small Rho-type GTP-binding protein with functions in cell wall synthesis and actin organization. A cortical pool of GFP-*AgRho1b* colocalizes with aniline-blue stained $\beta(1,3)$ -glucane (part III, figure 2), and the yeast homolog *ScRho1* was shown to be a catalytical subunit of the $\beta(1,3)$ glucan-synthase (Drgonova et al., 1996; Qadota et al., 1996). Therefore, GFP-*AgRho1b* localization is likely

to represent areas of $\beta(1,3)$ glucan synthesis. In contrast to the other polarity factors described here, GFP-*AgRho1b* was found to localize weakly at the cortex in the entire hyphae (not shown). Nevertheless it was strongly enriched in hyphal tips. GFP-*AgRho1b* did not localize in an apical body-like manner but the tip-enriched pool of GFP-*AgRho1b* extended with $6.68 \pm 0.45 \mu\text{m}$ (mean \pm S.D., n = 24) further along the cortex than any of the other factors discussed so far (table 3). GFP-*AgRho1b* localization in slow hyphae was different from localizations of all the factors described so far. It was not restricted to a small area in the hyphal tip but occupied a big part of

the hyphal cortex. At fast hyphal elongation rates, GFP-*AgRho1b* intensity was maximal at the cortex below the hyphal tip in all cases forming a “corset” around the tip region ($n = 24$) while such a localization pattern was only observed in 7 % of slow growing hyphae ($n = 15$, figure 13B).

Discussion

Growth-speed dependent localization of polarity factors into distinct zones in the *A. gossypii* hyphal tip.

A. gossypii hyphal tips are constantly polarized and, when maximally growing, produce enormous amounts of new surface in a very narrow zone of growth that is restricted to the hyphal tip. We found that factors involved in polar growth are organized into different zones in the tip of fast growing hyphae (figure 14). Such a differentiation of discrete polarity factor zones is not seen in slow hyphae. This demonstrates that localization of polarity factors changes with growth speed! The hyphal tip is a very dynamic environment, vesicles constantly fuse with the membrane leading to enlargement of the hyphal surface. Consequently, an imaginary probe that is attached to the cortex of the very tip of a fast growing hypha at time point zero is located already more than 1.5 μm behind the tip one minute later. Yet we observe zones of defined sizes where polarity factors are enriched. Therefore, the factors are either organized into a scaffold that is kept at its position or, alternatively, the zones we observe result from steady states between enrichment and dispersal of polarity factors. Importantly, the mechanism of localization may differ between the factors. Furthermore, proteins can be enriched at sites of activity but also at sites where they are stored. Keeping these points in mind, we will discuss here the polarity factors assayed during this study following a hierarchical pattern from cell polarity over polarization of the actin cytoskeleton to polarized secretion and cell wall synthesis.

The *AgCdc42* module and the PAK family kinase *AgCla4* localize together to the central apical cortex.

In hyphae that display an apical body, *AgCdc24* localized together with *AgBem1* and *AgCla4* to a region we termed the central apical cortex, which covers the first 1.3 μm of the tip (figure 14). GFP-*AgCdc42* was also present at the central apical cortex though covering a larger region than *AgCdc24*,

AgBem1 and *AgCla4*. However, GFP-*AgCdc42* was not proven to be fully functional and thus the GFP localization eventually does not faithfully reflect the localization pattern of untagged *AgCdc42*. The small GTPase *AgCdc42* was identified as a key regulator of cell polarity (Wendland and Philippsen, 2001). Also, deletion of *AgBEM1* is lethal though the terminal phenotype is heterogeneous: about 35 % of the *Agbem1* Δ cells lacked cell polarity completely and displayed a phenotype similar to *Agcdc42* Δ , another 35 % of the spores were able to form a first, misshaped germ tube while the rest of the germlings either formed potato-shaped cells or small, aberrant mycelia with swollen hyphae after 17 h (Daniele Cavichioli, unpublished data). In budding yeast it was found that GTP-bound *ScCdc42*, *ScBem1* and *ScCdc24* act in a positive feedback loop that ensures polarization of the cell even in the absence of cortical landmarks (Bose et al., 2001; Butty et al., 2002; Irazoqui et al., 2003; Wedlich-Soldner et al., 2004). The localization of *AgCdc24* and *AgBem1* to the same region of the hyphal tip together with the observation that *Agbem1* Δ has a severe polarity defect suggests that a positive feedback loop between *AgCdc42*, *AgCdc24*, and *AgBem1* might be conserved that guarantees maintenance of cell polarity. The central apical cortex is likely to represent the site where the GDP to GTP exchange of *AgCdc42* happens due to the presence of its only GEF *AgCdc24*. To test whether *AgCdc42* activity is restricted to this region, we analyzed the localization of *AgGic1/2* Δ C-YFP. Interestingly, *AgGIC1/2* Δ C-YFP covered a slightly bigger area than *AgCdc24*, *AgBem1*, and *AgCla4*. It is thus possible that an unknown mechanism shuts off *AgCdc42* activation and *AgBem1*, *AgCdc24* and *AgCla4* diffuse away while GTP-bound *AgCdc42* stays at the cortex until the *AgCdc42* bound GTP is hydrolyzed. Findings from yeast imply that the protein kinase *AgCla4* might negatively regulate *AgCdc42* by shutting of the positive feedback loop since some reports from budding yeast attribute to *ScCla4* a role in negative regulation of *ScCdc42* by mediating phosphorylation of *ScCdc24*, which triggers its dissociation from *ScBem1* after bud emergence (Gulli et al., 2000; Bose et al., 2001). Other targets of *ScCla4* are the septins *ScCdc3* (Wu et al., 1997; Versele and Thorner, 2004). If *AgCla4* would indeed negatively regulate *AgCdc42* activity in *A. gossypii*, one would expect an overactivation of *AgCdc42* in an *Agcla4* Δ strain. Therefore, deletion of *AgCLA4* and overactivation of *AgCdc42* either by abolishment of *AgCdc42* GTPase activity or by

deletion of GAPs should share some phenotypes. However, both an *Agcdc42^{Q61H}* strain that carries a GTPase deficient *AgCDC42* allele (figure 15A) and a deletion of the putative *AgCdc42* GAP *AgBem2* resulted in swollen, misshaped hyphae indicating polarity defects (Wendland and Philippsen, 2000) while hyphal morphogenesis was close to normal in *Agcla4Δ* (Ayad-Durieux et al., 2000). Therefore, rather than directly interfering with cell polarity, *AgCla4* might coordinate cell polarity with downstream events as for example septin assembly since septation was severely reduced in an *Agcla4Δ* strain (Ayad-Durieux et al., 2000).

The polarity maintenance factor *AgBoi1/2* occupies the entire apical cortex.

The cortical localization of *AgBoi1/2* extended with 2.4 μm further along the hyphal cortex than those of *AgCdc42* associated factors. We defined this zone as the entire apical cortex. *AgBoi1/2* is important for prevention of non-polar growth in *A. gossypii* since an *Agboi1/2Δ* strain displayed spherical enlargement at hyphal tips with concomitant

depolarization of the actin cytoskeleton (Knechtle et al., 2006).

An area of reduced fluorescence was observed at the most apical part of fast growing hyphae in strains expressing fluorescently tagged *AgBoi1/2* or *AgCdc42*-associated factors. We do not have evidence that the polarity factors described so far are localized to the plasma membrane through the secretory pathway since they were not observed in the apical body, which mainly consists of vesicles. Therefore, they may localize from the cytoplasm to the cortex of the hyphal tip by an unknown mechanism. Indeed, it was shown in yeast that *ScCdc42*, *ScCdc24*, *ScBem1*, and the CRIB-domain containing probe based on *ScGic1* are highly dynamic and show very quick exchange between the plasma membrane and the cytoplasm with half times between one and seven seconds (Wedlich-Soldner et al., 2004; Ozbudak et al., 2005). As quick as polarity factor recruitment might be, a small zone where the vesicles just fused with the plasma membrane might show a reduced density of polarity factors. This region would be visible as a zone of reduced fluorescence similar as observed it in fast growing hyphae. In slow hyphae, presumably fewer vesicles fuse with the hyphal tip and localization of polarity factors is fast enough to occupy the newly formed cortical surface.

The apical body of *A. gossypii*.

The polarity factors described so far were associated with different parts of the hyphal cortex. Nevertheless, proteins involved in regulation of the actin cytoskeleton or polarized exocytosis were found to localize to a vesicle based, dynamic structure in fast growing hyphae called the Spitzenkörper or apical body. The apical body was described more than 50 year ago for *Polystictus versicolor* and is present in most filamentous fungi examined so far (Girbardt, 1957; Grove and Bracker, 1970; Lopez-Franco, 1996).

Transmission electron microscopy of *A. gossypii* hyphae revealed that two main vesicle populations that differ in size are accumulated in the hyphal tip, which is in agreement with findings from other filamentous fungi. The smaller vesicles, which measured between 20 and 40 nm in *A. gossypii*, were previously named microvesicles, the bigger vesicle population with diameters between 70 and 100 nm were characterized as apical vesicles or macrovesicles (Harris et al., 2005; Steinberg, 2007). At least a part of these vesicles most likely are secretory vesicles for two reasons. (i) Cell wall construction, which was shown to be

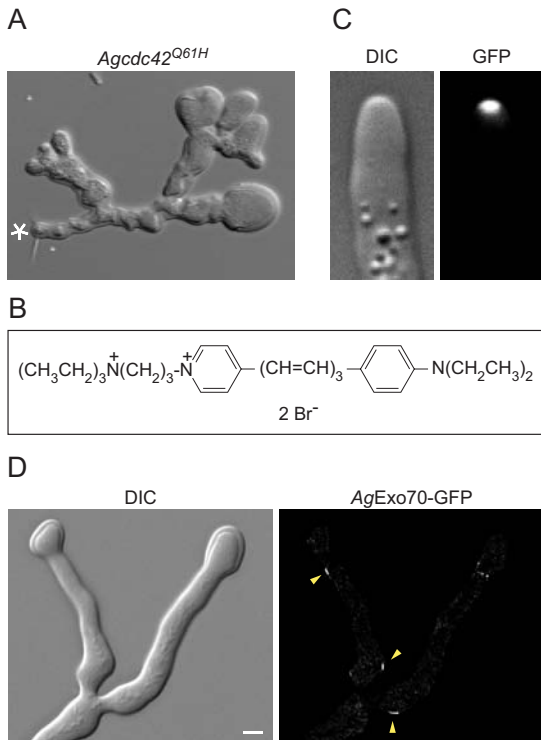


Figure 15 (A) Spores from a heterokaryotic *Agcdc42^{Q61H}* strain were inoculated for 24 h in AFM at 30 °C. The star denotes the position of the spore. (B) Chemical structure of the lipophilic styryl dye FM 4-64. (C) *AgMyo2*-GFP localizes in a spherical shape in the tip of *A. gossypii* hyphae (Hans-Peter Helfer, unpublished result). (D) *AgEXO70*-GFP was incubated with 200 μM latrunculin A. for 60 minutes. Scale bar = 5 μm.

maximal in hyphal tips (Bartnicki-Garcia and Lippman, 1969; Gooday, 1971), requires large amounts of cell wall proteins and enzymes that are synthesized, processed and often glycosylated in the endoplasmic reticulum and the Golgi apparatus. (ii) A GFP-fusion to *AgSec4*, a Rab-GTPase whose yeast ortholog is found on post-Golgi vesicles, accumulates in the apical body. Evidence for the presence of a second vesicle type besides secretory vesicles comes from the finding that FM 4-64 accumulates in the apical body. Due to its positively charged head group (figure 15B, FM 4-64 does not cross the membrane and can only be taken up into the cell via endocytosis. The observation that FM 4-64 fluorescence can be detected in the apical body before it is observed on extended intracellular membrane structures argues for a very quick resorting of endocytosed membranes back to the tip. For this reason, a certain part of the vesicles observed in the apical body may originate from recycling events (Fischer-Parton et al., 2000). It is tempting to speculate that the two types of vesicles that are distinguished by size represent vesicles of different origin.

An excellent study recently identified the myosin light chain *CaMlc1* as a component of the apical body in *Candida albicans* hyphae. Intriguingly, the same protein works at the cortex if *C. albicans* grows in the yeast form. These findings let the authors conclude that the apical body is a hypha-specific structure (Crampin et al., 2005). Our findings show that an apical body is not mandatory for hyphal morphogenesis *per se* but rather is required for an efficient organization of transport and secretion since we did not observe apical bodies or polarity factors localizing in an apical body-like shape in hyphae that grew slower than 0.83 $\mu\text{m}/\text{min}$. Importantly, this observation allows an alternative interpretation of findings that identified factors involved in apical body formation by mutagenesis. It is possible that mutations lead to a reduction of the maximal hyphal growth speed. Consequently, these mutations would impair formation of apical bodies indirectly by limiting hyphal extension rates rather than by disturbing apical body formation.

The polarisome components *AgSpa2* and *AgPea2* and the formin *AgBni1* localize to the apical body while a third polarisome component, *AgBud6*, is restricted to the cortex in fast growing hyphal tips.

In yeast, *ScSpa2*, *ScPea2*, and *ScBud6* were copurified in a 12S protein complex called the

polarisome (Sheu et al., 1998). It was found that all polarisome components interact with the formin *ScBni1* that nucleates actin filaments and serves as a processive capping protein for actin cables. In *A. gossypii*, the deletion strains *Agspa2 Δ* , *Agpea2 Δ* , and *Agbud6 Δ* all showed a similar reduction of radial growth speed while deletion of the formin *Agbni1 Δ* is lethal. These findings support the idea that *AgSpa2*, *AgPea2*, and *AgBud6* work together. In slow hyphae, all the polarisome components and *AgBni1* localized to the apical cortex. Strikingly, *AgBni1*, *AgSpa2*, and *AgPea2* localization expanded to the apical body in fast hyphae while *AgBud6* stayed in association with the hyphal cortex. This observation questions the idea of the polarisome being a tight protein complex. Alternatively, it is possible that *AgSpa2*, *AgPea2*, and *AgBud6* interact together and are active at the cortex while the differing localization patterns might reflect different modes of transport. Localization of *AgSpa2*, *AgPea2*, and *AgBni1* to the apical body could arise by transport of these factors on vesicles to the hyphal tip. To our knowledge, no association between secretory vesicles and a formin or a *Pea2* homolog is known. However, in yeast, *ScSpa2* interacts with the type V myosin *ScMyo2* and cosediments with secretory vesicles in a subcellular fractionation assay while *ScPea2* did not sediment during the same experiment (Shih et al., 2005). The hypothesis that *AgSpa2* localizes to the apical body in *A. gossypii* via vesicular, *AgMyo2*-mediated transport is supported by the finding that an *AgMyo2*-GFP fusion shows an apical body-like, spheroid distribution in the hyphal tip (figure 15C, Hans-Peter Helfer, unpublished data). Importantly, *AgBni1* was not uniformly distributed in the apical body. It was enriched in a central region of this structure and at the hyphal cortex. We were unable to detect actin cables with phalloidin-coupled dyes in the hyphal tip thus we do not know whether actin cables emanate from the cortical or the apical-body based pool of *AgBni1*. However, *AgBni1* is likely to nucleate actin cables at its cortical localization for two reasons. First, *AgCdc42*, which interacts with *AgBni1* (Schmitz et al., 2006), is active at the cortex. Small Rho-GTPases in their GTP-bound form stimulate actin assembly by disrupting an inhibitory, intramolecular interaction of formins (Alberts, 2001), a mechanism that is likely to be conserved in *A. gossypii* and yeast. Second, cortical *AgBud6* might stimulate *AgBni1*-mediated actin assembly since the *S. cerevisiae* *Bud6* binds to the carboxy-terminus of *ScBni1* and stimulates *ScBni1* activity *in vitro* (Moseley et al., 2004). *AgCdc42*

and *AgBud6* are unlikely to activate *AgBni1* in the central region of the apical body since they are only enriched at the cortex. However, *AgSpa2* might interact with *AgBni1* in the apical body because both proteins display a similar localization pattern with an enrichment in the centre of the apical body and because the Spa2-binding domain, which was identified in budding yeast *Bni1*, is conserved in *AgBni1* (Fujiwara et al., 1998; Schmitz et al., 2006). Nevertheless, activation of formins by Spa2 was not reported so far.

In yeast, the translation elongation factor EF1 α was shown to interact with the proline-rich FH1-domain of *ScBni1* and to possess actin bundling capacity (Demma et al., 1990; Yang et al., 1990; Umikawa et al., 1998). EF1 α , which is encoded by *ScTEF1* and *ScTEF2*, is associated with ribosomes during translation. Intriguingly, ribosomes are clustered in a central region in the apical body as can be seen on electron micrographs of the *A. gossypii* hyphal tip (see appendix, figure 5). It is currently not known whether the ribosomes and *AgBni1* colocalize in the apical body but it is tempting to speculate that translation in the apical body is linked to the actin cytoskeleton via *AgBni1*.

The localization of formins to the apical body is seen in other filamentous fungi as well. The formins SepA from *A. nidulans* and CaBni1 from *C. albicans* were found at this location (Sharpless and Harris, 2002; Crampin et al., 2005). Interestingly, the concept of a polarized, vesicle-based structure that is involved in actin organization seems to be conserved even beyond fungi. Fragile stonewort (*Chara globularis*), a green algae, forms tubular, gravity-sensing cells called rhizoids. Actin microfilaments emanate from a vesicle-based structure in the rhizoid tip that strongly resembles the apical body from filamentous fungi (Braun et al., 2004).

Interestingly, *AgBud6* was the only polarity factor described in this study that localized to the apical cortex evenly, also in fast growing hyphae. Contrary to *AgBoi1/2* and *AgCdc42*-associated factors, it did not exclude a zone at the very tip like. This observation suggests a different mechanism for *AgBud6* localization than for the other factors. It is possible that the speed of *AgBud6* localization from the cytoplasm to the cortex is very high thus *AgBud6* occupies newly formed plasma membrane virtually immediately. Alternatively, *AgBud6* forms a fixed, polarized protein scaffold that is kept at the tip during hyphal growth.

The exocyst localizes to the apical body in fast elongating hyphae.

The exocyst is an octameric complex that is conserved from yeast to mammals (Hazuka et al., 1997). It mediates polarized secretion in yeast but its exact mechanism of action is unknown. Presumably, it is assembled by the master regulator of post-Golgi trafficking, *ScSec4*, and activated by interaction with Rho type GTPases such as *ScCdc42*, *ScRho1* or *ScRho3*. All exocyst components, which are soluble cytoplasmatic proteins, are associated with secretory vesicles – with the exception of *ScSec3* (Guo et al., 1999; Boyd et al., 2004). It is thus believed that *ScSec3* serves as a cortical landmark that localizes to the site of exocytosis independently of the actin cytoskeleton, probably by recruitment through *ScCdc42*, which interacts with *ScSec3*. A partially assembled exocyst lacking *ScSec3* is thus thought to arrive on vesicles. Formation of the exocyst would be completed at the plasma membrane (Finger et al., 1998; Boyd et al., 2004). A new report challenges this view. Roumanie et al., 2005) found that *ScSec3* localization depends on actin-based transport and that interaction of the exocyst with *ScCdc42* (and *ScRho3*) functions in allosterically activating the exocyst but not in recruitment of these proteins. In *A. gossypii*, deletions of seven exocyst components analyzed so far were lethal. Interestingly, *AgExo70* and *AgSec3* localize to the apical body, which suggests localization of these exocyst components to vesicles that are abundant at this site. This observation is in disagreement with *AgSec3* being solely a cortical landmark and rather argues for the possibility that the entire exocyst complex can be assembled on vesicles in *A. gossypii*. One could imagine a recycling mechanism of exocyst proteins at the hyphal tip: the vesicles fuse with the plasma membrane and the exocyst components disassemble and diffuse away. The components then are re-recruited by *AgSec4* on vesicles in the apical body thus preparing these vesicles for fusion with the plasma membrane. Nevertheless, a non-actin based mechanism of exocyst localization is likely to exist. *A. gossypii* hyphae treated with latrunculin A displayed *AgExo70*-GFP enrichment at distinct sites on the cortex where *AgExo70*-GFP was not observed prior to destruction of the actin cytoskeleton (figure 15D). Therefore, recruitment of *AgExo70*-GFP to distinct sites can happen in the absence of filamentous actin. Whether these sites represent sites of polarity establishment is currently unknown.

AgRho1b localization and cell wall synthesis.

ScRho1 has a dual function in regulation of the actin cytoskeleton and cell wall integrity signalling in yeast. ScRho1 can be activated upon cell wall stress: Transmembrane cell wall sensors as ScWsc2 or ScMid2 recruit and activate the GEFs ScRom1 and ScRom2, which localize in a polarized manner (Ozaki et al., 1996; Manning et al., 1997; Philip and Levin, 2001). They activated ScRho1, which can regulate cell wall synthesis indirectly, via ScPkc1 mediated signaling, or directly, by associating with the glucan synthase ScFks1. Two homologs of ScRho1 were identified in *A. gossypii* and named *AgRHO1a* and *AgRHO1b*. During evolution, only *AgRho1b* maintained the function in control of the cell wall and can complement for loss of ScRho1 in yeast (see part III, figure 3). Deletion of *AgRHO1b* is lethal, few *Agrho1b* Δ spores are able to establish tiny mycelia that display extensive lysis (Wendland and Philippsen, 2001). Localization of a GFP-*AgRho1b* fusion overlapped with aniline-blue stained cell wall material that presumably represents newly synthesized $\beta(1,3)$ -

glucan (part III, figure 2). It is thus likely that cell wall synthesis takes place at sites where GFP-*AgRho1b* is enriched in the zone defined as the extended apical cortex. We observed a “corset”-like GFP-*AgRho1b* localization in fast growing hyphae instead of the tip-based cortical distribution seen for slow hyphae. This might indicate that cell wall synthesis is evenly distributed over the tip surface in slower hyphae while in fast hyphae, it is maximal behind the tip where hyphae reached their final diameter. The mechanism of growth-speed dependent localization of *AgRho1b* could be as follows: A transmembrane cell wall sensor is transported through vesicular traffic to the hyphal tip where it comes into contact with the cell wall. It immediately starts signalling and recruits potential GEFs, such as *AgRom1*, that activate *AgRho1b*. This process may take a constant amount of time. In slow growing hyphae, this time interval might be short enough to enable localization of *AgRho1b* to the hyphal tip. However, if hyphae grow fast, they might synthesize a considerable surface area during the time that elapses between signalling and GFP-*AgRho1b* activation and thus *AgRho1b*

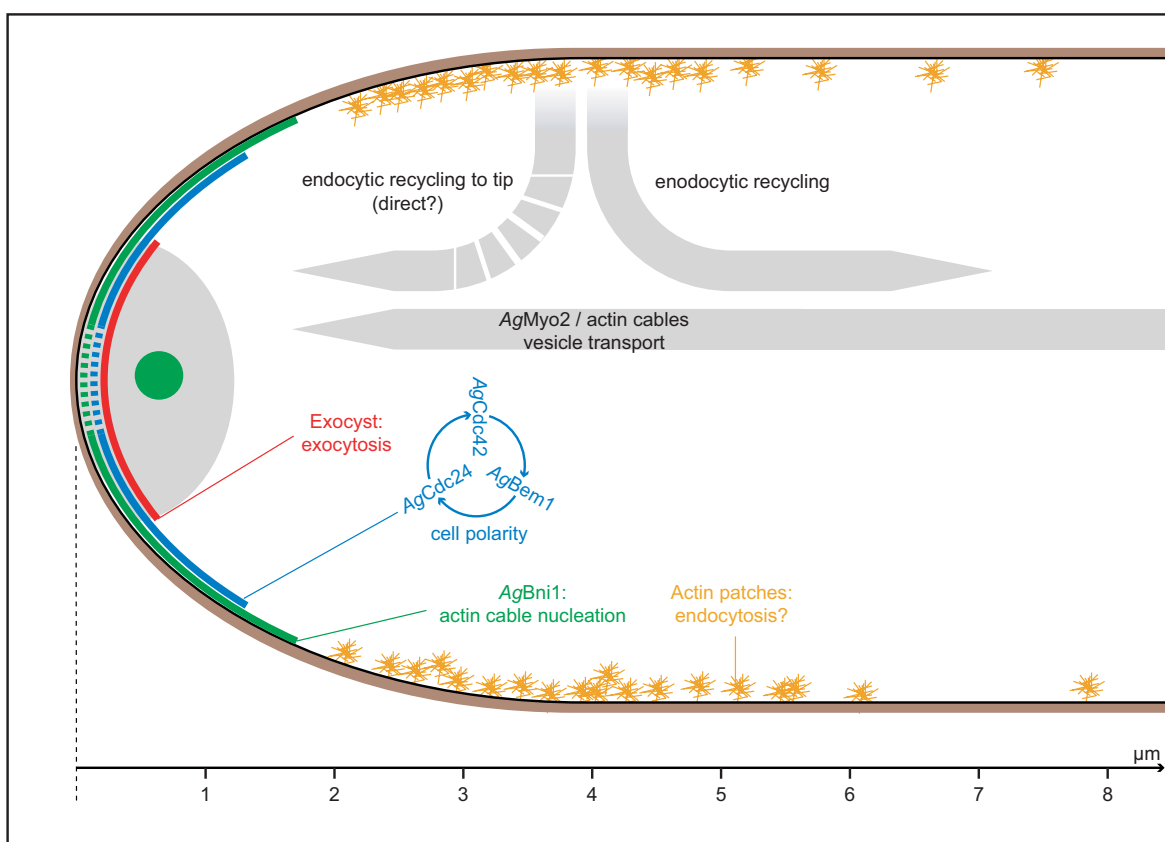


Fig. 16: Model of a fast-growing hyphal tip. The scheme shows a cross-section through a fast growing hyphal tip. For explanations see text.

enrichment happens behind the tip leading to the “corset” like distribution.

Model of a fast-growing hypha

A model of fast hyphal growth can be postulated based on the data presented in this study (figure 16). The *AgCdc42* module (figure 16, blue) is located at the central apical cortex regulating cell polarity where it activates the formin *AgBni1* (figure 16, green) at the cortex. The formin nucleates actin cables that serve as tracks for myosin-dependent transport of secretory vesicles. An additional pool of *AgBni1* in the apical body might be important for organization of the latter or for generation of sufficient actin cables to supply fast hyphal growth. Vesicles that are accumulated in the apical body (figure 16, light grey) fuse with the plasma membrane at the very tip where *AgExo70* is enriched (figure 16, red). Endocytosis is thought to take place mainly in a region behind the tip where actin patches (figure 16, orange) are very dense. A fraction of the endocytosed material is transported back to the tip. This is supported by the observations that FM 4-64 quickly accumulates in the apical body and that about 15 % of the actin patches display anterograde movement (Philippe Laissue, unpublished results). This cycle of polarized secretion and endocytosis may function in localization of polarity factors. It is possible that polarity factors are endocytosed and transported back to the tips. Indeed, it was shown that polarized secretion coupled with endocytosis is sufficient to generate a polarized localization pattern (Valdez-Taubas and Pelham, 2003) thus an exocytosis/endocytosis cycle may be involved in generation of the observed polarity factor localization patterns.

Materials and methods

DNA manipulations, plasmids and oligonucleotides

All DNA manipulations were performed according to Sambrook, 2001. The *E. coli* strain DH5alphaF' (Hanahan, 1983) was used as host for plasmid propagation. PCR was performed using Taq DNA polymerase, the Expand High Fidelity PCR system or the Expand Long Template PCR system following the manufacturer's instructions (Roche, Germany). Oligonucleotides were synthesized by MWG (Germany) or Microsynth (Switzerland).

Oligonucleotides that were longer than 30 bases were PAGE purified. DNA sequencing was performed in-house on an ABI377 automated sequencer using the BigDye Terminator Sequencing Kit or by Microsynth (Switzerland). All restriction enzymes came from New England BioLabs or Roche, restriction reactions were performed according to the enzyme's manufacturer. DNA was ligated using T4 DNA ligase (New England BioLabs, USA); DNA fragments that contained an origin of replication and that were not wished religate were treated with alkaline phosphatase (Roche). Homologous recombination was performed in the yeast strain DHD5 (Arvanitidis and Heinisch, 1994) using the protocol of Gietz et al., 1995. Plasmids were isolated from yeast as described in Schmitz et al., 2006 using the “High Pure Plasmid Purification Kit” (Roche, Germany). Oligonucleotides and plasmids used in this study are listed table in 5 and table 6, construction of plasmids that gave rise to *A. gossypii* strains is further explained under “*A. gossypii* strain construction”.

***A. gossypii* growth conditions**

A. gossypii was cultivated in AFM (*Ashbya* full medium) that contained 10 g/l yeast extract (Formedium, United Kingdom), 10 g/l peptone (Formedium, United Kingdom), 20 g/l glucose and 1 g/l myo-inositol (Merck). 5x concentrated AFM was filtered sterile and diluted prior to use with sterile, deionized water or with an autoclaved, 50 °C warm agar solution, final agar concentration was 15 g/l. G418 (Calbiochem) or ClonNat (Werner BioAgents, Germany) was added to a final concentration of 200 µg/ml and 50 µg/ml respectively from 50 mg/ml stock solutions. For auxotrophic selection using the *LEU2* marker, AMM-Leucine (*Ashbya* minimal medium without leucine) was used. AMM-Leucine contains 1.7 g/l YNB without amino acids and without (NH₄)₂SO₄ (Becton, Dickinson and Co., USA), 0.69 g/l CSM-Leucine (Bio101 Systems, USA), 2 g/l Glycine, 1 g/l myo-inositol, 0.01 g/l adenine HCl and 20 g/l glucose. A two fold solution was prepared, the [pH] was adapted to 6.3 with 5 M KOH and the medium was filtered sterile and stored in the dark at room temperature. Standard incubation temperature was 30 °C. Spores were either prepared from liquid cultures in AMM supplied with 0.2 g/l leucine if necessary or from mycelium that was stripped from AFM plates 5-8 days after inoculation. The mycelium/spore

mixture was washed once with sterile H₂O, then the mycelium was digested with either 2 mg/ml zymolyase (Seikagaku, 20T) or 3 mg/ml lysing enzyme from *Trichoderma harzianum* (Sigma) at 37 °C for 2 h under soft shaking. The spores were centrifuged at 2000 x g, the supernatant was removed and the spores were washed three times with 2 ml 0.03 % Triton X-100. Spores were stored at -70 °C in a 33 % glycerol solution and thawed prior to use at 4 °C. Mycelium was stored in a 40% glycerol solution in AFM at -70 °C.

A. *gossypii* transformation

Agleu2Δthr4Δ (Altmann-Johl and Philippsen, 1996) was used as a parental strain for all transformations if not mentioned otherwise and is referred to as “reference strain” or “Ag” in figures. *A. gossypii* transformation was performed as described in Wendland et al., 2000. Plasmidic transformation of heterokaryotic mycelium was achieved with an identical protocol. To obtain a homogenous culture of the desired heterokaryotic strain, 0.2 g of mycelium were stripped from an AFM plate and suspended in 0.5 ml AFM with a mortar. One volume of this suspension was inoculated with 1000 volumes of AFM containing the proper antibiotics for 12 h at 30 °C.

A. *gossypii* strain construction

The strains used in this study are listed in table 7, details to strain constructions are given below.

Gene deletions

Genes were deleted using the PCR-based, one-step gene targeting approach with heterologous markers described by Baudin et al., 1993; Wach et al., 1994; Wendland et al., 2000. The oligonucleotides were designed to have 40 to 50 bases of homology to the upstream- and downstream region of the sequence to be replaced and 20 bp homology to the PCR template. The name of the respective oligonucleotides and PCR templates can be found in the *A. gossypii* strain table. Primary transformants were heterokaryotic meaning that the mycelia contained both nuclei where a marker gene replaced the target sequence and wild-type nuclei. More than 99.8 % of *A. gossypii* spores are uninucleated (Claudia Birrer, unpublished), thus clonal purification of the mutation is performed by separating spores on selective medium. The spores give rise to homokaryotic mycelia where the target sequence is replaced by a marker gene

in each nucleus. Both hetero- and homokaryotic strains were verified by analytical PCR. It is possible to observe phenotypes of lethal, recessive mutations since spores carrying such mutations are readily obtained from heterokaryotic strains, development of these spores can be followed on selective medium.

GFP-fusion strains

GFP-fusion constructs were integrated at the site of the wilt-type gene in the *A. gossypii* genome under the control of the native promoter if not mentioned otherwise. Radial growth speeds of the constructed strains, the parental strain and of strains that carried deletions of the respective genes were compared to assess functionality of the GFP-fusion constructs. The growth speed measurements are mentioned only if differences between the parental strains and the GFP-fusion construct could be detected. The parts of the plasmids that were originally created in a PCR reaction were verified by sequencing prior to transforming them into *A. gossypii*. Genomic integration of the constructs was verified by analytical PCR. Furthermore, the homokaryotic fusion strains could be cultivated for more than one week on non-selective medium without losing the GFP-signal and the GFP-signal was present in every hypha at comparable intensities. In plasmidic transformants, the GFP-signal is lost when the strain is grown on non-selective medium and GFP- intensity can vary greatly between different hyphae; hyphae without any GFP are frequently observed.

GFP-AgBNII (K46 and K47)

Amino-terminal fusions to *AgBni1* were constructed because a strain with a carboxy-terminal *AgBni1*-GFP fusion (Schmitz et al., 2006) showed a reduced radial growth speed and was incapable to form apical bodies. In a first step, a cassette for amino-terminal GFP-tagging via PCR-based gene targeting was constructed since no such construct was available at the time. The plasmid pG3i was created by cloning the *GEN3* cassette cut with *PstI* into pUC19 to create plasmid that was identical to pAGT140 (pG3) with an inverted *GEN3* marker. After removal of the *PacI* restriction site, pG3i was digested with *XbaI* and religated with a *SpeI* cut GFP-containing 0.744 kbp fragment that was amplified from pAGT141 (pG3 GFP) with the primers 05.216 and 05.217 giving rise to pG3-NT-GFP. The *AgBNII* promoter was amplified from pAMK1 with the primers 05.220 and 05.221. The resulting 0.604 kbp product was digested

with *PacI* and ligated into *PacI*-cut pG3-NT-GFP resulting in pK16. This plasmid was then used as a template to create a 3.223 kbp long amino-terminal GFP-fusion cassette using the primers 05.215 and 05.222. This cassette was cotransformed into yeast together with pAMK1, the resulting pK15 encoded an amino-terminal GFP-*AgBni1*-fusion under the control of the *AgBni1* promoter. pK15 was digested with *KpnI*, the 3.864 kbp fragment was subcloned into *KpnI* cut pUC19. The resulting pK46 was propagated, about 15 µg DNA were cut with *KpnI* and transformed into *A. gossypii* resulting in the strain *K46* that expresses *GFP-AgBNI1* under the native *AgBNI1* promoter. A *GFP-AgBNI1* fusion whose expression was driven by the *S. cerevisiae HIS3* promoter was constructed to increase signal strength. The *ScHIS3* promoter (0.220 kbp) was amplified from pAGrPXC (Helfer and Gladfelter, 2006) with the primers 06.039 and 06.040 and cloned into pG3-NT-GFP cut with *PacI* giving rise to pK50. The 1.992 kbp fragment of *StyI* digested pK50 was ligated into *StyI* cut pK46 resulting in pK47. The plasmid pK47 was digested with *KpnI* and transformed into *A. gossypii*. Western blot analysis showed that the *ScHIS3* driven expression of *GFP-AgBNI1* resulted in roughly five to ten times increased proteins levels compared to expression driven from the native promoter (figure 5B). The presented results were obtained with *K47*, the localization patterns and speed dependences observed for *K46* were similar though, in slower hyphae, the GFP-*AgBni1* signal was often so weak that no explicit localization pattern could be assigned. *K47* showed increased radial growth speed compared to the carboxy-terminal *AgBNI1-GFP* fusion strain, however *K46* still displayed a decrease in radial growth speed compared to the parental strain (figure 5A).

GFP-AgBUD6 (K52)

GFP was fused amino-terminally to *AgBud6* because the 5' end of the predicted *AgBUD6* open reading frame overlapped with the open reading frame of *AFR494W*. The amino-terminal 2.851 kbp fusion cassette was amplified from pK50 with the primers 06.041 and 06.042 and recombined with pAG16044 (Dietrich et al., 2004) that contains *AgBUD6* by cotransformation into yeast. pK51 that contained a GFP-*AgBUD6* fusion was isolated and digested with *XhoI*. The 5.563 kbp fragment was cloned into *XhoI* cut pBluescript giving rise to pK52. About 15 µg of pK52 were cut with *XhoI* and used to transform *A. gossypii* resulting in *K52*.

AgPEA2-CFP and AgPEA2-YFP (K25 and K26)

CFP and YFP fusion cassettes were obtained with the primer pair 05.206/05.207 using pAGT142 (pG3 CFP, 2.570 kbp) and pAGT143 (pG3 YFP, 2.447 kbp) as templates. The cassettes were cotransformed together with pAG18591 that contains *AgPEA2*. The resulting pK21 (*AgPEA2-CFP*) and pK23 (*AgPEA2-YFP*) were isolated from yeast and digested with *SpeI*. The 9.434 kbp fragment of pK21 and the 9.341 kbp fragment of pK23 were recircularized giving rise to pK25 and pK26. Both pK25 and pK26 were cut with *SpeI* and *XhoI* for *A. gossypii* transformation giving rise to *K25* and *K26*. *AgPea2-CFP* was barley visible under the standard growth conditions used during this study; all results shown were obtained with *AgPea2-YFP*. Nevertheless, the localization patterns of *AgPea2-CFP* and *AgPea2-YFP* were identical in fast growing hyphae where both signals were easily detectable.

AgEXO70-GFP (K28)

AgEXO70 was amplified from genomic DNA with the primers 05.249 and 05.250. The 4.838 kbp fragment was digested with *HinDIII* and *NheI*, the resulting 4.684 kbp fragment that contained *AgEXO70* was cloned into *SpeI* and *NheI* digested pRS415 giving rise to pK27. The primers 05.201 and 05.202 were used to create a 2.892 kbp GFP fusion cassette with pAGT141 (pG3 GFP) as a template. This cassette was cotransformed together with pK27 into yeast giving rise to pK28. After isolation from yeast, pK28 was cut with *BsrBI* for transformation of *A. gossypii*.

AgSEC3-YFP (K33)

AgSEC3 was amplified from genomic DNA with the primers 05.229 and 05.230. The 4.874 kbp product was digested with *SpeI*, the resulting 4.830 kbp fragment was inserted into *SpeI* cut pRS415 giving rise to pK22. A YFP-fusion cassette (2.420 kbp) obtained with the primers 05.268 and 05.198 using pAGT103 as a template was cotransformed with pK22 into yeast resulting in pK33. This plasmid was isolated from yeast, digested with *NheI* and *SpeI* and used for transformation of *A. gossypii*.

AgGIC1/2-YFP (K39)

Please see part II.

Agcdc42Δ GFP-CDC42 (pK49): a selection-based process for generation of functional GFP-fusions constructs.

Plasmids containing an ARS sequence from yeast can replicate in *A. gossypii* freely and are not integrated into the genome (Wright and Philippsen, 1991). A heterokaryonic *Agcdc42Δ* strain was transformed with pK49 containing GFP-*AgCdc42* with different random linkers as described under “*A. gossypii* transformation”. The pK49 construct is based on pHPS248 (Hans-Peter Schmitz, unpublished), which contains an N-terminal GFP-fusion to the *AgRHO1a* open reading frame. First, the *AgCDC42* open reading frame and terminator were amplified by PCR (Primers: 04.162/04.163, template pCDC42), the 0.755 kbp was cloned into pHPS248 with *EcoRI* and *SpeI* replacing *AgRHO1a* resulting in pK5. The *AgCDC42* promoter was amplified with the primers 05.097 and 05.098 from pCDC42, the 0.508 kbp product was cloned into pK5 with *HinDIII* and *BamHI* giving rise to pK10. A *GEN3*-containing cassette was amplified from pCDC42kanr (Schmitz et al., 2006) with the oligonucleotides 05.099 and 05.100, the 1.900 kbp product was cloned behind the *GFP-AgCDC42* with *SpeI* giving rise to pK12. A system based on the yeast strain *DLY3067* (Moskow et al., 2000) was used to assess the functionality of different *GFP-AgCdc42* fusions. In this strain, *ScCDC42* is expressed under the control of the *ScGAL1* promoter. The plasmid pCDC42K containing *AgCDC42* was able to complement *DLY3067* on YPD while *GFP-AgCDC42* expressed from pK12 was not. In order to obtain functional *GFP-AgCdc42* fusions, *EcoRI* cut, dephosphorylated pK12 was cotransformed with a library of random linkers, the transformation was spread on YPD to select for functional *GFP-AgCDC42* fusions. The random linker library consisted of a linker sequence that coded for nine different random amino acids, flanked by sequences that were homologous to *GFP* and *AgCDC42* (fig. 8A). The nine random amino acids could either be leucine, proline, histidine, arginine, glycine, aspartate, alanine or valine. The linker library was obtained by annealing the two oligonucleotides 05.301 and 05.302 followed by a PCR-based fill-in reaction (denaturation at 95 °C for 5 min, addition of Expand High Fidelity PCR system polymerase mix at 55 °C, second denaturation step at 93 °C for 60s followed by repeated annealing and amplification rounds at 55 °C and 68 °C, temperatures were chosen in way that the double-stranded fragments where the fill-in reaction already has taken place were

not denatured any more). Transformants were repicked on YPD+G418 after three days. Plasmids were rescued from transformants that were able to grow at 37 °C and that showed a *GFP-AgCdc42* localization to the bud or the bud neck. The plasmids were sequenced, the *GEN3* marker was cut out with *SpeI* and the plasmids were religated to give rise to pK49RL04, pK49RL06 and pK49RL07. An alternative process was used to select for *GFP-AgCdc42* fusions that work best for *A. gossypii*. *DLY3067* strains that displayed *GFP-AgCdc42* at bud tips and bud necks were pooled; plasmids were rescued from the pooled culture. The *GEN3* cassette was cut out of the rescued plasmids giving rise to pK49 versions that differed in the sequence of the random linker. A heterokaryonic *Agcdc42::GEN3* strain was transformed with this plasmid collection and with the three pK49 plasmids rescued from yeast. The primary transformants were sporulated, spores were spread on AMM-Leucine containing G418 to select for spores with an *AgCDC42* deletion. The resulting homokaryonic *Agcdc42Δ* strains were verified by analytical PCR, radial growth speed was estimated to select for fusion constructs that displayed maximal radial growth speeds. The random linker of the pK49 version with the fastest growth speed was coding for the peptide APPRRLVHP. No difference in *GFP-AgCdc42* localization could be observed for the four different *GFP-AgCdc42* strains. Two bands were visible on western blots probed with antiGFP, one with the characteristic size of *GFP-AgCdc42*, one with the size of GFP alone. The single GFP-band was estimated to be about half as intense than the *GFP-AgCdc42* band. It is thus possible that about 1/3 of the *GFP-AgCdc42* molecules are proteolytically cleaved and that a considerable amount of untagged *AgCdc42* is present in the cells (figure 10C). *K49RL13* and *K49RL07* reached about 85 % respectively 75 % of the radial growth speed of an *Agcdc42Δ* strain that was complemented with pCDC42 on solid AFM at 30 °C (figure 10B).

Protein extraction and western blotting

A. gossypii was grown in liquid AFM for 15-18 h at 30 °C and collected by vacuum filtration. The wet weight of the harvested mycelium was between 80 and 300 mg. Protein extraction was performed as described by Helfer and Gladfelter, 2006, protein concentrations of the lysates were between 10 and 20 µg/µl. 30 to 150 µg proteins were separated by SDS-PAGE, the percentage of the poly-acrylamid

gel was between 5 and 10 % depending on the predicted molecular weight of the proteins to be observed. The gel was run at 4 °C and the proteins were transferred to nitrocellulose membranes (Amersham Biosciences) using standard conditions (Sambrook, 2001). The nitrocellulose membrane was blocked 3 times for 40 min with 60 ml 5 % MPBST (5 % non-fat milk powder (COOP, Switzerland), PBS according to Sambrook, 2001, 0.1 % Tween-20). The membrane was probed with monoclonal mouse anti-GFP (Roche, 10 ml of a 1 : 1000 dilution in 2.5 % MPBST) at 4 °C over night, washed four times ten minutes with 60 ml 5 % MPBST and two times ten minutes with PBST (PBS with 0.1 % Tween-20) at room temperature and was reprobed with HRP-conjugated goat anti-mouse antibodies (Jackson ImmunoResearch, 10 ml of a 1 : 5000 dilution in 2.5% MPBST) at room-temperature for two hours. Washing was repeated as above. ECL chemiluminescence (Amersham Biosciences) was used to develop the western blot according to the manufacturer's instructions; the chemiluminescence was detected with Kodak BioMax XAR films (Kodak).

Light microscopy, sample preparation and image processing.

The microscope set-up is described in Knechtle et al., 2003, the camera was a CoolSNAP HQ camera (Photometrics, USA), a 75 W XPO short arc lamp (Osram, Germany) or a Polychrome V monochromator (Till Photonics, Germany) was used as an illumination source. Mycelium from the borders of 2-3 days old, adult *A. gossypii* colonies were inoculated on „time-lapse slides“, glass slides with a cavity (Roth, Switzerland) that was filled with half concentrated AFM solidified with 1 % agarose. Strains harboring a plasmid (*GFP-AgRHO1b*, *GFP-AgSEC4*) were cultivated on ASC-Leucine (1.7 g/l YNB without amino acids and ammonium sulfate, 1.8 g/l SC-Leucine (Bio101 Systems, USA), 7g/l glutamic acid monopotassium salt monohydrate, 7 g/l aspartic acid potassium salt hemihydrate, 1 g/l myo-inositol, 20 g/l glucose) which allowed fast hyphal extension also under microscopy conditions (Andreas Kaufmann, personal communication). An air-bubble was included in the center of the time-lapse slide, fast growing hyphae were often observed in areas close to the bubble, either due to reduced pressure from the cover-slide in this region or due to increased oxygenation. FM 4-64 was kept in a 16 µM aqueous stock solution at -80 °C. It was diluted

with AFM to an FM 4-64 concentration of 11 µM and was applied directly to the sample prior to microscopy. FM 4-64 stained Spitzenkörper were observed after about 10 minutes of incubation with FM 4-64, image acquisition was stopped after 1 hour. DIC images were processed using the „Scale-image“ and the „Unsharp Mask“ feature from MetaMorph 6.2r6 (Molecular Devices Corp. USA). Z-stacks with a distance between 0.3 and 0.8 µm were acquired and processed either with the „Remove Haze“ function, with the „No Neighbours“ or the „Nearest Neighbour“ tool of MetaMorph. Fluorescent images shown are maximum projections or sum projections of two to four central planes of a processed Z-stack. Overlay images were performed with the „Overlay Images“ function of MetaMorph. Stacks that were submitted to blind deconvolution with AutoDeblur 7 (MediaCybernetics, USA) contained at least 32 image planes with a z-distance of maximally 0.3 µm. The presented images retrieved from the deconvoluted image stacks are maximum projections of 2 to 5 central planes.

Phase contrast microscopy was performed at the Arizona State University, Tempe AZ, USA in laboratory of Robert Roberson. *A. gossypii* was grown microscopy slides that were coated with AFM containing 19 % gelatin (gelatin powder, “baker analyzed”, J. T. Baker, USA). Microscopy was performed on a Axioskop microscope (Carl Zeiss, USA). Images were captured with a Roper Cool SNAP ES digital camera (Roper Scientific, USA).

Actin cytoskeleton staining

The actin cytoskeleton was stained as described in Knechtle et al., 2003. To ensure fast hyphal extension speeds, spores were plated on an AFM agar plate and incubated for 20 hours at 30 °C. The cells were fixed by pouring 5 ml fixative (4 % formaldehyde in PBS) directly on the plates. The mycelia were detached gently from the agar surface with a glass rod after 10 minutes of fixation, centrifuged down and postfixed for 30 minutes in fresh fixative. After the staining procedure, mycelia could be stored for several days at 4 °C in the dark without apparent loss of staining quality; the mycelia were suspended in PBS for microscopy.

Measurements and statistics

All measurements were performed on unprocessed images on the plane of the Z-stack that was the closest to the hyphal center. The measurements were evaluated with Microsoft Excel. Growth

speed was measured by acquisition of a DIC image followed by a time interval of 150 seconds and a DIC Z-stack. The first DIC image and the best plane of the DIC image stack were overlaid and the (X/Y) coordinates of the hyphal tip for $t=0$ and $t=150$ s were transferred to Microsoft Excel. Distances d were calculated as $((X_{t=150}-X_{t=0})^2 + (Y_{t=150}-Y_{t=0})^2)^{1/2}$. Growth speeds are given in $\mu\text{m}/\text{min}$ and were obtained by dividing d by Δt . Similar strategies were used to measure hyphal diameters and dimensions of GFP-signals. The standard deviations (S.D.) were calculated with Microsoft Excel, standard errors (S.E.) are given as the S.D. divided by the square root of the number of measurements. Depending on the context, the mean \pm the S. D. or the S. E. are given. The S.D. is used to give an impression of the range of normally distributed data; the S.E. is the estimated standard deviation of the error in the process of measuring.

Transmission electron microscopy

Electron microscopy was performed at the Arizona State University, Tempe AZ, USA in the laboratory of Robert Roberson. Sample preparation was performed according to McDaniel and Roberson, 2000. Mycelium was taken from the border of a 2-3 days old *A. gossypii* colony and inoculated on 4x4 mm big pieces of thin dialysis membrane on AFM agar plates over night at room temperature. Radial growth speed on the dialysis membrane was between 1.3 and 1.6 $\mu\text{m}/\text{min}$. The dialysis membranes with the small *A. gossypii* colonies were plunged into a liquid propane-ethene mixture with a temperature of approximately -185°C . The frozen samples were transferred into substitution solution (1 % glutaraldehyde and 1 % tannic acid (w/v) in HPLC grade anhydrous acetone) that was kept on dry ice. After an inoculation of 72 hours, the samples were rinsed three times in acetone on dry ice before placing them into a 1 % OsO_4 solution in acetone. The specimens were incubated one hour on dry ice, then they were allowed to warm up by placing them for two hours at -20°C followed by a two hours incubation at 4°C and a 30 to 60 minutes incubation at room temperature until the OsO_4 solution turned dark brown. The OsO_4 was washed out with acetone and the samples were embedded in Spurr's resin (Spurr 1969) by step-wise increasing of the Spurr's resin concentration. Samples were flat-embedded and the Spurr's resin was polymerized at 60°C . Selected hyphae were sectioned and post-stained for ten minutes

in 2 % uranyl-acetate in 50 % ethanol and for five minutes in Reynolds' lead citrate (Reynolds, 1963), sections were examined using a Philips CM12S TEM (Philips Electronic Instruments CO). Chemical fixation was performed directly on AFM plates. Mycelia were inoculated like for cryo-fixation. Four hours prior to fixation, the plates were shifted to 30°C to accelerate hyphal growth. Fixative (2 % glutaraldehyde in 0.05 M sodium phosphate buffer [pH 6.8]) was poured directly on the plates. After 60 minutes of fixation, samples were washed three times in cold 0.05 M sodium phosphate buffer [pH 7] and soaked in cold 0.5 % uranyl acetate over night. The mycelia were washed three times with water and dehydrated in ethanol. The ethanol was exchanged by acetone and the samples were embedded and processed for microscopy as described above.

Table 5: Oligonucleotides

	Name	Sequence*	Use**
-	AgCDC24-F1	GTAAAGGAGAGCAAAGAACGGATACTAAACGTTTGGGCATTGTGTT ggtgcaggcgctggagctg	rec
-	AgCDC24-F2	CGTACAGTCGCTCCTACATAGTCTGCACATTTGTTAATACCTCT agggacctggcaggagc	rec
-	AgPEA2-S1	GTAGTTCATGTATCAGAGCGATGGAGGACGATACAGTGCTTACGG gctagggataacaggtaat	gt
-	AgPEA2-S2	GGGAGTTCCTTAGACCACAATTGCGCCATATAGTTACCAATGCGG aggcatgcaagcttagatct	gt
01.060	AgBNI1-I1	CAGATCGGGCCTGTGTTACC	aPCR
01.084	V2*NAT1	GTGGTGAAGGACCCATCCAG	aPCR
02.036	AgCDC42	CGTTGTCGTACCCGTCGACGGACG	aPCR
02.103	V3PDC1T	GACCAGACAAGAAGTTGCCGACAGTCTGTTGAATTGGCCTG	aPCR
03.496	AgCDC42-S1	GGCAGGAGAACTAGAGTGCAAAGCAGGCAGCTGCACACAGGAAGTAGCA gctagggataacaggtaat	gt
03.497	AgCDC42-S2	CATGAATCATTGACCTATGTGTCTTTAGTACTTAAGTATCCAAAAGCCA aggcatgcaagcttagatct	gt
03.498	AgCDC42-G4	GCCACGTGATCGCACTATTG	aPCR
03.517	AgCDC42-I1	TGTTGACACTGCCGGGCAG	aPCR
04.011	green2.2	TGTAGTTCCCGTCATCTTTG	aPCR
04.017	G2.3	GGAGGTAGTTGCTGATTGG	aPCR
04.018	G3.3	ATGTTGGACGAGTCGGAATC	aPCR
05.028	SEQ-GCYFO	CAAGAGTGCCATGCCCGAAG	aPCR
05.082	AgBEM1-F1	CGGGGTAATCCAGGAGAAGCAGAAGATCATGGTTCTCGATGTCCAA ggtgcaggcgctggagctg	rec
05.083	AgBEM1-F2	TCTTATGTACGACACAAGCAATGGTATACCACCTTGCATGGGCGAT agggacctggcaggagc	rec
05.097	AgCDC42prom-5'	AGTaatgcttctgcagCCGCTGTATACTACATAGCC	pl, aPCR
05.098	AgCDC42prom-3'	actggatccCATTGCTACTTCTGTGTGTC	pl
05.099	AgCDC42term-5'	tgactagtTAACAGGGTAATACAGATATC	pl
05.100	AgCDC42term3'	tgactagtctgcagCCCATCCAACCGTATATACG	pl
05.160	AgSEC4-I1	GAACATCCGCCAGTGGTTC	aPCR
05.198	AgSEC3-F2	GGCAGAATAAAAGGCAGAACCCTGATTTGTAGAATACTAGAGACATT accatgattacgccaagcttgc	rec
05.201	AgEXO70-F1	AAGTATACACCGAATGAGTTAATGAACATTTGAATTCCTTAGGGAGA aaaacgacggccagtgaaattcg	rec
05.202	AgEXO70-F2	ATCACCATTTGTAATATAGCGAGCGCTTTATTAAGCAATAATCCTGAT accatgattacgccaagcttgc	rec
05.206	AgPEA2-F1	GAGCGGAATTACGGAAAAAGCTCGAGTCGCAGTTAGCGAAAAAGTTG aaaacgacggccagtgaaattcg	rec
05.207	AgPEA2-F2	AAAACACTCGGTGTTAATCTGCCTGGGAGTTCCTTAGACCACAATTGC accatgattacgccaagcttgc	rec
05.208	AgPEA2-I1	GCGATATGTTCCCGAAGTCC	aPCR
05.215	AgBNI1-NTF	GCCCCGCTGCTGTGTTTTGGAGTGTGTTGTTGAGTGCCTGGACTTCTT ggatcctctagtgtttaaacc	rec
05.216	GFP-Nterm	AGactagtaattaatgAGTAAAGGAGAAGAAGCTTTTCAC	pl
05.217	GFP-Cterm!	AGactagtgtttaaaccTTTGTATAGTTCATCCATGC	pl
05.220	AgBNI1prom-5'	GCttaattaaCTAATACCTCGTGCCATAG	pl
05.221	AgBNI1prom-3'	TCttaattaaATGTGCCAGCCGCCGACG	pl
05.222	Ag-BNI1-NF2	TCTACGCACCGTTGCCGCCACGTCGCTCGCGCGCAGCCGCCACCAC accatgattacgccaagcttgc	rec
05.229	AgSEC3-SpeI	taactAGTTGGCTGCGGTGCGGTGTC	pl
05.230	AgSEC3-5'	GTAACGCAGTTGGTGGTGTG	pl, aPCR
05.246	AgPEA2-G4	TGGCAAATGGGACCACTTTC	aPCR
05.247	AgEXO70-G1.2	TCCAAACTTAGAGCCCCGAAGTC	aPCR

05.248	AgEXO70-G4.2	CCGACCCAATTCTCAGTCAAG	aPCR
05.249	AgEXO70-us	GCGCGAAACCTCTTGAGGAACC	pl
05.250	AgEXO70-ds	AGTTATGAGGAGGCGCTAGAGG	pl
05.267	AgSEC3-G1.2	AGAAGATGAGCTGGCCCATGCG	aPCR
05.268	AgSEC3-F1.2	CTAAAAACGATATAATTAGTGCATTTCGAGGGCCATAAAAAATTGG aaaacgacggccagtgaaatcgag	rec
05.301	RandomLinker	GGGATTACACATGGCATGGATGAACTATACAAAGAATTC snysnysnysnysnysnysnysnysnyATGCAGACATTGAAGTGCGTGG***	rec
05.302	RL-complement	CAGCTCCGTCCECAACGACCACGCACCTCAATGTCTGCAT	rec
05.349	G2.3	GGAGGTAGTTTGTCTGATTGG	aPCR
06.006	AgPEA2-G1	AGTCGCCAGAAAAGATGAAG	aPCR
06.041	AgBUD6-NTF	AAGAAGTCCGCGACGTTCTTTGAGAGACGGGAACTGACAT ggatcctctagtgttfaaac	rec
06.042	AgBUD6-NF2	ATATAAAAACCAGAGGGTTGCTCTTTTGGATTTGCAAGCTTA accatgattacccaagcttgc	rec
06.043	AgBUD6-G4	GCGTGCCGTCCTTGATATAGTG	aPCR
06.044	AgBUD6-G1	TTCTGTGAACCGCACTAGC	aPCR
06.045	AgBUD6-I1	ACGATGATCTCCCGATGTG	aPCR
06.097	V2_NAT1	GTGTCGTCAAGAGTGGTACC	aPCR
06.098	V3_NAT1	ACATGAGCATGCCCTGCCCC	aPCR
06.122	AgBNII-G1	GCCGCTGGTTCATACTGTC	aPCR
06.139	AgBUD6-S1	CGCGTGATATAAAAACCAGAGGGTTGCTCTTTTGGATTTGCAAGCTTAA atgggtaccactcttgaagac	gt
06.140	AgBUD6-F2	ATTGCTTGAACCCTGCTTTTCATGGTCTGGGTTAAGTTCTGGACTCCA atgcttcggctcgtatgttg	gt
06.262	AgBUD6-G4.3	GCGCGTTCGATTGCTTGAACC	aPCR
06.263	AgBUD6-I2	TACATGGAGCAGTCGCATTCG	aPCR

* Bold lower case characters indicate the template-binding sequences of gene targeting- and recombination primers. All other lower case characters indicate nucleotides that are not homologous to the PCR template.

** aPCR = analytical PCR, gt = gene targeting, pl = plasmid construction, rec = recombination

*** s = g or c; n = g, a, t or c; y = t or c (IUB code for mixed base sites)

Table 6: Plasmids

Name	Backbone	Insert	Source
pBluescript	-	-	Short et al. 1988
pRS415	-	-	Sikorski and Hieter 1989
pRS416	-	-	Sikorski and Hieter 1989
pUC19	-	-	Vieira and Messing 1991
pYCPlac111	-	-	Bartel et al. 1993
pAG16044	pRS416	<i>AgBUD6</i>	Dietrich et al, 2004
pAG18591	pRS416	<i>AgPEA2</i>	Dietrich et al, 2004
pAGT103	pUC19	<i>YFP-NAT1</i> cassette	Kaufmann A., unpublished
pAGT140	pUC19	<i>GEN3</i> cassette	Kaufmann A., unpublished
pAGT141	pUC19	<i>GFP-GEN3</i> cassette	Kaufmann A., unpublished
pAGT142	pUC19	<i>CFP-GEN3</i> cassette	Kaufmann A., unpublished
pAGT143	pUC19	<i>YFP-GEN3</i> cassette	Kaufmann A., unpublished
pAMK1	pRS415	<i>AgBNII</i> with promoter and terminator	Schmitz et al. 2005
pCDC42	pRS415	<i>AgCDC42</i> with promoter and terminator	Schmitz et al. 2005
pCDC42K	pRS415	<i>AgCDC42</i> with <i>GEN3</i> cassette behind ORF	This study
pCDC42kanr	pRS415	pCDC42(Q61H) <i>GEN3</i> behind <i>AgCDC42</i> ORF	Schmitz et al.2005
pG3i	pUC19	pAGT140 with inverted <i>GEN3</i> cassette	This study
pG3-NT-GFP	pUC19	promoterless <i>GEN-GFP</i> cassette	This study
pGUG	pUC19	<i>GFP-GEN3</i> cassette	Knechtle et al. 2003

pHPS235	pYCPlac111	<i>GFP-AgSEC4</i>	Schmitz et al. 2005
pHPS248	pYCPlac111	<i>P_{RHO1a}-GFP-AgRHO1a</i>	Schmitz HP., unpublished
pHPS250	pYCPlac111	<i>P_{AgRHO1b}-GFP-AgRho1b</i>	Schmitz HP., unpublished
pK10	pYCPlac111	<i>P_{AgCDC42}-GFP-AgCDC42</i>	This study
pK15	pRS415	<i>GEN3-P_{AgBNI1}-GFP-AgBNI1</i>	This study
pK16	pUC19	<i>GEN3-P_{AgBNI1}-GFP cassette</i>	This study
pK21	pRS416	<i>AgPEA2-CFP-GEN3</i>	This study
pK22	pRS415	<i>AgSEC3 with promoter and terminator</i>	This study
pK23	pRS416	<i>AgPEA2-YFP-GEN3</i>	This study
pK25	pRS416	<i>AgPEA2-CFP-GEN3</i>	This study
pK26	pRS416	<i>AgPEA2-YFP-GEN3</i>	This study
pK27	pRS415	<i>AgEXO70 with promoter and terminator</i>	This study
pK28	pRS415	<i>AgEXO70-GFP-GEN3</i>	This study
pK33	pRS415	<i>AgSEC3-YFP-NAT1</i>	This study
pK46	pUC19	<i>GEN3-P_{AgBNI1}-GFP-AgBNI1</i> (nucleotides 1-1277)	This study
pK47	pUC19	<i>GEN3-P_{ScHIS3}-GFP-AgBNI1</i> (nucleotides 1-1277)	This study
pK49	pYCPlac111	<i>GFP-RL-AgCDC42</i> (RL = random linker)	This study
pK49RL04	pYCPlac111	<i>GFP-RL-AgCDC42</i> (RL codes for DHPRHGGPP)	This study
pK49RL06	pYCPlac111	<i>GFP-RL-AgCDC42</i> (RL codes for PRPALPRVA)	This study
pK49RL07	pYCPlac111	<i>GFP-RL-AgCDC42</i> (RL codes for PRPVRRVAP)	This study
pK49RL13	pYCPlac111	<i>GFP-RL-AgCDC42</i> (RL codes for APPRRLVHP)	This study
pK5	pYCPlac111	<i>P_{RHO1a}-GFP-AgCDC42</i>	This study
pK50	pRS416	<i>GEN3-P_{ScHIS3}-GFP cassette</i>	This study
pK51	pRS416	<i>GEN3-P_{ScHIS3}-GFP-AgBUD6</i>	This study
pK52	pBluescript	<i>GEN3-P_{ScHIS3}-GFP-AgBUD6</i>	This study
pVG006	pBluescript	<i>Agsec3Δ::GEN3</i>	Galati V., unpublished

Table 7: *A. gossypii* strains

Strain	Genotype	Construction	Source
<i>ATCC10895</i>	<i>wild type</i>	-	Ashby and Nowell, 1926
$\Delta\Delta t$	<i>AgIeu2Δ Agthr4Δ</i>	-	Altmann-Johl and Philippsen (1996)
<i>AgBem1-GFP</i>	<i>AgBEM1-GFP-GEN3</i> <i>AgIeu2Δ Agthr4Δ</i>	pGUG PCR 05.082/05.083	Cavicchiol D., unpublished
<i>AgBni1-GFP</i>	<i>AgBNI1-GFP-GEN3</i> <i>AgIeu2Δ Agthr4Δ</i>	-	Schmitz et al. 2005
<i>AgBoi1-GFP</i>	<i>AgBOI1-GFP-GEN3</i> <i>AgIeu2Δ Agthr4Δ</i>	-	Knechtle 2006
<i>AgCdc24-GFP</i>	<i>AgCDC24-GFP-GEN3</i> <i>AgIeu2Δ Agthr4Δ</i>	pGUG PCR AgCDC24-F1/AgCDC24-F2	Boudier K., unpublished
<i>AgCla4-GFP</i>	<i>AgCLA4-GFP-GEN3</i> <i>AgIeu2Δ Agthr4Δ</i>	-	Ayad-Durieux 2000
<i>AgPXL1-GFP</i>	<i>AgPXL1-GFP</i>	-	
<i>AgSpa2-GFP</i>	<i>AgSPA2-GFP-GEN3</i> <i>AgIeu2Δ Agthr4Δ</i>	-	Knechtle 2003
<i>GFP-AgRho1b</i>	<i>GFP-AgRho1b</i> (pHPS250) <i>AgIeu2Δ Agthr4Δ</i>	pHPS250	Schmitz HP., unpublished
<i>GFP-AgSec4</i>	<i>GFP-AgSEC4</i> (pHPS235) <i>AgIeu2Δ Agthr4Δ</i>	-	Schmitz et al. 2005
<i>K25</i>	<i>AgPEA2-CFP-GEN3</i> <i>AgIeu2Δ Agthr4Δ</i>	pK25; <i>SpeI</i> , <i>XmmI</i>	This study
<i>K26</i>	<i>AgPEA2-YFP-GEN3</i> <i>AgIeu2Δ Agthr4Δ</i>	pK26; <i>SpeI</i> , <i>XmmI</i>	This study

K28	<i>AgEXO70-GFP-GEN3</i> <i>Agleu2Δ Agthr4Δ</i>	pK28; <i>BsrBI</i>	This study
K33	<i>AgSEC3-YFP-NAT1</i> <i>Agleu2Δ Agthr4Δ</i>	pK33; <i>NheI, SpeI</i>	This study
K39	<i>AgGIC1/2(aa1-173)-YFP-GEN3</i> <i>Agleu2Δ Agthr4Δ</i>	pK39; <i>AatII, SacII</i>	This study, chapter III
K46	<i>GEN3-P_{AgBNI1}-GFP-AgBNI1</i> <i>Agleu2Δ Agthr4Δ</i>	pK46; <i>KpnI</i>	This study
K47	<i>GEN3-P_{ScHIS3}-GFP-AgBNI1</i> <i>Agleu2Δ Agthr4Δ</i>	pK47; <i>StyI</i>	This study
K49-RL07	<i>GFP-RL07-AgCDC42 (pK49RL07)</i> <i>Agcdc42Δ Agleu2Δ Agthr4Δ</i>	pK49RL07	This study
K49-RL13	<i>GFP-RL13-AgCDC42 (pK49RL13)</i> <i>Agcdc42Δ Agleu2Δ Agthr4Δ</i>	pK49RL13	This study
K52	<i>GEN3-P_{ScHIS3}-GFP-AgBUD6</i> <i>Agleu2Δ Agthr4Δ</i>	pK52; <i>XhoI</i>	This study
<i>Agbud6Δ</i>	<i>Agbud6Δ::NAT1</i> <i>Agleu2Δ Agthr4Δ</i>	pAGT140, PCR 06.139/06.140	This study
<i>Agcdc42Δ</i>	<i>Agcdc42Δ::GEN3</i> <i>Agleu2Δ Agthr4Δ</i>	pGEN3, PCR 03.496/03.497	This study
<i>Agexo70Δ</i>	<i>Agexo70Δ::GEN3</i> <i>Agleu2Δ Agthr4Δ</i>	pGEN3, PCR 05.341/05.342	Galati V., unpublished
<i>Agpea2Δ</i>	<i>Agpea2Δ::GEN3</i> <i>Agleu2Δ Agthr4Δ</i>	pGEN3 PCR AgPEA2-S1/AgPEA2-S2	Brachat S., unpublished
<i>Agsec3Δ</i>	<i>Agsec3Δ::GEN3</i> <i>Agleu2Δ Agthr4Δ</i>	pVG006; <i>MunI, StuI</i>	Galati V., unpublished

Part II

AgGic1/2 is important for cell polarity establishment but not for maintenance of fast hyphal growth in *Ashbya gossypii*.

Establishment of a fungal mycelium depends on constant hyphal elongation and formation of new hyphae, which arise by branching. Emergence of a lateral branch requires establishment of a novel axis of cell polarity at the hyphal cortex, an event which might *a priori* not involve an identical set of polarity factors needed for sustained polar growth. Therefore, I looked for *Ashbya gossypii* candidate genes the deletion of which could generate mycelia with severely reduced or even absent lateral branching while tip expansion was unchanged. I found that loss of *AgGic1/2* resulted in such a phenotype. *AgGic1/2* also plays a role in the first polarity establishment during germination since spores lacking *AgGic1/2* display delayed germ tube emergence. The data reported in this PhD-thesis clearly indicate that *AgGic1/2* is important for cell polarity establishment but dispensable for polarity maintenance in *A. gossypii*. In *Saccharomyces cerevisiae* the homologous proteins *ScGic1* and *ScGic2* act as effectors of the key polarity factor *ScCdc42*. This molecular function is probably conserved in *A. gossypii* since *AgGic1/2* interacts with *AgCdc42* in a two-hybrid assay. Degradation of *AgGic1/2* is likely to be mediated by its carboxy-terminal PEST domains, which are not predicted in the homologous yeast proteins *ScGic1* and *ScGic2*. *AgGic1/2* may have a regulatory function in branch initiation based on the finding that an *AgGIC1/2* allele lacking the part that encodes the PEST domains induces an increase in branching if expressed from a strong promoter. It is possible that controlled degradation of *AgGic1/2* constitutes a simple mechanism that is involved in regulating emergence of new lateral branches.

Introduction

The formation of a fungal mycelium depends on two essential mechanisms: polarity establishment to generate hyphae, either during spore germination or at the cortex of growing hyphae for initiation of lateral branches, and sustained polar growth that leads to elongation of hyphal tips. A plethora of factors was identified that are involved in hyphal tip extension in the filamentous fungi *Ashbya gossypii*, *Neurospora crassa*, *Aspergillus nidulans*, *Ustilago maydis* and many other species (for a review see Steinberg, 2007). Factors influencing the frequency of lateral branches are known from hyperbranching mutants and are frequently observed. Contrary, mutants with reduced branching, which indicates reduced polarity establishment, are very rare (Watters and Griffiths, 2001). A well-described example is a temperature-sensitive mutation of the *nimX* gene of *A. nidulans* that encodes a cyclin-dependent kinases (Lin and Momany, 2004). Also, deletions of *AgSPA2* and *AgBEM4* in *A. gossypii* led to reduced lateral branching (Knechtle et al., 2003; Winkler, 2007). Strains carrying these mutations do not reach wild-type hyphal growth speeds. Therefore, these factors are important for polarity establishment as indicated by the reduced lateral branching and for hyphal elongation as well. To our knowledge no mutation was described so far that reduces lateral branching while leaving hyphal tip extension unchanged.

We found in this work that disruption of *AgGIC1/2* in *A. gossypii* does not alter hyphal elongation but, under certain conditions, almost entirely abolishes emergence of lateral branches. The *Saccharomyces cerevisiae* genes *GIC1* and *GIC2* (GTPase interactive component) are syntenic homologs of *AgGIC1/2*. They emerged from a single ancestor gene during the whole-genome duplication that took place in the *S. cerevisiae* lineage (Dietrich et al., 2004). They both encode proteins that contain a CRIB (Cdc interactive binding) domain and interact specifically with GTP-bound *ScCdc42*. While single deletions of either *ScGIC* gene has no effect, double deletion leads to a temperature-sensitive phenotype. At 37 °C, cells are spherical and display delocalized chitin depositions and a depolarized actin cytoskeleton. Spindle mispositioning, multiple spindles, and multinucleated cells were observed at elevated temperatures. The mitotic defects are likely to be a consequence of the severely disturbed cellular morphology since they are mostly observed in cells with aberrant shapes (Brown et al., 1997; Chen et al., 1997). Consistent with their role in morphogenesis, both *ScGic1* and *ScGic2* localize to sites of bud emergence. *ScGic1* forms a cap in small-budded cells and localizes to the bud neck in medium and large budded cells. *ScGic2* behaves differently, it localizes to the entire cortex of tiny buds as well as to the neck. The portion of *ScGic2*

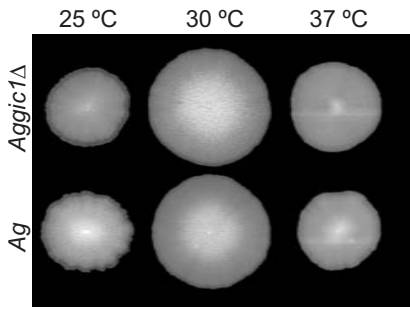


Fig. 1: Deletion of *AgGIC1/2* does not influence radial growth speed. Samples from the borders of *Aggic1/2Δ* and reference strain (*Ag*) mycelia were inoculated in the centers of AFM agar plates and incubated for 6 days at the indicated temperatures.

that is associated with the bud cortex disappears as the bud grows. (Brown et al., 1997; Chen et al., 1997; Iwase et al., 2006). Different studies found that the two Gic proteins link activated *ScCdc42* to downstream events like actin cytoskeleton control or septin recruitment (Jaquenoud and Peter, 2000; Iwase et al., 2006). It was reported that *ScGic2* localizes polarisome components to sites of cell polarity. The CRIB domain as well as the tryptophan 23 of *ScGic2* are necessary for interactions with *ScBud6* and *ScPea2*, and localization of *ScBud6* and *ScBni1* largely depends on the presence of at least one *GIC* homolog (Jaquenoud and Peter, 2000). Furthermore, both, *ScGic1* and *ScGic2*, interact

with the septin *ScCdc12* and are essential for septin recruitment at elevated temperatures in haploid cells (Iwase et al., 2006). *ScGic2* but not *ScGic1* protein levels depend on the cell cycle stage (Brown et al., 1997; Jaquenoud et al., 1998; Hofken and Schiebel, 2004). Upon interaction with *ScCdc42*, *ScGic2* is phosphorylated at its carboxy-terminus, ubiquitinated and degraded in the proteasome. The yeast Skp1-culling-F-box complex in association with *ScGrr1* (*SCF^{Grr1}*) acts as an ubiquitin ligase in this process with the F-box protein *ScGrr1* mediating substrate specificity. Consistently, truncation of the carboxy-terminus or the CRIB domain of *ScGic2* leads to protein stabilization. However, the significance of *ScGic2* degradation is not clear. Overexpression of a stabilized *ScGic2* variant led to multiple buds on one cell thus *ScGic2* degradation may ensure that only one bud per cell cycle is formed (Jaquenoud et al., 1998).

In this study, we show that lack of the *AgCdc42* effector *AgGic1/2* results in delayed germ tube outgrowth and strongly reduced lateral branching in *A. gossypii* while hyphal extension is not altered. This finding suggests that *AgGic1/2* is important for polarity establishment but dispensable for sustained polar growth and maximal hyphal extension. *AgGic1/2* is probably degraded in *A. gossypii* since truncation of the carboxy-terminal domains that

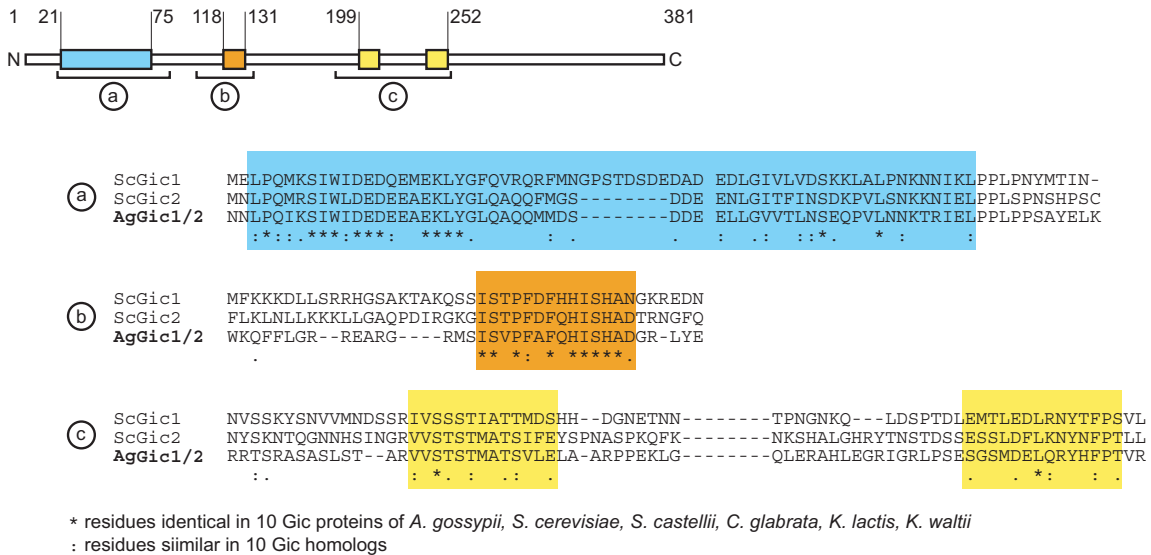


Fig. 2: Sequence analysis of *AgGic1/2*. The protein sequences of 10 GIC homologs of *A. gossypii*, *S. cerevisiae*, *Saccharomyces castellii*, *Candida glabrata*, *Kluyveromyces lactis*, *Kluyveromyces waltii*, and *Saccharomyces kluyveri* (<http://wolfe.gen.tcd.ie/ygob/>) were aligned using ClustalW. Only parts of the *A. gossypii* and corresponding *S. cerevisiae* sequences are shown that contain conserved amino acids (*) or amino acids that are similar for the ten Gic proteins (:). A conserved region shown in light blue was detected at the amino-terminus stretching the amino acids 21-75 of *AgGic1/2*. A second, shorter conserved sequence, which confers to the CRIB domain of *ScGic1* and *ScGic2*, reaches from amino acid 118 to 131 of *AgGic1/2* (orange box). Two short, conserved regions in the carboxy-terminal half of *AgGic1/2* are highlighted in yellow.

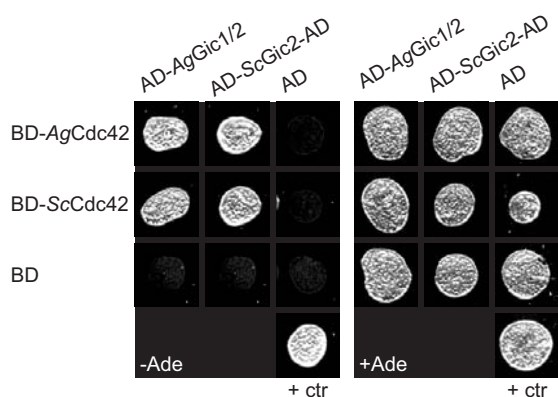


Fig. 3: *AgGic1/2* interacts with *AgCdc42* in a two-hybrid assay. *ScCdc42*^{Q61L} and *AgCdc42*^{Q61H} were fused to the DNA binding domain of *GAL4* (BD), *AgGic1/2* and *ScGic2* to the activator domain of *GAL4* (AD). 5 μ l liquid culture ($OD_{600} = 1$) of the yeast strain *PJ69-4a/α* harboring different combinations of binding- and activator domain fusions were spotted on minimal medium without adenine, which selects for interaction between bait and prey (left panel), or on plates with adenine as a growth control (right panel).

contain three PEST sequences led to an increase in *AgGic1/2* protein levels. We suggest a key role for *AgGic1/2* in regulation of lateral branching based on the finding that an *AgGIC1/2* allele lacking the part that encodes the PEST domains induces an increase in branching if expressed from a non-endogenous promoter.

Results

Deletion of *Aggic1/2Δ* does not influence radial growth speed.

The open reading frame encoding the putative *AgCdc42* effector *AgGic1/2* was deleted in *A. gossypii*. The radial growth of the mycelia was unaffected (figure 1). This was surprising since deletions of putative polarity factors in *A. gossypii* so far resulted without exception in decreased hyphal elongation rates or even lethality (Ayad-Durieux et al., 2000; Wendland and Philippsen, 2001; Knechtle et al., 2003; Bauer et al., 2004; Knechtle et al., 2006; Schmitz et al., 2006). A double deletion of the two syntenic *GIC* homologs in yeast, *ScGIC1* and *ScGIC2*, cannot grow at 37 °C (Brown et al., 1997; Chen et al., 1997). However, neither high nor low temperatures seemed to reduce the capacity of *Aggic1/2Δ* for radial growth compared to the reference strain (figure 1).

Three conserved regions can be identified in the protein sequence of *GIC* homologs.

The Gic proteins from budding yeast were initially identified in the yeast genomic sequence due to the presence of a CRIB domain that is typical for Cdc42 effectors. Strangely, no CRIB domain was predicted for *AgGic1/2* by InterProScan, a bioinformatics tool that integrates different protein signature recognition methods (Zdobnov and Apweiler, 2001) while CRIB domains were faithfully identified in *ScGic1* and *ScGic2* (data not shown). Ten syntenic *GIC* homologs were found in seven different yeast species (Dietrich et al., 2004; Byrne and Wolfe, 2006). Multiple alignment of the predicted protein

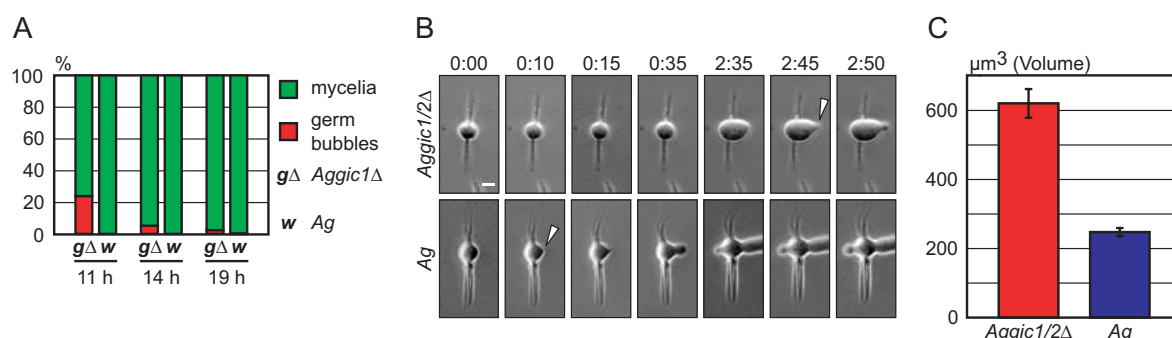


Fig. 4: Deletion of *AgGIC1/2* delays germ tube outgrowth. (A) Spores of *Aggic1/2Δ* (*gΔ*) and the reference strain (*w*) were spread on agar plates and inoculated for the given times at 30 °C. 150 spores that germinated were counted per time point and strain, the ratio between cells that still were in the germ-bubble phase (red) and cells that formed at least a germ tube (green) are shown. (B) Spores of *Aggic1Δ* and the reference strain (*Ag*) were spread on AFM agar, covered with a glass slide and incubated at 25 °C. The first pictures were acquired 10 hours after spore inoculation. Pictures were acquired every 5 minutes, time is given in hours. The arrowheads depict the emerging germ tubes in both strains. Scale bar = 5 μ m. (C) The volume of *Aggic1/2Δ* and reference strain spores (*Ag*) in the last frame prior to germ tube emergence was estimated. The bars represent the average volume, the bars the standard error ($n = 9$ and $n = 10$ respectively). The shape of the germ bubble was approximated as a prolate ellipsoid. The volume was calculated as $4/3\pi ab^2$ with a being the long and b the short axis of the ellipsoid.

sequences with ClustalW (Thompson et al., 1994) revealed the presence of three conserved regions. In figure 2, sequences of *AgGic1/2* and *S. cerevisiae* Gic1 and Gic2 are shown that contain conserved amino acids (marked with asterisks). The amino-terminal conserved region, which we will call GCN (Gic conserved amino-terminus) during this study, comprises amino acid 21 to 75 in *AgGic1/2* (figure 2a). Another conserved region from amino acid 118 to 131 corresponds to the CRIB domains of *ScGic1* and *ScGic2* (figure 2b, Brown et al., 1997; Chen et al., 1997). Therefore, *AgGic1/2* might contain a CRIB domain despite the fact that protein sequence analysis tools did not predict one. The carboxy-terminal halves of the Gic proteins are more diverged showing only two short, conserved sequence segments between amino acids 199 and 252 of *AgGic1/2* (figure 2c). This observation will be discussed later together with the phenotype of the carboxy-terminal deletion.

***AgGic1/2* interacts with *AgCdc42*.**

The fact that some amino acids that are characteristic for CRIB domains are conserved in *AgGic1* does not necessarily imply that *AgGic1/2* does bind to *AgCdc42*. In a two-hybrid assay it was tested whether *AgGic1/2* physically interacts with *AgCdc42* using the yeast proteins *ScGic2* and *ScCdc42* as positive controls. Both *CDC42* genes carried a mutation that abolished GTP hydrolase activity of the encoded proteins thus locking them in the GTP-bound state that binds to effectors. Furthermore, the four last amino acids were truncated to prevent geranylgeranylation and thus membrane localization. *AgCdc42* interacted with both *AgGic1/2* and with *ScGic2*. Similarly, *ScCdc42* interacted with both Gic proteins (figure 3). This finding confirms that *AgGic1/2* is an effector of the key polarity factor *AgCdc42* suggesting that *AgGIC1/2* is involved in cell polarity signaling pathways.

***Aggic1/2Δ* displays a defect in polarity establishment.**

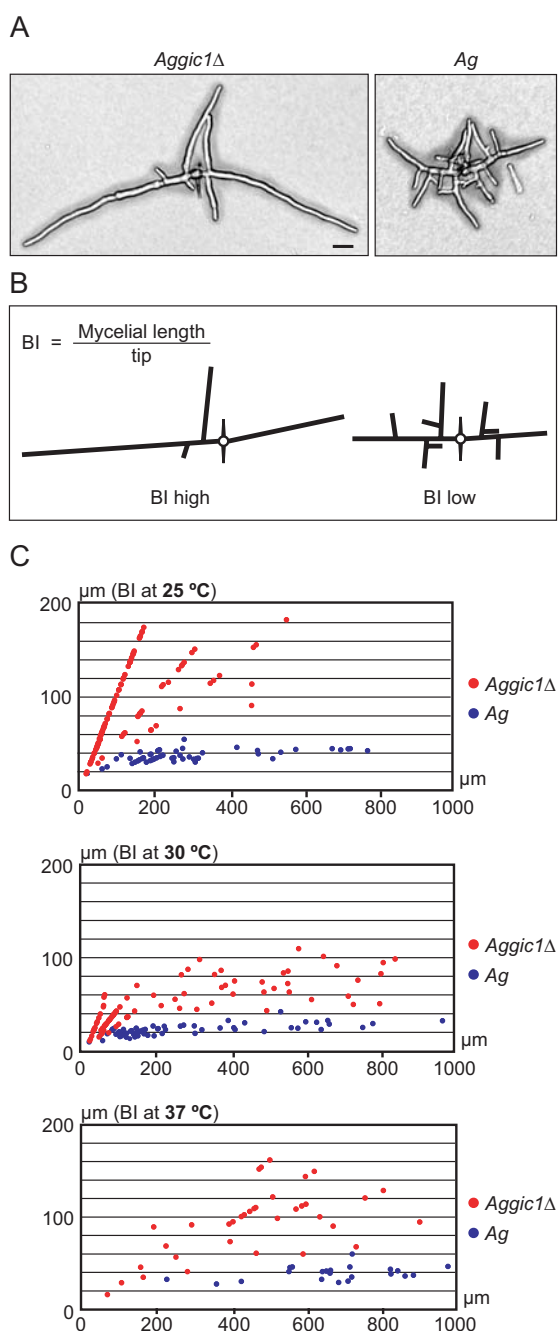
As we could not see an effect of *Aggic1/2Δ* on radial growth on AFM agar plates, we wondered whether *Aggic1/2Δ* has an effect on germination or development of young *A. gossypii* mycelia rather than affecting adult, fast growing mycelium. Germination of the needle-shaped *A. gossypii* spores is initiated by formation of a spherical germ bubble, two germ tubes sequentially emerge at opposite sites perpendicular to the spore needle. While the germ tubes continue to elongate, new sites of cell polarity are established resulting in the emergence

of lateral branches and thus formation of a mycelium (Knechtle et al., 2003; Wendland and Walther, 2005). *Aggic1/2Δ* strains were compared to the reference strain by following the development of spores that had been spread on AFM agar plates. After eleven hours of incubation at 30 °C, all germinating spores from the reference strain have formed at least one germ tube (n = 150). In contrast, germ bubbles of the *Aggic1Δ* strain still lacked a germ tube in many cases. This effect was quantified by assessing more than 150 spores that germinated per time-point and per strain (figure 4A). The amount of cells that displayed at least one germ tube in the *Aggic1/2Δ* strain increased over time (figure 4A) from 76 % after 11 hours to 98 % after 19 hours of incubation. Therefore, most cells did not die during the germ bubble stage. Rather, establishment of germ tubes seems delayed in *Aggic1/2Δ*. Time-lapse movies of germinating spores were acquired to find out whether isotropic growth that leads to germ bubble expansion or germ tube emergence was disturbed (figure 4 B). While germ tubes emerged from spores of the reference strain, germ bubbles of *Aggic1/2Δ* continued isotropic growth. As a consequence, the volume of *Aggic1/2Δ* germ bubbles just prior to germ tube emergence was $620 \pm 42 \mu\text{m}^3$ while germ bubbles of the reference strain had a volume of $248 \pm 11 \mu\text{m}^3$ (mean \pm S.E., n = 9 and n = 10 respectively, figure 4C). This observation suggests that the isotropic growth phase in *Aggic1/2Δ* is prolonged due to delayed germ tube emergence leading to larger germ bubbles. Evidently, outgrowth of a germ tube requires establishment of cell polarity at the corresponding site of the cortex. If polarity establishment was disturbed in *Aggic1/2Δ* mutants, formation of lateral branches should be affected as well since lateral branch emergence requires the establishment of new sites of cell polarity at the cortex of existing hyphae. Indeed, young reference strain and *Aggic1/2Δ* mycelia of the same age appeared differently, *Aggic1/2Δ* established much less branches than the reference strain (figure 5A).

Table 1: PEST domains in *AgGic1/2*

aa of <i>AgGic1/2</i>	PEST score*	Sequence
259 – 270	6.57	REEPPAAFETPR
324 – 336	10.23	KETFTESQTPNER
347 – 362	7.66	HQGETDSTLTGPNR

* PEST score ranges from -50 to + 50, values > 5 are considered as good hits (<https://embl.bcc.univie.ac.at/toolbox/pestfind.htm>)



We quantified this effect by assaying the branching index (BI; Trinci, 1970), which is defined as the total length of the mycelium divided by the number of hyphal tips. The branching index is a reciprocal value. If a mycelium displays few tips for a given total mycelial length, the branching index is high. If many tips are observed for the same total mycelial length, the branching index is low (figure 5B). Hyphal elongation increases the branching index while establishment of new branches leads to a decrease of this ratio. After germination, the branching index increases until it reaches a plateau

Fig. 5: Deletion of *AgGIC1/2* reduces lateral branching. (A) Mycelia that grew for 14 hours at 30 °C from an *Aggic1Δ* and from a reference strain (*Ag*) spore. Scale bar = 20 μm. (B) The branching index is defined as total hyphal length divided by the number of tips. Two mycelia of equal total hyphal length are outlined. The mycelium on the left has fewer tips and thus a higher branching index than the mycelium on the right. (C) The branching index of *Aggic1Δ* mycelia (red dots) and reference strain mycelia (*Ag*, blue dots) was determined at 25 °C, 30 °C and 37 °C (represented by three graphs). Total hyphal lengths and associated tip numbers were assayed for individual mycelia between 11 and 21 hours after spreading of the spores depending on the incubation temperature. The branching index (BI) was calculated and plotted against mycelial length. All numbers are given in μm.

where tip growth and lateral branch establishment counterbalance each other. The branching index is plotted as a function of total mycelial length in figure 5C, one dot represents one measurement of one mycelium. Obviously, the branching indices of an *Aggic1/2* strain (figure 5C, red dots) were higher than the branching indices of the reference strain (figure 5C, blue dots) for a given mycelial length. The effect was most pronounced at 25 °C where virtually no lateral branches were observed for *Aggic1/2Δ*. Interestingly, the branching index of the reference strain depended on temperature and was higher at 25 °C than at 30 °C or 37 °C. To summarize, deletion of *AgGIC1/2* interferes with polarity establishment leading to delayed outgrowth of germ tubes and reduced numbers of lateral branches. However, constant polar growth was not affected by the lack of *AgGic1/2*. These observations raise the question how an *Aggic1/2Δ* strain can form a normal mycelium despite a defect in generation of new hyphal tips?

Tip splitting is not disturbed by deletion of *AgGIC1/2*.

A. gossypii not only generates new hyphal tips by polarity establishment along the hyphal cortex as described above but also by symmetrical splitting of growing tips forming Y-shaped bifurcations. This so-called tip splitting does not take place in young mycelia but is the main mode for generation of new tips in older mycelium, for example at the border of growing colonies (Knechtle et al., 2003; Philippsen et al., 2005; Schmitz et al., 2006). Surprisingly, tip splitting was observed in *Aggic1/2Δ* strains earlier than in the reference strain (movie S3, figure 6A). After incubation on AFM agar for 13 hours, 22.8 % of all *Aggic1/2Δ* mycelia have undergone tip splitting at least once while no tip splitting event was observed in mycelia of the reference strain ($n > 250$, data not shown). For the wild type, growth speed of hyphae that performed tip splitting

Table 2: Branching index of K38, K39 and K40

Strain	BI*	Length**	n
K38 (<i>AgGIC1/2ΔC</i>)	42.8 ± 2.0 μm	462 μm	40
K39 (<i>AgGIC1/2ΔC-YFP</i>)	42.5 ± 1.5 μm	419 μm	45
K40 (<i>AgGIC1/2-YFP</i>)	58.0 ± 4.2 μm	429 μm	38
reference strain	41.1 ± 2.2 μm	480 μm	27
<i>Aggic1Δ</i>	90.0 ± 12.4 μm	190 μm	20

* BI was measured on mycelia that grew at 25 °C for 17 h and for 21 h. Mean ± S.E.

** Average length of the assessed mycelia

was above 1.4 μm/min (Schmitz et al., 2006). Thus it is either possible that an *Aggic1/2Δ* strain reaches the elongation speeds that are associated with tip splitting earlier or, alternatively, aberrant tip splitting occurs in this strain at lower hyphal growth speeds. To distinguish these two options, we measured the growth speed of hyphae during a time interval of ten minutes prior to splitting in time-lapse movies. The speed of *Aggic1/2Δ* hyphae prior to tip splitting was 1.80 ± 0.06 μm/min (mean ± S.E., n = 17 from 4 movies), which is very similar to the 1.85 ± 0.04 μm/min (mean ± S.E., n = 6 from 2 movies) measured for the reference strain as shown in figure 6B. Hence, tip splitting occurs at normal growth speeds in *Aggic1/2Δ* but hyphal elongation rates that are characteristic for this event are reached much earlier during mycelial development.

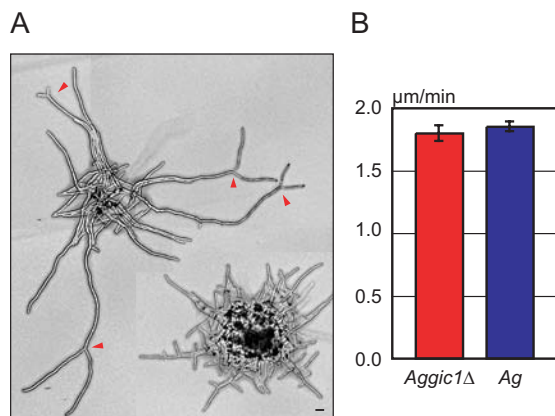


Fig. 6: Tip splitting in *Aggic1/2Δ*. (A) An *Aggic1/2Δ* (upper left) and a reference strain mycelium (lower right) 19 hours after spore inoculation at 30 °C. Tip splitting events were observed in most of the *Aggic1/2Δ* mycelia while they were rare in reference strain mycelia of that age. Tip splitting can be recognized by the characteristic Y-shaped bifurcation (arrowheads) and by the similar length of the two branches that originate from a tip splitting. (B) Comparison of hyphal growth speeds prior to tip branching. Time-lapse movies from four *Aggic1/2Δ* mycelia and two reference strain mycelia that grew from a single spore were analyzed. The bars represent the average growth speed in a ten minutes time period prior to tip branching for *Aggic1/2Δ* and the reference strain (*Ag*) respectively. Error bars represent the S.E.

Truncation of the carboxy-terminal PEST domains of *AgGic1/2* leads to increased protein levels.

As mentioned before, the amino-terminal halves of proteins encoded by *GIC* homologs are conserved while the carboxy-termini show more variation between species. We were able to identify three PEST domains in the *AgGic1/2* carboxy-terminus (table 1) using the PESTfind bioinformatic tool (Rogers et al., 1986). PEST domains contain proline, aspartate or glutamate and serine or threonine and are not interrupted by positively charged amino acids. They are found in proteins that are polyubiquitinated and subsequently degraded by the 26S proteasome and were shown to mediate a decreased protein half-life period (reviewed by Rechsteiner and Rogers, 1996). Interestingly, the carboxy-terminus of *ScGic2* was reported to mediate proteasome-mediated degradation upon phosphorylation and subsequent ubiquitination (Jaquenoud et al., 1998) though the PESTfind software did not find a PEST domain for *ScGic2* or *ScGic1*. In a first step, we deleted the region of *AgGIC1/2* that encodes the three predicted PEST domains and the two small, conserved regions in the *AgGic1/2* carboxy terminus. The resulting construct will be referred to as *AgGIC1/2ΔC* (figure 7A). Replacement of *AgGIC1/2* with *AgGIC1/2ΔC* did not influence radial growth speed or morphogenesis (figure 7B and 7C). Furthermore, the branching index of mycelia expressing *AgGIC1/2ΔC* was identical to the reference strain, even at 25 °C where the *Aggic1/2Δ* phenotype is most pronounced. The average branching indices are given in table 2 together with the average total length of the assessed mycelia. This finding shows that the carboxy-terminally truncated *AgGic1/2ΔC* is functional. We further wanted to test whether deletion of the PEST domains influences protein abundance. YFP was fused to the carboxy-terminus of both *AgGic1/2* and *AgGic1/2ΔC*. Both strains displayed wild-type radial growth (figure 8A). Branching was frequently observed at 25 °C

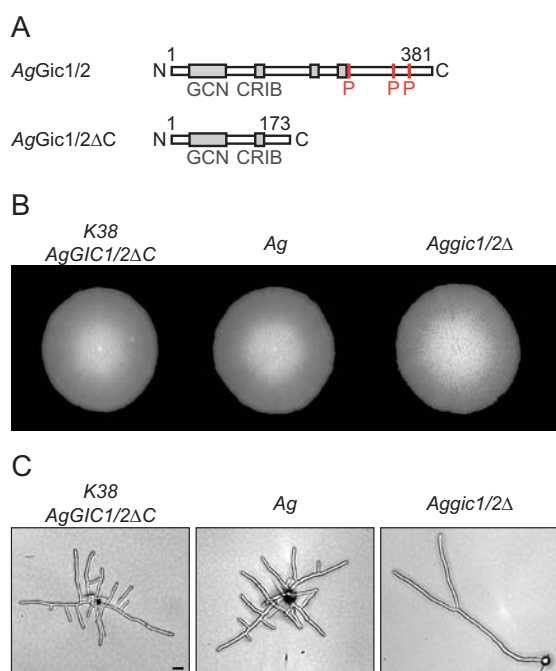


Fig. 7: The *AgGic1/2* carboxy terminus contains three PEST domains and is not necessary for *AgGic1/2* function. (A) Schematic representation of *AgGic1/2* and *AgGic1/2ΔC* lacking the amino acids 174 – 381 of *AgGic1/2*. The grey boxes represent the conserved GCN, the CRIB domain and the conserved carboxy-terminal residues. The letter P indicates the location of PEST domains (see also table 1). (B) Radial growth after 6 days at 30 °C of K38 (*AgGIC1/2ΔC*), the reference strain (*Ag*) and *Aggic1/2Δ*. (C) Spores from K38, the reference strain (*Ag*) and *Aggic1/2Δ* were inoculated for 21 hours at 25 °C. The corresponding branching indices are shown in table 2.

for both *AgGIC1/2-YFP* and *AgGIC1/2ΔC-YFP* (figure 8B) thus both YFP fusions were functional. Nevertheless, a slightly elevated branching index was seen for *AgGIC1/2-YFP* (table 2) thus indicating that a carboxy-terminal YFP fusion to full length *AgGic1/2* resulted in a mild polarity establishment defect. Protein levels were estimated by western blotting. The *AgGic1/2-YFP* band was weak while the band corresponding to *AgGic1/2ΔC-YFP* was intense thus truncation of the PEST domains led to elevated levels of *AgGic1/2ΔC-YFP* (figure 8C). This finding was confirmed microscopically, *AgGic1/2-YFP* was barely detectable while the *AgGic1/2ΔC-YFP* intensity was rather high (not shown). Since deletion of *AgGIC1/2* displays fewer branches, one would expect *AgGic1/2-YFP* at sites of branch outgrowth. Time-lapse movies were acquired of *AgGIC1/2ΔC-YFP* due to the weak *AgGic1/2-YFP* signal (movie S4). As shown in figure 8D, *AgGic1/2ΔC-YFP* accumulated at the cortex prior to outgrowth of a lateral branch as expected. Surprisingly, *AgGic1/2ΔC-YFP* was seen also at

hyphal tips but not at sites of septation (figure 8E). The tip localization cannot be a consequence of the carboxy-terminal truncation of *AgGic1/2ΔC-YFP* since a YFP-fusion to the full length *AgGic1/2* also localized to hyphal tips (figure 8E).

Expression of *AgGIC1/2* alleles from the *AgCDC42* promoter.

The deletion phenotype of *Aggic1/2Δ* could be explained by two different mechanisms. First, *AgGic1/2* may work as a simple adapter between *AgCdc42* and effectors. In this case, overexpression of *AgGic1/2* would have no effect on the branching index. However, *AgGic1/2* may function in the decision making process whether a branch is established at a certain site or not. In this case, overexpression of *AgGic1/2* might lead to an increase in lateral branching and thus to a decrease of the branching index. In order to elevate *AgGic1/2* levels, the *AgCDC42* promoter was inserted in front of GFP-*AgGIC1/2* and GFP-*AgGIC1/2ΔC* (figure 9A). About nine times more *AgCDC42* than *AgGIC1/2* mRNA is present in nine hours old mycelia (Riccarda Rischatsch, unpublished results), thus the *AgCDC42* promoter is likely to be stronger than the *AgGIC1/2* promoter while minimizing the risk that overexpression of *AgGIC1/2* leads to titration of *AgCdc42* as it was observed for yeast where expression of a carboxy-terminally truncated *ScGIC2* allele from the *ScGAL1* promoter is lethal (Jaquenoud et al., 1998). Replacement of *AgGIC1/2* with both GFP-*AgGIC1/2* and GFP-*AgGIC1/2ΔC* under the control of the *AgCDC42* promoter did not disturb radial expansion of the mycelium on AFM agar plates (figure 9B), both GFP-*AgGic1/2* and GFP-*AgGic1/2ΔC* localized to hyphal tips (figure 9C). However, the GFP-intensities of both fusion proteins were similar to the fluorescence intensities of the corresponding carboxy-terminally tagged fusion constructs that are expressed from the native promoter (not shown). Western blot analysis of strains expressing GFP alleles confirmed the observation that expression of the amino-terminally tagged *AgGIC1/2* alleles under the control of the *AgCDC42* promoter did not result in an increase of protein levels (figure 9D). Interestingly, we observed a double-band for *AgGic1/2-GFP* and *AgGic1/2ΔC-GFP* (figure 9D, marked by asterisk) that could represent a phosphorylated state. Since protein levels of GFP-*AgGic1/2* and GFP-*AgGic1/2ΔC* respectively were not drastically increased, we did not expect tremendous changes of the branching indices in these strains. Indeed, young mycelia of both GFP-*AgGIC1/2*

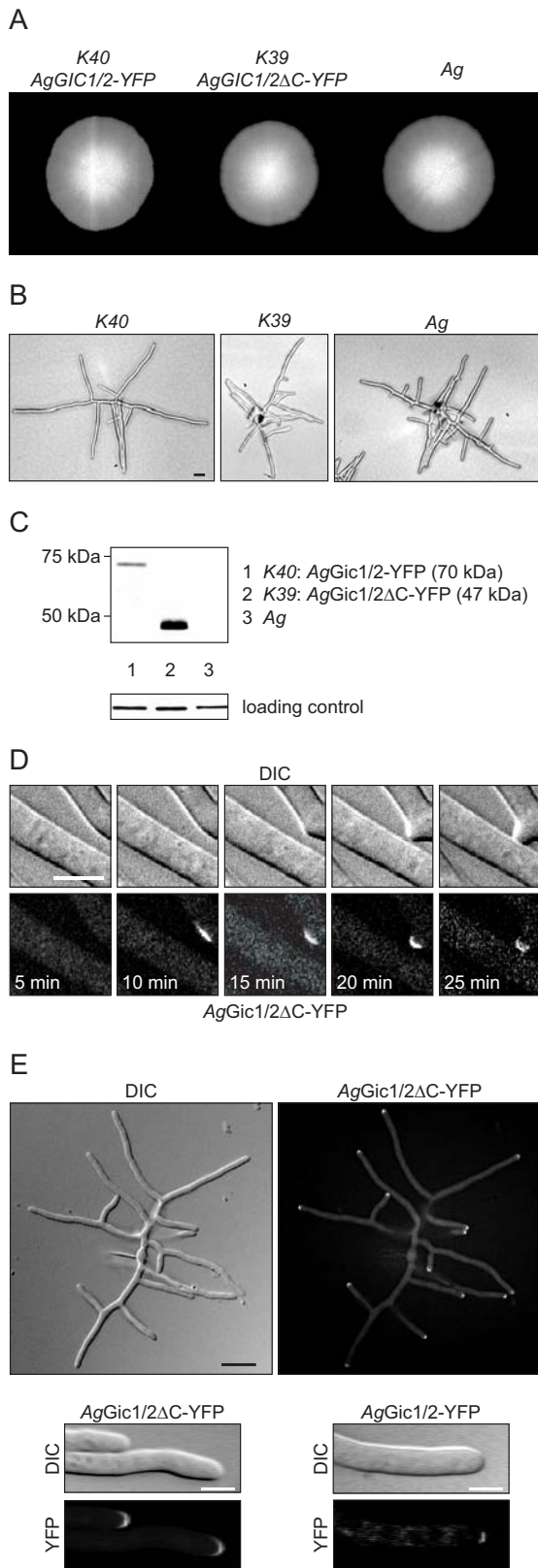


Fig. 8: YFP-fusions to *AgGic1/2* and *AgGic1/2ΔC* localize to hyphal tips. (A) Radial growth of *K40* (*AgGIC1/2-YFP*), *K39* (*AgGIC1/2ΔC-YFP*) is normal. Mycelium was inoculated for 6 days at 30 °C. (B) Spores from *K40*, *K39* and the reference strain (*Ag*) were inoculated for 21 hours at 25 °C. The corresponding branching indices can be found in table K38-K40. (C) Western blot probed with antiGFP. 100 μg protein from *K40*, *K39* and the reference strain (*Ag*) grown for 16 hours in liquid medium at 30 °C were separated and transferred to a nitrocellulose membrane. *AgGic1/2-YFP* has a predicted molecular weight of 70 kDa, *AgGic1/2ΔC-YFP* of 47 kDa. A 105 kDa band that crossreacts with antiGFP from Roche was used as a loading control. (D) Frames from a time-lapse movie (movie S4) showing establishment of a lateral branch in a strain expressing *AgGic1/2ΔC-YFP*. Scale bar = 5 μm. (E) Young *K39* mycelium that grew from a spore. *AgGic1/2ΔC-YFP* can be seen at hyphal tips but not at sites of septation. Scale bar = 20 μm. (D) *AgGic1/2ΔC-YFP* and *AgGic1/2-YFP* localize to hyphal tips.

and GFP-*AgGIC1/2ΔC* strains appeared normal (figure 9E). Nevertheless, we measured a reduced branching index for GFP-*AgGIC1/2ΔC* compared to both the reference strain and GFP-*AgGIC1/2* (table 3). A similar effect was observed if the branching index was assessed for mycelia that grew at 23 °C (figure 9F). A two sample t-test confirmed this differences to be significant with p-values smaller than 0.001 for the 30 °C measurements and smaller than 0.01 for the 23 °C measurements. In summary, GFP-*AgGIC1/2ΔC* that is expressed under the control of the *AgCDC42* promoter decreases the branching index thus suggesting that *AgGic1/2* may have a regulatory function in morphogenesis.

Discussion

We show that the *AgCdc42* effector *AgGic1/2* is important for cell polarity establishment but dispensable for fast hyphal elongation and thus polarity maintenance. To our knowledge, *Aggic1/2Δ* is the first mutation that displays a severe reduction in establishment of cell polarity without affecting polarity maintenance. Furthermore, *AgGic1/2* degradation is likely to be mediated by its carboxy-terminal PEST domains, which are not predicted in the homologous yeast proteins *ScGic1* and *ScGic2*. We speculate that *AgGic1/2* might have a regulatory function in branch initiation based on the finding that an *AgGIC1/2* allele lacking the part that encodes the PEST domains induces a slight increase in branching if expressed from a non-endogenous promoter.

AgGic1/2 is an *AgCdc42* effector.

Sequence alignments indicate two conserved regions in the amino-terminal half of *AgGic1/2*, the

GCN (Gic1/2 conserved amino-terminus) and the CRIB domain. We showed in a two-hybrid assay that *AgGIC1/2* was able to bind to *AgCdc42* thus the CRIB domain is likely to be functional despite the failure of protein sequence analysis tools to predict it. Therefore, it is likely that *AgGic1/2* is a *Cdc42* effector like the yeast *Gic* proteins. The GCN lies between the CRIB domain and the amino-terminus of *Gic* proteins. It is possible that the GCN mediates interaction of *AgGic1/2* with the polarisome since mutation of a conserved tryptophan in yeast abolishes interaction of *ScGic2* with the polarisome components *ScBud6* and *ScPea2* but not with *ScCdc42* (Jaquenoud and Peter, 2000).

***AgGic1/2* is involved in cell polarity establishment but is not needed for maximal polar growth.**

Deletion of *AgGIC1/2* had two effects: Germ bubbles grew isotropically to more than twice the volume of the reference strain prior to establishment of a germ tube (figure 10, 8 h), and the generation of lateral branches that emerge from the cortex of an already existing hypha was severely reduced (figure 10, 12 h). Both observations indicate that absence of *AgGic1/2* reduces but does not abolish establishment of new sites of polar growth. Formation of lateral branches is disturbed at a very early stage of branch formation since localization of the two cell polarity markers *AgBem1*-GFP or

Fig. 9: Expression of *GFP-AgGIC1/2* and *GFP-AgGIC1/2ΔC* under the control of the *AgCDC42* promoter. (A) Schematic representation of the *AgGIC1/2* locus in the strains *K77* ($P_{AgCDC42}$ -*GFP-AgGIC1/2*) and *K79* ($P_{AgCDC42}$ -*GFP-AgGIC1/2ΔC*). The amino-terminal GFP fusions are expressed under the control of the *AgCDC42* promoter. (B) Radial growth of *K77* and *K79* is normal. Mycelium was inoculated for 6 days at 30 °C. (C) Both *GFP-AgGic1/2* and *GFP-AgGic1/2ΔC* localize to hyphal tips. Scale bar = 5 μm. (D) Western blot probed with antiGFP comparing protein levels of strains expressing *AgGIC1/2-GFP* and *AgGIC1/2ΔC-GFP* from the endogenous promoter with strains that express amino-terminal fusions from the *AgCDC42* promoter. The arrowheads denote the bands that confer to GFP-fusions to full length *AgGic1/2*, the open arrowheads GFP fusions to *AgGic1/2ΔC*. The asterisks mark double-bands that are specifically observed in carboxy-terminal GFP-fusions. 100 μg protein isolated from 15 hours old liquid cultures grown at 30 °C were separated and transferred to a nitrocellulose membrane. A 105 kDa band that crossreacts with the antiGFP antibody from Roche was used as a loading control. (E) Mycelia that grew from spores of *K77*, *K79*, the reference strain (*Ag*) and *Aggic1/2Δ* inoculated for 15 hours at 30 °C. The corresponding branching indices are shown in table 3. (F) Branching index comparison of *K79* that expresses *GFP-AgGIC1/2ΔC* under the control of the *AgCDC42* promoter with *K77* and the reference strain (*Ag*). The bars represent the branching indices of the strains denoted below, the error bars represent the S.E. The branching index of *K79* was lower than *K77* or the reference strain respectively ($p < 0.0007$ and $p < 0.0002$, Welch two-sample t-test) at 30 °C and at 23 °C ($p < 0.003$, Welch two-sample t-test).

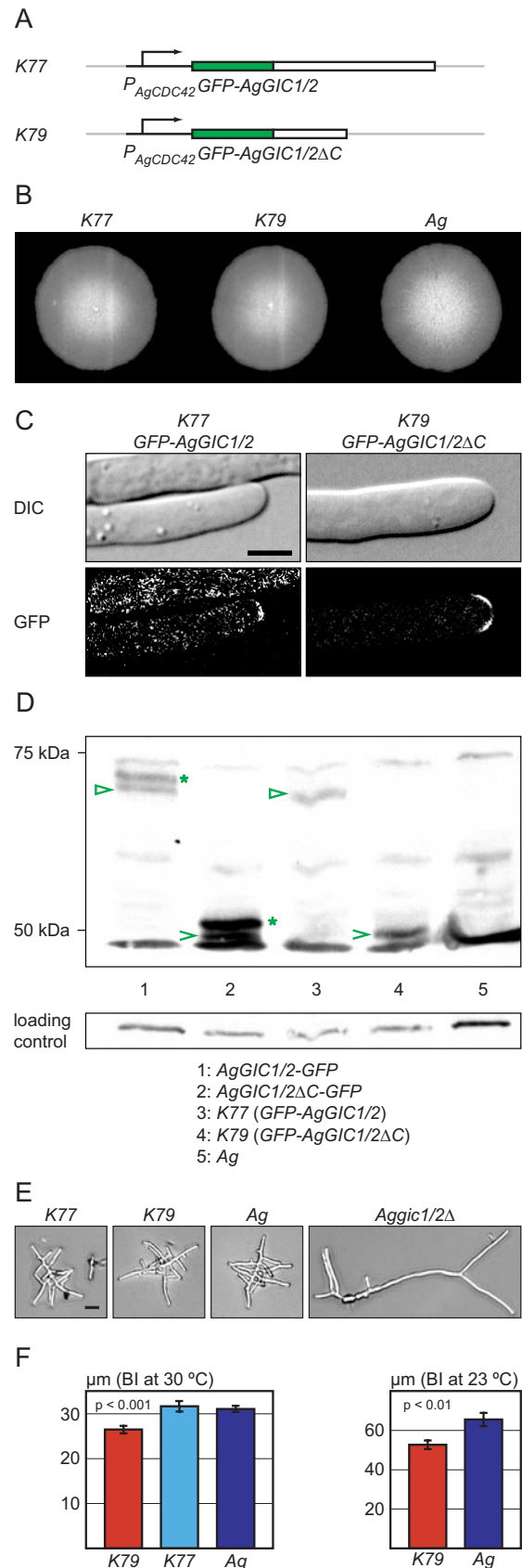


Table 3: Branching index of K77 and K79

Strain	BI*	Length**	n
<i>K77 (GFP-AgGIC1/2)</i>	31.6 ± 1.2 μm	395 μm	31
<i>K79 (GFP-AgGIC1/2ΔC)</i>	26.5 ± 0.8 μm	415 μm	22
reference strain	31.1 ± 0.7 μm	453 μm	24
<i>Aggic1Δ</i>	89.2 ± 8.1 μm	874 μm	20

* BI was measured on mycelia that grew at 30 °C for 15 h. Mean ± S.E.

** Average length of the assessed mycelia

AgSpa2-GFP to sites at the hyphal cortex was not observed in an *Aggic1/2Δ* strain (Winkler, 2007). In yeast, *ScGic1* and *ScGic2* interact with the septin *ScCdc12* and are involved in septin recruitment. We were not able to detect an effect of the *Aggic1/2* deletion on localization of the septin *AgShs1-GFP* during preliminary experiments (data not shown). Septa, which are chitinous partition walls that are preceded by septin rings, are spaced with the same distance as they are in the reference strains and appear undisturbed (Winkler, 2007). These findings however do not exclude that *AgGic1/2* is involved in septin recruitment or organization in *A. gossypii*. This is supported by the fact that also in yeast, septins can be recruited by a *Gic*-independent pathway (Iwase et al., 2006).

As in wild type, hyphae that form a mature *Aggic1/2Δ* mycelium arise by tip splitting. Tip splitting is not observed in young mycelia but is the main mode of branching if hyphal growth speeds reach values of about 1.4 μm/min (Schmitz et al., 2006). To our surprise, tip splitting happened earlier in *Aggic1/2Δ* than in the reference strain after inoculation of spores (figure 10, 12 h). The time span between the first polarity establishment and the first tip splitting event was thus massively shortened in *Aggic1/2Δ* as indicated by the square bracket in figure 10. However, the hyphal growth speeds prior to tip splitting were identical for *Aggic1/2Δ* and the reference strain. Thus, *Aggic1/2Δ* reached growth speeds necessary for tip splitting sooner after germination rather than displaying aberrant tip splitting at lower hyphal extension rates. It was reported by Knechtle et al., 2003) that emergence of a lateral branch is accompanied by a reduction in growth speed of the main hypha, presumably because resources are redirected to newly emerging branches. The reduction in lateral branches observed in *Aggic1/2Δ* may thus allow the hyphae to accelerate faster and subsequently to reach speeds associated with tip splitting earlier than the wild type.

The carboxy-terminal PEST domains of *AgGic1/2* mediate protein degradation.

The carboxy-terminal half of *Gic*-proteins is less conserved than the amino-terminal part. Sequence analysis of the *AgGic1/2* carboxy-terminus revealed three PEST motives that were not conserved in *S. cerevisiae*. *AgGic1/2ΔC*, which lacks the PEST domains, had no effect on the branching index and thus is functional. As expected, protein levels of *AgGic1/2ΔC* were higher than *AgGic1/2* indicating that the PEST motives indeed mediate protein instability. In yeast, despite the absence of a predictable PEST domain, *ScGic2* is at least partially degraded after bud emergence. Upon phosphorylation, *ScGic2* is polyubiquitinated and targeted to the proteasome. *ScGic1* is stable but displays cell-cycle dependent modifications. (Jaquenoud et al., 1998; Hofken and Schiebel, 2004). It is unlikely that *AgGic1/2* levels are coupled to the nuclear cycle in *A. gossypii* since nuclei that share a common cytoplasm are in different stages (Gladfelter et al., 2006). However, it might be possible that *AgGic1/2* is degraded upon a yet to be defined signal as will be discussed later. Furthermore, the conserved amino-termini of *Gic* proteins may link *Cdc42* to the polarisome and septins while the carboxy-termini are more variable, which might reflect the need to regulated *Gic* proteins differently.

Carboxy-terminally truncated *AgGic1/2* that is expressed from the *AgCDC42* promoter leads to a decreased branching index.

AgGic1/2 could be an adaptor between *AgCdc42* and other factors. However, *AgGic1/2* protein levels might have a regulatory function in branch initiation and germ tube emergence. This hypothesis was tested with the attempt to overexpress *AgGIC1/2* from the *AgCDC42* promoter. In 9 hours old mycelia, *AgCDC42* mRNA is 9 times more abundant than *AgGic1/2* mRNA. However, protein levels of the *AgGIC1/2* alleles that were expressed from the *AgCDC42* promoter were not increased.

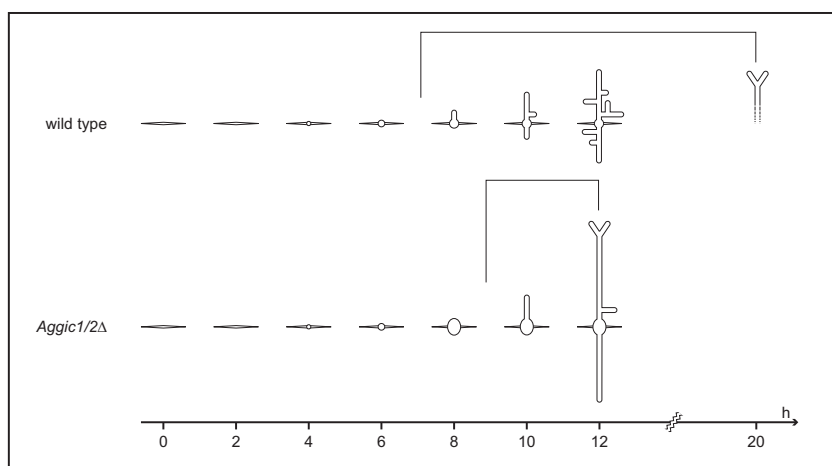


Fig. 10: Overview: development of wild type and *Aggic1/2Δ*. Early development of wild type and *Aggic1/2* are compared. The timeline indicates time in hours after inoculation of spores on AFM agar at 30 °C. Note that the timing of the developmental steps strongly depends on environmental factors and differs between experiments. The square brackets indicate the time span between germ tube emergence and the first apical branching in both strains.

This might have several reasons: mRNA abundance is not only regulated by the rate of transcription but also by mRNA stability, which might account for the difference in mRNA abundance between *AgGIC1/2* and *AgCDC42* rather than a difference in promoter strength. Furthermore, the carboxy-terminally labeled *AgGic1/2* proteins might be artificially stabilized by the GFP tag or else, *AgGic1/2* levels might be tightly regulated in the cell and the *AgGic1/2* surplus is very efficiently degraded. The observation that, independent of the promoter, the ratio between stabilized *AgGic1/2ΔC* that lacks the PEST domains and full length *AgGic1/2* is similar argues against the latter two possibilities unless a second, PEST independent degradation pathway exists. Though we could not see an increase in *AgGic1/2* levels, we were able to see a small decrease of the branching index if *AgGic1/2ΔC* was expressed from the *AgCDC42* promoter. This means that more sites of polarity were established in this strain, which supports the hypothesis that *AgGic1/2* might have a regulatory function in branch establishment. However, the effect was rather small, future experiment will show whether higher concentrations of *AgGic1/2* will be able to induce hyperbranching. Recently, a regulable promoter was described for *A. gossypii* (Dunkler and Wendland, 2007) that may be helpful to further specify the role of *AgGic1/2* in polarity establishment.

Suggested roles of *AgGic1/2* in *A. gossypii* morphogenesis.

AgGic1/2ΔC was observed at sites where new lateral branches emerged, which is consistent with the observation that *AgGic1/2* is involved in polarity establishment. However, GFP-fusions to full length and truncated *AgGic1/2* also localized to hyphal tips, which could mean that *AgGic1/2* has

a redundant function at this cellular location. It is likely that *AgGic1/2* binds to activated *AgCdc42* at growing tips since *AgCdc42* and its GEF, *AgCdc24*, are found at this location (part I, figure 11). Furthermore, it is known from yeast that *ScGic2* is only phosphorylated and degraded upon interaction with activated *ScCdc42*. Hence, one can speculate that growing *A. gossypii* tips represent sites that degrade *AgGic1/2*. Consequently, the *AgGic1/2* concentration would be lower in the proximity of growing hyphal tips, which is represented by low *AgGic1/2* activity (white color) in figure 11. Lack of *AgGic1/2* would make outgrowth of lateral branches at this site unlikely. However, *AgGic1/2* concentration would be higher at sites that are further away from the hyphal tips (purple color, figure 11). There, potential branching sites (arrowheads, figure 11) could be activated. As soon as a branch is established, *AgGic1/2* is degraded in this region leading to a drop in *AgGic1/2*-activity, and branching in the proximity of the new tip becomes very unlikely (figure 11A2). As soon as the newly established hypha reached a certain length, *AgGic1/2* levels would rise again enabling establishment of more lateral branches (figure 11A3 and 11A4). This model would explain the observation that genetically identical spores that are spread on a homogenous AFM agar surface give rise to mycelia that are easily distinguishable from one another though general parameters like the branching index are similar between individuals. There are always small fluctuations in the system that allow outgrowth of a lateral branch from a potential branching site. As soon as the branch is established, *AgGic1/2* might be degraded in this region in an *AgCdc42*-dependent manner making it very unlikely for a second branch to emerge. Such a rather simple mechanism would be sufficient to generate a balance between hyphal elongation and

polarity establishment without the need of a fixed body plan like it is present in higher eukaryotes. Additional to the local regulation of branching, *AgGic1/2* might serve as global regulator that allows *A. gossypii* to adjust cell morphology to its environment. Indeed, it is frequently observed that *A. gossypii* shows few lateral branches under certain conditions. Reduced branching is observed for dense *A. gossypii* cultures or for mycelia that are grown on glass-covered microscopy slides where oxygen and nutrients presumably are low. Thus, it might be possible that *A. gossypii* adapts its morphology to harsh or competitive conditions by reducing lateral branches and thereby focusing growth on fewer tips that might reach regions with more benign conditions. Starvation, low oxygen, quorum or other signals might be associated with low levels of *AgGic1/2* (figure 11B, left branch) and consequently with a reduction in lateral branches. Alternatively, it is possible that favorable conditions might stabilize *AgGic1/2* (figure 11B, right branch). It was shown that *A. gossypii* reacts to starvation with a decrease of the nuclear density that is mediated by *AgSwe1*-dependent inhibition of the *A. gossypii* cyclin dependent kinase (Helfer and Gladfelter, 2006), maybe controlled *AgGic1/2* degradation constitutes a pathway to adapt morphogenesis to environmental conditions?

Materials and methods

Please consult the “Materials and methods” section of part I for general information and techniques. Here, only methods are described that were not mentioned otherwise, oligonucleotides and plasmids are listed in table 4 and 5. PCR-generated parts of plasmids that were used to transform *A. gossypii* were sequenced prior to transformation.

Nomenclature

Both *ScGIC1* and *ScGIC2* are syntenic homologs of the gene *AAL047C*. The sequence identities between *AAL047C* and *ScGIC1* and *AAL047* and *ScGIC2* are similar (38 % and 40 % respectively). For this reason, *AAL047C* was named *AgGIC1/2*.

A. *gossypii* strains

The various *AgGIC1/2* based constructs replace *AgGIC1/2* at its chromosomal locus under the control of the *AgGIC1/2* promoter if not mentioned otherwise. The functionality of the different

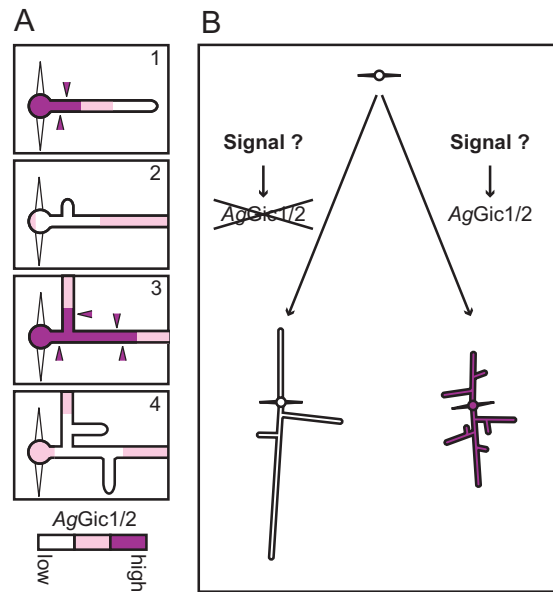


Figure 11: Possible roles of *AgGic1/2* in regulation of lateral branching. (A) Model: Establishment of new lateral branches is suppressed by growing hyphal tips. The four images illustrate the development of single *A. gossypii* mycelium. *AgGic1/2* activity is represented by three different colors: purple for high *AgGic1/2* activity, pink for medium and white for low *AgGic1/2* activity. *AgGic1/2* is constantly synthesized in the entire mycelium and targeted for degradation at hyphal tips leading to low *AgGic1/2* activity in apical regions. Potential sites of polarity establishment where *AgGic1/2* activity is high are marked with arrowheads. (B) Model: *AgGic1/2* is used to adapt cellular morphology to external signals. *AgGic1/2* can be stabilized or degraded upon external signals. Degradation of *AgGic1/2* results in a morphology that resembles the *Aggic1/2* Δ strain, stabilization of *AgGic1/2* leads to a highly branched mycelium like it is observed for the wild type grown on AFM agar.

constructs is discussed in the “Results” section, the strains are listed in table 6. The reference strain, *Agleu2* Δ *thr4* Δ , is referred to as “Ag” in the figure legends.

K38 (*AgGIC1/2* Δ C)

A 2.154 kbp PCR product containing a stop-codon followed by the *ScURA3* terminator and the *GEN3* resistance cassette was obtained with the primers 05.304 and 05.307 using pAGT141 as a template. This DNA fragment was cotransformed into the yeast strain DH5D (Arvanitidis and Heinisch, 1994) together with pK37, which contains the *AgGIC1/2* gene. The resulting pK38 contained *AgGIC1/2* Δ C, which codes for the first 173 amino acids of *AgGic1/2*. The plasmid pK38 was isolated from yeast, about 15 μ g of DNA were cut with *PvuII* and *StuI* and used for transformation of *A. gossypii*.

K39 and K65 (*AgGIC1/2ΔC-YFP* and *AgGIC1/2ΔC-GFP*).

The plasmid pK39 was created by recombination of a 2.819 kbp *YFP-GEN3* cassette (primers 05.305/05.307, template pAGT143) with pK37 in yeast. About 15 μg of pK39 was digested with *AatII* and *SacII* for *A. gossypii* transformation resulting in a strain that expressed the first 173 amino acids of *AgGIC1/2* fused to YFP. The strain *K65* carries an *AgGIC1/2ΔC-GFP* fusion but is otherwise identical to *K39*. The plasmid pK65, which was used to create *K65*, was constructed based on pK39. In a first step, the 4.366 kbp fragment of *AatII* digested pK39 was cloned into *AatII* cut pUC19 resulting in pK63. Second, the *GFP* containing 1.571 kbp fragment of *NcoI* and *NruI* digested pAGT141 was used to replace the *YFP* in pK63 cut with *NcoI* and *NruI* giving rise to pK65.

K40 and K66 (*AgGIC1/2-YFP* and *AgGIC1/2-GFP*).

The plasmid pK40 was obtained by cotransformation of pK37 with a 2.819 kbp carboxy-terminal fusion cassette (primers 05.306/05.307, template pAGT143). Transformation of *AatII* digested pK40 into *A. gossypii* resulted in an *AgGIC1/2-YFP* fusion. *K66* is identical to *K40* with the only difference that *GFP* instead of YFP is fused to *AgGIC1/2*. In order to create pK66, the *AgGIC1/2-YFP* containing 3.488 kbp fragment of *AatII* digested pK40 was cloned into pUC19 resulting in pK64. *YFP* was replaced by *GFP* by ligating the 1.571 kbp fragment of *NcoI* and *NruI* cut pAGT141 into pK64 that was digested with *NcoI* and *NruI*.

K77 ($P_{AgCDC42}$ -*GFP-AgGIC1/2*)

In a first step, a promoterless *GFP-AgGIC1/2* fusion was created via yeast cotransformation. The plasmid pAG6266 containing *AgGIC1/2* was recombined with a 3.150 kbp fusion cassette (primers 06.362/06.363, template pG3iNyEGFP) resulting in pK76 that encoded yEGFP-*AgGic1/2*. The plasmid pK77 was created by digesting pK76 with *PacI* and inserting the 0.497 kbp *AgCDC42* promoter that was amplified from genomic DNA with the primers 06.365 and 06.366 and digested with *PacI*. *A. gossypii* was transformed with *SacII* digested pK77 to give rise to *K77*, which expressed yEGFP-*AgGIC1/2* under the control of the *AgCDC42* promoter.

K79 ($P_{AgCDC42}$ -*GFP-AgGIC1/2ΔC*)

The plasmid pAG6266 was cut open with *BipI* and recombined with a 3.150 kbp *GEN3-yEGFP*

cassette (primers 06.362/06.363, template pG3iNyEGFP) and with a 0.342 kbp PCR fragment that contained the *ScURA3* terminator (primers 05.304/06.364, template pAGT141) in a single yeast cotransformation. The resulting plasmid, pK78, contained a promoterless *GFP*-fusion to *AgGIC1/2ΔC* that encoded amino acids 1-173 of *AgGIC1/2*. The *AgCDC42* promoter was inserted as mentioned for pK77 in the paragraph above resulting in pK79. Transformation of *ApaI* and *XhoI* cut pK79 into *A. gossypii* resulted in a strain expressing yEGFP-*AgGIC1/2ΔC* under the control of the *AgCDC42* promoter. For simplicity, yEGFP will be referred to as *GFP* during this work.

Light microscopy, sample preparation and image processing.

Samples were prepared as described in part I for fluorescence microscopy. Alternatively, mycelia that were growing in liquid culture were pipetted on glass slides and observed immediately. For high magnification germination time-lapse movies, spores were spread on glass slides that were coated with 1 ml AFM agar, immediately covered with a cover slide and incubated for 9 hours prior to microscopy at 25 °C. Mycelia growing on AFM agar plates were observed with an Axioplane2 microscope (Carl Zeiss, Switzerland) using the Plan Neofluar 10x Ph1 numerical aperture (N.A.) 0.3 objective and the Plan Neofluar 20x Ph2 N.A. 0.5 objective. Images were acquired with a MicroMAX TE-CCD-800 PE digital camera (Princeton Instruments, USA) that was controlled by MetaMorph 6.2r6 (Molecular Devices Corp. USA).

Branching index measurements

The branching index was determined for mycelia that grew from single spores on AFM agar plates. Images were acquired between 11 and 21 hours after spore inoculation, depending on the incubation temperature. The total mycelial length was measured using the “Measure regions” tool of MetaMorph and transferred to Microsoft Excel. The branching index was determined as mycelial length divided by the number of tips (Trinci, 1970).

Two hybrid analysis

The plasmids pK32 and pK35 were transformed into the yeast strain *PJ69-4a* (James et al., 1996), pK31 and pK36 into *PJ69-4α* (Uetz et al., 2000). The above mentioned plasmids were constructed by ligating *EcoRI* and *BamHI* digested PCR

products into *EcoRI* and *BamHI* cut pGBKT7 (for pK32 and pK35) or pGADT7 (for pK31 and pK36). The plasmid pK32 contained *AgCDC42^{Q61H}* lacking the bases that code for the carboxy-terminal prenylation signal (primers 02.005/04.156, template pCdc42cons). The plasmid pK35 was constructed likewise containing *ScCDC42^{Q61L}* (primers 05.271/05.272, template pMOSB66). The plasmid pK31 contained *AgGIC1/2* (primers 05.269/05.270 template pAG6266) and the plasmid pK36 contained *ScGIC1/2* (primers 05.273/05.274, template pMOSB230). The PCR-generated inserts were sequenced before transformation. Yeast strains were allowed to mate, diploids were selected on plates lacking tryptophan and leucine but containing a four-fold concentration of adenine (80 mg/ml). The activity of the reporter gene was monitored by spotting 5 μ l of liquid culture with an OD₆₀₀ of 1 on medium lacking adenine. The empty vectors, pGADT7 and pGBKT7 were used as negative and pTD1 and pVA3 as positive controls.

Statistics

The Welch two-sample t-test was applied using the open source R statistical computing and graphics environment (<http://www.r-project.org/>).

Table 4: Oligonucleotides

	Name	Sequence*	Use**
02.005	AgCDC42-ATG	gatcgaattcATGCAGACATTGAAGTGCGTGGTC	pl
04.011	green2.2	TGTAGTCCCGTCATCTTTG	aPCR
04.156	AgCDC42-TAG.2	cgacggatcctACTTCTTGCTCTTCTTGATGACC	pl
04.314	G3.2	CTCCAACCTCGGCACTATTTTAC	aPCR
04.473	URA3T_XmaI	gcccgggggattATAAGTAAATGCATGTATAC	aPCR
05.161	AgGIC1/2-NS1	GCAGAATCCCCTGTTTGAGGCAATTCGGGCGGGGCCATATATAACAGA Gccagtgaattcgagctcgg	gt
05.162	AgGIC1/2-F2	ATAAGCGGTTTTGTAAAGTGTAACTGAGTGTCTATGTAAACAAGCGGCAac catgattacccaagcttgc	gt
05.163	AgGIC1/2-G1	GAGGCGGTAGACAGTATAAC	aPCR
05.164	AgGIC1/2-G4	ATTGTCCGTTCCCTCCAGTC	aPCR
05.165	AgGIC1/2-I	CGCCCATTCTCTGCATGAAG	aPCR
05.269	AgGIC1/2-ATG	gatcgaattcATGTGTAGCAGGCGAGCCACGGGC	pl
05.270	AgGIC1/2-TAG	cgacggatcctTCACATGTATGCATCTCCCTCC	pl
05.271	ScCDC42-ATG	gatcgaattcATGCAAACGCTAAAAGTGTG	pl
05.272	ScCDC42-TAG	cgacggatcctaTTTTTACTTTTCTTGATAACAGG	pl
05.273	ScGIC2-ATG	gatcgaattcATGACTAGTGCAAGTATTACC	pl
05.274	ScGIC2-TAG	cgacagatctaTTAAGTTGCAGGGGCTCG	pl
05.303	AgGIC1/2-ds	CCGCTGTTCGCATGGTAACTG	aPCR
05.304	AgGIC1/2ΔC-FX	CGCCGACGGCGTCGCCGCTGGAGGACGCGCGCGCGCGG tagggcgcgccattataag	rec
05.305	AgGIC1/2ΔC-Tag-F1	CGCCGACGGCGTCGCCGCTGGAGGACGCGCGCGCGCGG aaaacgagggcagtgattcg	rec
05.306	AgGIC1/2-F1	ACCTCCAGCCGTGCACCGGAGGAGATGCATACATG aaaacgagggcagtgattcg	rec
05.307	AgGIC1/2-F2	TGTAAGTGTAACTGAGTGTCTATGTAAACAAGCGGCAC acctgattacccaagcttgc	rec
05.349	G2.3	GGAGGTAGTTTGCTGATTGG	aPCR
06.305	GFP-NTF	GGTGATGGTCCAGTCTTGTTAC	aPCR
06.362	AgGIC1/2-NR5	GTGGTTTCCGTCACGCAGAATTCCTGTTTGAGGCAATT acacaggaaacagctatgac	rec
06.362	AgGIC1/2-NR5	GTGGTTTCCGTCACGCAGAATTCCTGTTTGAGGCAATT acacaggaaacagctatgac	rec
06.363	AgGIC1/2-NR3	TGCTCCTGCACCCGCTGCCCGTGGCTCGCTGCTACACAT caatgaccgtcactgc	rec
06.363	AgGIC1/2-NR3	TGCTCCTGCACCCGCTGCCCGTGGCTCGCTGCTACACAT caatgaccgtcactgc	rec
06.364	AgGIC1/2-URA3t3	CGACGTCGCCATCGTCGACGTCGACACCACCCGCGCCGT accgagctctatgctccatc	rec
06.365	AgCDC42p-PAC3	gacttaattaaCTGTGTGCAGCTGCCTGC	pl
06.366	AgCDC42p-PAC5	gcattaattaaCCGCTGTATACTACATAGCCG	pl
06.391	AgGIC1/2-G4.2	CGTGGCTGATGTGCTGGAAC	aPCR

* Bold lower case characters indicate the template-binding sequences of gene targeting- and recombination primers. All other lower case characters indicate nucleotides that are not homologous to the PCR template.

** aPCR = analytical PCR, gt = gene targeting, pl = plasmid construction, rec = recombination

Table 5: Plasmids

Name	Backbone	Insert	Source
pGEN3	-	-	Wendland et al. 2000
pUC19	-	-	Vieira and Messing 1991
pGADT7	-	two-hybrid <i>GAL4</i> -activation domain (AD)	Chien et al. 1991
pGBKT7	-	two-hybrid <i>GAL4</i> -DNA binding domain (BD)	Louvet et al. 1997
pAG6266	pRS416	<i>AgGIC1/2</i> (no terminator)	Dietrich et al. 2004
pAGT141	pUC19	<i>GFP-GEN3</i> cassette	Kaufmann A., unpublished
pAGT143	pUC19	<i>YFP-GEN3</i> cassette	Kaufmann A., unpublished
pCDC42cons		<i>AgCDC42(Q61H)</i>	Schmitz et al, 2006
pG3iNyEGFP	pUC19	<i>GEN3-yEGFP</i> cassette	Kaufmann A., unpublished
pMOSB230		<i>ScGIC2</i>	Jaquenoud et al. 1998
pMOSB66		<i>ScCDC42(Q61L, C189S)</i>	Gladfelter et al. 2001
pTD1		two-hybrid positive control vector	Clonetech, USA
pVA3		two-hybrid positive control vector	Clonetech, USA
pK31	pGADT7	<i>AD-AgGIC1/2</i>	This study
pK32	pGBKT7	<i>BD-AgCDC42(Q61H)</i>	This study
pK35	pGBKT7	<i>BD-ScCDC42(Q61L)</i>	This study
pK36	pGADT7	<i>AD-ScGIC2</i>	This study
pK37	pRS416	<i>AgGIC1/2</i>	This study
pK38	pRS416	<i>AgGIC1/2ΔC-GEN3</i>	This study
pK39	pRS416	<i>AgGIC1/2ΔC-YFP-GEN3</i>	This study
pK40	pRS416	<i>AgGIC1/2-YFP-GEN3</i>	This study
pK63	pUC19	<i>AgGIC1/2ΔC-YFP-GEN3</i>	This study
pK64	pUC19	<i>AgGIC1/2-YFP-GEN3</i>	This study
pK65	pUC19	<i>AgGIC1/2ΔC-GFP-GEN3</i>	This study
pK66	pUC19	<i>AgGIC1/2-GFP-GEN3</i>	This study
pK76	pRS416	<i>GEN3-yEGFP-AgGIC1/2</i> (promoterless)	This study
pK77	pRS416	<i>GEN3-P_{AgCDC42}-yEGFP-AgGIC1/2</i>	This study
pK78	pRS416	<i>GEN3-yEGFP-AgGIC1/2ΔC</i> (promoterless)	This study
pK79	pRS416	<i>GEN3-P_{AgCDC42}-yEGFP-AgGIC1/2ΔC</i>	This study

Table 6: *A. gossypii* strains.

Strain	Genotype	Construction	Source
$\Delta/\Delta t$	<i>Agleu2Δ Agthr4Δ</i>	-	Altmann-Johl and Philippsen 1996
<i>Aggic1/2Δ</i>	<i>Aggic1/2Δ::GEN3 Agleu2Δ Agthr4Δ</i>	pGEN3 PCR 05.161/05.162	This study
<i>K38</i>	<i>AgGIC1/2ΔC-GEN3 Agleu2Δ Agthr4Δ</i>	pK38; <i>PvuII, StuI</i>	This study
<i>K39</i>	<i>AgGIC1/2ΔC-YFP-GEN3 Agleu2Δ Agthr4Δ</i>	pK39; <i>AatII, SacII</i>	This study
<i>K40</i>	<i>AgGIC1/2-YFP-GEN3 Agleu2Δ Agthr4Δ</i>	pK40; <i>AatII</i>	This study
<i>K65</i>	<i>AgGIC1/2ΔC-GFP-GEN3 Agleu2Δ Agthr4Δ</i>	pK65; <i>AatII</i>	This study
<i>K66</i>	<i>AgGIC1/2-GFP-GEN3 Agleu2Δ Agthr4Δ</i>	pK66; <i>AatII</i>	This study
<i>K77</i>	<i>GEN3-P_{AgCDC42}-GFP-AgGIC1/2 Agleu2Δ Agthr4Δ</i>	pK77; <i>SacII</i>	This study
<i>K79</i>	<i>GEN3-P_{AgCDC42}-GFP-AgGIC1/2ΔC Agleu2Δ Agthr4Δ</i>	pK79; <i>ApaLI, XhoI</i>	This study

Part III

The work presented in this part of my PhD thesis resulted from a collaboration with Hans-Peter Schmitz and Sabrina Buck from the University of Osnabrück, Germany. My personal contributions were the characterization of the *Agrho1a* Δ mutant (figure 1), the microscopy shown in figure 2C and construction of the strains *Aglrg1* Δ , *Agrho1aQ68H* and *Agrho1bQ69H* shown in figure 6B.

The function of two closely related Rho proteins is determined by regulator specificity, not by effector interaction

Michael Köhli¹, Sabrina Buck² and Hans-Peter Schmitz^{2,3}

¹Applied Microbiology, Biozentrum Universität Basel, Klingelbergstr. 50-70, 4056 Basel, Switzerland

²Department of Genetics, University of Osnabrück, Barbarastr. 11, 49076 Osnabrück, Germany

It is generally believed that the vast number of small GTP-binding proteins present in cells of higher organisms today has evolved by gene duplications of a common ancestor. Furthermore it is taken for granted that after duplication mutations alter the protein's effector interactions, thereby changing its function. In contrast to these assumptions we show here for the two duplicated *RHO1* genes from the filamentous fungus *Ashbya gossypii* that the different functions of the encoded proteins are not due to different effector interactions. Instead we found that both proteins are regulated by different GAP-proteins and that GAP specificity is determined by either a tyrosine or a histidine at a single position in the switch I region of the two Rho1 proteins. An analogous histidine residue is found in some atypical GTP-binding proteins of higher eukaryotes, suggesting that the evolutionary mechanism we describe here might be a common way for diversification of GTP-binding protein function.

Introduction

Gene duplication is the motor of genetic evolution (Ohno, 1970). Single loci, chromosomal fragments or even whole genomes duplicate, and duplicated genes undergo different fates. However, how mutations change the function of the encoded proteins often remains unclear. Here we investigate duplicated genes of small GTP-binding proteins for several reasons: Small GTP-binding proteins are a ubiquitous protein class, in eukaryotic cells. They are involved in diverse processes like cancer development, cell morphogenesis or vesicle trafficking (Takai et al., 2001). The structure and mode of action of this protein class is highly conserved and well understood, and effects of mutations mimicking active and inactive forms can be generalized. Activation of small GTP-binding proteins is characterized by a GDP-GTP exchange involving regulators called guanine nucleotide exchange factors (GEFs). The active, GTP-bound form of a GTP-binding protein binds and activates effectors. Inactivation is mediated by the binding of a GTPase activating protein (GAP) that increases the intrinsic GTPase activity of the GTP-binding protein dramatically. It is generally assumed that small GTP-binding proteins have evolved by gene duplication followed by mutation of the effector binding regions, potentially resulting in novel protein function. In this study, we used a comparative analysis of duplicated and non-duplicated Rho proteins to understand the

mechanism how Rho proteins can gain functional specificity after gene duplication.

Yeasts provide an excellent tool for studying gene duplication (Wolfe, 2006). With the well-annotated genome of *Saccharomyces cerevisiae* and several other complete yeast genomes, identification of duplicated genes is very reliable. Taking synteny information into account, duplicated genes can be identified with confidence. *A. gossypii* is especially well suited for studies on evolution of gene function in combination with the budding yeast *S. cerevisiae* (Philippson et al., 2005). The gene content of the *A. gossypii* genome is very similar to *S. cerevisiae* but *A. gossypii*, unlike *S. cerevisiae*, did not go through a whole genome duplication since the two species diverged leading to a very compact genome (Dietrich et al., 2004). In comparison with *S. cerevisiae*, only a few (~26) genes in *A. gossypii* are duplicated, while many (~496 pairs) are found in *S. cerevisiae*, thus providing a total of more than 500 candidates for studies on functional changes by gene duplication. In contrast to other, closely related yeast species, *A. gossypii* shows exclusively filamentous growth and does not grow by budding. This different life style compared to yeast cells increases the possibility to observe changes in function of gene-products that are involved in such elementary processes like polar growth, cell division and cell cycle control.

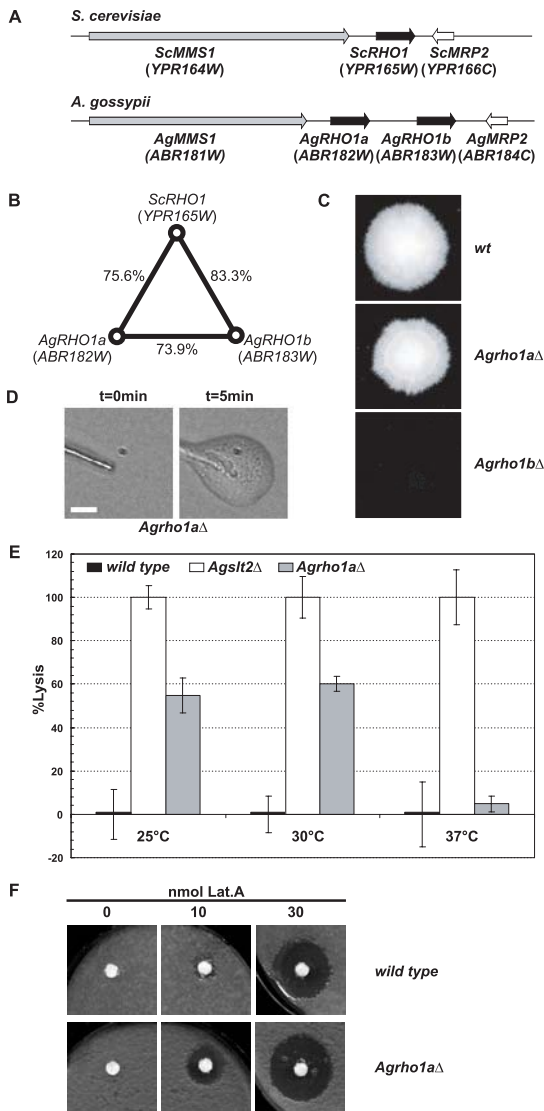


Fig. 1: Lysis phenotypes of an *Agrho1a* deletion strain. (A) Genomic organization of *RHO1* loci and neighboring genes in *S. cerevisiae* and *A. gossypii*. Homologous genes are shaded identically. (B) Percent identity of Rho1 proteins derived from comparisons with the needle program of the EMBOSS package (Rice et al., 2000). (C) Representative mycelia of wild type and deletions of *AgRHO1a* and *AgRHO1b*. For the deletion mutants, spores from a heterokaryotic mycelium were spotted on medium selective for the marker of the deletion. Wild type spores contained a plasmid carrying the same marker gene to allow for growth on the selective medium. (D) Hyphal lysis of *Agrho1aΔ*. Still images of individual hyphae that lysed during a time-lapse movie (movie S5). Sections of frames from time points prior to and after lysis are shown ($\Delta t = 5$ min). The size of the bar is 25 μ m. (E) Quantification of mycelial lysis (see Materials and Methods). The alkaline phosphatase release of wild-type cells was set to 0% and the release of an *AgsIt2Δ* to 100%. Values are given for at least 3 individual experiments. (F) Latrunculin A sensitivity of *Agrho1aΔ*. A dense spore suspension of wild-type (upper panel) or *Agrho1aΔ* spores (lower panel) was mixed with AFM-Agar and overlaid on AFM plates. Filter discs were placed on the AFM agar plates and the indicated amount of latrunculin A was spotted on discs in a volume of 5 μ l DMSO. Plates were incubated at 25°C for 36h.

The Rho1 protein from *S. cerevisiae* is a typical member of the Rho GTP-binding protein family. Its function and regulation is complex but well understood (Levin, 2005). Deletion of the *ScRHO1* gene is lethal (Madaule et al., 1987), which reflects the multitude of functions that have been attributed to the encoded protein. Two major functions of *ScRHO1* are represented by two different complementation groups of *Scrho1* mutants (Saka et al., 2001). The functions assigned to these groups are the regulation of cell wall biosynthesis and the regulation of the actin cytoskeleton. Cell wall biosynthesis is controlled by interaction of *ScRho1* with the glucan-synthase complex (Drgonova et al., 1996; Mazur and Baginsky, 1996; Qadota et al., 1996), which produces β -(1,3)-glucan, the major component of the yeast cell wall. Initially, *ScRho1* was isolated as the regulatory subunit of this complex. Actin regulation is achieved by interaction with two different effector-proteins: The formin *ScBni1* (Kohno et al., 1996) and the single *S. cerevisiae* protein kinase C *ScPkc1* (Nonaka et al., 1995). While the connection to actin regulation via formins is direct because proteins of this class catalyze polymerization of actin cables, actin regulation via *ScPkc1* is not understood in detail, and the targets of *ScPkc1* responsible for actin regulation are unknown. In addition to these two main roles of Rho1, there is evidence for a variety of other functions (reviewed by Levin, 2005). Even though these processes seem to be quite diverse, they might all be reduced to actin regulation because they all involve actin-dependent transport processes.

A first *A. gossypii* homolog of *S. cerevisiae* *RHO1* was cloned before the second *RHO1* copy was detected during the genome-sequencing project (Wendland and Philippsen, 2001). Deletion mutants of *AgRHO1* (open reading frame *ABR183W*) grew slowly, suffered from significant cell-lysis and died within 4 days. This phenotype suggested *AgRho1b* functions that are similar to the *S. cerevisiae* Rho1. A second *RHO1* homolog (*ABR182W*), directly upstream of *AgRHO1*, was identified after the genome sequence became available (Dietrich et al., 2004). The genomic organization of the *AgRHO1* genes together with the neighboring genes in *A. gossypii* and *S. cerevisiae* is shown in figure 1A. The two *AgRHO1* copies very likely originate from a tandem-duplication event. Only little is known about the function of *ABR182W*. Deletion mutants have been reported to display a slightly increased lysis phenotype and a weak sensitivity to

the chitin-binding-dye Calcofluor white (Walther and Wendland, 2005).

To get insight into the evolution of small GTP-binding protein genes, we investigated the functional changes that occur after duplication of such genes. We studied the differences in function of a pair of duplicated *RHO*-type GTP-binding proteins in *A. gossypii* and compared them to their single homolog in budding yeast. Furthermore, we wanted to identify the change in the duplicated sequence that might have led to an initial separation of function of the duplicated gene copies. Surprisingly, we found that a single residue, which is altered in the switch I region of *AgRho1a*, determines protein function and causes a different GAP-specificity without altering effector interaction. Since a similar residue is found in the switch I region of some atypical small GTP-binding proteins in higher eukaryotes, the evolution of the *AgRho1* proteins we describe here might reflect a general mechanism for diversification of GTP-binding protein function.

Results

The lytic phenotype of *Agrho1a*Δ is temperature-dependent.

Before investigation of a possible mechanism for diversification of duplicated gene function, we first had to characterize the Rho1 proteins in *Ashbya gossypii* to verify that both gene copies developed different functions during evolution. Alignment of the protein sequences shows that *AgRho1a* is 73.9% identical to *AgRho1b* and 75.6% identical to *ScRho1* while the latter two proteins show the highest identity with 83.3% (figure 1B). As a first step towards defining functional difference between *AgRHO1a* and *AgRHO1b*, we compared the phenotypes of deletion mutants. While *Agrho1a*Δ strains formed a mature mycelium that grew slightly slower than the wild type, deletion of *Agrho1b* resulted in cells which never reached the state of a mature mycelium and died due to cell lysis (figure 1C). *Agrho1a*Δ cells also lysed but only few hyphae were affected. Figure 1D shows an examples of lysing hyphae taken from movie S5. We also monitored the strain deleted for *AgRHO1a* at different growth temperatures. Lysis of adult mycelia was quantified by an assay that visualizes the release of cytoplasmic alkaline phosphatase upon lysis by a color reaction (figure 1E, for details refer to Material and Methods). An

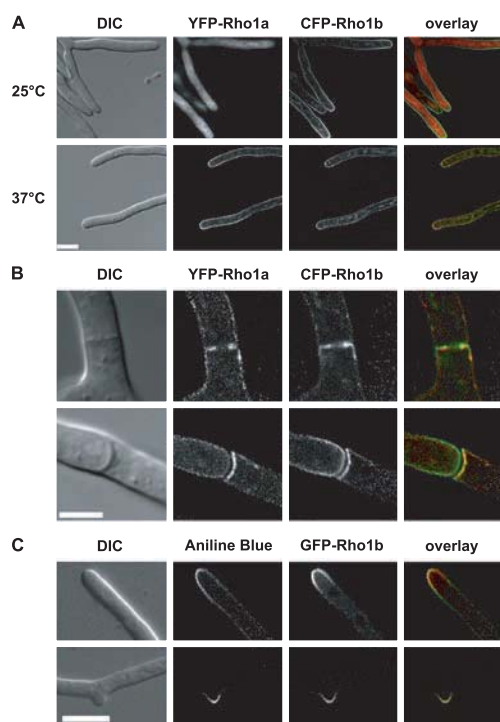


Fig. 2: Localization of *AgRho1* proteins. Amino-terminal fusions of Yellow-Fluorescent-Protein (YFP) to *AgRho1a* and Cyan-Fluorescent-Protein (CFP) to *AgRho1b* localizing at the tip (A) and at the septum (B). Mycelia were placed on a slide with a small cavity containing solid time-lapse medium. The slides were incubated for 1 h at the given temperature prior to microscopy. The overlay uses green for YFP-*AgRho1a* and red for CFP-*AgRho1b*. The size bar represents 5 μ m. C). Colocalization of GFP-*AgRho1b* with β -(1,3)-glucan biosynthesis at the tip. Mycelia that were grown on microscopy slides were incubated with 1 mg/ml Aniline blue in AFM for visualization of β -(1,3)-glucan biosynthesis for 5-10 minutes prior to microscopy. Aniline blue is shown in red and GFP-*AgRho1b* in green on the overlay image. The size bar is 10 μ m.

*Agslt2*Δ strain was used as a lysis control. *AgSLT2* is the homolog of the *S. cerevisiae* MAP-kinase responsible for maintenance of cellular integrity (Torres et al., 1991). In contrast to *Agrho1b*Δ, *Agslt2* deletion mutants can form a mature mycelium despite frequent hyphal lysis (our own unpublished results). At 25°C and 30°C, *Agrho1a*Δ mutants release about half as much alkaline phosphatase as the *Agslt2*Δ mutants. To our surprise, lysis of the *Agrho1a*Δ strain decreases to almost wild-type levels at 37°C. Cold-sensitive phenotypes are often associated with mutants of actin and its regulators. However, we did not observe significant differences between the actin cytoskeleton of wild-type and *Agrho1a*Δ cells stained with rhodamine-phalloidin (data not shown). Since visualization of actin requires fixation of cells, differences in actin

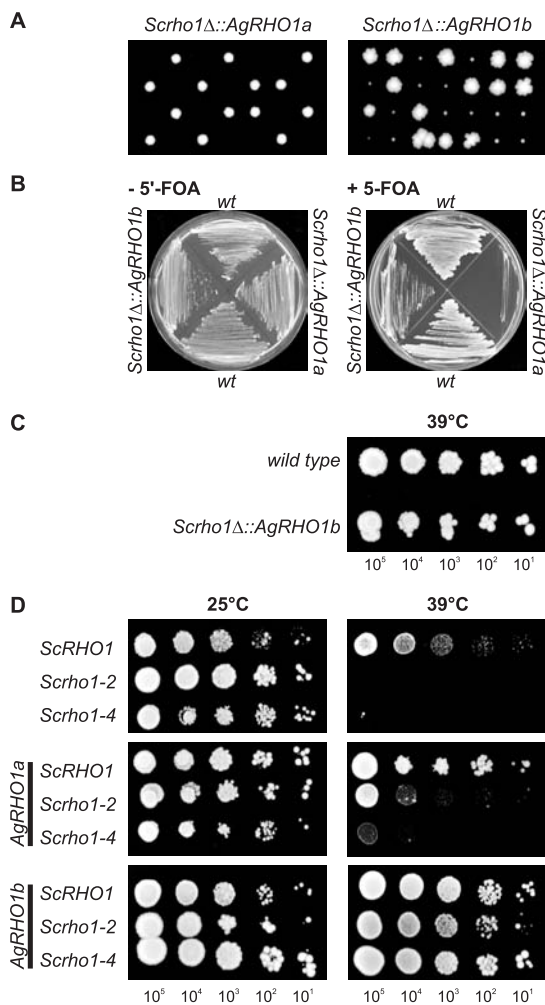


Fig. 3: Complementation of *S. cerevisiae rho1* mutants by *AgRHO1* genes. (A) Complementation of *Scrho1Δ*. The open reading frame of *ScRHO1* was replaced by either *AgRHO1a* or *AgRHO1b* in a diploid strain. After sporulation the resulting strains were subjected to tetrad analysis. Growth for seven representative tetrads is shown for *AgRHO1a* (left) and *AgRHO1b* (right). (B) Plasmid loss experiment. Strains with the indicated genotypes were transformed a plasmid containing the *URA3* marker and the *ScrHO1* gene with promoter and terminator and streaked on medium without or with counterselection for *URA3* by 5-fluorootic acid. (C) Two segregants from a tetrad shown in A were tested for temperature sensitivity at 39°C in a drop dilution assay. Cultures were grown to an OD₆₀₀ of 1. The number of cells given below the image were spotted on agar plates and incubated for 3 days 39°C. (D) Complementation of different *Scrho1* temperature-sensitive mutants from different complementation groups by the two *AgRHO1* genes. Drop dilution assays of culture that was grown to OD₆₀₀ 1 are shown. Strains that carry the wild-type *ScRHO1* allele or either allele from each *Scrho1* complementation group were combined with a *Scrho1* deletion (top row), *AgRHO1a* (middle row) or *AgRHO1b* (bottom row). The strains were incubated at the permissive (25°C, left image) or the restrictive temperature (39°C, right image).

dynamics might have been missed. Therefore, we tested wild type and *Agrho1aΔ* for sensitivity to the actin monomer sequestering drug latrunculin A. Figure 1F shows that mutant *Agrho1aΔ* cells are more sensitive to actin perturbation than wild-type cells, best visible for 10nmol latrunculin A. This result suggests an involvement of *AgRho1a* in actin regulation. The observed lysis of hyphae could therefore be an indirect consequence of the actin defects while the lethal lysis phenotype of the *Agrho1b* deletion might be the consequence of direct defects in cell wall biosynthesis.

Different localization patterns of *AgRho1a* and *AgRho1b*

The two main functions of Rho1 that are known from studies in *S. cerevisiae* are cell wall biosynthesis and regulation of the actin cytoskeleton. In filamentous fungi, growth, and therefore cell wall biosynthesis, is restricted to the tip area of hyphae. Actin patches in *A. gossypii* also localize to the tip region but they are absent at the most apical part of the tip cortex. In addition, actin-cables are found in the whole mycelium and actin rings form at sites of septation. Proteins that are involved in regulation of either cell wall biosynthesis or the regulation of the actin cytoskeleton should therefore show a distinct localization pattern. To test if this is true for the *AgRho1* proteins, we localized fusions of both proteins to YFP (*AgRho1a*) or CFP (*AgRho1b*) simultaneously by fluorescence microscopy. Since we observed temperature-dependent lysis for the *Agrho1aΔ* mutants, we speculated that temperature is an important factor for the *AgRho1a* function. To test this, cells were grown either at 25°C or at 37°C. Figure 2A shows that, at 25°C, *AgRho1b* localizes mainly to the cortex and the cytoplasm at the tip of the growing hyphae while *AgRho1a* localizes to the entire cytoplasm. Interestingly, a 1h heat shock at 37°C led to a different localization pattern for both proteins. Now they were found at the cortex of the entire hyphae. In contrast to the localization pattern of *AgRho1b* at 25°C, membrane association is not restricted to the tip region of the hyphae. This implies that, at higher temperatures, both proteins might share more functions than at lower temperatures and might be one reason for the reduced lysis at higher temperature observed for *Agrho1aΔ*.

While localization of the two *AgRho1* proteins differs at the tip region of hyphae, we found both proteins at developing (figure 2B, first row) and mature septa (figure 2B, second row) suggesting that both feature in septum formation. To test whether

Table 1: Interaction of *AgRho1* proteins with potential effector-proteins

	<i>AgRho1a</i>	<i>AgRho1a</i> Q68H	<i>AgRho1a</i> H39Y,Q68H	<i>AgRho1b</i>	<i>AgRho1b</i> Q69H	vector
<i>AgBni1</i>	-	++	++	-	++	-
<i>AgPkc1</i>	-	++	++	-	++	-
<i>AgSec3</i>	-	-	-	-	+	-
<i>AgFks1/2</i>	-	-	-	-	-	-
<i>AgSkn7</i>	-	-	-	-	-	-
<i>AgSte4</i>	-	-	-	-	-	-
vector	-	-	-	-	-	-

the area of *AgRho1b* localization at the tip at 25°C overlaps with the area of cell wall biosynthesis, we observed a GFP-fusion to *AgRho1b* in aniline blue stained hyphae. Aniline blue is incorporated with $\beta(1,3)$ -glucan into the forming cell wall (Kippert and Lloyd, 1995). Therefore, short incubation times with aniline blue preferentially stain the sites of cell wall biosynthesis. As shown in figure 2C, an overlap of aniline blue staining and GFP-*AgRho1b* is observed in growing tips and newly emerging branches. This is indicative of a direct connection between localization of *AgRho1b* and cell wall biosynthesis.

***AgRHO1a* does not function in glucan biosynthesis**

We performed complementation assays of yeast mutants to test the conclusion from the experiments above. *S. cerevisiae* is a close relative of *A. gossypii* but has no duplicated *RHO1* gene. Therefore, complementation of *S. cerevisiae rho1* mutants can be used to assay how the function of the *A. gossypii RHO1* genes may have evolved. We constructed *S. cerevisiae* strains with an ORF-replacement of the *ScRHO1* gene by each of the *A. gossypii* homologs resulting in a fusion of the *A. gossypii* genes to the *ScRHO1* promoter. Figure 3A shows representative examples of a tetrad analysis of heterozygous strains carrying *ScRHO1* and either *AgRHO1a* (left side) or *AgRHO1b* (right side). Out of 50 tetrads analyzed for *AgRHO1a*, all showed a 2:2 segregation for viability and none of the viable spores carried the marker for *AgRHO1a* proving that *AgRHO1a* is unable to complement loss of *ScRHO1*. In contrast, segregants of a similar strain where *ScRHO1* is replaced by *AgRHO1b* are viable even though a 2:2 segregation with bigger and smaller colonies was observed. The small colonies carried the marker of *AgRHO1b* in

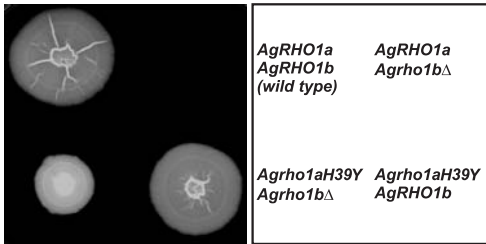
all cases. In addition to tetrad-analysis, we tested whether haploid cells, in which the genomic copy of *ScRHO1* was replaced by either one of the *AgRHO1* alleles, can be forced to lose a plasmid with an *URA3* marker carrying the *ScRHO1* gene on medium with 5-fluoroorotic acid. Consistent with the results from the tetrad analysis, plasmid loss was possible for *Scrho1 Δ ::AgRHO1b* but not for *Scrho1 Δ ::AgRHO1a*. However, in contrast to the tetrad analysis where *Scrho1 Δ ::AgRHO1b* segregants were smaller, the *Scrho1 Δ ::AgRHO1b* strain grew like the wild type suggesting that the reason for the small size of the segregants is delayed germination and not a growth defect. To verify this, we tested the growth of the *Scrho1 Δ ::AgRHO1b* strain at high temperature (figure 3C). At 39°C, the *Scrho1 Δ ::AgRHO1b* mutant behaves like the wild type suggesting that there is no growth defect associated with this ORF replacement.

The complementation assay indicates that *AgRho1b* and *ScRho1* functions are conserved while the functions of *AgRho1a* and *ScRho1* have diverged and that the functions of *AgRho1b* and *ScRho1* probably reflect the functions of the common ancestor Rho1 protein. This raises the question whether *AgRho1a* lost the capability to act in both or only in one branch of ancestral Rho1 signalling. We performed complementation tests with temperature-sensitive alleles from both *ScRHO1* complementation groups (Saka et al., 2001) to answer this question. Again, we used ORF-replacements of *ScRHO1* with either *A. gossypii RHO1*, but in addition we integrated temperature sensitive *ScRHO1* alleles at the *LEU2* locus. We used the *Scrho1-2* mutant that has a defect in the actin branch of Rho1 signalling and the *Scrho1-4* mutant that has a defect in the glucan biosynthesis branch of Rho1 signalling (Saka et al., 2001). As shown in figure 3D (first row), cells with

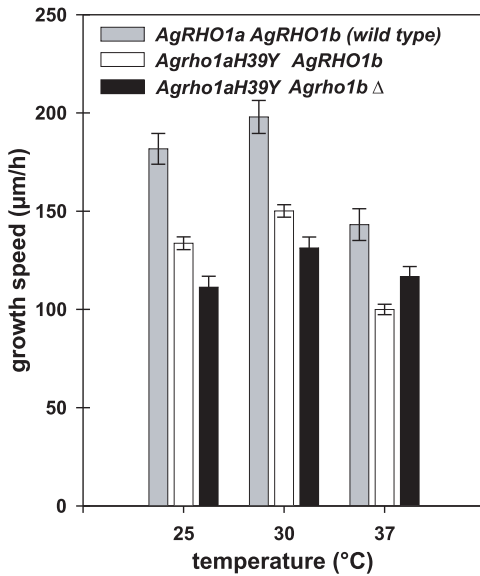
A

conserved residues	Y PTVF	
<i>A.gossypii</i> Rho1a (Abr182w)	FFELIVPTVFENYV	(35-49)
<i>A.gossypii</i> Rho1b (Abr183w)	FFQVYVPTVFENYV	(36-50)
<i>K.waltii</i> Rho1 Kwal_55.21937	FFPEYVPTVFENYV	(35-49)
<i>K.waltii</i> Rho1 Kwal_55.21941	FFQVYVPTVFENYV	(37-51)
<i>S.cerevisiae</i> Rho1 (Ypr165w)	FFPEYVPTVFENYV	(35-49)
<i>S.pombe</i> Rho1 (SPAC1F7.04)	FFPEYVPTVFENYV	(31-45)
<i>C.elegans</i> RhoA (51H4A.3)	FFPEYVPTVFENYV	(30-44)
<i>D.melanogaster</i> Rho1 (CG8416)	FFPEYVPTVFENYV	(30-44)
<i>M.musculus</i> RhoA	FFPEYVPTVFENYV	(30-44)
<i>H.sapiens</i> RhoA	FFPEYVPTVFENYV	(30-44)

B



C



D

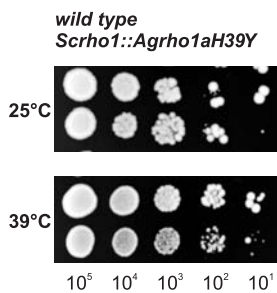


Fig. 4: An atypical histidine in the switch I region of *AgRho1a*.

(A) Representative alignment of the switch I region of Rho-type proteins from several model organisms. Non-homologous residues are shaded grey. The residues corresponding to position 39 of *AgRho1a* is boxed. (B) An *A. gossypii* mutant with an exchange of histidine 39 for tyrosine (C115T) in *AgRho1a* is able to complement the lethality of an *Agrho1b* deletion. Spores from mycelia that are heterokaryotic for the indicated mutation were spotted on plates selective for the marker of the mutations to allow only growth of spores with indicated genotype. Plates were incubated for 4 days at 30°C. (C) Growth speed of the mutants shown in B. Identically sized inoculums of homokaryotic mycelia were placed on full medium plates and incubated at 30°C for 4 days. Growth speed was determined as the quotient of mycelial diameter and incubation time. (D) The *Agrho1aH39Y* mutant is able to complement the deletion of *Scrho1* in *S. cerevisiae*. Yeast cells of the indicated strains were grown at 25°C in liquid medium to an OD₆₀₀ of 1. Dilutions with the indicated cell number were spotted on agar plates and incubated at the indicated temperatures for 2 days.

the *Scrho1* mutants from both complementation groups can grow at the permissive temperature (25°C) but die at the restrictive temperature (39°C). *AgRHO1a* partially complements the mutant with a defect in actin regulation (figure 3D, second row). Together with the latrunculin A sensitivity of the *A. gossypii rho1aΔ* strain, this indicates that *AgRho1a* is involved in actin regulation. The major loss of function of *AgRHO1a* might have occurred in glucan biosynthesis as emphasized by the complete failure of *AgRHO1a* to complement the *Scrho1-4* mutant with a defect in glucan biosynthesis. As expected from the ability of *AgRHO1b* to complement the loss of *SCRHO1*, *AgRHO1b* is able to fully complement the defects of mutants from both *SCRHO1* complementation groups (figure 3D, third row).

An atypical switch I region in *AgRho1a*

Since we were interested in the mechanism of evolution of the GTP-binding protein function after gene duplication, we wanted to know the molecular basis of the observed changes in *AgRHO1a* function. To identify differences between *AgRho1a* and *AgRho1b*, we compared the sequences of the homologs with each other and with more than 300 other Rho-type GTP-binding proteins from different organisms. We identified a single histidine residue at position 39 in the switch I region of *AgRho1a* that is a highly conserved tyrosine in all 323 Rho-type GTP-binding proteins we examined. This atypical switch I region is shown in an alignment with Rho-proteins of other model organisms in figure 4A. Resequencing of the *AgRHO1a* ORF verified the presence of the atypical histidine residue thus excluding a sequencing error. We speculated that

this single residue might contribute significantly to the difference in *AgRho1a* and *AgRho1b* function. If so, a mutant *AgRho1a* protein with a histidine to tyrosine exchange at position 39 should be able to take over the function of *AgRho1b* and consequently should be able to rescue the otherwise lethal deletion of *AgRHO1b*. To test this hypothesis, we mutated the cytosine at position 115 of *AgRHO1a* to a thymine resulting in a change from histidine 39 to tyrosine and integrated the mutated allele into an *A. gossypii* wild-type strain at the original *AgRHO1a* locus. The resulting strain was viable (figure 4B) although its radial growth speed was slightly reduced compared to wild type (figure 4C). We then combined this mutation with a deletion of *AgRHO1b*. A strain with a heterokaryotic deletion of *AgRHO1b* was used as a control. Spores from the strain deleted for *AgRHO1b* did not give rise to a mycelium. However, the presence of *Agrho1aH39Y* restored growth and cells formed a mature mycelium in an *Agrho1b*Δ background (figure 4B). As shown in figure 4C, the growth speed of this strain was slower than wild type and the difference in growth speed was less pronounced at 37°C. We hypothesized that, unlike the wild-type *AgRHO1a*, the mutant *Agrho1aH39Y* would be capable to complement the lethality of an *Scrho1* deletion. To test this, we replaced the *ScrHO1* ORF with *Agrho1aH39Y* (figure 4D). In contrast to the wild-type *AgRHO1a* allele (figure 3A and 3B), *Agrho1aH39Y* fully restores growth in an *Scrho1*Δ background even under heat stress at 39°C. The complementation of the growth defects of an *Agrho1b* and an *Scrho1* deletion is a strong indicator for the importance of the histidine 39 of *AgRho1a* for divergence of protein function between the two *AgRho*-proteins.

Histidine 39 of *AgRho1a* is responsible for GAP-specificity

We wondered how a single residue could influence the function of *AgRho1a* in such a dramatic way. The switch I region of small GTP-binding proteins, where the atypical histidine in *AgRho1a* is located, is one of the regions that undergo a nucleotide-dependent conformational change (Milburn et al., 1990) and thus is part of the major interaction interface with other proteins (Vetter and Wittinghofer, 2001). A survey of protein structures shows that the tyrosine residue that is homologous to histidine 39 in *AgRho1a* is directly involved in interaction of RhoA, Rac1 and Cdc42 with other proteins (Dvorsky et al., 2004). Interestingly, none of the 13 different structures of protein complexes

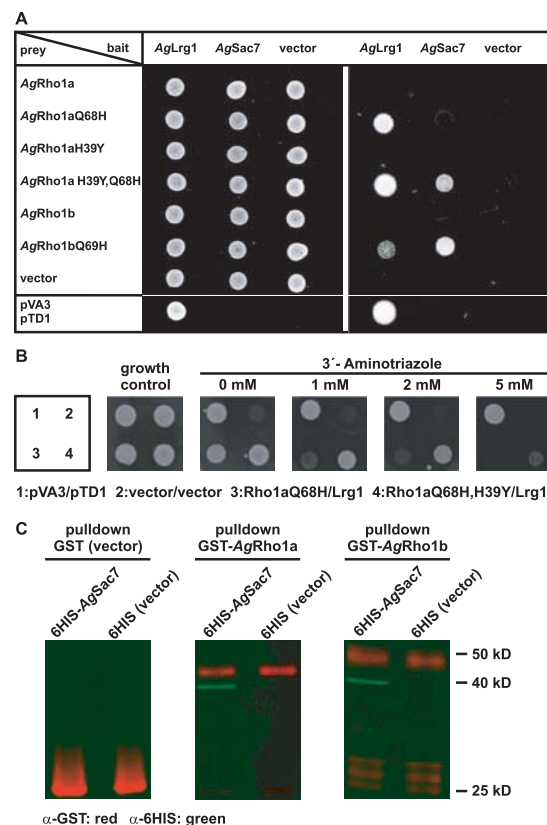


Figure 5: Rho-proteins and GAP interactions. (A) Two-hybrid analysis of interactions between the *AgRho1* proteins and potential GTPase activating proteins. The carboxy-terminal lipid-modification motif of the small GTP-binding proteins was truncated from their coding sequence to allow two-hybrid testing. The glutamate to histidine exchange in switch II mimics the GTP-bound state of the proteins. The histidine to tyrosine exchange is indicated by H39Y. The left panel shows a growth control on medium selective only for prey and bait plasmids. The medium in the right panel is also selective for interaction. (B) The H39Y mutation increases interaction strength of *AgRho1a* with *AgLrg1*. The indicated pray/bait combinations from A were additionally tested on medium containing different concentrations of 3-Aminotriazole to test interaction strength of the *AgRho1aH39Y* mutant protein with *AgLrg1*. The first image on the left side is the growth control. (C) Pull-down experiment in the presence of aluminium fluoride. Glutathion-S-Transferase (GST) or *AgRho1a* proteins fused to GST were bound to Glutathion-sepharose and washed. The eluted proteins were subjected to Western-blot analysis. The blot was probed with anti-GST (red) and anti-6HIS (green).

where the conserved tyrosine in the switch I region participated in the interaction interface involved an effector molecule. Instead, all complexes were formed with regulators of small GTP-binding proteins like GEFs, GDP-dissociation inhibitors (GDIs), and mainly GAPs. This suggests that the different functions of the two *AgRho1* proteins are not caused by different effector interactions. Consistently, two-hybrid assays revealed that *AgRho1* proteins do not differ greatly in their

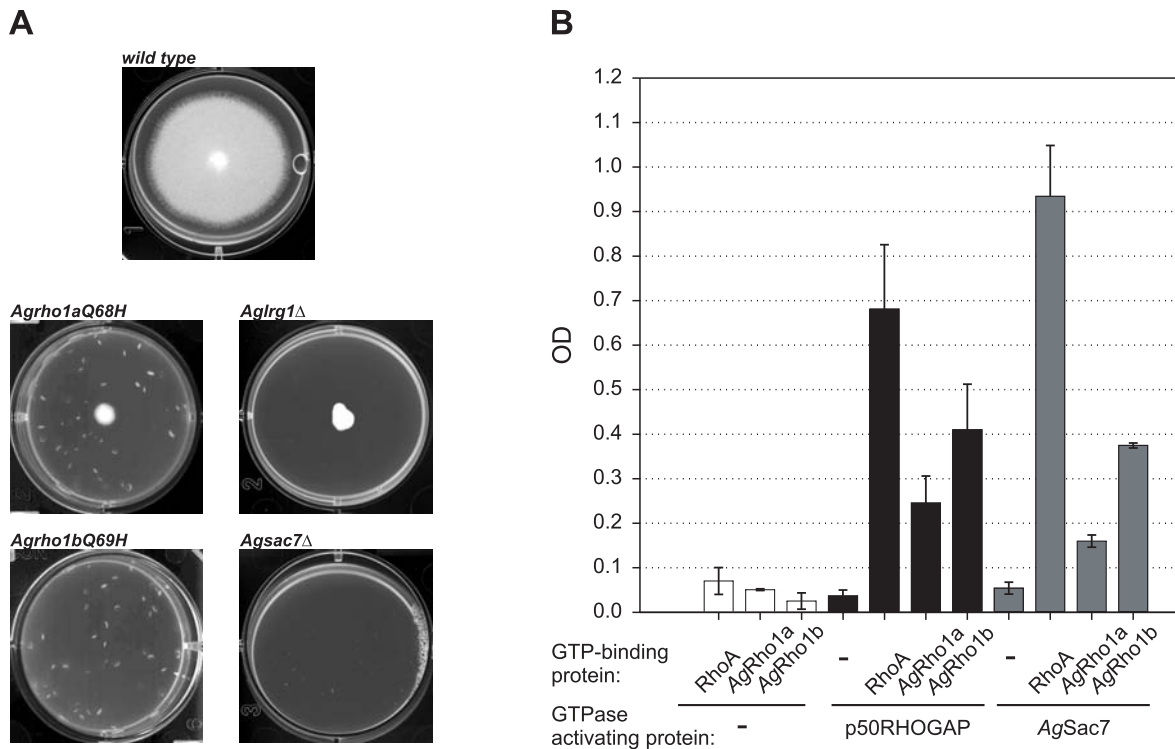


Fig. 6: GAP-activity on *AgRho1* proteins. (A) Correlation of growth phenotypes of a mutant expressing GTP-locked *AgRho1aQ68H* with *Aglrg1Δ* and GTP-locked *AgRho1b* with *Agsac7Δ*. Spores from mycelia that are heterokaryotic for the indicated allele were spotted on medium selecting for the mutation in 6 well plates with a diameter of 3.5 cm per well. Plates were incubated at 30°C for 2 days. The speckles are air bubbles in the agar. (B) *AgSac7* GAP-activity towards *AgRho1* proteins. The activities were determined as described in Material and Methods using 5 μg of each protein (Rho and GAP) or buffer as a control. The optical density at 650 nm was determined against a control reaction with buffer only.

interaction with putative effector molecules that are known from *S. cerevisiae*. The only difference we observed was a weak interaction between *AgRho1b* and *AgSec3* that is not found with *AgRho1a* (table 1). However, this difference is not responsible for the functional differences observed for the *AgRho1* proteins since the interaction with *AgSec3* was not influenced by a *Agrho1bY40H* or an *Agrho1aH39Y* mutation (not shown). Instead, we speculated that the difference in function of the *AgRho1* proteins might come from a different affinity of *AgRho1a* and *AgRho1b* to regulatory proteins. Since two important regulators of the different branches of *ScRho1* signalling in *S. cerevisiae* are the two GAPs *ScLrg1* and *ScSac7* (Lorberg et al., 2001; Schmidt et al., 2002; Watanabe et al., 2001), we set up a two-hybrid assay to test for interaction of the homologous GAPs from *A. gossypii* with the *AgRho1* proteins. As only the GTP-bound forms of the GTP-binding proteins interact with the GAPs, we used both, the wild-type and variants that carry a glutamine to histidine mutation in the switch I region, resulting in GTP-locked variants of the proteins. As shown in figure 5A, GTP-*AgRho1a* interacts with *AgLrg1*

but interaction with *AgSac7* was barely detectable. This raises the question whether this interaction is completely absent or whether it is too weak to be detected by a two-hybrid assay. We addressed these possibilities by performing a coprecipitation of the two proteins in presence of aluminium fluoride. Aluminium fluoride forms a stable complex with GTP-binding proteins in the GDP-bound form and their GAPs mimicking a transition state of GTP hydrolysis (Ahmadian et al., 1997). If *AgRho1a* and *AgSac7* interact, the complex between GAP, GTP-binding protein and aluminium fluoride can be pulled down even if the interaction is transient and weak. We performed this test by expression of GST-tagged *AgRho1a* and *AgRho1b* and the hexahistidine-tagged GAP-domain of *AgSac7* in *E. coli*. The GAP-domain of *AgSac7* can be pulled down with both *AgRho1a* and *AgRho1b* (figure 5C). Attempts to perform a similar experiment with *AgLrg1* were unsuccessful because we were unable to express soluble *AgLrg1* or *AgLrg1* fragments. However, together with the two-hybrid data, the results for *AgSac7* show that *AgRho1a* and *AgSac7* do interact and can be copurified if the complex is stabilized although this interaction

is probably so weak that it is close to the detection level of the two-hybrid assay.

The situation for *AgRho1b* is exactly opposite to *AgRho1a*. GTP-*AgRho1b* shows only a weak two-hybrid interaction with *AgLrg1* but a strong interaction with *AgSac7* (figure 5A). *AgLrg1* interaction with *AgRho1b* is stronger than the background detected with a vector control but clearly weaker than the interaction between *AgSac7* and *AgRho1b*. We also tested *AgRho1aH39Y* to see if the mutation influences binding to a GAP. Indeed, the switch I-mutation resulted in a stronger interaction between *AgRho1a* and *AgSac7*. This change in interaction strength is probably the reason for the capability of an *AgRho1aH39Y* mutant to take over *AgRho1b* function. While increased interaction strength between *AgRho1aH39Y* and *AgSac7* is obvious, we used 3-aminotriazole to estimate interaction strength for *AgLrg1* (figure 5B). In this assay, yeast cells can grow on higher concentrations of 3-aminotriazole if they contain more of the *HIS3* gene product. Therefore, stronger interaction between the bait and the prey of a two-hybrid assay leads to higher resistance against 3-aminotriazole. While yeast cells with wild-type *AgRho1a* as a bait and *AgLrg1* as a prey do not grow on 2 mM 3-aminotriazole, a strain with *AgRho1aH39Y* can grow even on 5 mM 3-aminotriazole indicating a much stronger interaction between mutant *AgRho1aH39Y* and *AgLrg1* compared to wild-type *AgRho1a*.

We constructed strains carrying a mutation that encodes dominant active forms of *AgRho1a* and *AgRho1b* and compared the phenotypes of these strains with phenotypes of strains deleted for either *AgSAC7* or *AgLRG1*. Removal of a GAP from the regulatory circuit of a small GTP-binding protein should lead to an accumulation of a GTP-bound Rho protein and therefore to a phenotype that is similar to the GTPase-deficient form of the small GTP-binding protein. In support of our hypothesis, a deletion of *AgLRG1* and introduction of a GTPase-deficient allele of *AgRHO1a* result in slow growth compared to wild type while deletion of *AgSAC7* and a GTPase-deficient allele of *AgRHO1b* is lethal (figure 6A). Together with the two-hybrid data, these phenotypes support the idea that *AgRho1a* is the preferred target of *AgLrg1* while *AgRho1b* might be the preferred target of *AgSac7*.

Our results suggest that GTP-hydrolysis of *AgRho1a* should be lower than GTP-hydrolysis of *AgRho1b* in presence of *AgSac7*. To test this, we expressed the GTP-binding proteins and the GAP-domains of these *A. gossypii* proteins in

E. coli and purified them for an *in vitro* GAP-assay (figure 6B). The assay we used detects the release of phosphate from GTP-hydrolysis by a color reaction that can be monitored by an increase in absorbance of orange light ($\lambda = 650$ nm). GTP-hydrolysis of all control reactions, each GTP-binding protein and GAP on its own, is below OD 0.1. We used the GAP p50RhoGAP and the GTP-binding protein RhoA as a positive control. RhoA has the highest rate of GTP-hydrolysis with both human p50RhoGAP and the *AgSac7* GAP-domain. With both of these GAPs, GTP-hydrolysis of *AgRho1b* was significantly higher than GTP-hydrolysis of *AgRho1a*. The results obtained with *AgSac7* show that the difference in interaction between the two *AgRho1* proteins and *AgSac7* results in different GTP hydrolysis and therefore in a different activation state of the two *AgRho1* proteins in the cell.

Discussion

The initial question we addressed in this study was how the function of a Rho-type GTP-binding protein evolves after gene duplication. We found that during evolution, alteration of a single tyrosine to a histidine in one of the two encoded proteins can influence interaction with GTPase activating proteins. This simple change in the protein sequence has the dramatic effect of changing the function of the proteins thereby rewiring a whole signal transduction network without altering the specificity for effector proteins.

A condition that had to be met to study the mechanism of functional diversification of Rho-type GTP-binding proteins was that the duplicated genes have taken over different functions within the cell. We could show in the first part of our study that *AgRho1a* has diverged functionally from *AgRho1b*, while the function of the latter remained similar to the single *ScRho1* of *S. cerevisiae*. The data from deletion analysis, localization and complementation studies indicate that *AgRho1a* is still involved in actin regulation but has lost the glucan biosynthesis function that is preserved in *ScRho1* and *AgRho1b*. In addition, *AgRho1a* gained a novel function that prevents cell lysis at lower temperatures. The fact that both Rho1 proteins have different functions in *A. gossypii* raises the question why this could be an advantage for the cell. Different aspects have to be taken into account when answering this question. One

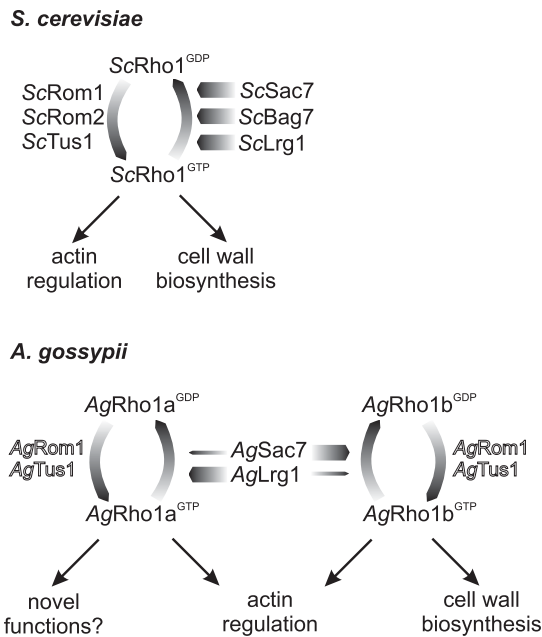


Figure 7: Model of Rho1 regulatory networks in *S. cerevisiae* and *A. gossypii*. *A. gossypii* homologs of Rho1 regulators known from *S. cerevisiae* that were not subject of our studies are printed in outline. Note that *ScROM1/ScROM2* and *ScSAC7/ScBAG7* are “Twin-ORFs”, remnants of a whole genome duplication that occurred in the *S. cerevisiae* lineage (Dietrich et al., 2004).

aspect is that there are far more Rho1 regulators present in *S. cerevisiae* than in *A. gossypii*. Figure 7 compares the core machinery of the Rho1 regulatory network of both organisms. The GEFs *ScRom1* and *ScRom2* (Ozaki et al., 1996), as well as the GAPs *ScSac7* and *ScBag7* (Schmidt et al., 2002), are so-called “Twin-ORFs”, remnants of a whole genome duplication that occurred in the *S. cerevisiae* lineage (Dietrich et al., 2004).

The increased number of regulatory proteins in *S. cerevisiae* adds a level of complexity to *ScRho1* regulation and thus might allow the adaptation of *ScRho1* activity in response to a variety of intra- and extracellular signals. The *RHO1* duplication in *A. gossypii* might have been maintained in the genome because it simply expands the organism’s capacity to fine-tune Rho1 activity to a similar level as it is possible with duplication of several GAPs or GEFs.

Furthermore, duplication of the *AgRHO1* genes might be advantageous for the filamentous life style of *A. gossypii*. In budding yeast, cell growth, cell cycle and cell division are tightly connected (Philippson et al., 2005). The majority of glucan biosynthesis occurs during polar growth when the new bud is formed. Thus, full Rho1 activity

in glucan biosynthesis is only required during a specific period of the cell cycle, the two different branches of *ScRho1* activity might be temporally restricted. Temporal restriction of polar growth is not present in *A. gossypii*. Rather, polar growth is active in the filamentous fungus all the time (Philippson et al., 2005) and requires a highly active glucan biosynthesis. Thus presence of a second, independently regulated Rho1 protein that is not involved in cell wall synthesis would allow the cell to uncouple the different branches of the Rho1 signalling pathway.

This raises the question how this uncoupling is reflected in the protein sequence or, with other words, what is the mechanism behind functional diversification after gene duplication? It is commonly assumed that, after such a duplication event, mutations alter the specificity of the Rho and its effectors. However, a large study of switch-of-function mutations with the Ras-Superfamily revealed that mutations outside the effector interaction interface can induce a switch of function (Heo and Meyer, 2003). In addition it was suggested for three closely related Rac proteins that their different function is not due to different effector proteins. Instead a different nucleotide binding capability and a different activation by a GEF are responsible for functional diversification (Haeusler et al., 2003). Our data strongly supports the idea of an effector-independent functional diversification of the *A. gossypii* Rho1 proteins because they share most of the effectors already known from *S. cerevisiae*. The only difference between *AgRho1a* and *AgRho1b* we detected on the effector level using the two-hybrid system was the very weak interaction of *AgSec3* with *AgRho1b* but not with *AgRho1a*. As *Sec3* in *S. cerevisiae* is a component of the exocyst, which is responsible for the delivery of vesicles to the growing tip (Guo et al., 2001), it is possible that this also contributes to the cell wall biosynthesis pathway that is regulated by *AgRho1b*. However this interaction is not affected by a tyrosine to histidine mutation in the switch I region, which makes it very unlikely that it contributes to the functional switch we observe in the *Agrho1aH39Y* mutant.

If it is not the different effectors that are responsible for the different *AgRho1a* and *AgRho1b* functions, it can only be the regulatory proteins, namely GEFs and GAPs. As stated above, a duplication of a Rho-encoding gene alone is not sufficient to gain novel functions. One or both of the encoded proteins would have to change their GAP- and GEF specificity in order to be differently regulated.

This diversification could only arise by mutation in the concerned genes. The histidine at position 39 of *AgRho1a* represents a mutation that occurred during evolution and alters interaction of *AgRho1a* with regulatory proteins. The homologous residue in the 323 other Rho-proteins (including *AgRho1b* and *ScRho1*) was, without exception, a conserved tyrosine. Consistently, it was possible to revert *AgRho1a* function to *AgRho1b* function by simply changing histidine 39 of *AgRho1a* to a tyrosine. The resulting *AgRho1aH39Y* was able to compensate for the loss of *AgRHO1b* while an *Agrho1b* Δ mutant alone was not viable. The atypical histidine 39 of *AgRho1a* is found in the switch I region, which is known to interact with GAPs in various small GTP-binding proteins. For this reason, we investigated the interactions of *AgRho1a* and *AgRho1b* with the two Rho1 GAPs *AgLrg1* and *AgSac7*. We found that Rho1a interacts preferentially with *AgLrg1* and only weakly with *AgSac7*.

AgRho1b on the other hand shows strong interaction *AgSac7*. The difference in two-hybrid interaction strength is reflected by the ability of *AgSac7* to activate GTP-hydrolysis more efficiently for *AgRho1b* than for *AgRho1a* as shown in an *in-vitro* GTPase activity assay. Interestingly, strong interaction with the Rho GAPs seems to be crucial for *AgRho1b* function, since *AgRho1aH39Y* can provide cell viability in absence of *AgRho1b* and shows GAP interaction similar to *AgRho1b*. This finding implies that precisely controlled GTP-hydrolysis is critical for the different *AgRho1* functions. First, it could be possible that not only GAP but also GEF interactions, which were not tested in this study, are altered. However, a GTPase deficient *AgRHO1a* allele was not able to rescue *Agrho1b* Δ (our own unpublished data). Thus, increasing the GTP-bound pool of *AgRho1a*, which would be a consequence of increased GEF affinity, did not have a similar effect as the *Agrho1aH39Y* mutation. Second, it is possible that *AgLrg1* and *AgSac7* localization and/or activity are controlled by input from other signalling pathways. An example for this is the Cdc28-dependent phosphorylation of *Sac7* in budding yeast (Ubersax et al., 2003). Subsequently, GAP-activity is not uniformly distributed in the cell. A difference in GAP-specificity could thus lead to a completely different temporal and spatial distribution of GTP- and GDP-bound *AgRho1a* and *AgRho1b*. Since interactions with known Rho1 effectors are virtually identical between *AgRho1a* and *AgRho1b*, the *AgRho1aH39Y* GAP-affinity

that resembles the GAP-affinity of *AgRho1b* might lead to a *AgRho1b*-like distribution of GTP-bound *AgRho1aH39Y* and thus to an activation of downstream events that are otherwise regulated by *AgRho1b*. Third, small GTP-binding proteins often not only work as on/off switches. The cycling between the GDP- and the GTP-bound form is important for functionality as it was shown for Cdc42 in yeast (Gladfelter et al., 2002). The same study characterized an *Sccdc42* mutant that had a tyrosine to histidine exchange like it is present in *AgRho1a*. In agreement with our results, this *Sccdc42* mutant could not be activated to the same level of GTPase activity by its GAP compared to wild-type *ScCdc42* with a tyrosine in switch I. Therefore, *AgRho1a H39Y* might be able to compensate for loss of *AgRHO1b* by having similar GDP/GTP cycling properties as *AgRho1b* and thus mimic *AgRho1b* action.

Even though the *AgRho1a* histidine residue in the switch I region is atypical for Rho-type proteins, it can be found in other GTP-binding proteins suggesting that the histidine mutation in the switch I region might be a general theme in evolution for diversification of small GTP-binding protein functions. Rin, Rit and Ric are examples of GTP-binding proteins that also have a histidine residue at a homologous position (Lee et al., 1996; Wes et al., 1996). Rit and Rin were shown to have a slower intrinsic GTP-hydrolysis rate than most other GTP-binding proteins, which might be caused by the histidine residue in their switch I region (Shao et al., 1999). Taking the knowledge from our study into account, it might be possible that these proteins, like *AgRho1a*, did not diverge from other GTP-binding proteins by altering effector but regulator interaction. Interestingly, these proteins, like the *AgRho1* proteins, seem to be important for sustained polar growth. They are found in neuronal cells, and Rit as well as Rin were recently shown to act in neurite outgrowth by interaction with the key cell polarity regulator PAR6 (Hoshino and Nakamura, 2003; Hoshino et al., 2005). It might be an interesting hypothesis to test if GTP-binding proteins with a histidine in switch I have an altered cycling-kinetic that is advantageous for polar growth.

Taken together, we find that GTP-binding protein function can evolve independently from effector interaction. In addition, we could show that a single change in the protein sequence was the most important step during this evolution.

Material and methods

Nomenclature

According to the guidelines used for the *A. gossypii* gene annotation, we refer in this manuscript to *ABR183W* as *AgRHO1b* and to *ABR182W* as *AgRHO1a*, while in an initial characterization the authors referred to *AgRHO1a* as *RHOH* (Walther and Wendland, 2005).

Ashbya gossypii strains and growth conditions

Ag1eu2Δthr4Δ was used as a reference strain. Deletion strains were constructed by PCR-based gene targeting according to the method described by Wendland et al. (2000). All oligonucleotides and corresponding mutants are listed in Supplemental Table S1. Plasmid pGEN3 was used as a template if the mutant strain is G418 resistant and plasmid pUC19NATPS was used in the case of CloNAT resistance. The strains were verified by PCR with primers binding inside the marker genes and primers binding close to the integration site.

Mutants carrying single amino acid exchanges in the genome were constructed as follows. The *Agrho1aC115T* mutants were generated by transformation of either the reference strain (for *Agrho1aC115T*) or the *Agrho1b* deletion strain (for *Agrho1aC115T Agrho1bΔ*) with the 4.2 kb *EcoRI/SalI* fragment from pHPS299. This fragment contained the mutated *Agrho1a* gene together with the Gen3 marker and flanking regions for integration via homologous recombination. The *Agrho1aQ68H* strain was generated by transformation of the reference strain with the 3.9 kb *SphI* fragment from pMK1a*. This fragment is similar to the one above except for the mutation in *Agrho1a*. The *Agrho1bQ69H* strain was generated by transformation of the reference strain with the 3.8 kb *PstI* fragment from pMK1b*. This fragment carries the mutated *Agrho1b* also together with the Gen3 marker and regions for homologous integration. Mutated alleles were amplified by PCR and checked by restriction digest for presence of the desired mutation. Primers used for amplification were *Rho1a_compl* and *AgRho1a-mutrev* for *Agrho1aC115T* resulting in a 510 bp fragment, *AgRho1a-ATG* and *AgRho1a-TAG* for *Agrho1aQ68H* resulting in a 620 bp fragment and *AgRho1b-ATG* and *AgRho1b-TAG* for *Agrho1bQ69H* resulting in a 620 bp

fragment. The mutation introduced inserted a *BglIII* restriction site into the *Agrho1aC115T* construct and to *BssSI* restriction sites in both other mutant fragments. Presence of the mutation was indicated by fragments of 328 bp and 182 bp for the digest of the *Agrho1aC115T* product and by fragments of 410 bp and 210 bp for the digest of both other PCR-products. In addition the correct integration of the mutated alleles was verified with PCR. The primers are listed in Supplemental Table S3.

Integration of deletion cassettes and mutagenized alleles always occurred only in few nuclei of the multinucleated mycelium leading to a heterokaryotic situation, where some nuclei still carried the wild-type allele. Homokaryotic strains that carry the desired mutation in all nuclei were generated by separation of single spores with single nuclei followed by selection on the marker of the mutation.

Strains were grown at the temperature indicated either in AFM (*Ashbya* Full Medium) with or without Geneticin or ClonNAT, or in synthetic medium when selecting for auxotrophic markers (Knechtle et al., 2003).

Saccharomyces cerevisiae strains and growth conditions

The genotypes of all strains used in this study are listed in Supplemental Table S2. DSH1 was constructed by PCR-based gene targeting according to the method described by Wach et al. (1994) using primers pC1-ScRHO1 and pC2-ScRHO1 together with pCORE as a template. HPS2 and HPS3 were constructed similarly with primers Sc-AgRHO1a-ATG (for *AgRHO1a*) or AgRHO1b-ATG (for *AgRHO1b*) and *Rho1* integrator using either pHPS262 (for *AgRHO1a*) or pHPS263 (for *AgRHO1b*) as a template. These vectors contain either one of the *AgRho1* genes together with the *KanMX* resistance cassette. Transformation of the product from such a PCR leads to replacement of the *S. cerevisiae* *RHO1* gene by its *A. gossypii* homologs generating a fusion with the *ScRHO1* promoter and thereby preventing artefacts that come from differences in function of heterologous promoters. The three strains DSH1, HPS2 and HPS3 built the basis for all other strains. All three were transformed with integrative vectors (pHPS254, pHPS256, pHPS258) cut with *EcoRV* for integration into the *LEU2* locus. The plasmids contained *ScRHO1*, *ScRHO1-2* or *ScRHO1-4* together with promoter and terminator. Using this method yielded the diploid strains *HPS4*, *HPS5*,

HPS7, *HPS9*, *HPS10*, *HPS12*, *HPS31*, *HPS34* and *HPS24*. Haploid strains carrying both integrated constructs were selected by tetrad analysis. The strain HPS40 was generated similar to HPS2 except for the fact that the *Agrho1aC115T* was first integrated into a vector containing the *ScRHO1* with flanking regions. The resulting vector pHPS317 was then used as template in a PCR reaction with the primers Sc-AgRHO1a-ATG and Rho1 integrator. The resulting product was transformed into *S. cerevisiae* for homologous integration.

S. cerevisiae strains were grown at 30° C. If different temperatures were used, this is indicated in the Figures. Media were used according to Amberg et al. (2005).

DNA manipulations and sequencing

All DNA Manipulations were carried out according to Sambrook et al. (2001) with DH5 α F' as host (Hanahan, 1983). Sequencing was done using an ABI DNA Sequencer according to the instructions of the manufacturer. Plasmids were isolated from yeast using the Roche "High Pure Plasmid Purification Kit" according to the instruction manual for plasmid preparation from *E. coli* but with the following modifications: 5 ml of a yeast culture were collected by centrifugation and the supernatant discarded. The cells were resuspended in solution 1 and 0.2 g of 0.5 mm glass beads were added. Cells were lysed by vortexing for 8 min at 4 °C. From here on the instructions of the manufacturer were followed, only the elution volume was decreased to 20 μ l. 10 μ l of the eluted fraction were transformed into *E. coli* for plasmid amplification.

Plasmids and constructs

All plasmids and constructs are listed in Supplemental Table S4 together with construction details. Sequences of most plasmids constructed for this study are available from the authors upon request.

Overlay assay for lysis quantification

The overlay assay for detection of cellular lysis was adopted from Saka et al. (2001). 4 μ l of a mycelia suspension was spotted on AFM plates for every strain and incubated at 30°C for 36 h. The plates were then shifted to 25°C, 30°C or

37°C over night (about 14 h) and overlaid in the morning with lysis indicator agarose containing 10 mM BCIP (5-Bromo-4-chloro-3-indonyl phosphate disodium salt). Lysis indicator agarose (10 ml of 0.05 M Glycine-HCl buffer pH 9.5 in and 1 % agarose for routine use (Sigma-Aldrich, St. Louis, USA) was boiled in a microwave oven and allowed to cool down to 50°C under constant stirring. The BCIP was added and dissolved and the warm agar was immediately poured over the mycelia. The plates were scanned after 90 min of incubation at room temperature using an EPSON Perfection 1200 PHOTO scanner (Long Beach, USA) and the average signal intensity of the blue channel of an area of 2960 pixels of the RGB image was determined using Metamorph v6.2 software (Universal Imaging Corporation, Downingtown, USA). Lysis of deletion strains was calculated relative to negative (wild type) and positive control strains (*Ags12* deletion).

Image acquisition and processing

For microscopy, cells were grown overnight in selective full or in selective synthetic minimal medium. Cells were then placed on slides with small cavities that were filled with half concentrated AFM with 2% glucose and 0.5% agarose and grown for 2 hours at the temperature indicated before they were placed under the microscope. The setup used for in vivo fluorescence microscopy consisted of a Zeiss Axioplan2e (Carl Zeiss, Jena, Germany) equipped with 100x alpha-Plan Fluor objective (NA 1.45) and differential-interference-contrast. Images were acquired using a Photometrics CoolSNAP HQ Camera (Roper Scientific, Tucson, USA). Fluorescence was excited with a Xenon-lamp and appropriate filtersets were used to adjust excitation and emission wavelengths. The setup was controlled by Metamorph v6.2 (Universal Imaging Corporation, Downingtown, USA). Brightfield images were acquired as single planes using differential-interference-contrast. Images were scaled using Metamorphs scale image command and Huygens essential software was used for deconvolution of the images. The processed images were overlaid using Metamorphs overlay images command.

Two-hybrid experiments

For two-hybrid experiments prey and bait plasmids were transformed into a and α derivatives of *S. cerevisiae* strain PJ69-4a. Strains were crossed

and selected on minimal medium without leucine and tryptophane but containing a four-fold concentration (80 mg/l) of adenine. Transformants were grown in the same liquid medium to an OD_{600} of about 1. Of these, 5 μ l were spotted on plates without leucine, tryptophane and histidine for selection on interaction. To test the strength of interactions 5-aminotriazole was added to the media at the concentration indicated.

Protein expression and Purification

All proteins were expressed using *E. coli* BL21 (DE3) as a host (Stratagene, La Jolla, USA). Induction, expression and GST-purification was performed as described in detail by Smith and Rittinger (2002). Purification of the hexa-histidine-tagged *AgSac7p* was performed using an ÄKTA FPLC system (GE Healthcare Life Sciences, Pittsburgh, USA) with 1 ml HisTrap FF column according to the instructions of the manufacturer. Lysis buffer consisted of 100mM Tris-HCl pH 8.0, 300mM NaCl and 2mM β -Mercaptoethanol. Elution buffer was 100mM Tris-HCl pH 8.0, 300mM NaCl, 2mM β -Mercaptoethanol and 500mM Imidazol.

Pulldown assays

GST-pulldown of GAP and GTP-binding proteins was performed in the presence of aluminiumfluoride by addition of 10 mM NaF and 450 μ M $AlCl_3$ to lysis and washing buffers for stabilization of the complex. Apart from the addition of aluminiumfluoride buffers and conditions used were similar to the purification of GST-tagged proteins described above. Western blots were visualized using an Odyssey infrared imaging system (Li-Cor, Lincoln, Nebraska USA) according to the protocol of the manufacturer using anti-GST from rabbit (G7781 Sigma, St. Louis, USA) and anti-Penta-HIS from mouse (34660 Qiagen, Hilden, Germany) as primary and anti-rabbit coupled to IRdye700 (611-730-127, Rockland Immunochemicals Inc., Gilbertsville, USA) and anti-mouse coupled to IRdye800 (926-32210, Li-Cor, Lincoln, USA) as secondary antibodies.

In vitro GAP-assay

The *in vitro* GAP-assay was performed using the “RhoGAP assay Biochem Kit” (BK105, Cytoskeleton Inc., Denver, USA) according to

the instructions of the manufacturer. RhoA and p50RhoGAP were controls supplied with the kit.

Acknowledgements

Thanks to Peter Philippsen and Jürgen J. Heinisch for constant support. Thanks to Peter Philippsen, Amy S. Gladfelter and Anja Lorberg for discussions and critical reading of the manuscript. Thanks to Alfred Wittinghofer, Reza Ahmadian and Stefan Hohmann for discussions. Thanks to Peter Uetz, Mike Hall, Yoshikazu Ohya and D. Hoepfner for strains and plasmids. Finally thanks to Lars Molzahn, Lynn Ullmann and Déborah Ley for their work during their lab internship.

Table 2: *A. gossypii* strains

strain	genotype	reference
<i>Alt</i>	<i>Agleu2Δ Agthr4Δkan^r</i>	Altmann-Johl and Philippsen 1996
<i>Agrho1aΔ</i>	<i>Agleu2Δ Agthr4Δ Agrho1aΔ::Gen3</i>	this study
<i>Agrho1bΔ</i>	<i>Agleu2Δ Agthr4Δ Agrho1bΔ::Gen3</i>	this study
<i>Agslt2Δ</i>	<i>Agleu2Δ Agthr4Δ Agslt2Δ::Gen3</i>	this study
<i>Aglrg1Δ</i>	<i>Agleu2Δ Agthr4Δ Aglrg1Δ::CloNAT</i>	this study
<i>Agsac7Δ</i>	<i>Agleu2Δ Agthr4Δ Agsac7Δ::Gen3</i>	this study
<i>Agrho1aC115T</i>	<i>Agleu2Δ Agthr4Δ Agrho1aC115T::Gen3</i>	this study
<i>Agrho1aC115T Agrho1bΔ</i>	<i>Agleu2Δ Agthr4Δ Agrho1aC115T::Gen3</i>	this study
<i>Agrho1aQ68H</i>	<i>Agleu2Δ Agthr4Δ Agrho1aC115T::Gen3</i>	this study
<i>Agrho1bQ69H</i>	<i>Agleu2Δ Agthr4Δ Agrho1aC115T::Gen3</i>	this study

Table 3: *S. cerevisiae* strains

strain	genotype	reference
<i>DHD5</i>	<i>MATa/MATα ura3-52/ura3-52 leu2-3,112/leu2-3,112 his3-11,15/his3-11,15</i>	Arvanitidis and Heinisch 1994
<i>PJ69-4a</i>	<i>MATa trp1-901 leu2-3,112 ura3-52 his3-200 gal4Δ gal80Δ LYS2::GAL1-HIS3 GAL2-ADE2 met2::GAL7-lacZ</i>	James et al. 1996
<i>PJ69-4α</i>	<i>MATα trp1-901 leu2-3,112 ura3-52 his3-200 gal4Δ gal80Δ LYS2::GAL1-HIS3 GAL2-ADE2 met2::GAL7-lacZ</i>	Uetz et al. 2000
<i>HPS2</i>	<i>MATa/MATα ura3-52/ura3-52 leu2-3_112/leu2-3_112 his3-11,15/his3-11,15 RHO1/rho1::AgRHO1a-HISMX</i>	this study
<i>HPS3</i>	<i>MATa/MATα ura3-52/ura3-52 leu2-3_112/leu2-3_112 his3-11,15/his3-11,15 RHO1/rho1::AgRHO1b-HISMX</i>	this study
<i>DSH1</i>	<i>MATa/MATα ura3-52/ura3-52 leu2-3_112/leu2-3_112 his3-11,15/his3-11,15 Δrho1::KanMX-KIURA3/RHO1</i>	this study
<i>HPS4</i>	<i>MATa/MATα ura3-52/ura3-52 leu2-3_112/leu2-3_112::LEU2-RHO1 his3-11,15/his3-11,15 RHO1/rho1::AgRHO1a-HISMX</i>	this study
<i>HPS5</i>	<i>MATa/MATα ura3-52/ura3-52 leu2-3_112/leu2-3_112::LEU2-rho1-2 his3-11,15/his3-11,15 RHO1/rho1::AgRHO1a-HISMX</i>	this study
<i>HPS7</i>	<i>MATa/MATα ura3-52/ura3-52 leu2-3_112/leu2-3_112::LEU2-rho1-4 his3-11,15/his3-11,15 RHO1/rho1::AgRHO1a-HISMX</i>	this study
<i>HPS9</i>	<i>MATa/MATα ura3-52/ura3-52 leu2-3_112/leu2-3_112::LEU2-RHO1 his3-11,15/his3-11,15 RHO1/rho1::AgRHO1b-HISMX</i>	this study
<i>HPS10</i>	<i>MATa/MATα ura3-52/ura3-52 leu2-3_112/leu2-3_112::LEU2-rho1-2 his3-11,15/his3-11,15 RHO1/rho1::AgRHO1b-HISMX</i>	this study
<i>HPS12</i>	<i>MATa/MATα ura3-52/ura3-52 leu2-3_112/leu2-3_112::LEU2-rho1-4 his3-11,15/his3-11,15 RHO1/rho1::AgRHO1b-HISMX</i>	this study
<i>HPS31</i>	<i>MATa/MATα ura3-52/ura3-52 leu2-3_112/leu2-3_112::LEU2-RHO1 his3-11,15/his3-11,15 Δrho1::KanMX-KIURA3/RHO1</i>	this study
<i>HPS34</i>	<i>MATa/MATα ura3-52/ura3-52 leu2-3_112/leu2-3_112::LEU2-rho1-2 his3-11,15/his3-11,15 Δrho1::KanMX-KIURA3/RHO1</i>	this study
<i>HPS24</i>	<i>MATa/MATα ura3-52/ura3-52 leu2-3_112/leu2-3_112::LEU2-rho1-4 his3-11,15/his3-11,15 Δrho1::KanMX-KIURA3/RHO1</i>	this study
<i>HPS32</i>	<i>MATa ura3-52 leu2-3_112::LEU2-RHO1 his3-11,15 Δrho1::KanMX</i>	this study
<i>HPS35</i>	<i>MATa ura3-52 leu2-3_112::LEU2-rho1-2 his3-11,15 Δrho1::KanMX</i>	this study
<i>HPS57</i>	<i>MATa ura3-52 leu2-3_112::LEU2-rho1-4 his3-11,15 Δrho1::KanMX</i>	this study
<i>HPS17</i>	<i>MATa ura3-52 leu2-3_112::LEU2-rho1-4 his3-11,15 rho1::AgRHO1a-HISMX</i>	this study
<i>HPS29</i>	<i>MATa ura3-52 leu2-3_112::LEU2-RHO1 his3-11,15 rho1::AgRHO1a-HISMX</i>	this study
<i>HPS54</i>	<i>MATa ura3-52 leu2-3_112::LEU2-rho1-2 his3-11,15 rho1::AgRHO1a-HISMX</i>	this study
<i>HPS19</i>	<i>MATa ura3-52 leu2-3_112::LEU2-RHO1 his3-11,15 rho1::AgRHO1b-HISMX</i>	this study
<i>HPS46</i>	<i>MATa ura3-52 leu2-3_112::LEU2-rho1-2 his3-11,15 rho1::AgRHO1b-HISMX</i>	this study
<i>HPS47</i>	<i>MATa ura3-52 leu2-3_112::LEU2-rho1-4 his3-11,15 rho1::AgRHO1b-HISMX</i>	this study
<i>HPS40</i>	<i>MATa; ura3-52; leu2-3_112; his3D1; MAL2-8C; SUC2; rho1::SpHIS3/RHO1a(C₁₁₅T)</i>	this study

Table 4: Oligonucleotides

name	sequence	use
Rho1a-S1	CTTATACTCGGACAATAACAGGCTGGGAAGTGACAGTTTCAGAAATgctaggg ataacagggtaat	<i>Agrho1a</i> deletion
Rho1a-S2	GGATATGTATGTAATTGACCGATGACTATGGATGCGGCGGCCGCTaggcatgc aagcttagatct	<i>Agrho1a</i> deletion
Rho1b-S1	GACCACTAGCTCGTTGCGCTGCAATATAATAATAAGAACGAGgctagggataacag gtaaat	<i>Agrho1b</i> deletion
Rho1b-S2	GTATTCAATCAACTATGTGAGTAGTTTCTTGTAGGCAGTCTCCagcatgcaagcct agatct	<i>Agrho1b</i> deletion
Slh2-S1	CGGGAGTAAAAGTGAAATAAATAACGAACTACTTACGGAACTATAGgctaggg ataacagggtaat	<i>Agslh2</i> deletion
Slh2-S2	CATCGGGCTCACGGGCGCACGACGTGAACGACGGAGAACGAAACAGCAAG aggcatgcaagcttagatct	<i>Agslh2</i> deletion
AgLrg1-NAT5'	GGTACCAATACGATCAGCAAGGGTAAGATAGGAAGTGCTACTGTTTTTCatg ggtaccactcttgacgac	<i>AgLrg1</i> deletion
AgLrg1-NAT3'	TAAGAGTCTGATAGTACATACTCATTATATTGAAAATGAGATCTGGgcttag gggcaggcatgctc	<i>AgLrg1</i> deletion
AgSAC7-F2	ATATAGACATATTCAGCAATTACGATACTATACTTTACTTTCATCCcatgattacgc caagcttgc	<i>Agsac7</i> deletion
AgSAC7-NS1	GACCGGCGCGCAGAAGCAGGGGACAGTGAGCGTGGGAGGGGCGGAGccagtg aattcgagctcgg	<i>Agsac7</i> deletion
V2_NAT1	GTGTCGTCAAGAGTGGTACC	CloNAT verification
V3_NAT1	ACATGAGCATGCCCTGCCCC	CloNAT verification
G3	TCGCAGACCGATAACCAGGATC	Gen3 verification
G2.3	GGAGGTAGTTTGCTGATTGG	Gen3 verification
delRho1aG1	GCGTTTCCATAGCTCAAGCAGCGCCC	<i>Agrho1aΔ</i> verification
delRho1aG4	CAGCGGACAACGGCTCGGCGTTGCTC	<i>Agrho1aΔ</i> verification
G1:Rho1b_vPCR_sense	CCACTAGCTCGTTGCGCTGC	<i>Agrho1bΔ</i> verification
G4:Rho1b_vPCR_ant	CCCGCCCATCACCAGTAAAC	<i>Agrho1bΔ</i> verification
Slh2-G1	GCCGGTATGACGCCATGTTC	<i>Agslh2Δ</i> verification
Slh2-G2	CGACGTGAACGACGGAGAAC	<i>Agslh2Δ</i> verification
AgLrg1-G1	GCGATGCCCGCCATTCTATTTTC	<i>AgLrg1Δ</i> verification
AgLrg1-G4	TGTTGCGGGATGCTTTGCTG	<i>AgLrg1Δ</i> verification
AgSAC7-G1	CGTCGCACTGAAGCACTGAGCC	<i>Agsac7Δ</i> verification
AgSAC7-G4	GGTTGGATGCTGATTCTGCTG	<i>Agsac7Δ</i> verification
AgRho1a-C115T	GGGCAGTCCCAGGAGATcATGTGCCAC	mutagenesis
AgRho1a-mutrev	GATCTCCGGGAACCTGCCCTTTGGAGAACAC	mutagenesis
AgRho1b-C118-120T	GGGAAAGTCCCACAGGTGcAcGTTCTACGG	mutagenesis
AgRho1b-mutrev	CACCTGTGGGAACCTTCCCTTGGCAAACAC	mutagenesis
AgRHO1a-TAGneu	CGACGGATCCTATTTCTTCTTCTTGTCCACC	cloning, verification
AgRHO1a-ATG	GAGATCGAATTCATGGCGTACCAGACAGGCGGCA	cloning, verification
AgRHO1b-TAGneu	CGACGGATCCTACTTTTTCTTCTTCTTGTCCAGAC	cloning, verification
AgRHO1b-ATG	GATCGAATTCATGTCTCAGCAAATGCATAAC	cloning, verification
G4_rho1a*_ins	CTTCCCTTGCCAAACA	<i>Agrho1aQ68</i> <i>H</i> verification
G4_Rho1b*_ins	GAAACACGGCTTTACCTACG	<i>Agrho1bQ69</i> <i>H</i> verification
AgRHO1a	TGCGGCCATTGTCGTACCCG	<i>Agrho1aQ68</i> <i>H</i> verification

AgRHO1b	TACGGCCGTTATCGTACCCAGACTCC	<i>Agrho1bQ69</i>
Rho1a_comp1	CTATGAGACTTCCGCTCCAATAGC	<i>H</i> verification
AgRho1a-mutrev	GATCTCCGGAACTGCCCTTTGGAGAACAC	verification
Sc-AgRHO1a-ATG	CTAATAGAAAATCATAGAACTTTAAAAATTATACTAGAAAAGatggcgtaccagaca ggcgg	<i>ScRHO1</i> ORF replacement
Sc-AgRHO1b-ATG	CTAATAGAAAATCATAGAACTTTAAAAATTATACTAGAAAAGatgctcagcaaatgc ataac	<i>ScRHO1</i> ORF replacement
Rho1-integrator	GCAGTATCTGCCACTAAGTTAACGACTGAGAGATCGAGACACTCgaattcagact cgtttaaac	<i>ScRHO1</i> ORF replacement
pGADAGLRG1-ATG	CGATGATGAAGATACCCACCAAACCCAAAAAAGAGATCATGACTAATA TACAGAAGCCACAGC	<i>in vivo</i> rekombination
pGADAGLRG1-TAG	GGGTTTTTCAGTATCTACGATTCATAGATCTCTGCAGGTCGACTTATTTATG GATTTCTACCTTCGTC	<i>in vivo</i> rekombination
pGADAgSAC7-ATG	CTATTCGATGATGAAGATACCCACCAAACCCAAAAAAGAGATCATGAG TGAGCAGGGCGCGCTG	<i>in vivo</i> rekombination
pGADAGSAC7-TAG	GGTTTTTCAGTATCTACGATTCATAGATCTCTGCAGGTCGACTATGTTGCTG ACCTAGAGCGGCTC	<i>in vivo</i> rekombination
behindAgRho1aS1	CCACGGTGACAAGAAGAAGAAGAAATGTCTGGTCTGTGAgctaggataacaggg taat	integration
behindAgRho1aS2	GTATGTAATTGACCGATGACTATGGATGCGGCGGCCGCTagcatgcaagcttagat ct	integration
behindAgRho1aS1	CCACGGTGACAAGAAGAAGAAGAAATGTCTGGTCTGTGAgctaggataacaggg taat	integration
behindAgRho1aS2	GTATGTAATTGACCGATGACTATGGATGCGGCGGCCGCTagcatgcaagcttagat ct	integration
AgLRG1-LoxATG	GAAGTTATCAGTCGACTgactaatatacagaagccacagc	cloning
AgLRG1-LoxTAA	ATGGTCTAGAAAAGCTTtattatgatttctaccttcgtcac	cloning
AgSAC7-LoxATG	GAAGTTATCAGTCGACTgagtgcagggcgctg	cloning
AgSAC7-LoxTAA	ATGGTCTAGAAAAGCTTatgttgcctacctagcggctcc	cloning
pGEXAgRho1aBam	CCGCGTGGATCCATGGCGTACCAGACAGGCGGCAAC	cloning
pGEXAgRho1aEco	CACGATGAATTCACAGGACCAGACATTTCTTCTTC	cloning
pGEXAgRho1bBam	GCGTGGATCCATGTCTCAGCAAAATGCATAACCC	cloning
pGEXAgRho1bEco	CACGATGAATTCCTACAAGACCACACATTTTCTTTC	cloning
AgSAC7GAP-BGLII	GCGCAGATCTCCGGCGTCCGTCACGCGGTGCCG	cloning
AgSAC7GAP-HINDIII	GCGCAAGCTTATCCGCAACATTACTATACTGG	cloning
AgLRG1GAP-BGLII	CGCGAGATCTCTTCTGCCCCAAAACCCCAAGTC	cloning
AgLRG1GAP-HINDIII	GCGCAAGCTTATTAATCAGGTAATCCACAGTTTCAATG	cloning
Rho1aQH1	GTGGACATCGACGGGCGACGCGTAGAGCTGGCACTGTGGGATACAGCGGG CCACGAGGAC	mutagenesis
Rho1aQH2	CATTGGAATCCGGGTACGACAATGGCCGACCCGGTCTAGTCTCTCGTGCC CCGCTGTAT	mutagenesis
Rho1a-pC1	GGGCGACGCGTAGAGCTGGCACTGTGGGATACAGCGGGCCgagctcgttttcgact gg	mutagenesis
Rho1a-pC2	GGAATCCGGGTACGACAATGGCCGACCCGGTCTAGTCTCTccttaccattagtt gatc	mutagenesis
Rho1b_Q-H_as_ok	CATTGGAGTCTGGGTACGATAACGGCCGTAGCCTGTCTGTAATCCTCGTGAG CCGTAT	mutagenesis
Int_Rho1a*_s1	CCGCCTACATATCCTACTATAAGCGTACATCTGCTGCGCGgctaggataacaggtaat	integration
Int_Rho1a*_s2*	AGCGATCAATAGTTAATAATCCGTAGCCTCGGCAACGCAGaagcttagatctgatgag gccg	integration
Int_Rho1b*_s1	CCGCATAGCACTGGAGCGAAATGATCTGCAAAATCCGAAgctaggataacagggt aat	integration
Int_Rho1b*_s2	GCTCAAGTTTCTTTATTGATGGGACAGACGTGCTGTCCGGgagcatgcaagcttagatc t	integration
Rho1b_del_S1	CCACTAGCTCGTTGCGCTGCAATATAATAAAGAACGAGgctaggataacagggt aat	deletion
Rho1b_del_S2	GTATTCAACTAATGATGTGAGTAGTTTCTGTAGGCAGTCagcatgcaagcttagatc t	deletion
pGADAgPkc1ATG	TGAAGATACCCACCAAACCCAAAAAAGAGATCGAATTCatgggagcagcagatga tgaac	<i>in vivo</i> rekombination
pGADAgPkc1TAG	AGTATCTACGATTCATAGATCTCTGCAGGTCGACGGATCctatagcacaagatcatca g	<i>in vivo</i> rekombination
AgSec3-Bam	GTATAAGTTGGATCCGGCGAGAAGGCGGAAAAGCTCCTTG	cloning
AgSec3-Eco	GAGATCGAATTCATGTTGAAGCGCTTTTCGCACAGCAG	cloning
pGADSKN7P	CCACCAAACCCAAAAAAGAGATCGAATTTCCCGGGATCCGGATGGCTGA GGAGATA	<i>in vivo</i> rekombination
pC1-ScRHO1	CTAATAGAAAATCATAGAACTTTAAAAATTATACTAGAAAAGgagctcgttttcgacac tgg	<i>Scrho1</i> deletion
pC2-ScRHO1	GCAGTATCTGCCACTAAGTTAACGACTGAGAGATCGAGACACTCtcttaccattaa gttgatc	<i>Scrho1</i> deletion

pGADSKN7T	CTTGCGGGGTTTTTCAGTATCTACGATTCATAGATCTCTGCAGTCACACCCT GGGTTTCTTC	<i>in vivo</i> rekombination
GFP-Bam	CGGGATCCAGTAAAGGAGAAGAAGCTTTTCAC	cloning
GFP-Eco	CGCGAATTCTTTGTATAGTTTCATCCATGCC	cloning
Rho1b-ECO	CGCGAATTCTCTCAGCAAATGCATAACCC	cloning
Rho1b-SPE	CACCAACTAGTGATATATAATGAAGCGAGGAG	cloning
Rho1a-ECO	CGCGAATTCGCGTACCAGACAGGCGGCAAC	cloning
Rho1a-SPE	CACCAACTAGTCAGTGTAGCACTTCGGTATC	cloning
Rho1bP-BAM	GCCGGATCCCATCTCGTTCTTATTATTATATTGCAGCG	cloning
Rho1bP-HIND	GGAAGCTTGCAGCCGCCGCATCCATAGTC	cloning
Rho1aP-BAM	GCCGGATCCCATATTTCTGAAACTGTCACTTC	cloning
Rho1aP-HIND	GGAAGCTTGAGACTTCCGCTCCAATAGC	cloning
AgRho1a-C115T	GGGCAGTTCGCGGAGATCTATGTGCCAC	mutagenesis
AgRho1a-mutrev	GATCTCCGGGAACTGCCCTTTGGAGAACAC	mutagenesis
Rho1a-HIS3F1	GAAGGTCCACGGTGACAAGAAGAAGAAATGTCTGGTCTGTGAACggat ccccgggtaataa	marker integration
Rho1a-HIS3R1	GGATATGTATGTAATTGACCGATGACTATGGATGCGGCGGCCGgaattc tcgttaaac	marker integration
pGADSTE4atg	GTACCAGATTACGCTCATATGGCCATGGAGGCCAGTGAATTCatgtagcattaga tatccatcc	<i>in vivo</i> rekombination
pGADSTE4taa	TTTTCAGTATCTACGATTCATCTGCAGCTCGAGCTCGATGGATCCtccatattagga ggtgaccacac	<i>in vivo</i> rekombination

*Bases are highlighted as follows: introduced restriction sites are underlined, altered codon for mutagenesis are printed bold, primers used for *in vivo* recombination are printed in capital letters for the homology region used for recombination and in small letters for the region used for annealing during the PCR reaction.

Table 5: Plasmids

Name ^a	Used	Content	Construction details or reference
pDH5			NCRR Yeast Resource Center, University of Washington
pDH3			NCRR Yeast Resource Center, University of Washington
pGUG			Knechtle et al. 2003
pUC19			Vieira and Messing 1991
pET-23a+			Novagen, Inc., Madison, Wisconsin, U.S.A.
pGEX-2t			GE Healthcare Life Sciences, Pittsburgh, USA
pGEN3			Wendland et al. 2000
RHO1L		<i>ScRHO1</i>	1.4kb XbaI/XhoI fragment cloned XbaI/SalI into YEPlac195 kindly provided by M. Hall
pUC19NATPS			kindly provided by D. Hoepfner (unpublished)
pCORE			Storici et al. 2001
pFA6a-HISMx			Longtine et al. 1998
YCPlacIII			Gietz and Sugino 1988
Yiplac128			Gietz and Sugino 1988
pGADT7			Clontech, Mountain View, CA, U.S.A.
pGAD424			James et al. 1996
pGBT9			James et al. 1996
pYO748			Qadota et al. 1996
pYO750			Qadota et al. 1996
pYO760			Qadota et al. 1996
pAG11194			Wendland and Philippsen 2001
pHPS291	Fig. 2	<i>YFP-AgRHO1a</i> <i>CFP-AgRHO1b</i>	<i>in vivo</i> recombination of PCR product with primers behindAgRho1aS1 and behindAgRho1aS1 from pGEN3 into pHPS289
pHPS289			<i>in vivo</i> recombination of HindIII/BglI fragment from pHPS286 into EcoRV/SpeI cut pHPS285
pHPS285			PCR product with GFP-Bam and GFP-Eco from pDH5 cut with EcoRI/BamHI in pHPS248 cut EcoRI/BamHI
pHPS286			PCR product with GFP-Bam and GFP-Eco from pDH3 cut with EcoRI/BamHI in pHPS250 cut EcoRI/BamH
			this study
			this study
			this study
			this study

pHPS250			PCR product with Rho1b-Eco and Rho1b-Spe from pAG11194 in pHPS247 cut EcoRI/SpeI	this study
pHPS248			PCR product with Rho1a-Eco and Rho1a-Spe from pAG11194 in pHPS246 cut EcoRI/SpeI	this study
pHPS247			PCR product with GFP-Bam and GFP-Eco from pGUG cut with EcoRI/BamHI in pHPS244 cut EcoRI/BamHI	this study
pHPS246			PCR product with GFP-Bam and GFP-Eco from pGUG cut with EcoRI/BamHI in pHPS245 cut EcoRI/BamHI	this study
pHPS245			PCR product with Rho1bP-BAM and Rho1bP-HIND from pAG11194 cut with BamHI/HindIII in YCPlac111 cut BamHI/HindIII	this study
pHPS244			PCR product with Rho1bP-BAM and Rho1bP-HIND from pAG11194 cut with BamHI/HindIII in YCPlac111 cut BamHI/HindIII	this study
pHPS250	Fig. 2	<i>GFP-AgRHO1b</i>	see above	this study
pHPS254	Fig. 3	<i>ScrHO1</i>	BamHI/SalI fragment from pYO760 in Yiplac128 cut BamHI/SalI	this study
pHPS256	Fig. 3	<i>Scrhol-2</i>	BamHI/SalI fragment from pYO748 in Yiplac128 cut BamHI/SalI	this study
pHPS258	Fig. 3	<i>Scrhol-4</i>	BamHI/SalI fragment from pYO750 in Yiplac128 cut BamHI/SalI	this study
pHPS299	Fig. 4	<i>Agrho1Y39H</i>	SpeI/SacI fragment from pHPS296 in pUC19 cut XbaI/SacI	this study
pHPS296			<i>in vivo</i> recombination of PCR with behindRho1aS1 and behindRho1aS1 into pHPS292	this study
pHPS292			PfoI/EheI fragment from pHPS276 in pHPS290 cut PfoI/EheI	this study
pHPS290			PCR with Rho1aP-HIND Rho1b-SPE from pAG11194 cut with HindIII/SpeI in YCPlac111 cut with HindIII/SpeI	this study
pHPS276	Fig. 5	<i>Agrho1aY39H</i> 2-hybrid	Quick change mutagenesis with primers AgRho1a-C115T and AgRho1a-mutrev of pHPS264	this study
pHPS264			PCR with Rho1a-ATG and Rho1a-TAGneu from pAG11194 cut EcoRI/BamHI in pGBT9 cut EcoRI/BamHI	this study
pHPS305	Fig. 4	<i>Agrho1aY39H</i> Δ <i>Agrho1b</i>	SpeI/SacI fragment from pHPS304 in pUC19 cut XbaI/SacI	this study
pHPS304			<i>in vivo</i> recombination of PCR product with Rho1b-S1 and Rho1b-S2 from pGen3 into pHPS292	this study
pHPS317	Fig. 4	<i>Agrho1aY39H</i>	BbsI/XhoI from pHPS299 in pHPS262 cut BbsI/XhoI	this study
pHPS262			HindIII/KpnI of pHPS260 in pUC19 cut HindIII/KpnI	this study
pHPS260			Sc-AgRHO1a-ATG and Rho1-integrator from pHPS253 into RHO1L	this study
pHPS253			<i>in vivo</i> recombination of PCR with Rho1a-HIS3F1 and Rho1a-HIS3R1 from pFa6a His3 and pAG11194	this study
pHPS313	Fig. 5	<i>AgLRG1</i> 2-hybrid	<i>in vivo</i> recombination of PCR with pGADLRG1-ATG and pGADLRG1-TAG from genomic Δ <i>lt</i> DNA into pGAD424 cut EcoRI/BamHI	this study
pHPS314	Fig. 5	<i>AgSAC7</i> 2-hybrid	<i>in vivo</i> recombination of PCR with pGADSAC7-ATG and pGADSAC7-TAG from genomic Δ <i>lt</i> DNA into pGAD424 cut EcoRI/BamHI	this study
pHPS333	Fig. 5	<i>6his-AgSAC7</i>	PCR with AgSAC7GAP-BGLII and AgSAC7GAP-HINDIII from genomic Δ <i>lt</i> DNA cut HindIII/BamHI in pET-23a+ cut HindIII/BglII	this study
pHPS334	Fig. 5	<i>6his-AgLRG1</i>	PCR with AgLRG1GAP-BGLII and AgLRG1GAP-HINDIII from genomic Δ <i>lt</i> DNA cut HindIII/BamHI in pET-23a+ cut HindIII/BglII	this study
pHPS270	Fig. 5	<i>GST-AgRho1a</i>	PCR with pGEXAgRho1aBam and pGEXAgRho1aEco from pAG11194 cut EcoRI/BamHI in pGEX-2t cut EcoRI/BglII	this study
pHPS272	Fig. 5	<i>GST-AgRho1b</i>	PCR with pGEXAgRho1bBam and pGEXAgRho1bEco from pAG11194 cut EcoRI/BamHI in pGEX-2t cut EcoRI/BglII	this study
pHPS277	Fig. 5	<i>Agrho1aY39H</i> , Q68H 2-hybrid	Quick change mutagenesis with primers AgRho1a-C115T and AgRho1a-mutrev of pHPS265	this study
pHPS265			PCR with Rho1a-ATG and Rho1a-TAGneu from pHPS212 cut EcoRI/BamHI in pGBT9 cut EcoRI/BamHI	this study

pHPS212			<i>in vivo</i> recombination with annealed primers Rho1aQH1 and Rho1aQH2 and pHPS210 cut with BamHI/AflIII	this study
pHPS210			<i>in vivo</i> recombination of PCR with Rho1a-pC1 and Rho1a-pC2 from pCORE into pAG11194	this study
pMK1a_int	Fig. 6	<i>Agrho1aQ68H</i>	SphI fragment of pRho1a*_kanr in pUC19 cut SphI	this study
pRho1a*_kanr			<i>in vivo</i> recombination of PCR with Int_Rho1a*_s1 and Int_Rho1a*_s1 from pGEN3 into pHPS212	this study
pMK1b_int	Fig. 6	<i>Agrho1bQ69H</i>	PstI fragment of pRho1b*_kanr in pUC19 cut PstI	this study
pRho1b*_kanr			<i>in vivo</i> RK mit PCR Int_Rho1b*_s1 Int_Rho1b*_s1 von pGEN3	this study
pRho1b*			<i>in vivo</i> recombination with annealed primers Rho1aQH1 and Rho1aQH2 and Rho1b_cas	this study
Rho1b_cas			<i>in vivo</i> recombination of PCR with Rho1b-pC1 and Rho1b-pC2 from pCORE into pAG11194	this study
pHPS205	Table 1	<i>AgPKC1</i> 2-hybrid	<i>in vivo</i> recombination of PCR with pGADAgPkc1-ATG and pGAD-AgPkc1-TAA from genomic <i>Δt</i> DNA and pGAD424 cut EcoRI/BamHI	this study
pHPS214	Table 1	<i>AgBNI1</i> 2-hybrid	<i>in vivo</i> recombination of PCR with pGADBNI1-ATG and pGADBNI1-TAA from genomic <i>Δt</i> DNA and pGAD424 cut EcoRI/BamHI	this study
pHPS224	Table 1	<i>AgSKN7</i> 2-hybrid	<i>in vivo</i> recombination of PCR with pGADAgSKN7P and pGADAgSKN7T from genomic <i>Δt</i> DNA and pGAD424 cut BamHI	this study
pHPS237	Table 1	<i>AgSTE4</i> 2-hybrid	<i>in vivo</i> recombination of PCR with pGADAgSte4-ATG and pGADSte4-TAA from genomic <i>Δt</i> DNA and pGADT7 cut EcoRI/BamHI	this study
pHPS275	Table 1	<i>AgSEC4</i> 2-hybrid	BamHI/EcoRI fragment from pHPS274 in pGAD424 cut BamHI/EcoRI	this study
pHPS274			PCR with AgSec3-Bam and AgSec3-Eco genomic <i>Δt</i> DNA cut BamHI/EcoRI in pUC19 cut BamHI/EcoRI	this study

^anames aligned left are base vectors or were used in the Figures or tables listed in column 2. Names aligned right are constructs that the other vectors are based on.

Appendix

Introduction

Hyphal growth allows filamentous fungi to spread rapidly through their substrate in search for nutrients or mating partners, or to penetrate host organisms (figure 1). Single hyphae can elongate with 20 $\mu\text{m}/\text{min}$, fungal mycelia are known to cover hectares (Smith et al., 1992). Attempts to understand hyphal growth have led to the description of the Spitzenkörper or apical body by Girbardt in 1957. He observed that the apical body, which was visible as a phase-dense structure in the hyphal tip, is only present in growing hyphae and that its location in the hyphal tip correlates with the direction of hyphal growth. Electron microscopy of different fungal species revealed that the appearance of the apical body varies between different species but that it shares some common features. Most prominently, vesicles are accumulated in the apical body. They surround a distinct core region, which either appears as a dense cluster of vesicles, as a meshwork of microfilaments or, sometimes, as a structure with low contrast in the EM (Grove and Bracker, 1970; Howard, 1981; Harris et al., 2005, Robert W. Roberson, unpublished results). Microtubules extend into and through the apical body though no microtubule organizing centers (MTOC) could be identified in the tips of higher fungi (Han et al., 2001; Freitag et al., 2004, Robert W. Roberson and Claudia Birrer, unpublished results).

A role for the apical body in polarized secretion was assumed since it mainly consists of vesicles. How tightly hyphal morphogenesis and the apical body might be connected was found in the late eighties by computer simulations. It was shown that hyphal shapes arise by simply moving a vesicle supply center (VSC), which is a theoretical construct that distributes vesicles in all directions, with a constant speed. The predicted position of such a VSC and the position of the apical body coincided, which led to the theory that post-Golgi vesicles accumulate in the apical body before they are redistributed to the growing tip (Bartnicki-Garcia et al., 1989; Bartnicki-Garcia et al., 1995). Importantly, one has to consider that the VSC hypothesis only defines minimal requirements for hyphal morphogenesis and does not take into consideration factors like endocytosis or the possibility that not the entire plasma membrane might be compatible for vesicular fusion. Nevertheless, this hypothesis implied that understanding the apical body is of great importance to understand fast and efficient hyphal growth. A first insight on a molecular level came from *C. albicans* hyphae where the formin *CaBni1* as well as the myosin light chain *CaMlc1* were found to localize to the apical body (Crampin et al., 2005). In *Ashbya gossypii*, we found that the formin *AgBni1*, the polarisome components *AgSpa2* and *AgPea2*, and the exocyst components *AgExo70* and *AgSec3* localize in an apical body-like pattern suggesting that it might play a role

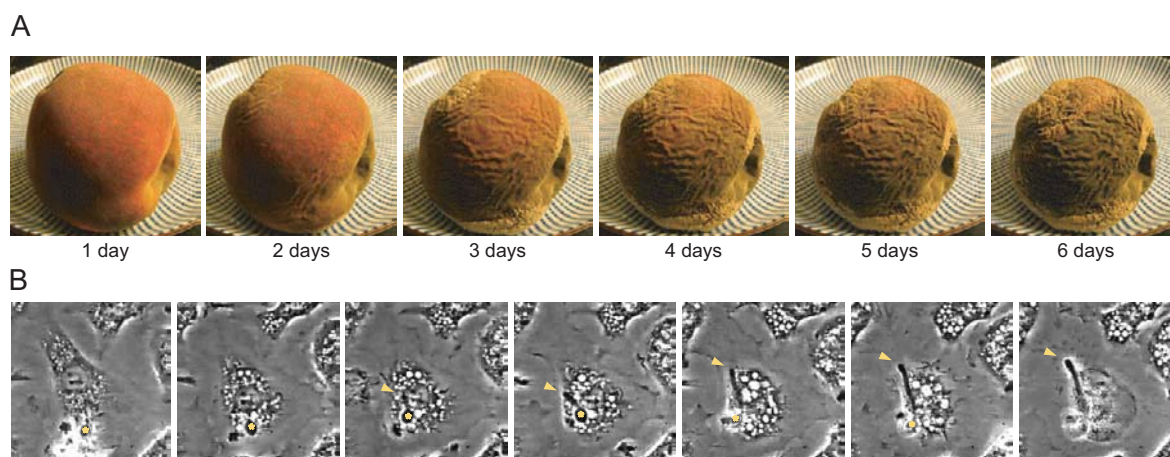


Fig. 1: Hyphal growth allows filamentous fungi to spread. (A) Fungal spread on a peach. The pictures were taken with a time-interval of one day. (B) The fungal pathogen *C. albicans* (asterisk) is engulfed by a mouse bone marrow macrophage. *C. albicans* responds by growing a germ tube (arrowhead) which eventually pierces the macrophage from the inside, killing the attacking macrophage while the fungus survives. The image series cover 75 minutes in real time. Pictures were taken by Julie Theriot and Julie Koehler, Stanford University Medical School, USA (<http://cmgm.stanford.edu/theriot/index.html>).

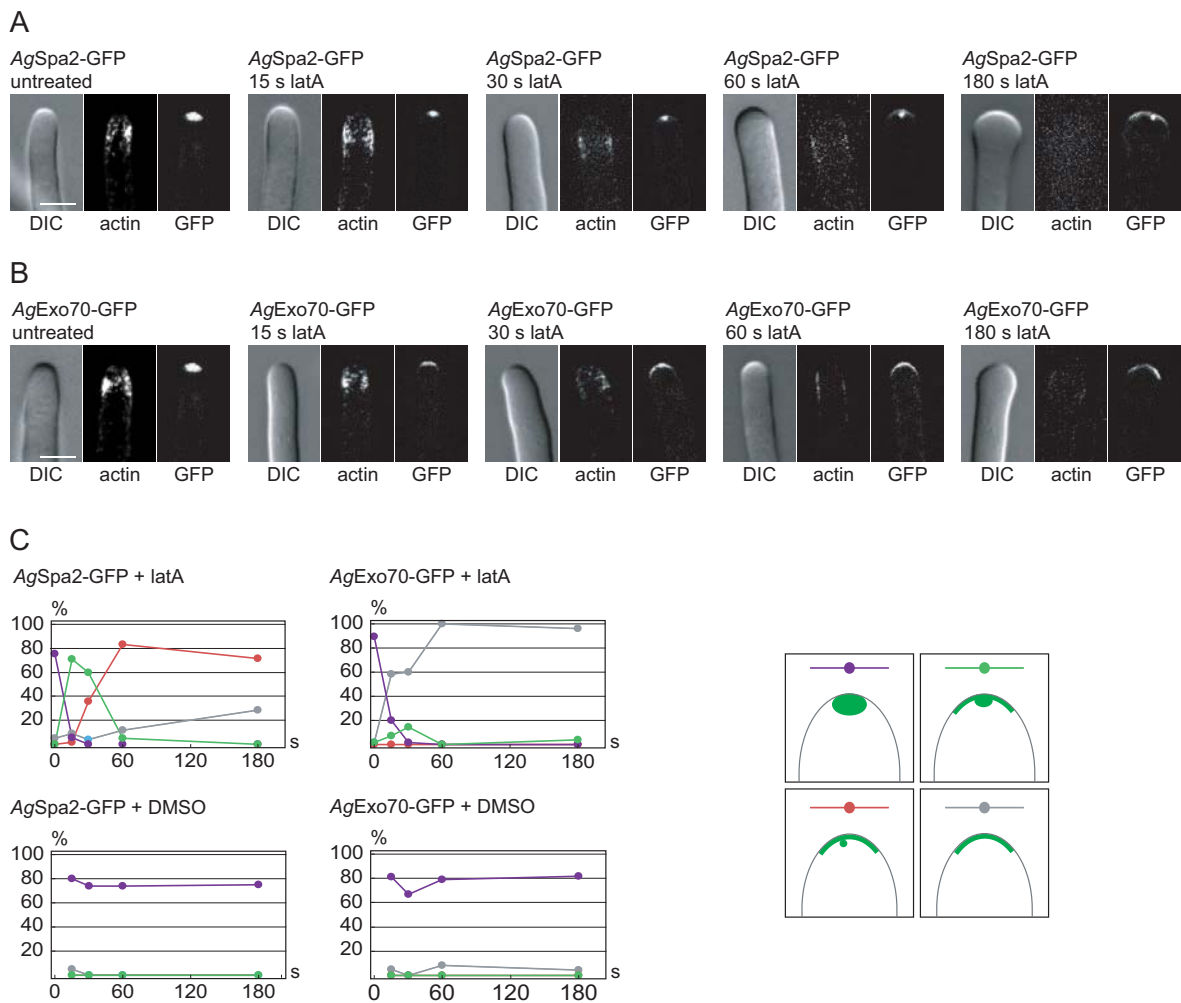


Fig. 2: Disruption of the actin cytoskeleton leads to formation of an AgSpa2-GFP containing spherule. (A) Latrunculin A was added to a 20 hours old liquid culture of a strain that expresses *AgSpa2-GFP*. Samples were fixed prior to and 15, 30, 60 and 180 seconds after addition of the drug. Disruption of the actin cytoskeleton was monitored by staining of the hyphae with Alexa568-coupled phalloidin. Representative pictures are shown for the different time points. (B) Images of *AgExo70-GFP* expressing hyphae that were treated as described above. (C) Quantification of different, characteristic localization patterns that were observed upon treatment of 20 hours old mycelia with latrunculin A or DMSO. 40 to 60 leading hyphae were analyzed for the latrunculin A treated samples and more than 20 for the DMSO controls. The purple line represents the hyphae that displayed apical body-like localization of *AgSpa2-GFP* or *AgExo70-GFP*, the green line hyphae that displayed a “condensed” spherical localization pattern, the red line hyphae with small and bright GFP spherules and the grey line cortical localization of *AgSpa2-GFP* or *AgExo70-GFP*. Schemes of the different localization patterns are shown next to the graphs. Note that the different categories do not add up to 100 % since few hyphae were observed that displayed crescent-like or aberrant localizations of the GFP-tagged factors, which are not included in the graphs. Scale bar = 5 μ m.

in organization of the actin cytoskeleton and, eventually, in organization of polarized secretion. The experiments described in the appendix are only loosely connected characterizing different aspects of fast hyphal growth and the apical body. First, we show that loss of filamentous actin leads to accumulation of *AgBni1* and *AgSpa2* in small spherules. In a sharp contrast, *AgExo70* was restricted to the cortex upon actin cytoskeleton disruption. Microtubules are frequently observed in the hyphal tip. However, apical body-like localization of *AgExo70*-GFP and fast hyphal growth are microtubule-independent. The endoplasmic reticulum reaches into the region occupied by the apical body but does not form a distinct sphere like it is observed for other organisms.

***AgSpa2* and *AgBni1* form distinct structures upon actin cytoskeleton disruption.**

Filamentous actin is indispensable for polarized growth of fungal cells (Novick and Botstein, 1985; Akashi et al., 1994; Ayscough et al., 1997; Fuchs et al., 2005). Loss of filamentous actin in *Candida albicans* hyphae resulted in depolarized cell growth leading round, enlarged hyphal tips (Crampin et al., 2005) thus the actin cytoskeleton is necessary for polar growth but not for surface expansion *per se*. Here, we studied the effect of latrunculin A on different polarity factors of *A. gossypii*. Latrunculin A is a toxin from the sponge *Latrunculia magnifica*. It sequesters monomeric actin (Coue et al., 1987), actin structures disappear quickly due to the dynamic nature of the actin cytoskeleton (Ayscough et al., 1997).

Loss of actin cables, either due to latrunculin A treatment or due to loss of the formin *AgBNI1*, leads to dispersal of the post-Golgi vesicle marker GFP-*AgSec4* in *A. gossypii* (Schmitz et al., 2006). We wondered how other factors that localize to the apical body behave upon disruption of the actin cytoskeleton. For this reason, spores of *AgSPA2-GFP* and *AgEXO70-GFP* were inoculated in liquid AFM for 20 hours at 30 °C. The cultures were split, one half was treated with 200 μM latrunculin A, the other half with DMSO as a control. Samples were taken after different time-points, fixed and stained for actin. Already after 15 seconds, apical body localization of *AgExo70*-GFP and *AgSpa2*-GFP was not observed

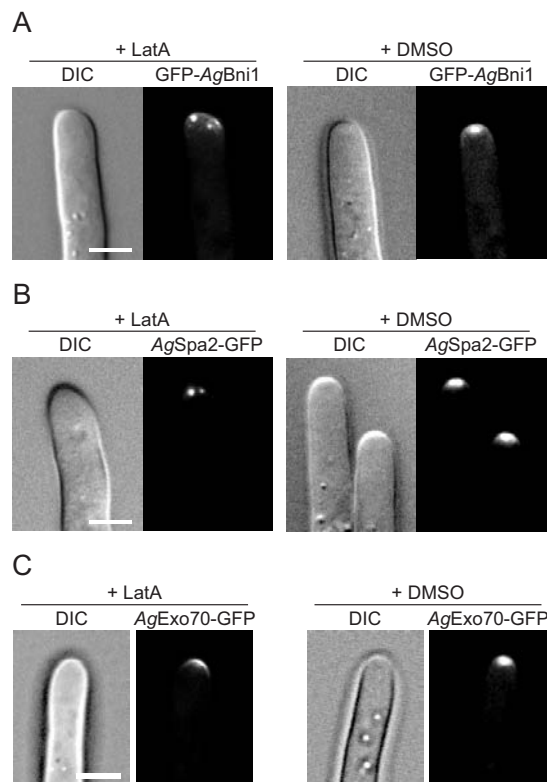


Fig. 3: *AgBni1*-GFP concentrates in a spherule upon latrunculin A treatment. (A) GFP-*AgBNI1* hyphae growing on a time lapse slide (glass slide with a cavity that is filled with AFM microscopy agar) were treated with 5 μl 400 μM latrunculin A in AFM or with a DMSO control. The pictures show hyphae three minutes after addition of the drug. (B) *AgSPA2-GFP* and (C) *AgEXO70-GFP* were treated as described for GFP-*AgBNI1*. Scale bars = 5 μm.

any more for most hyphae. While *AgExo70*-GFP was found at the cortex in the majority of latrunculin treated hyphae, the *AgSpa2*-signal was observed in a localization pattern that could be best described as a “condensed apical body” (figure 2, 15 s time point). After 60 seconds, *AgSpa2*-GFP mostly formed a single, small spherule (figure 2A and 2C, 60s time point). This structure seemed to be rather stable since it was still visible three minutes after addition of latrunculin A when hyphal tips were enlarging isotropically (figure 2A, 180s and 2C). Five minutes after administration of the drug, some *AgSpa2*-GFP spherules were still visible (data not shown). Most of the GFP-*AgBNI1* hyphae displayed a cortical or crescent-like localization pattern even if treated with DMSO only thus the GFP-*AgBni1* distribution in fixed hyphae seems not to reflect the localization patterns known from live hyphae. For this reason, latrunculin treated GFP-*AgBNI1* hyphae were observed by time-lapse microscopy. Latrunculin A induced swelling of hyphal tips after about ten minutes and lysis of

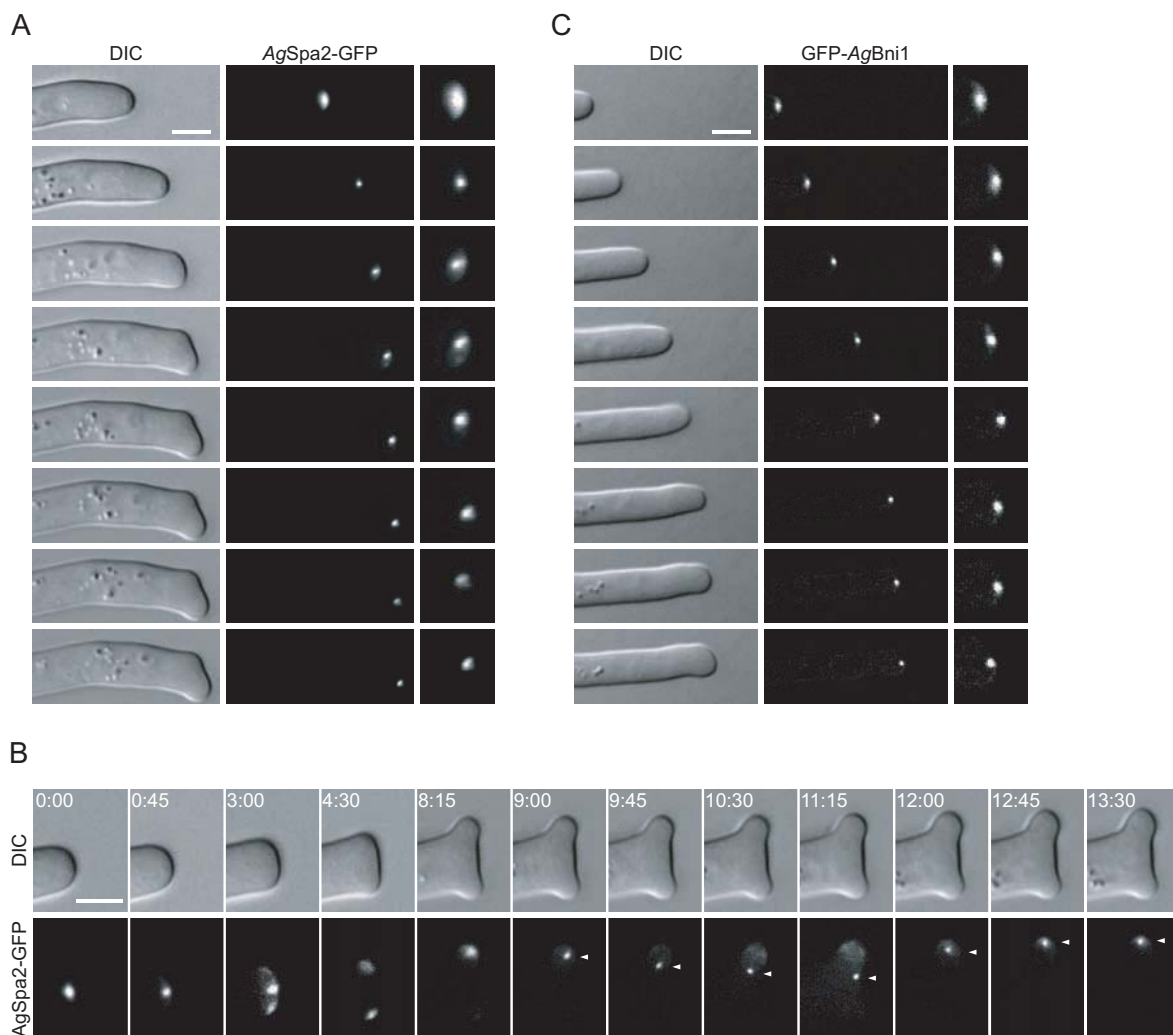


Fig. 4: Microscopy-induced stress leads to formation of *AgSpa2-GFP* and *GFP-AgBni1* spherules.

(A) Frames from a time-lapse movie of an *AgSpa2-GFP* hypha (movie S6). The time interval between the images is 3 minutes, the second column shows the *AgSpa2-GFP* signal that is correlated with the DIC pictures. The third column displays an enlargement of the tip region in the GFP-channel. (B) Frames from a time-lapse movie of *AgSpa2-GFP* are shown (movie S7). The white numbers indicate the times in minutes. The white arrowhead designates an *AgSpa2-GFP* spherule that moves inside the hypha. (C) Frames from a time-lapse movie of a *GFP-AgBni1* expressing strain (movie S8). The time interval between the images is 3 minutes. Scale bars = 5 μm .

some hyphae after 15 minutes in mycelia grown on time-lapse slides, which are glass slides with a cavity that is filled with AFM microscopy agar. The slower reaction of hyphae to latrunculin A on solid medium compared to liquid culture might result from the lower growth temperatures under microscopy conditions. *GFP-AgBni1* was concentrated in a bright spherule along with one to four less intense *GFP-AgBni1* foci in 76 % of all hyphae ($n = 17$) three minutes after application of latrunculin A (figure 3A). The *GFP-AgBni1* spherules were not stable since they were not detected in hypha that grew isotropically (not shown). Similarly, *AgSpa2-GFP* was observed in a bright spherule in 87 % of all cases, accompanied

by some smaller, less intense *AgSpa2-GFP* dots in 48 % of the hyphae ($n = 23$, figure 3B). The small *AgSpa2* spots have not been observed in hyphae that were treated with latrunculin A in liquid culture. Therefore, they might be the consequence of the slowed actin cytoskeleton disruption under microscopy conditions. Formation of *AgExo70-GFP* spherules was not observed (figure 3C) confirming the findings from the previous experiment. Intriguingly, *AgSpa2-GFP* and *GFP-AgBni1* spherules not only occurred if the actin cytoskeleton was disrupted. Frequently, spherule formation accompanied by deceleration of hyphal growth was observed in hyphae upon prolonged exposure to intensive blue light during

acquisition of time-lapse movies (figure 4A and movie S6). Interestingly, the spherule seemed not necessarily to be associated with the tip since extensive movement of an *AgSpa2*-GFP spherule was observed (figure 4B and movie S7). Microscopy stress had a similar effect on *AgBni1*: GFP-*AgBni1* spherule formation accompanied cessation of hyphal growth (figure 4C and movie S8).

In summary, apical body-like localization of the polarisome component *AgSpa2*, the formin *AgBni1* and the exocyst component *AgExo70* was sensitive to latrunculin A. In contrast, the polarized, cortex-associated pools of these factors stayed at hyphal tips even during non-polar growth that resulted from disruption of the actin cytoskeleton. Additionally, *AgBni1* and *AgSpa2* but not *AgExo70* concentrated in a spherule in the hyphal tip. In fast growing hyphae, *AgSpa2* and *AgBni1* are enriched in a core-like structure in the apical body as shown in part I on figure 8, it is thus tempting to speculate that the spherules observed upon disruption of the actin cytoskeleton are remnants of this core structure. In budding yeast, the formin *ScBni1* displays retrograde movement on actin cables. Loss of polymerized actin abolishes retrograde transport with enhanced targeting of *ScBni1* to the bud tip (Buttery et al., 2007). If the mechanism of actin-dependent *AgBni1* dispersal is conserved in *A. gossypii*, it is possible that destruction of the actin cytoskeleton leads to *AgBni1* accumulation at the sites where it is recruited at the tip cortex and, eventually, in the center of the apical body. Interestingly, we saw a decrease in cytoplasmatic fluorescence of GFP-*AgBni1* upon latrunculin A treatment which supports this hypothesis (data not shown). Future experiments will show whether *AgSpa2* and *AgBni1* colocalize in the core region of the apical body or the spherules observed upon disruption of the actin cytoskeleton respectively. Interestingly, formation of *AgSpa2* and *AgBni1* spherules was observed upon prolonged exposure to intensive, blue light. This similarity between latrunculin A and light-stress induced cessation of hyphal growth may indicate that quick deceleration of hyphal growth could be mediated by loss of actin cables. Indeed, it was discovered in budding yeast that the actin cytoskeleton depolarizes upon heat shock (Delley and Hall, 1999). Thus, it would be possible that an unknown mechanism deactivates the machinery responsible for generation of polarized actin cables resulting in spherule formation in the hyphal tip. However,

this is highly elusive. We do not know how blue light influences the mycelium or whether heat shock has similar effects on *A. gossypii* and on *Saccharomyces cerevisiae*.

Microtubules are not necessary for apical body-like localization of *AgExo70*-GFP and hyphal growth in *A. gossypii*.

Microtubules are frequently observed in the apical body by transmission electron microscopy (figure 5A). This was further confirmed by immunofluorescence staining of microtubules in an *AgEXO70-GFP* strain (figure 5C). Spherical localization of *AgExo70*-GFP was taken as an indication for the presence of an apical body since *AgExo70*-GFP localized to the FM 4-64 stained apical body as shown in part I, figure 3. In 88 %

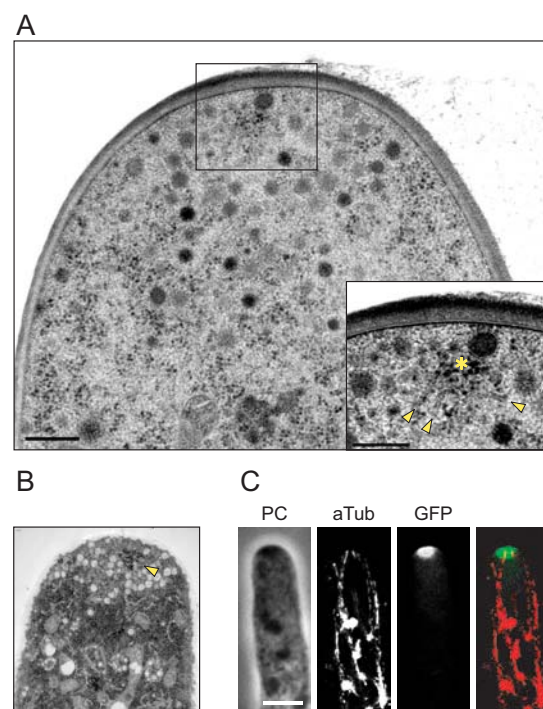
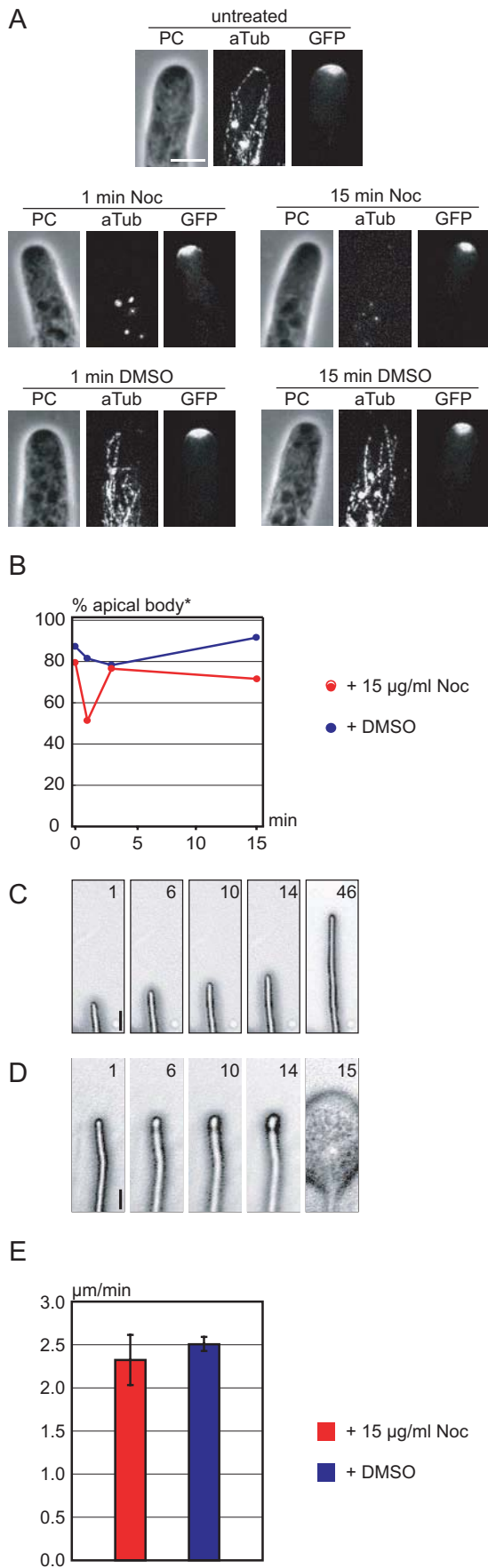


Fig. 5: Electron microscopy of the hyphal tip: microtubules and ribosomes in the apical body. (A) Transmission electron microscopy micrograph (TEM) of a cryo-fixed *A. gossypii* hyphal tip. The inset shows a higher magnification of the region that is marked with a rectangle on the bigger image. The star denotes a cluster of ribosomes, the arrowheads point to microtubules. Scale-bars = 0.3 μm and 0.2 μm respectively. (B) TEM micrograph of a chemically fixed hypha. The arrowhead points to a ribosomal cluster that is surrounded by a dense array of vesicles. (C) Immunofluorescence staining of microtubules in an *AgExo70*-GFP expressing strain. Microtubules (aTUB) are shown in red and *AgExo70*-GFP (GFP) in green in the overlay image. Scale bar = 5 μm .



of the cases, one or two microtubules penetrated into the *AgExo70-GFP* labeled zone, in about 10 % of the cases, no microtubules were observed in this region while one hypha displayed 3 microtubules in the apical body (n = 32). The apical body was hypothesized to be a switching center between microtubule-based long-range transport and short-range actin-mediated transport (Harris et al., 2005). If this were true for *A. gossypii*, one would expect an effect on the apical body upon microtubule destruction. To test this hypothesis, microtubules were disrupted with 15 µg/ml nocodazole in a 19 hours old culture. After one minute of treatment, the cytoplasmic microtubules disappeared. After 15 minutes, no mitotic spindles were detected any more. Lack of microtubules did not influence hyphal morphogenesis neither did it cause changes in the *AgExo70-GFP* localization (figure 6A). 50 to 70 tips were analyzed for presence of an apical body that is indicated by spherical localization of *AgExo70-GFP*. Interestingly, a decrease in the number of apical bodies was observed after one minute of nocodazole treatment. Nevertheless, spherical *AgExo70-GFP* localization was observed in a majority of the hyphae at all time-points (figure 6B). Even 4 hours after microtubule loss, many hyphae appeared undisturbed (data not shown). It was reported that hyphal growth continues in the absence of microtubules (Gladfelter et al., 2006, supplemental figures), however it might still be possible that hyphal elongation speed is reduced. To test this possibility, the border of 3 days old mycelium that was growing on AFM agar plates was treated with nocodazole and observed

Fig. 6: Microtubules are not necessary for apical body-like localization of *AgExo70-GFP* and hyphal growth. (A) Immunofluorescence staining of microtubules (aTUB) in an *AgExo70-GFP* (*GFP*) strain that was treated with 15 µg/ml nocodazole. Spores were inoculated in liquid AFM and incubated for 20 hours at 30 °C. The images are taken from samples that were fixed and processed one minute and 15 minutes after addition of nocodazole. Scale bar = 5 µm. (B) The relative occurrence of hyphae displaying *AgExo70-GFP* in an apical-body like localization is plotted on the y-axis, the time after addition of nocodazole or DMSO on the x-axis. The red line represents the data from the nocodazole-treated hyphae, and the blue line the DMSO treated control. Between 45 and 70 leading hyphae were assessed per time point. (C) AFM containing 30 µg/ml nocodazole was pipetted onto the border of a 2 days old mycelium, pictures of an image sequence are shown. The numbers indicate the time after addition of nocodazole in minutes. (D) Control treatment with 400 µM latrunculin A. Scale-bars for C and D = 20 µm. (E) AFM containing 30 µg/ml nocodazole or DMSO was pipetted onto the border of a 3 days old mycelium. Hyphal growth speeds were measured over 12 minutes. The bars represent the mean from 3 experiments, 15-25 hyphae were assessed per experiment. Error bars = S.E.

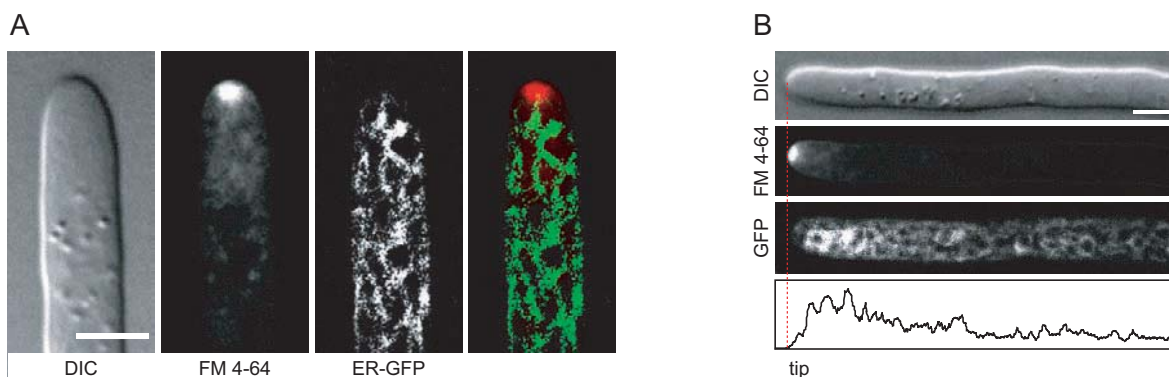


Fig. 7: The ER does not localize in an apical body-like manner in the hyphal tip. (A) ER-GFP (green in the overlay) in a hypha that was stained with FM 4-64 (red in the overlay). The strain *K81* was stained with FM 4-64 as described in part I. (B) Image of an ER-GFP expressing hypha that was stained with FM 4-64. The intensity profile of ER-GFP was measured in the direction of the hyphal axis with the “line scan”-tool of the MetaMorph software and is shown in the lowest panel. The x-axis indicates the distance from the tip and the y-axis relative GFP fluorescence intensity. Scale bars = 5 μ m.

microscopically during the following 50 minutes (figure 6C). Growth continued while treatment with latrunculin A led to immediate cessation of hyphal growth, swelling and lysis (figure 6D). Furthermore, the average hyphal elongation rate was measured during a time period of 12 minutes after nocodazole treatment. Growth speeds of nocodazole- and DMSO treated hyphae did not differ (figure 6E).

To summarize, we could not find an indication that microtubules are directly involved in hyphal growth of *A. gossypii* despite the fact that they are frequently observed in the hyphal tip. Disruption of microtubules by nocodazole neither abolished apical body-like localization of *AgExo70* nor did it slow down hyphal growth. It is thus unlikely that the apical body in *A. gossypii* serves as a switching center between microtubule- and actin-based vesicle transport since, in this case, one would at least expect a reduction of hyphal growth speed. Nevertheless, microtubules are essential for formation of a mycelium due to their role in nuclear transport and mitosis. In the basidiomycete *Ustilago maydis*, loss of microtubules does not influence morphogenesis as well but reduces hyphal growth speed (Fuchs et al., 2005). Disruption of microtubules in *Aspergillus nidulans* resulted in a severe reduction of hyphal growth though morphogenesis seemed normal (Horio and Oakley, 2005) thus indicating that microtubules play a direct role in hyphal growth of filamentous fungi. However, benomyl was used as a microtubule-destabilizing agent in both studies instead of nocodazole. We found that a mix of benomyl and nocodazole led to transient swelling of hyphal tips and dispersal of *AgExo70*-GFP in *A. gossypii* (data

not shown). This cell polarity defect is likely to be a side effect of benomyl rather than a consequence of microtubule disruption since nocodazole alone disrupts microtubules without affecting polar growth.

The endoplasmic reticulum displays a polarized distribution in *A. gossypii* and reaches into the apical body.

Ribosomes, which are visualized as small, electron-dense dots by transmission electron microscopy, are highly abundant in the cytosol. The ribosomal density seems reduced in the peripheral region of the apical body while an enrichment of ribosomes in a core region is obvious (figure 5A and 5B). We wondered whether the space devoid of ribosomes could represent the lumen of endoplasmic reticulum (ER) since ER fragments are associated with the apical body of the green algae *Chara globularis* (Braun, 2001). We tested this hypothesis by localization of ER-GFP, which consists of GFP flanked by a signal peptide and an ER retention signal (Hettema et al., 1998). ER-GFP localized in network through the hypha and extended into the region that was stained with FM 4-64 in 13 out of 14 cases (figure 7A). However, the ER was not observed in a spherical localization that resembled the apical body in its shape. Nevertheless, it displays a polarized distribution in hyphae (figure 7B) since the ER-GFP signal was more intense in the proximity of the hyphal tip in all observed cases (n = 19).

In summary, the ER reaches into the zone of the hyphal tip that is occupied by the apical body. Yet the part of the apical body poor in ribosomes does not represent ER lumen since the tip-base ER did not resemble the apical body in its shape. Therefore, it might be possible that a dense array of different proteins and vesicles excludes ribosomes from parts of the apical body. The endoplasmic reticulum seems to be denser close to hyphal tips as indicated by the higher ER-GFP fluorescence in this region. Apical accumulation of ER seems to be a general theme in filamentous fungi since it was also observed in *U. maydis* (Wedlich-Soldner et al., 2002) and might be beneficial for hyphal growth.

Material and methods

Please see the “Materials and methods” section of part I for general information on strains and techniques. Here, only materials and methods are described that were not mentioned otherwise, plasmids and strains are listed in table 1 and 2.

A. *gossypii* strain construction

ER-GFP (pK81 and pK82)

The plasmids pK81 and pK82 that encode an ER-GFP fusion protein were transformed into *Agლე2Δthr4Δ* to give rise to a strain with a luminal endoplasmic reticulum (ER) marker. ER-GFP is a fusion protein of the *ScSuc2* amino-terminus that contains a signal peptide for ER import, GFP and the ER retention signal from *ScKar2* (Hettema et al., 1998). Expression of *ER-GFP* was driven by the *ScHIS3* promoter. The plasmids pK81 and pK82 were generated by ligating the *EcoRI/HinDIII* digested, T4 DNA polymerase treated 1

kbp fragment of pAgIntER-GFP into *PvuII* cut pRS415 and pAG503.

Immunofluorescence staining of microtubules

Immunofluorescence was performed as described previously by Gladfelter et al., 2006. *A. gossypii* spores were inoculated in AFM and grown for 20 hours. The culture was checked microscopically to ensure the presence of fast-growing hyphae. Samples that displayed signs of starvation like heavily vacuolated hyphae were discarded (Helfer and Gladfelter, 2006). The culture was fixed for one hour by adding formaldehyde to a final concentration of 4 %. A rat anti-tubulin antibody (YOL34; Serotec, United Kingdom) was used at a dilution of 1:50, AlexaFluor568 goat anti-rat (Invitrogen, USA) at a dilution of 1:200.

Cytoskeleton disruption

Latrunculin A, which binds to and sequesters monomeric actin, was stored at -20 °C in a 0.237 M stock (100 µg/µl) in DMSO and was added to liquid cultures to a final concentration of 200 µM. For live imaging, 5 µl of 400 µM latrunculin A in AFM was added on time-lapse slides, effectiveness of the latrunculin A treatment was confirmed by swelling of hyphal tips and lysis. Microtubules were disrupted with nocodazole, which was kept in a stock of 3 mg/ml in DMSO at -65 °C and added to liquid cultures to a final concentration of 15 µg/ml. For live imaging, 15 µl of 30 µg/ml nocodazole were added to the mycelia.

Table 1: Plasmids

Name	Backbone	Insert	Source
pAG503	pRS415	<i>ScLEU2</i> of pRS415 replaced with GEN3	Knechtle 2002
pAgIntER-GFP	pAgINTLAC	<i>P_{ScHIS3}-ER-GFP</i>	Schlatter I., unpublished
pK81	pRS415	<i>P_{ScHIS3}-ER-GFP</i>	This study
pK82	pAG503	<i>P_{ScHIS3}-ER-GFP</i>	This study

Table 2: *A. gossypii* strains

Strain	Genotype	Construction	Source
K81	<i>ER-GFP</i> (pK81) <i>Agcdc42Δ Agლე2Δ Agthr4Δ</i>	pK81	This study
K82	<i>ER-GFP</i> (pK82) <i>Agcdc42Δ Agლე2Δ Agthr4Δ</i>	pK82	This study

References

References

- Adamo, J. E., G. Rossi and P. Brennwald (1999). The Rho GTPase Rho3 has a direct role in exocytosis that is distinct from its role in actin polarity. *Mol Biol Cell* **10**(12): 4121-33.
- Adams, A. E., D. I. Johnson, R. M. Longnecker, B. F. Sloat and J. R. Pringle (1990). CDC42 and CDC43, two additional genes involved in budding and the establishment of cell polarity in the yeast *Saccharomyces cerevisiae*. *J Cell Biol* **111**(1): 131-42.
- Ahmadian, M. R., R. Mittal, A. Hall and A. Wittinghofer (1997). Aluminum fluoride associates with the small guanine nucleotide binding proteins. *FEBS Lett* **408**(3): 315-8.
- Akashi, T., T. Kanbe and K. Tanaka (1994). The role of the cytoskeleton in the polarized growth of the germ tube in *Candida albicans*. *Microbiology* **140** (Pt 2): 271-80.
- Alberts, A. S. (2001). Identification of a carboxyl-terminal diaphanous-related formin homology protein autoregulatory domain. *J Biol Chem* **276**(4): 2824-30.
- Altmann-Johl, R. and P. Philippsen (1996). AgTHR4, a new selection marker for transformation of the filamentous fungus *Ashbya gossypii*, maps in a four-gene cluster that is conserved between *A. gossypii* and *Saccharomyces cerevisiae*. *Mol Genet* **250**(1): 69-80.
- Amberg, D. C., D. J. Burke and S. J. N. (2005). *Methods in Yeast Genetics: A Cold Spring Harbor Laboratory Course Manual.*, Cold Spring Harbors Laboratory Press, U.S.
- Arvanitidis, A. and J. J. Heinisch (1994). Studies on the function of yeast phosphofructokinase subunits by in vitro mutagenesis. *J Biol Chem* **269**(12): 8911-8.
- Ashby and Nowell (1926). *Annals of Botany* **XL**.
- Ayad-Durieux, Y., P. Knechtle, S. Goff, F. Dietrich and P. Philippsen (2000). A PAK-like protein kinase is required for maturation of young hyphae and septation in the filamentous ascomycete *Ashbya gossypii*. *J Cell Sci* **113** Pt 24: 4563-75.
- Ayscough, K. R., J. Stryker, N. Pokala, M. Sanders, P. Crews and D. G. Drubin (1997). High rates of actin filament turnover in budding yeast and roles for actin in establishment and maintenance of cell polarity revealed using the actin inhibitor latrunculin-A. *J Cell Biol* **137**(2): 399-416.
- Bartnicki-Garcia, S. and E. Lippman (1969). Fungal morphogenesis: cell wall construction in *Mucor rouxii*. *Science* **165**(890): 302-4.
- Bartnicki-Garcia, S., D. D. Bartnicki, G. Gierz, R. Lopez-Franco and C. E. Bracker (1995). Evidence that Spitzenkörper behavior determines the shape of a fungal hypha: a test of the hyphoid model. *Exp Mycol* **19**(2): 153-9.
- Bartnicki-Garcia, S., F. Hergert and G. Gierz (1989). Computer simulation of fungal morphogenesis and the mathematical basis for hyphal (tip) growth. *Protoplasma* **153**(1): 46-57.
- Batra, L. R. (1973). Nematosporeaceae (Hemiascomycetidae): Taxonomy, pathogenicity, distribution, and vector relations. *USDA Technical Bulletin* **1469**: 1-71.
- Baudin, A., O. Ozier-Kalogeropoulos, A. Denouel, F. Lacroute and C. Cullin (1993). A simple and efficient method for direct gene deletion in *Saccharomyces cerevisiae*. *Nucleic Acids Res* **21**(14): 3329-30.
- Bauer, Y., P. Knechtle, J. Wendland, H. Helfer and P. Philippsen (2004). A Ras-like GTPase is involved in hyphal growth guidance in the filamentous fungus *Ashbya gossypii*. *Mol Biol Cell* **15**(10): 4622-32.
- Benton, B. K., A. Tinkelenberg, I. Gonzalez and F. R. Cross (1997). Cla4p, a *Saccharomyces cerevisiae* Cdc42p-activated kinase involved in cytokinesis, is activated at mitosis. *Mol Cell Biol* **17**(9): 5067-76.
- Bose, I., J. E. Irazoqui, J. J. Moskow, E. S. Bardes, T. R. Zyla and D. J. Lew (2001). Assembly of scaffold-mediated complexes containing Cdc42p, the exchange factor Cdc24p, and the effector Cla4p required for cell cycle-regulated phosphorylation of Cdc24p. *J Biol Chem* **276**(10): 7176-86.
- Boyd, C., T. Hughes, M. Pypaert and P. Novick (2004). Vesicles carry most exocyst subunits to exocytic sites marked by the remaining two subunits, Sec3p and Exo70p. *J Cell Biol* **167**(5): 889-901.
- Braun, M. (2001). Association of spectrin-like proteins with the actin-organized aggregate of endoplasmic reticulum in the Spitzenkörper of gravitropically tip-growing plant cells. *Plant Physiol* **125**(4): 1611-9.
- Braun, M., J. Hauslage, A. Czogalla and C. Limbach (2004). Tip-localized actin polymerization and remodeling, reflected by the localization of ADF, profilin and villin, are fundamental for gravity-sensing and polar growth in characean rhizoids. *Planta* **219**(3): 379-88.

References

- Brown, J. L., M. Jaquenoud, M. P. Gulli, J. Chant and M. Peter (1997). Novel Cdc42-binding proteins Gic1 and Gic2 control cell polarity in yeast. *Genes Dev* **11**(22): 2972-82.
- Burbelo, P. D., D. Drechsel and A. Hall (1995). A conserved binding motif defines numerous candidate target proteins for both Cdc42 and Rac GTPases. *J Biol Chem* **270**(49): 29071-4.
- Buttery, S. M., S. Yoshida and D. Pellman (2007). Yeast formins Bni1 and Bnr1 utilize different modes of cortical interaction during the assembly of actin cables. *Mol Biol Cell* **18**(5): 1826-38.
- Butty, A. C., N. Perrinjaquet, A. Petit, M. Jaquenoud, J. E. Segall, K. Hofmann, C. Zwahlen and M. Peter (2002). A positive feedback loop stabilizes the guanine-nucleotide exchange factor Cdc24 at sites of polarization. *Embo J* **21**(7): 1565-76.
- Byrne, K. P. and K. H. Wolfe (2006). Visualizing syntenic relationships among the hemiascomycetes with the Yeast Gene Order Browser. *Nucleic Acids Res* **34**(Database issue): D452-5.
- Chen, G. C., Y. J. Kim and C. S. Chan (1997). The Cdc42 GTPase-associated proteins Gic1 and Gic2 are required for polarized cell growth in *Saccharomyces cerevisiae*. *Genes Dev* **11**(22): 2958-71.
- Chien, C. T., P. L. Bartel, R. Sternglanz and S. Fields (1991). The two-hybrid system: a method to identify and clone genes for proteins that interact with a protein of interest. *Proc Natl Acad Sci U S A* **88**(21): 9578-82.
- Coue, M., S. L. Brenner, I. Spector and E. D. Korn (1987). Inhibition of actin polymerization by latrunculin A. *FEBS Lett* **213**(2): 316-8.
- Crampin, H., K. Finley, M. Gerami-Nejad, H. Court, C. Gale, J. Berman and P. Sudbery (2005). *Candida albicans* hyphae have a Spitzenkorper that is distinct from the polarisome found in yeast and pseudohyphae. *J Cell Sci* **118**(Pt 13): 2935-47.
- Cvrckova, F., C. De Virgilio, E. Manser, J. R. Pringle and K. Nasmyth (1995). Ste20-like protein kinases are required for normal localization of cell growth and for cytokinesis in budding yeast. *Genes Dev* **9**(15): 1817-30.
- Dammer, K. H. and Grillo-Ravelo (1996). Verseuchung von *Leptoglossus gonagara* (Fabr.) mit *Nematosporea caryli* und *Ashbya gossypii* (Ashby et Nowell) Guilliermond in einer Zitrusanlage der Republik Kuba. Berlin, Arch. Phytopathol. Pflanzenschutz: 26:71.78.
- Delley, P. A. and M. N. Hall (1999). Cell wall stress depolarizes cell growth via hyperactivation of RHO1. *J Cell Biol* **147**(1): 163-74.
- Demain, A. L. (1972). Riboflavin oversynthesis. *Annu Rev Microbiol* **26**: 369-88.
- Demma, M., V. Warren, R. Hock, S. Dharmawardhane and J. Condeelis (1990). Isolation of an abundant 50,000-dalton actin filament bundling protein from *Dictyostelium amoebae*. *J Biol Chem* **265**(4): 2286-91.
- Dietrich, F. S., S. Voegeli, S. Brachat, A. Lerch, K. Gates, S. Steiner, C. Mohr, R. Pohlmann, P. Luedi, S. Choi, R. A. Wing, A. Flavier, T. D. Gaffney and P. Philippsen (2004). The *Ashbya gossypii* genome as a tool for mapping the ancient *Saccharomyces cerevisiae* genome. *Science* **304**(5668): 304-7.
- Dijksterhuis, J. (2003). Confocal microscopy of Spitzenkorper dynamics during growth and differentiation of rust fungi. *Protoplasma* **222**(1-2): 53-9.
- Dong, Y., D. Pruyne and A. Bretscher (2003). Formin-dependent actin assembly is regulated by distinct modes of Rho signaling in yeast. *J Cell Biol*.
- Drgonova, J., T. Drgon, K. Tanaka, R. Kollar, G. C. Chen, R. A. Ford, C. S. Chan, Y. Takai and E. Cabib (1996). Rho1p, a yeast protein at the interface between cell polarization and morphogenesis. *Science* **272**(5259): 277-9.
- Dunkler, A. and J. Wendland (2007). Use of MET3 promoters for regulated gene expression in *Ashbya gossypii*. *Curr Genet*.
- Dvorsky, R., L. Blumenstein, I. R. Vetter and M. R. Ahmadian (2004). Structural insights into the interaction of ROCK1 with the switch regions of RhoA. *J Biol Chem* **279**(8): 7098-104.
- Evangelista, M., D. Pruyne, D. C. Amberg, C. Boone and A. Bretscher (2002). Formins direct Arp2/3-independent actin filament assembly to polarize cell growth in yeast. *Nat Cell Biol* **4**(1): 32-41.
- Evangelista, M., K. Blundell, M. S. Longtine, C. J. Chow, N. Adames, J. R. Pringle, M. Peter and C. Boone (1997). Bni1p, a yeast formin linking cdc42p and the actin cytoskeleton during polarized morphogenesis. *Science* **276**(5309): 118-22.
- Finger, F. P., T. E. Hughes and P. Novick (1998). Sec3p is a spatial landmark for polarized secretion in budding yeast. *Cell* **92**(4): 559-71.

- Fischer-Parton, S., R. M. Parton, P. C. Hickey, J. Dijksterhuis, H. A. Atkinson and N. D. Read (2000). Confocal microscopy of FM4-64 as a tool for analysing endocytosis and vesicle trafficking in living fungal hyphae. *J Microsc* **198** (Pt 3): 246-59.
- France, Y. E., C. Boyd, J. Coleman and P. J. Novick (2006). The polarity-establishment component Bem1p interacts with the exocyst complex through the Sec15p subunit. *J Cell Sci* **119**(Pt 5): 876-88.
- Freitag, M., P. C. Hickey, N. B. Raju, E. U. Selker and N. D. Read (2004). GFP as a tool to analyze the organization, dynamics and function of nuclei and microtubules in *Neurospora crassa*. *Fungal Genet Biol* **41**(10): 897-910.
- Fuchs, U., I. Manns and G. Steinberg (2005). Microtubules are dispensable for the initial pathogenic development but required for long-distance hyphal growth in the corn smut fungus *Ustilago maydis*. *Mol Biol Cell* **16**(6): 2746-58.
- Fujiwara, T., K. Tanaka, A. Mino, M. Kikyo, K. Takahashi, K. Shimizu and Y. Takai (1998). Rho1p-Bni1p-Spa2p interactions: implication in localization of Bni1p at the bud site and regulation of the actin cytoskeleton in *Saccharomyces cerevisiae*. *Mol Biol Cell* **9**(5): 1221-33.
- Gietz, R. D. and A. Sugino (1988). New yeast-*Escherichia coli* shuttle vectors constructed with in vitro mutagenized yeast genes lacking six-base pair restriction sites. *Gene* **74**(2): 527-34.
- Gietz, R. D., R. H. Schiestl, A. R. Willems and R. A. Woods (1995). Studies on the transformation of intact yeast cells by the LiAc/SS- DNA/PEG procedure. *Yeast* **11**(4): 355-60.
- Girbardt, M. (1957). Der Spitzenkoerper von *Polystictus versicolor*. *Planta* **50**: 47-50.
- Gladfelter, A. S. (2006). Nuclear anarchy: asynchronous mitosis in multinucleated fungal hyphae. *Curr Opin Microbiol* **9**(6): 547-52.
- Gladfelter, A. S., A. K. Hungerbuehler and P. Philippsen (2006). Asynchronous nuclear division cycles in multinucleated cells. *J Cell Biol* **172**(3): 347-62.
- Gladfelter, A. S., I. Bose, T. R. Zyla, E. S. Bardes and D. J. Lew (2002). Septin ring assembly involves cycles of GTP loading and hydrolysis by Cdc42p. *J Cell Biol* **156**(2): 315-26.
- Gladfelter, A. S., J. J. Moskow, T. R. Zyla and D. J. Lew (2001). Isolation and characterization of effector-loop mutants of CDC42 in yeast. *Mol Biol Cell* **12**(5): 1239-55.
- Gooday, G. W. (1971). An autoradiographic study of hyphal growth of some fungi. *J. Gen. Microbiol.* **67**: 125-133.
- Grove, S. N. and C. E. Bracker (1970). Protoplasmic organization of hyphal tips among fungi: vesicles and Spitzenkorper. *J Bacteriol* **104**(2): 989-1009.
- Gulli, M. P., M. Jaquenoud, Y. Shimada, G. Niederhauser, P. Wiget and M. Peter (2000). Phosphorylation of the Cdc42 exchange factor Cdc24 by the PAK-like kinase Cla4 may regulate polarized growth in yeast. *Mol Cell* **6**(5): 1155-67.
- Guo, W., D. Roth, C. Walch-Solimena and P. Novick (1999). The exocyst is an effector for Sec4p, targeting secretory vesicles to sites of exocytosis. *Embo J* **18**(4): 1071-80.
- Guo, W., F. Tamanoi and P. Novick (2001). Spatial regulation of the exocyst complex by Rho1 GTPase. *Nat Cell Biol* **3**(4): 353-60.
- Haeusler, L. C., L. Blumenstein, P. Stege, R. Dvorsky and M. R. Ahmadian (2003). Comparative functional analysis of the Rac GTPases. *FEBS Lett* **555**(3): 556-60.
- Han, G., B. Liu, J. Zhang, W. Zuo, N. R. Morris and X. Xiang (2001). The *Aspergillus* cytoplasmic dynein heavy chain and NUDF localize to microtubule ends and affect microtubule dynamics. *Curr Biol* **11**(9): 719-24.
- Hanahan, D. (1983). Studies on transformation of *Escherichia coli* with plasmids. *J Mol Biol* **166**(4): 557-80.
- Harris, S. D., N. D. Read, R. W. Roberson, B. Shaw, S. Seiler, M. Plamann and M. Momany (2005). Polarisome meets spitzkorper: microscopy, genetics, and genomics converge. *Eukaryot Cell* **4**(2): 225-9.
- Hazuka, C. D., S. C. Hsu and R. H. Scheller (1997). Characterization of a cDNA encoding a subunit of the rat brain rsec6/8 complex. *Gene* **187**(1): 67-73.
- Helfer, H. and A. S. Gladfelter (2006). AgSwe1p regulates mitosis in response to morphogenesis and nutrients in multinucleated *Ashbya gossypii* cells. *Mol Biol Cell* **17**(10): 4494-512.
- Heo, W. D. and T. Meyer (2003). Switch-of-function mutants based on morphology classification of Ras superfamily small GTPases. *Cell* **113**(3): 315-28.
- Hettema, E. H., C. C. Ruigrok, M. G. Koerkamp, M. van den Berg, H. F. Tabak, B. Distel and I. Braakman (1998). The cytosolic DnaJ-like protein djp1p is involved specifically in peroxisomal protein import. *J Cell Biol* **142**(2): 421-34.

References

- Hofken, T. and E. Schiebel (2004). Novel regulation of mitotic exit by the Cdc42 effectors Gic1 and Gic2. *J Cell Biol* **164**(2): 219-31.
- Horio, T. and B. R. Oakley (2005). The role of microtubules in rapid hyphal tip growth of *Aspergillus nidulans*. *Mol Biol Cell* **16**(2): 918-26.
- Hoshino, M. and S. Nakamura (2003). Small GTPase Rin induces neurite outgrowth through Rac/Cdc42 and calmodulin in PC12 cells. *J Cell Biol* **163**(5): 1067-76.
- Hoshino, M., T. Yoshimori and S. Nakamura (2005). Small GTPase proteins Rin and Rit Bind to PAR6 GTP-dependently and regulate cell transformation. *J Biol Chem* **280**(24): 22868-74.
- Howard, R. J. (1981). Ultrastructural analysis of hyphal tip cell growth in fungi: Spitzenkorper, cytoskeleton and endomembranes after freeze-substitution. *J Cell Sci* **48**: 89-103.
- Huckaba, T. M., A. C. Gay, L. F. Pantalena, H. C. Yang and L. A. Pon (2004). Live cell imaging of the assembly, disassembly, and actin cable-dependent movement of endosomes and actin patches in the budding yeast, *Saccharomyces cerevisiae*. *J Cell Biol* **167**(3): 519-30.
- Imamura, H., K. Tanaka, T. Hihara, M. Umikawa, T. Kamei, K. Takahashi, T. Sasaki and Y. Takai (1997). Bni1p and Bnr1p: downstream targets of the Rho family small G-proteins which interact with profilin and regulate actin cytoskeleton in *Saccharomyces cerevisiae*. *Embo J* **16**(10): 2745-55.
- Iraoqui, J. E., A. S. Gladfelter and D. J. Lew (2003). Scaffold-mediated symmetry breaking by Cdc42p. *Nat Cell Biol* **5**(12): 1062-70.
- Iwase, M., J. Luo, S. Nagaraj, M. Longtine, H. B. Kim, B. K. Haarer, C. Caruso, Z. Tong, J. R. Pringle and E. Bi (2006). Role of a Cdc42p effector pathway in recruitment of the yeast septins to the presumptive bud site. *Mol Biol Cell* **17**(3): 1110-25.
- James, P., J. Halladay and E. A. Craig (1996). Genomic libraries and a host strain designed for highly efficient two-hybrid selection in yeast. *Genetics* **144**(4): 1425-36.
- Jaquenoud, M. and M. Peter (2000). Gic2p may link activated Cdc42p to components involved in actin polarization, including Bni1p and Bud6p (Aip3p). *Mol Cell Biol* **20**(17): 6244-58.
- Jaquenoud, M., M. P. Gulli, K. Peter and M. Peter (1998). The Cdc42p effector Gic2p is targeted for ubiquitin-dependent degradation by the SCFGrr1 complex. *Embo J* **17**(18): 5360-73.
- Jonsdottir, G. A. and R. Li (2004). Dynamics of yeast Myosin I: evidence for a possible role in scission of endocytic vesicles. *Curr Biol* **14**(17): 1604-9.
- Kamada, Y., H. Qadota, C. P. Python, Y. Anraku, Y. Ohya and D. E. Levin (1996). Activation of yeast protein kinase C by Rho1 GTPase. *J Biol Chem* **271**(16): 9193-6.
- Kippert, F. and D. Lloyd (1995). The aniline blue fluorochrome specifically stains the septum of both live and fixed *Schizosaccharomyces pombe* cells. *FEMS Microbiol Lett* **132**(3): 215-9.
- Knechtle, P. (2002). *AgSPA2* and *AgBOI* control landmarks of filamentous growth in the filamentous ascomycete *Ashbya gossypii*. *Philosophisch-Naturwissenschaftliche Fakultät*. Basel, University of Basel.
- Knechtle, P., F. Dietrich and P. Philippsen (2003). Maximal polar growth potential depends on the polarisome component AgSpa2 in the filamentous fungus *Ashbya gossypii*. *Mol Biol Cell* **14**(10): 4140-54.
- Knechtle, P., J. Wendland and P. Philippsen (2006). The SH3/PH domain protein AgBoi1/2 collaborates with the Rho-type GTPase AgRho3 to prevent nonpolar growth at hyphal tips of *Ashbya gossypii*. *Eukaryot Cell* **5**(10): 1635-47.
- Kohno, H., K. Tanaka, A. Mino, M. Umikawa, H. Imamura, T. Fujiwara, Y. Fujita, K. Hotta, H. Qadota, T. Watanabe, Y. Ohya and Y. Takai (1996). Bni1p implicated in cytoskeletal control is a putative target of Rho1p small GTP binding protein in *Saccharomyces cerevisiae*. *Embo J* **15**(22): 6060-8.
- Kurtzman, C. P. (1995). Relationships among the genera *Ashbya*, *Eremothecium*, *Holleya* and *Nematospira* determined from rDNA sequence divergence. *J Ind Microbiol* **14**(6): 523-30.
- Lee, C. H., N. G. Della, C. E. Chew and D. J. Zack (1996). Rin, a neuron-specific and calmodulin-binding small G-protein, and Rit define a novel subfamily of ras proteins. *J Neurosci* **16**(21): 6784-94.
- Levin, D. E. (2005). Cell wall integrity signaling in *Saccharomyces cerevisiae*. *Microbiol Mol Biol Rev* **69**(2): 262-91.

- Lin, X. and M. Momany (2004). Identification and complementation of abnormal hyphal branch mutants *ahbA1* and *ahbB1* in *Aspergillus nidulans*. *Fungal Genet Biol* **41**(11): 998-1006.
- Longtine, M. S., A. McKenzie, 3rd, D. J. Demarini, N. G. Shah, A. Wach, A. Brachat, P. Philippsen and J. R. Pringle (1998). Additional modules for versatile and economical PCR-based gene deletion and modification in *Saccharomyces cerevisiae*. *Yeast* **14**(10): 953-61.
- Lopez-Franco, R., Bracker, Charles E. (1996). Diversity and dynamics of the Spitzenkörper in growing hyphal tips of higher fungi. *Protoplasma* **195**(1-4): 90-111.
- Longberg, A., H. P. Schmitz, J. J. Jacoby and J. J. Heinisch (2001). Lrg1p functions as a putative GTPase-activating protein in the Pkc1p-mediated cell integrity pathway in *Saccharomyces cerevisiae*. *Mol Genet Genomics* **266**(3): 514-26.
- Louvet, O., F. Doignon and M. Crouzet (1997). Stable DNA-binding yeast vector allowing high-bait expression for use in the two-hybrid system. *Biotechniques* **23**(5): 816-8, 820.
- Madaule, P., R. Axel and A. M. Myers (1987). Characterization of two members of the rho gene family from the yeast *Saccharomyces cerevisiae*. *Proc Natl Acad Sci U S A* **84**(3): 779-83.
- Manning, B. D., R. Padmanabha and M. Snyder (1997). The Rho-GEF Rom2p localizes to sites of polarized cell growth and participates in cytoskeletal functions in *Saccharomyces cerevisiae*. *Mol Biol Cell* **8**(10): 1829-44.
- Mazur, P. and W. Baginsky (1996). In vitro activity of 1,3-beta-D-glucan synthase requires the GTP-binding protein Rho1. *J Biol Chem* **271**(24): 14604-9.
- McDaniel, D. P. and R. W. Roberson (2000). Microtubules Are required for motility and positioning of vesicles and mitochondria in hyphal tip cells of *Allomyces macrogynus*. *Fungal Genet Biol* **31**(3): 233-44.
- Milburn, M. V., L. Tong, A. M. deVos, A. Brunger, Z. Yamaizumi, S. Nishimura and S. H. Kim (1990). Molecular switch for signal transduction: structural differences between active and inactive forms of protooncogenic ras proteins. *Science* **247**(4945): 939-45.
- Moseley, J. B., I. Sagot, A. L. Manning, Y. Xu, M. J. Eck, D. Pellman and B. L. Goode (2004). A conserved mechanism for Bni1- and mDia1-induced actin assembly and dual regulation of Bni1 by Bud6 and profilin. *Mol Biol Cell* **15**(2): 896-907.
- Moskow, J. J., A. S. Gladfelter, R. E. Lamson, P. M. Pryciak and D. J. Lew (2000). Role of Cdc42p in pheromone-stimulated signal transduction in *Saccharomyces cerevisiae*. *Mol Cell Biol* **20**(20): 7559-71.
- Mulholland, J., D. Preuss, A. Moon, A. Wong, D. Drubin and D. Botstein (1994). Ultrastructure of the yeast actin cytoskeleton and its association with the plasma membrane. *J Cell Biol* **125**(2): 381-91.
- Nelson, W. J. (2003). Adaptation of core mechanisms to generate cell polarity. *Nature* **422**(6933): 766-74.
- Nonaka, H., K. Tanaka, H. Hirano, T. Fujiwara, H. Kohno, M. Umikawa, A. Mino and Y. Takai (1995). A downstream target of RHO1 small GTP-binding protein is PKC1, a homolog of protein kinase C, which leads to activation of the MAP kinase cascade in *Saccharomyces cerevisiae*. *Embo J* **14**(23): 5931-8.
- Novick, P. and D. Botstein (1985). Phenotypic analysis of temperature-sensitive yeast actin mutants. *Cell* **40**(2): 405-16.
- Ohno, S. (1970). *Evolution by gene duplication*. Berlin, Springer.
- Ozaki, K., K. Tanaka, H. Imamura, T. Hihara, T. Kameyama, H. Nonaka, H. Hirano, Y. Matsuura and Y. Takai (1996). Rom1p and Rom2p are GDP/GTP exchange proteins (GEPs) for the Rho1p small GTP binding protein in *Saccharomyces cerevisiae*. *Embo J* **15**(9): 2196-207.
- Ozaki-Kuroda, K., Y. Yamamoto, H. Nohara, M. Kinoshita, T. Fujiwara, K. Irie and Y. Takai (2001). Dynamic localization and function of Bni1p at the sites of directed growth in *Saccharomyces cerevisiae*. *Mol Cell Biol* **21**(3): 827-39.
- Ozbudak, E. M., A. Becskei and A. van Oudenaarden (2005). A system of counteracting feedback loops regulates Cdc42p activity during spontaneous cell polarization. *Dev Cell* **9**(4): 565-71.
- Philip, B. and D. E. Levin (2001). Wsc1 and Mid2 are cell surface sensors for cell wall integrity signaling that act through Rom2, a guanine nucleotide exchange factor for Rho1. *Mol Cell Biol* **21**(1): 271-80.
- Philippsen, P., A. Kaufmann and H. P. Schmitz (2005). Homologues of yeast polarity genes control the development of multinucleated hyphae in *Ashbya gossypii*. *Curr Opin Microbiol* **8**(4): 370-7.

References

- Qadota, H., C. P. Python, S. B. Inoue, M. Arisawa, Y. Anraku, Y. Zheng, T. Watanabe, D. E. Levin and Y. Ohya (1996). Identification of yeast Rho1p GTPase as a regulatory subunit of 1,3-beta-glucan synthase. *Science* **272**(5259): 279-81.
- Rechsteiner, M. and S. W. Rogers (1996). PEST sequences and regulation by proteolysis. *Trends Biochem Sci* **21**(7): 267-71.
- Reynolds, E. S. (1963). The use of lead citrate at high pH as an electron-opaque stain in electron microscopy. *J Cell Biol* **17**: 208-12.
- Rice, P., I. Longden and A. Bleasby (2000). EMBOSS: the European Molecular Biology Open Software Suite. *Trends Genet* **16**(6): 276-7.
- Rogers, S., R. Wells and M. Rechsteiner (1986). Amino acid sequences common to rapidly degraded proteins: the PEST hypothesis. *Science* **234**(4774): 364-8.
- Roumanie, O., H. Wu, J. N. Molk, G. Rossi, K. Bloom and P. Brennwald (2005). Rho GTPase regulation of exocytosis in yeast is independent of GTP hydrolysis and polarization of the exocyst complex. *J Cell Biol* **170**(4): 583-94.
- Sagot, I., A. A. Rodal, J. Moseley, B. L. Goode and D. Pellman (2002). An actin nucleation mechanism mediated by Bni1 and profilin. *Nat Cell Biol* **4**(8): 626-31.
- Saka, A., M. Abe, H. Okano, M. Minemura, H. Qadota, T. Utsugi, A. Mino, K. Tanaka, Y. Takai and Y. Ohya (2001). Complementing yeast rho1 mutation groups with distinct functional defects. *J Biol Chem* **276**(49): 46165-71.
- Salminen, A. and P. J. Novick (1987). A ras-like protein is required for a post-Golgi event in yeast secretion. *Cell* **49**(4): 527-38.
- Sambrook, J. a. D. R. (2001). *Molecular Cloning: A Laboratory Manual*. Cold Spring Harbor, Cold Spring Harbor Laboratory Press.
- Schmidt, A., T. Schmelzle and M. N. Hall (2002). The RHO1-GAPs SAC7, BEM2 and BAG7 control distinct RHO1 functions in *Saccharomyces cerevisiae*. *Mol Microbiol* **45**(5): 1433-41.
- Schmitz, H. P., A. Kaufmann, M. Kohli, P. P. Laissue and P. Philippsen (2006). From Function to Shape: A Novel Role of a Formin in Morphogenesis of the Fungus *Ashbya gossypii*. *Mol Biol Cell* **17**(1): 130-45.
- Shao, H., K. Kadono-Okuda, B. S. Finlin and D. A. Andres (1999). Biochemical characterization of the Ras-related GTPases Rit and Rin. *Arch Biochem Biophys* **371**(2): 207-19.
- Sharpless, K. E. and S. D. Harris (2002). Functional characterization and localization of the *Aspergillus nidulans* formin SEPA. *Mol Biol Cell* **13**(2): 469-79.
- Sheu, Y. J., B. Santos, N. Fortin, C. Costigan and M. Snyder (1998). Spa2p interacts with cell polarity proteins and signaling components involved in yeast cell morphogenesis. *Mol Cell Biol* **18**(7): 4053-69.
- Shih, J. L., S. L. Reck-Peterson, R. Newitt, M. S. Mooseker, R. Aebersold and I. Herskowitz (2005). Cell polarity protein Spa2P associates with proteins involved in actin function in *Saccharomyces cerevisiae*. *Mol Biol Cell* **16**(10): 4595-608.
- Smith, M. L., J. N. Bruhn and J. B. Anderson (1992). The fungus *Armillaria bulbosa* is among the largest and oldest living organisms. *Nature* **356**(6368): 428-431.
- Smith, S. J. and K. Rittinger (2002). Preparation of GTPases for structural and biophysical analysis. *Methods Mol Biol* **189**: 13-24.
- Stahmann, K. P., H. N. Arst, Jr., H. Althofer, J. L. Revuelta, N. Monschau, C. Schlupen, C. Gatgens, A. Wiesenburg and T. Schlosser (2001). Riboflavin, overproduced during sporulation of *Ashbya gossypii*, protects its hyaline spores against ultraviolet light. *Environ Microbiol* **3**(9): 545-50.
- Stahmann, K. P., J. L. Revuelta and H. Seulberger (2000). Three biotechnical processes using *Ashbya gossypii*, *Candida famata*, or *Bacillus subtilis* compete with chemical riboflavin production. *Appl Microbiol Biotechnol* **53**(5): 509-16.
- Steinberg, G. (2007). Hyphal growth: a tale of motors, lipids, and the Spitzenkorper. *Eukaryot Cell* **6**(3): 351-60.
- Storici, F., L. K. Lewis and M. A. Resnick (2001). In vivo site-directed mutagenesis using oligonucleotides. *Nat Biotechnol* **19**(8): 773-6.
- Takai, Y., T. Sasaki and T. Matozaki (2001). Small GTP-binding proteins. *Physiol Rev* **81**(1): 153-208.
- TerBush, D. R., T. Maurice, D. Roth and P. Novick (1996). The Exocyst is a multiprotein complex required for exocytosis in *Saccharomyces cerevisiae*. *Embo J* **15**(23): 6483-94.

- Thompson, J. D., D. G. Higgins and T. J. Gibson (1994). CLUSTAL W: improving the sensitivity of progressive multiple sequence alignment through sequence weighting, position-specific gap penalties and weight matrix choice. *Nucleic Acids Res* **22**(22): 4673-80.
- Torres, L., H. Martin, M. I. Garcia-Saez, J. Arroyo, M. Molina, M. Sanchez and C. Nombela (1991). A protein kinase gene complements the lytic phenotype of *Saccharomyces cerevisiae* *lyt2* mutants. *Mol Microbiol* **5**(11): 2845-54.
- Trinci, A. P. J. (1970). Kinetics of apical and lateral branching in *Aspergillus nidulans* and *Geotrichum lactis*. *Trans. Br. Mycol. Soc.* **55**: 17-28.
- Ubersax, J. A., E. L. Woodbury, P. N. Quang, M. Paraz, J. D. Blethrow, K. Shah, K. M. Shokat and D. O. Morgan (2003). Targets of the cyclin-dependent kinase Cdk1. *Nature* **425**(6960): 859-64.
- Uetz, P., L. Giot, G. Cagney, T. A. Mansfield, R. S. Judson, J. R. Knight, D. Lockshon, V. Narayan, M. Srinivasan, P. Pochart, A. Qureshi-Emili, Y. Li, B. Godwin, D. Conover, T. Kalbfleisch, G. Vijayadomodar, M. Yang, M. Johnston, S. Fields and J. M. Rothberg (2000). A comprehensive analysis of protein-protein interactions in *Saccharomyces cerevisiae*. *Nature* **403**(6770): 623-7.
- Umikawa, M., K. Tanaka, T. Kamei, K. Shimizu, H. Imamura, T. Sasaki and Y. Takai (1998). Interaction of Rho1p target Bni1p with F-actin-binding elongation factor 1alpha: implication in Rho1p-regulated reorganization of the actin cytoskeleton in *Saccharomyces cerevisiae*. *Oncogene* **16**(15): 2011-6.
- Valdez-Taubas, J. and H. R. Pelham (2003). Slow diffusion of proteins in the yeast plasma membrane allows polarity to be maintained by endocytic cycling. *Curr Biol* **13**(18): 1636-40.
- Versele, M. and J. Thorner (2004). Septin collar formation in budding yeast requires GTP binding and direct phosphorylation by the PAK, Cla4. *J Cell Biol* **164**(5): 701-15.
- Vetter, I. R. and A. Wittinghofer (2001). The guanine nucleotide-binding switch in three dimensions. *Science* **294**(5545): 1299-304.
- Vieira, J. and J. Messing (1991). New pUC-derived cloning vectors with different selectable markers and DNA replication origins. *Gene* **100**: 189-94.
- Wach, A., A. Brachat, R. Pohlmann and P. Philippsen (1994). New heterologous modules for classical or PCR-based gene disruptions in *Saccharomyces cerevisiae*. *Yeast* **10**(13): 1793-808.
- Walch-Solimena, C., R. N. Collins and P. J. Novick (1997). Sec2p mediates nucleotide exchange on Sec4p and is involved in polarized delivery of post-Golgi vesicles. *J Cell Biol* **137**(7): 1495-509.
- Walther, A. and J. Wendland (2005). Initial molecular characterization of a novel Rho-type GTPase RhoH in the filamentous ascomycete *Ashbya gossypii*. *Curr Genet* **48**(4): 247-55.
- Watanabe, D., M. Abe and Y. Ohya (2001). Yeast Lrg1p acts as a specialized RhoGAP regulating 1,3-beta-glucan synthesis. *Yeast* **18**(10): 943-51.
- Watters, M. K. and A. J. Griffiths (2001). Tests of a cellular model for constant branch distribution in the filamentous fungus *Neurospora crassa*. *Appl Environ Microbiol* **67**(4): 1788-92.
- Wedlich-Soldner, R., I. Schulz, A. Straube and G. Steinberg (2002). Dynein supports motility of endoplasmic reticulum in the fungus *Ustilago maydis*. *Mol Biol Cell* **13**(3): 965-77.
- Wedlich-Soldner, R., S. C. Wai, T. Schmidt and R. Li (2004). Robust cell polarity is a dynamic state established by coupling transport and GTPase signaling. *J Cell Biol* **166**(6): 889-900.
- Wendland, J. and A. Walther (2005). *Ashbya gossypii*: a model for fungal developmental biology. *Nat Rev Microbiol* **3**(5): 421-9.
- Wendland, J. and P. Philippsen (2000). Determination of cell polarity in germinated spores and hyphal tips of the filamentous ascomycete *Ashbya gossypii* requires a rhoGAP homolog. *J Cell Sci* **113** (Pt 9): 1611-21.
- Wendland, J. and P. Philippsen (2001). Cell polarity and hyphal morphogenesis are controlled by multiple rho-protein modules in the filamentous ascomycete *Ashbya gossypii*. *Genetics* **157**(2): 601-10.
- Wendland, J., Y. Ayad-Durieux, P. Knechtle, C. Reibischung and P. Philippsen (2000). PCR-based gene targeting in the filamentous fungus *Ashbya gossypii*. *Gene* **242**(1-2): 381-91.
- Wes, P. D., M. Yu and C. Montell (1996). RIC, a calmodulin-binding Ras-like GTPase. *Embo J* **15**(21): 5839-48.
- Wild, A. C., J. W. Yu, M. A. Lemmon and K. J. Blumer (2004). The p21-activated protein kinase-related kinase Cla4 is a coincidence detector of signaling by Cdc42 and phosphatidylinositol 4-phosphate. *J Biol Chem* **279**(17): 17101-10.

References

- Winkler, J. (2007). *AgGic1 and AgBem4: Two proteins in polarity establishment* (Master Thesis).
- Wolfe, K. H. (2006). Comparative genomics and genome evolution in yeasts. *Philos Trans R Soc Lond B Biol Sci* **361**(1467): 403-12.
- Wright, M. C. and P. Philippsen (1991). Replicative transformation of the filamentous fungus *Ashbya gossypii* with plasmids containing *Saccharomyces cerevisiae* ARS elements. *Gene* **109**(1): 99-105.
- Wu, C., V. Lytvyn, D. Y. Thomas and E. Leberer (1997). The phosphorylation site for Ste20p-like protein kinases is essential for the function of myosin-I in yeast. *J Biol Chem* **272**(49): 30623-6.
- Yang, F., M. Demma, V. Warren, S. Dharmawardhane and J. Condeelis (1990). Identification of an actin-binding protein from *Dictyostelium* as elongation factor 1a. *Nature* **347**(6292): 494-6.
- Zdobnov, E. M. and R. Apweiler (2001). InterProScan--an integration platform for the signature-recognition methods in InterPro. *Bioinformatics* **17**(9): 847-8.
- Zhang, X., E. Bi, P. Novick, L. Du, K. G. Kozminski, J. H. Lipschutz and W. Guo (2001). Cdc42 interacts with the exocyst and regulates polarized secretion. *J Biol Chem* **276**(50): 46745-50.
- Zigmond, S. H., M. Evangelista, C. Boone, C. Yang, A. C. Dar, F. Sicheri, J. Forkey and M. Pring (2003). Formin leaky cap allows elongation in the presence of tight capping proteins. *Curr Biol* **13**(20): 1820-3.

Supplemental movies

The supplemental movies can be found on the enclosed CD.

Movie S1

A time-lapse movie of an *A. gossypii* hyphal tip grown on a thin agar layer that contained 19 % gelatine was acquired during 60 seconds (see part I, figure 2).

Movie S2

Time-lapse movies of *AgEXO70-GFP* expressing hyphae. The movie represents 15 minutes in real time (see part I, figure 3).

Movie S3

Germination of *Aggic1/2Δ* and the reference strain. The movie represents 16 hours in real time (see part II, figure 6).

Movie S4

Time-lapse movie of *AgGIC1/2Δ-YFP*. The arrow indicates a lateral branching event (see part II, figure 8). The movie was taken during 50 minutes. Scale bar = 20 μm.

Movie S5

Time-lapse movie acquired at the border of an *Agrho1aΔ* mycelium. Arrows indicate hyphal lysis (see part III, figure 1). Scale bar = 50 μm.

Movie S6

Time-lapse movie of *AgSPA2-GFP*. The movie represents 21 minutes of real time (see appendix, figure 4). Scale bar = 5 μm.

Movie S7

Time-lapse movie of *AgSPA2-GFP*. The movie represents 30 minutes of real time (see appendix, figure 4). Scale bar = 5 μm.

Movie S8

Time-lapse movie of *GFP-AgBNI1*. The movie represents 41 minutes of real time (see appendix, figure 4). Scale bar = 5 μm.

Acknowledgements

Acknowledgements

Some people supported me during my time as a PhD student in a very direct manner by helping me working and thinking. Others were just there when I was tired, frustrated, or angry. I want to express my deepest feelings of gratitude to all of those who made this work possible.

I am very grateful to Peter Philippsen for giving me the opportunity to do my PhD in his laboratory. Peter took care that I didn't spend my entire time in the microscopy room. He sent me to Arizona to have a closer look at the *Ashbya gossypii* hyphal tip and to numerous conferences where I had the chance to present my work to the scientific community. Peter was never short of advice, anecdotes and chocolate to support my scientific work.

I want to thank Hans-Peter Schmitz who introduced me into laboratory work. He always had time to answer my questions or to help me with my experiments. Hans-Peter found the atypical histidine residue in *AgRho1a* and did a big part of the work presented in Part III of my thesis.

Robert W. Roberson welcomed me in his team at the Arizona State University, Tempe, USA. He and his PhD student, Maho Uchida, were supporting me on my quest for the Spitzenkörper in *Ashbya gossypii*.

I want to thank the members of my thesis committee, Yves Barral and Anne Spang for the time they sacrificed for me and for agreeing on having a Friday night PhD exam.

I always enjoyed working in the Philippsen group and I want to thank all present and former group members for their help and the good times we spent together. Especially, I want to thank Andreas Kaufmann for critically reading my manuscript and for helping me with my computer problems, Katrin Hungerbühler and Hans-Peter Helfer for never being tired to listen to my theories about *Ashbya* during our Tuesday night dinners, Claudia Birrer for bringing back the dancing days, Jeannine Winkler for working with me on *AgGic1/2*, and Virginie Galati for deleting the exocyst genes.

Many thanks to my friends Charlotte Jäggi who has been living with me under the same roof for the last four years and to Franziska Fürholz for countless evenings spent with a glass of wine.

Very special thanks to Sébastien Derada to whom it was perfectly clear that filamentous fungi are not on the "Most-Important-Things-In-Live"-list.

I feel the deepest gratitude towards my family who have supported me through my entire live.

Curriculum vitae

Curriculum vitae

Michael Köhli
 Buchenstrasse 4
 4054 Basel
 koehli@gmx.ch

Personal Information

Born on March 21, 1979 in Solothurn, Switzerland.
 Son of Monika Köhli-Christ and Heinz Köhli.

Education

PhD

2003 - 2007

PhD project "From polarity establishment to fast hyphal growth in the filamentous fungus *Ashbya gossypii*" at the Biozentrum of the University of Basel, Switzerland under the supervision of Prof. Peter Philippsen.

Thesis committee

Prof. Peter Philippsen, Biozentrum, Basel, Switzerland
 Prof. Yves Barral, ETH Zürich, Switzerland
 Prof. Anne Spang, Biozentrum, Basel, Switzerland

Diploma in Biology II

1999 – 2003

University of Basel, Switzerland
 Graduation: Molecular Microbiology
 Main subjects: biochemistry, biophysical chemistry, molecular genetics, cell biology

Matura typus C

1996-1999

Kantonsschule Solothurn, Switzerland
 Focus on mathematics and physics

Meetings

24th Fungal Genetics Conference

2007, Pacific Grove, California, USA

Talk and poster with the title "Functional topology of the growing hyphal tip"

Swiss yeast meeting 2006

2006, Basel, Switzerland

Talk and poster with the title: "Functional topology of the growing *Ashbya gossypii* hyphal tip"

1st meeting "Biology of Yeasts and Filamentous Fungi"

2006, Frankfurt am Main, Germany

Poster prize for the poster "Functional topology of the growing *Ashbya gossypii* hyphal tip"

23th Fungal Genetics Conference

2005, Pacific Grove, California, USA

Talk and poster with the title "Spitzenkörper and Polarisome of *Ashbya gossypii*".

7th European Conference on Fungal Genetics

2004, Copenhagen, Denmark

Poster with the title "The AgBNI1 formin homology protein is essential for hyphal formation in *Ashbya gossypii*"

Publication

Schmitz, H.P., Kaufmann, A., Köhli, M., Laissue, P. P., and Philippsen P. (2006). From function to shape: a novel role of a formin in morphogenesis of the fungus *Ashbya gossypii*. *Mol Biol Cell* **17**, 130-145

Erklärung

Erklärung

Ich erkläre, dass ich die Dissertation “From polarity establishment to fast hyphal growth in the filamentous fungus *Ashbya gossypii*“ nur mit der darin angegebenen Hilfe verfasst und bei keiner anderen Universität und bei keiner anderen Fakultät der Universität Basel eingereicht habe.

Basel, 12. Juni 2007

Michael Köhli